Western Australian School of Mines

Impurity control by precipitation in synthetic atmospheric nickel laterite sulfate leach solutions

Ndishavhelafhi Mbedzi

This thesis is presented for the Degree of
Doctor of Philosophy
of
Curtin University

September 2020

DECLARATION

To the best of my knowledge and belief this thesis contains no material previously published by any other person except where due acknowledgement has been made.

This thesis contains no material which has been accepted for the award of any other degree or diploma in any university.

Signature: .....

Date: 11 September 2020

ACKNOWLEDGEMENTS

My research study was funded through the BHP Billiton scholarship, and I would like to take this opportunity to acknowledge and express my gratitude for their financial support.

I would also like to express my sincere gratitude to many people for their help and support during this study.

First, I would like to thank my supervisors: Associate Professor Don Ibana, Associate Professor Richard Browner and Dr Laurence Dyer for their invaluable input, guidance and constructive suggestions.

To WASM staff members, academic, technical and support staff, thank you for the help and friendship. Special thanks to Veronica Avery and Elaine Miller of the X-Ray Diffraction and Scattering Facility and the Microscopy & Microanalysis Facility (John de Laeter Centre, respectively for your assistance with the XRD and SEM analysis. To Mujesira Vukancic, Anusha Shantha Kumara and Melina Miralles from WASM, thank you for the technical support, friendship and support.

I am also grateful to my fellow HDR colleagues for their warmth and support. To Zela Tanlega and Behrooz Rahimi, I appreciate the daily support and encouragement. It was an honour being around you. I learnt a lot from you my dear brothers and thank you.

A special thank you to my husband, Richard Nyengera for your support, love and encouragement.

ABSTRACT

In light of fast depleting nickel sulfide ore reserves and increasing demand for nickel, the future of the nickel industry lies in the hydrometallurgical processing of the relatively abundant low-grade nickel laterite ores. Hence the increased interest in the use of atmospheric leaching (AL) and heap leaching (HL) as potential alternatives or an adjunct to HPAL. The leach solutions produced contain significant amounts of impurities: iron, aluminium, chromium, magnesium, manganese and many others. The processing of these sulfate leach solutions from nickel laterites is proving to be particularly challenging despite decades of intense research and development work. The removal of the major impurities of iron and aluminium by precipitation processes is associated with significant nickel and cobalt losses.

This thesis is a compilation of research on understanding the effect of various process parameters on impurity removal and the associated nickel and cobalt losses from simulated nickel laterite solutions.

Modelling of the selective removal of the trivalent ions of iron, aluminium and chromium from the divalent ions of nickel and cobalt by precipitation was carried out using Visual MINTEQ software. Experimental studies were carried out on the relationships between the various process parameters and the impurities removal and the associated nickel and cobalt losses from simulated nickel laterite solutions of different metallic ion combinations.

Modelling showed the precipitation of the trivalent ions and the major precipitates; however, it was not possible to predict the co-removal of nickel from dilute sulfate solutions. Initial experimental studies on the precipitation of ferric ion from the simple ternary sulfate system [Fe(III)+Ni(II)+Co(II)] revealed that the amount of nickel and cobalt losses was dependent on the type of neutralising agent. The affinity for nickel and cobalt uptake by the iron precipitates produced via the neutralising agents tested was in the following order: MgO slurry > $MgCO_3$ slurry > NaOH solution > $CaCO_3$ slurry. Also, the extent of nickel and cobalt losses was found to increase as the elemental components in sulfate solutions increased. Higher nickel and cobalt losses occurred during the co-removal of iron, aluminium and chromium and in the presence of magnesium in the process solution.

The effect and importance of process parameters on the removal efficiency of trivalent ions of iron, aluminium and chromium and the associated nickel and cobalt losses was investigated using multi-element sulfate solutions using full factorial design and one variable at a time approach. The parameters, pH, temperature and concentration of $CaCO_3$ slurry were found to be of significance to the impurity removal process. Increasing equilibrium pH and temperature of the solution favoured the removal of the trivalent ions of iron, aluminium and chromium by precipitation but at the cost of greater nickel and cobalt losses to the precipitate. The precipitation products were a mixture of amorphous iron phases and metastable iron phases, schwertmannite and ferrihydrite and gypsum.

Ferrous ion, a common impurity when processing magnesium silicate-rich ores, can only be removed by oxidative precipitation at low pH to reduce nickel and cobalt losses. This study also investigated the influence of process parameters on ferrous ion removal efficiency, the associated nickel and cobalt losses and the co-removal of any residual aluminium and chromium from the first impurity removal process by oxidative precipitation. Type of oxidant, pH and temperature were found to influence the process. Higher pH and temperature favoured the removal of ferrous ion, aluminium and chromium but at the cost of greater nickel and cobalt losses. The amount of nickel and cobalt losses, however, can be reduced by using multistage oxidative precipitation. Hydrogen peroxide is a better oxidant than air and pure oxygen, with faster oxidation rates which can increase plant throughput. Although it was apparent that high pH promotes oxidative precipitation of ferrous ion, the optimum pH to be used in this process is determined by aluminium removal efficiency.

The best purification technique based on the results of investigations into the removal of iron aluminium and chromium was a two-stage precipitation process. The first stage is purely precipitation for the removal of the bulk of the trivalent ions of iron, aluminium and chromium. The second stage is oxidative precipitation targeted to remove ferrous ion and any ferric ion, aluminium and chromium remaining in solution after the first precipitation stage. The optimum conditions for the first stage were an equilibrium pH value of 3.5 and a temperature of 85 °C that produced nickel and cobalt losses of less than 10%. In the second stage, the optimum conditions when using hydrogen peroxide as oxidant were a combination of oxidative precipitation and ageing pH values of 3.5 and 4.5, respectively. Using a pH of 4.5 allows for aluminium

removal of more than 99.5% and complete removal of both iron and chromium. This is however at the cost of approximately 11% nickel and 2% cobalt losses. The amount of nickel losses in the first step can be minimised to less than 2% by using lower pH values, but this produces high Al concentrations in the oxidative precipitation process and build-up of aluminium if the precipitates are recycled. Low ferric ion concentration in oxidative precipitation did not affect the nature of the iron precipitates.

Manganese can be present in significant amounts in nickel laterite sulfate leach solutions and different purification routes are used to process the solutions following iron, aluminium and chromium removal. Oxidative precipitation with potassium permanganate as the oxidant using simulated process sulfate solutions was used to study the removal efficiency of manganese and the associated nickel and cobalt losses. The effect of process parameters was investigated. $KMnO_4$ dosage and temperature were found to play a significant role in manganese removal efficiency while pH, initial manganese concentration and $KMnO_4$ dosage are significant factors on cobalt and nickel losses to the precipitate. A reduction in manganese removal efficiency was observed when the slurries are aged. The removal of cobalt from the solution was very high, and oxidative precipitation was used for its co-removal with manganese. The removal of manganese and cobalt was favoured at high pH values but, at the cost of increased nickel losses while high temperatures resulted in a decrease in manganese removal efficiency. The optimum conditions for oxidative precipitation of manganese were, at temperature 25 ℃, pH value 4 and oxidant dosage of 1.54 mg $KMnO_4$/mg Mn(II) (Mode C). Manganous ion was precipitated as a dense brownish to black precipitate identified as manganese dioxide.

A purification process is proposed with initial two stage precipitation for the removal of iron (ferrous and ferric ion), aluminium and chromium followed by oxidative precipitation to remove both cobalt and manganese for future cobalt removal and nickel recovery. Such a scheme will overcome the issues of ferrous ions and manganese in subsequent downstream process steps.

TABLE OF CONTENTS

LIST OF FIGURES

LIST OF TABLES

CHAPTER 1
INTRODUCTION

1.1 Nickel production

Nickel production has continued to rise since 1950 (Dalvi et al., 2004) and is expected to continue, though with some cyclic fluctuations following global economic trends and events (Goonan et al., 2017). For instance, 2008 marked the onset of the global recession which resulted in a significant decline in stainless steel production and consequently nickel production and price in the years 2008 and 2009 as shown in Figure 1.1. The mean annual nickel price in 2008 was recorded at $21104/tonne and was 43% less than the 2007 year average and continues to fall (Kuck, 2008). Despite the continuing instability in nickel price following the global recession, the world nickel production has since increased tremendously (Figure 1.1), which is a clear indication of the importance of nickel in our modern society. The excellent alloying properties of nickel with other metals to produce final products with better corrosion resistance, toughness and strength over a wide range of temperatures make it invaluable in industrial, domestic and technology applications.

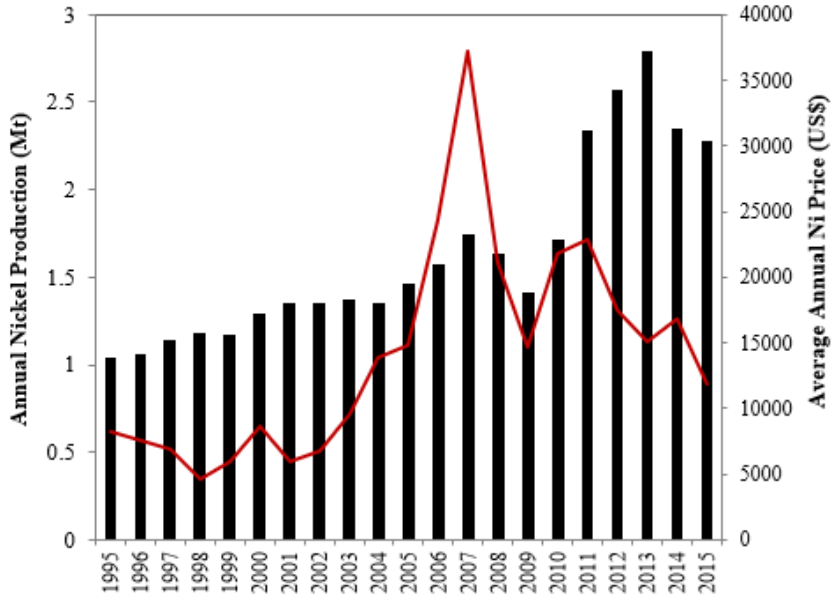

Figure 1. 1: World nickel production (bar graphs) (data extracted from nickel commodity summaries 1995 to 2017) (Kelly et al., 2014, Ober, 2018, Goonan et al., 2017) and nickel price (line graph) (Department of Mines, 2017).

Nickel laterite and sulfide ores are the principal sources of global nickel metal, with the former estimated to make up almost 60% of known global nickel resources with at least 1% Ni grade and the remaining 40% being nickel sulfide ores (McRae, 2018). For over a century, since the discovery of sulfide deposits of Sudbury in Canada, the high grade and easier to process nickel sulfide ores have been the dominant source of nickel metal, leading to their fast depletion. Nickel consumption has been increasing particularly over the last century and to meet the nickel demand there is a need for expansion in the exploitation of the relatively abundant but low-grade nickel laterite ores. The mining of nickel laterites is much cheaper compared to that of nickel sulphides, as they are close to the surface. The processing, however, is proving to be particularly challenging and expensive despite decades of intense research and development work.

1.2 Nickel laterite ores processing

The processing of nickel laterite ores is relatively complex due to their variable and complex mineralogy (Zhu et al., 2012). Early processing of nickel laterite ores was done using pyrometallurgical methods (ferronickel and matte smelting) and dates back in 1879 at Doniambo, New Caledonia with the production of ferronickel (Dalvi et al., 2004). The drawback of pyrometallurgical processing is that they are suited for high Ni grade ores and not low-grade ores which make up the bulk of the nickel laterite resource. As higher ore grades were fast depleting and the nickel demand continued to increase, there was a need for the development of alternative methods for exploiting the low-grade nickel laterite ores. The quest for better processing options for nickel laterite ores led to the establishment of two hydrometallurgical processing methods in the 1950s, the Caron Process and the high pressure acid leaching (HPAL).

The Caron Process, a hybrid of pyrometallurgical and hydrometallurgical processing was developed by M.H Carron and first used in a large scale operation at Nicaro, Cuba in 1952 (Caron, 1950). In the Caron process, the ore is first subjected to high temperatures (≈750°C) in a reducing environment followed by leaching of the enriched nickel and cobalt phases with an ammonia-ammonium carbonate solution at ambient conditions to extract both nickel and cobalt as amine complexes (Reid and Barnett, 2002). Nickel and cobalt from the solution are separated by a combination of processes

including, solvent extraction, carbonate precipitation and thermal decomposition (Fittock, 1993). The process is sensitive to ore composition, especially silicate content and is more suitable for limonite ores or blends of limonite and saprolite ores (Dalvi et al., 2004). Since its inception, only five commercial Caron Process operations have been developed, Nicaro and Punta Gorda in Cuba, Surigao in the Philippines, Yabulu in Australia and Tocantins in Brazil and all have since stopped operation. The high energy expenditure for drying and reduction roasting and the low recoveries of nickel (<90%) and cobalt (<80 %) makes the process less economic and lucrative, and its future is most unlikely (Kyle, 2010).

Pressure acid leaching of nickel laterite ores in sulfate medium dates back in 1959 when the first HPAL plant was built at Moa Bay, Cuba (Mayze, 1999). The Moa Bay operation was the first generation of HPAL plants and is still in operation. The second generation of HPAL plants was commissioned in Australia in the late twentieth and early twenty-first century endorsed as a technology that is robust and cost-effective (Moskalyk and Alfantazi, 2002). The capital and operation costs, production capacity and ramp up times were not as projected and the three projects, Bulong, Cawse and Murrin Murrin struggled financially (O'Shea, 2003). Bulong and Cawse were later on closed after running for less than three years, and Murrin Murrin survived the financial crisis and is still operational though it remains vulnerable to nickel price fluctuations (Mudd, 2007).

In HPAL, the ore is leached under extreme temperatures (>245 °C), pressure (>4 MPa) and acidity in titanium lined autoclaves (Kyle, 2010). The extreme conditions allow for fast leaching rates and high extractions of nickel and cobalt of more than 90% (Kyle, 1996, Georgiou and Papangelakis, 1998, Dalvi et al., 2004). The process is sensitive to ore type, best suited for limonite ores and blends of limonite and saprolite ores with a low magnesium content (< 4 %) and aluminium content (Dalvi et al., 2004). High magnesium and aluminium content result in excessive acid consumption. The high temperatures used in HPAL promote hydrolysis precipitation of significant amounts of trivalent ions of Fe, Al and Cr following their dissolution which results in less contaminated leach solutions with regards to the trivalent ions (Carlson and Simons, 1960). Regardless of the high nickel and cobalt dissolution and the lowering of the impurities (Fe, Al and Cr) in PAL, the capital and operating costs are very high. It is believed that the high capital and operational costs of HPAL contributed to the

demise of the second generation HPAL plants in Australia and the shift to atmospheric leaching (Harris et al., 2003). In the past decades, there has been mounting interest on using atmospheric leaching (AL) and heap leaching (HP), which are promoted as more cost-effective alternatives for the processing of nickel laterite ores (McDonald and Whittington, 2008b, McDonald and Whittington, 2008a).

AL also referred to as column and agitation leaching is carried out under atmospheric pressure and temperatures below the boiling point of the slurry which circumvents the need for expensive titanium lined autoclaves and the excessive energy requirements compared to HPAL. AL has been applied commercially at Ravensthorpe nickel project as an adjunct to PAL, a process they termed enhanced pressure acid leaching (EPAL), which is a version of the AMAX acid leach process (Duyvesteyn et al., 1979). EPAL aims at minimising overall acid consumption by processing both limonite ores and saprolite ores. Limonite ores are leached by HPAL and the residual acid from the hydrolysis precipitation of Fe, Al and Cr is used to leach saprolite ore under atmospheric pressure and temperature (White et al., 2006).

Heap leaching although a well-established process in the processing of a heap or bed of low-grade ores under atmospheric pressure and temperature is still in its infancy in the processing of nickel laterite ores. The liquid-solid separation step which follows leaching is eliminated in HP, and its economic viability depends on good bed permeability and stability (Steemson and Smith, 2009). HP is, therefore, less suited for treating limonite ores with a high content of fines and iron which could be detrimental to bed permeability and stability, respectively (Taylor, 2014). Early test work on heap leaching of laterite ores was conducted on Greek laterite ores (Agatzini-Leonardou et al., 2009, Agatzini-Leonardou and Zafiratos, 2004, Agatzini-Leonardou and Dimaki, 1994). The commercialisation of heap leaching was done by Murrin Murrin was it was successfully integrated into the main plant to process what they refer to as scats (Queneau and Chou, 1976). Several other demonstration projects such as the Caldag project in Turkey, Coje project in the Philippines and the GME resources in Australia have been developed (Steemson and Smith, 2009). The major drawbacks of HP are lower nickel and cobalt extractions, higher acid consumption and longer leach cycles compared to both AL and HPAL. For example, 79.4% Ni and 82% Co extractions from leaching Caldag ore for 548 days were obtained (Oxley et al., 2007).

Despite the challenges faced in HPAL, AL and HP processes, hydrometallurgical technology remains the only viable option for processing low-grade nickel laterite ores, especially AL and HP as an adjunct to HPAL. This is evidenced by the launching of several newer HPAL laterite operations, such as the Ravensthorpe, Coral Bay, Goro, Gordes, Ramu, Taganito and Ambatovy (Taylor, 2013, Tsuchida, 2015), after the demise of the second generation of HPAL plants in Australia. Also, the continuing research and development on AL using both sulphuric acid (Büyükakinci and Topkaya, 2009) and nitric acid (Nickel, 2013) shows the indisputable potential of hydrometallurgical processing as the future of laterite processing. Recently, there has been an interest in the development of a valuable by-product, scandium which makes HPAL even more attractive (Mihaylov et al., 2017). The use of AL as an adjunct to HPAL is appealing and arguably the way forward in the nickel industry.

1.3 Statement of the problem

A major weakness of the leaching of nickel laterite ores with sulfuric acid solutions is that the extraction degree of nickel and cobalt and the impurities are comparable (Chang et al., 2008). As a result, the leach solutions produced contain significant amounts of impurities such as iron, aluminium, chromium, magnesium and manganese. The relative concentration of impurities is dependent on the leaching technology used, and the type of ore processed. AL and HP are suited to process ores high in magnesium silicates that are not economically suitable for HPAL (Dalvi et al., 2004, Arroyo and Neudorf, 2001). AL and HP solutions contain higher amounts of Fe, Al, Cr, and Mg than solutions from HPAL and iron is often present as a mixture of ferrous ion and ferric ion in magnesium silicates (Rubisov and Papangelakis, 2000). Unlike ferric ion, ferrous ion is relatively stable in acidic conditions and its removal can only be achieved by oxidative precipitation. The various impurities contained in the sulfate leach solutions must be removed to recover high purity and saleable nickel and cobalt products.

Iron is ubiquitous in nickel laterite leach solutions, and its removal is a priority and usually the first step in the purification process of the acidic solutions. Ferric ion removal by precipitation as ferric oxyhydroxides and oxyhydroxysulfates occurs when process parameters such as pH and temperature are manipulated. The precipitation of

iron occurs simultaneously with that of aluminium and chromium. One major problem in precipitating iron, aluminium and chromium is the loss of nickel and cobalt to the precipitates. The nickel and cobalt losses can be significant and vary among the different iron precipitation processes.

The nickel and cobalt sulfate solutions obtained following iron, aluminium and chromium precipitation still contain impurities mainly manganese, calcium, copper, magnesium and zinc. Various process flowsheets for the purification of the nickel and cobalt sulfate solutions are used in different nickel laterite operations. For example, direct solvent extraction (DSX) used at the Goro nickel project (Mihaylov et al., 2000) and Bulong nickel operation (Donegan, 2006), mixed hydroxide precipitate (MHP) is used at Ravensthorpe and Cawse nickel operations (White et al., 2006) and mixed sulfide precipitation (MSP) at Murrin Murrin operation (Motteram et al., 1996). Clearly, there is no obvious processing route of choice, and the purifying options remain marginal.

It is clear from the above discussion that a need exists for further investigations on the removal of iron and the processing of nickel and cobalt sulfate solutions following iron, aluminium and chromium removal.

1.4 Aim and scope of the study

This study aims to identify and evaluate the factors affecting the precipitation of iron and co-removal of aluminium and chromium and the associated nickel and cobalt losses from synthetic sulfate solutions simulating sulfate solutions of nickel laterite ores. The study is also aimed at exploring an alternative method for processing nickel and cobalt solutions following the removal of iron, aluminium and chromium. This was achieved by implementing the following steps:

- Investigate the effect of various factors on iron precipitation, the co-removal of aluminium and chromium and the associated nickel and cobalt losses. Initially, the likely behaviour of the divalent ions of nickel and cobalt and the trivalent ions of iron, aluminium and chromium in a sulfate system was studied using Visual MINTEQ software (version 3.1). This was followed by the investigations into the correlation of different factors on iron removal

efficiency and the amount of nickel and cobalt losses from synthetic sulfate solutions. The factors investigated were:

(i) The neutralising agents, their effect on iron removal efficiency and the amount of nickel and cobalt losses from synthetic sulfate ternary system [Fe(III)+Ni(II)+Co(II)] and multi-element sulfate solution.

(ii) The effect of the presence of major impurities, aluminium, chromium and magnesium in solution on the level of nickel and cobalt losses during iron precipitation and the nature of the iron precipitates.

(iii) The effect of pH, temperature and concentration of neutralising agent on iron, aluminium and chromium removal and their effect on nickel and cobalt losses.

- Investigate the oxidative precipitation of ferrous ion from acidic sulfate solution, using different oxidising agents. The effect of various factors on the process, the co-removal of aluminium and chromium and the level of nickel and cobalt losses was evaluated. The factors studied include pH, temperature, type of neutralising agent used and ferrous on concentration.
- Explore oxidative precipitation of manganous ion from slightly acidic synthetic sulfate solution using potassium permanganate solution. This was investigated as an alternative process for purifying nickel and cobalt solutions that have composition comparable to the solutions from iron precipitation.

1.5 Significance of the study

Iron precipitation using partial neutralisation is an important integral step of the hydrometallurgical processing of nickel laterite sulfate solutions. It is preferred that at atmospheric conditions, iron is removed as goethite because it has better filtration and washing properties, which lowers nickel and cobalt losses to the precipitate, and it is environmentally stable than jarosites. However, in actual practice, the iron precipitates obtained using either the Vielle Montagne method (V.M.) or the Electrolytic Zinc method (E.Z.) contain significant amounts of amorphous and metastable iron phases that have poor filtration properties and high adsorption capacity for nickel and cobalt and other impurities which can contaminate the environment than goethite. It is fair to

conclude that dilution and reduction of ferric ion in laterite sulfate solutions do not guarantee the removal of iron as goethite, but a large amount of water and the reductants used continue to contribute to the operational cost of the process. Nickel laterite ores are often located in regions where the water quality and supply are not good. In Australia, for example, the nickel laterite deposits are found in the arid regions (Brand et al., 1998), with an inadequate water supply and mainly the hypersaline underground water. The large amounts of jarosite-forming cations such as the monovalent ions of Na and K in hypersaline water promote the formation of jarosite-type compounds (Dutrizac and Jambor, 2000).

This study investigated iron precipitation at high (Chapter 3) and low (Chapter 4) ferric ion concentration in solution during precipitation which provides an insight on the effect of ferric ion concentration and the other impurities on the nature of the precipitates. The finding of this study will give insight in whether dilution using large quantities of water in the E.Z. method is important as envisaged and if the precipitation of goethite in multi-element solution is far from reach due to other factors. This can serve as an economic incentive as it could lead to lower dilutions chosen and therefore reduced water usage and cost.

The study also attempted to remove manganese by oxidative precipitation as an alternative process following iron precipitation. This could pave way to the development of a new process route for nickel and cobalt sulfate solutions, which is more cost effective than the MHP route. A process route including the process could be more cost effective because the process has a potential to produce manganese as a by-product and a manganese precipitate can be used as an oxidising agent for ferrous ion upstream in leaching.

1.6 Thesis structure

This thesis consists of six chapters. Chapter 1 presents a brief overview of the production and processing of nickel laterite ores. It also includes the statement of the problem, aims and the likely significant contributions of the study in the processing of nickel laterite sulfate solutions.

Chapter 2 provides a review of studies relating to the impurities in sulfate leach solutions and their removal from process solutions. An overview of the origin of the

major impurities in nickel laterite sulfate solutions and the iron removal processes as used in zinc and nickel industry is presented in this chapter. Also, the chemistry of iron and the co-precipitation of iron, aluminium and chromium and manganese by precipitation and the associated nickel and cobalt losses were discussed. This chapter also provides an overview of the familiar purification routes used following iron precipitation process and the fundamentals of reactive crystallisation (precipitation).

Chapter 3 gives an extensive investigation of iron, aluminium and chromium removal and nickel and cobalt losses from synthetic nickel laterite solutions. The first part employs Visual MINTEQ (version 3.1) software to investigate the behaviour of Ni, Co, Al, Fe and Cr cations in dilute sulfate systems. The second part is an investigation of the effect of key variables on the impurity removal efficiency and nickel and cobalt losses to the precipitates using synthetic sulfate solutions using full factorial design experiments and one variable at a time approach.

Chapter 4 describes the experimental work on the oxidative precipitation of ferrous ion and its effect on nickel and cobalt losses from synthetic sulfate leach solutions. The effect of key factors like oxidant type, pH, temperature, type of neutralising agent and ferrous ion concentration are investigated using one variable at a time approach. The effect of using multistage oxidative precipitation on nickel and cobalt losses from the solution is also studied.

Chapter 5 is an exploratory study on oxidative precipitation of manganese as an alternative process following partial neutralisation steps to purify the solutions by separating nickel from cobalt and manganese. The effects of oxidant dose, pH, temperature and concentration of manganese in solution are investigated using full factorial design experiments and one variable at a time approach.

Chapter 6 gives a summary of the findings of the study and future work that may be undertaken based on the outcome of this thesis.

References

ARROYO, J. C. & NEUDORF, D. A. 2001. Atmospheric leach process for the recovery of nickel and cobalt from limonite and saprolite ores. Google Patents.

BRAND, N., BUTT, C. & ELIAS, M. 1998. Nickel laterites: classification and features.

BÜYÜKAKINCI, E. & TOPKAYA, Y. A. 2009. Extraction of nickel from lateritic ores at atmospheric pressure with agitation leaching. *Hydrometallurgy,* 97**,** 33-38.

CARLSON, E. & SIMONS, C. 1960. Acid leaching Moa Bay's nickel. *JOM,* 12**,** 206-213.

CARON, M. 1950. Fundamental and practical factors in ammonia leaching of nickel and cobalt ores. *JOM-Journal of the Minerals, Metals and Materials Society,* 2**,** 67-90.

CHANG, Y.-F., ZHAI, X.-J., FU, Y., LI, B.-C. & ZHANG, T.-A. 2008. Sulphuric acid leaching kinetics of pre-reduced laterite ores [J]. *Journal of Molecular Science,* 4**,** 005.

DALVI, A. D., W., G. B. & OSBORNE, R. C. 2004. The Past and the Future of Nickel Laterites. *PDAC 2004 International Convention.*

DEPARTMENT OF MINES, I. R. A. S. 2017. Major commodities resources.

DONEGAN, S. 2006. Direct solvent extraction of nickel at Bulong operations. *Minerals Engineering,* 19**,** 1234-1245.

DUTRIZAC, J. E. & JAMBOR, J. L. 2000. Jarosites and their application in hydrometallurgy. *Reviews in Mineralogy and Geochemistry,* 40**,** 405-452.

DUYVESTEYN, W., WICKER, G. & DOANE, R. An omnivorous process for laterite deposits. International Laterite Symposium, 1979. 553-570.

FITTOCK, J. E. 1993. NICKEL AND COBALT REFINING BY QNI PTY LTD, YABULU, QLD. *Mawby"-AUSIMM Monograph 19 Volume.*

GEORGIOU, D. & PAPANGELAKIS, V. G. 1998. Sulphuric acid pressure leaching of a limonitic laterite: chemistry and kinetics. *Hydrometallurgy,* 49**,** 23-46.

GOONAN, T. G., KUCK, P. H. & SCHNEBELE, E. K. 2017. Mineral Commodity Summaries.

HARRIS, B., MAGEE, J. & VALLS, R. 2003. Beyond PAL: the Chesbar option, AAL. *ALTA Nickel-Cobalt-9, Perth, WA.*

KELLY, T., MATOS, G., WITH BUCKINGHAM, D., DIFRANCESCO, C., PORTER, K., BERRY, C., CRANE, M., GOONAN, T. & SZNOPEK, J. 2014. Historical statistics for mineral and material commodities in the United States. *Data Series.* 2014 Version: Updated annually with the most recent supply-demand statistics ed. Reston, VA.

KUCK, P. H. 2008. Mineral Commodity Summaries *Minerals Yearbook.*

KYLE, J. 1996. Pressure acid leaching of Australian nickel/cobalt laterites. *Nickel,* 96**,** 245-250.

KYLE, J. 2010. Nickel laterite processing technologies – where to next? . *ALTA 2010 Nickel/Cobalt/Copper Conference,*. Perth, Western Australia.

MAYZE, R. An engineering comparison of the three treatment flowsheets in WA nickel laterite projects. Proceedings ALTA Nickel/Cobalt Pressure Leaching & Hydrometallurgy Forum, 1999.

MCDONALD, R. G. & WHITTINGTON, B. I. 2008a. Atmospheric acid leaching of nickel laterites review. Part II. Chloride and bio-technologies. *Hydrometallurgy,* 91**,** 56-69.

MCDONALD, R. G. & WHITTINGTON, B. I. 2008b. Atmospheric acid leaching of nickel laterites review: Part I. Sulphuric acid technologies. *Hydrometallurgy,* 91**,** 35-55.

MCRAE, M. E. 2018. Mineral Commodity Summaries*In:* SURVEY, U. S. G. (ed.).

MIHAYLOV, I., KRAUSE, E., COLTON, D., OKITA, Y., DUTERQUE, J.-P. & PERRAUD, J.-J. 2000. The development of a novel hydrometallurgical process for nickel and cobalt recovery from Goro laterite ore. *CIM bulletin,* 93**,** 124-130.

MIHAYLOV, I., PETERSON, R., SINGHAL, A. & MASSEY, C. 2017. Method for recovering scandium from intermediate products formed in the hydrometallurgical processing of laterite ores. Google Patents.

MOSKALYK, R. R. & ALFANTAZI, A. M. 2002. Nickel laterite processing and electrowinning practice. *Minerals Engineering,* 15**,** 593-605.

MOTTERAM, G., RYAN, M., BEREZOWSKY, R. & RAUDSEPP, R. Murrin-Murrin Nickel/Cobalt Project-Project Development Overview. Nickel and Cobalt Pressure Leaching and Hydrometallurgy Forum, Alta Metallurgical Service, Perth, Western Australia, 1996.

MUDD, G. M. 2007. An analysis of historic production trends in Australian base metal mining. *Ore Geology Reviews,* 32**,** 227-261.

NICKEL, D. 2013. Available: www.directnickel.com [Accessed].

O'SHEA, J. Pressure Acid Leaching of Nickel-Cobalt Laterites: Status and Likely Developments. Proc."ALTA, 2003.

OBER, J. A. 2018. Mineral commodity summaries 2018. US Geological Survey.

OXLEY, A., SIRVANCI, N. & PURKISS, S. 2007. Çaldağ nickel laterite atmospheric heap leach project. *Metalurgija,* 13**,** 5-10.

QUENEAU, P. B. & CHOU, E. C. 1976. High temperature neutralization of laterite leach slurry. Google Patents.

REID, J. & BARNETT, S. Nickel laterite hydrometallurgical processing update. ALTA 2002 Nickel/Cobalt, 2002 Perth. ALTA Metallurgical Services.

RUBISOV, D. H. & PAPANGELAKIS, V. G. 2000. Sulphuric acid pressure leaching of laterites - speciation and prediction of metal solubilities `at temperature'. *Hydrometallurgy,* 58**,** 13-26.

STEEMSON, M. & SMITH, M. The development of nickel laterite heap leach projects. Proceedings of ALTA 2009 Nickel/Cobalt conference, 2009.

TAYLOR, A. 2013. Laterites—Still a Frontier of Nickel Process Development. *TMS2013, San Antonio, Texas, USA***,** 3-7.

TAYLOR, A. Technical and Cost Comparison of Laterite Treatment Processes, Part 1. Proc. 5th ALTA Ni–Co–Cu Conf, 2014.

TSUCHIDA, N. HPAL in past, present and future. Nickel-Cobalt-Copper Conference, 2015 Perth, Australia. ALTA Metallurgical Services

WHITE, D., MILLER, M. & NAPIER, A. 2006. Impurity disposition and control in the Ravensthorpe acid leaching process. *Iron Control Technologies—3rd International Symposium on Iron Control in Hydrometallurgy, Canadian Inst. Min. Metall. & Petroleum.*

ZHU, D.-Q., CUI, Y., HAPUGODA, S., VINING, K. & PAN, J. 2012. Mineralogy and crystal chemistry of a low grade nickel laterite ore. *Transactions of Nonferrous Metals Society of China,* 22**,** 907-916.

CHAPTER 2
REVIEW OF STUDIES ON THE IMPURITIES IN LATERITE SOLUTIONS AND THEIR REMOVAL FROM PROCESS SOLUTIONS

2.1 Introduction

This chapter is a review of studies relating to the purification of multi-element sulfuric acid leach solutions produced during the hydrometallurgical processing of nickel laterite ores. First, a brief overview of nickel laterite ores and the gangue and host minerals is provided. The application of a precipitation process for the removal of iron and manganese from the acidic sulfate solutions is discussed, with particular reference to the successful implementation of iron precipitation in both zinc and nickel laterite industries. The effect of iron and manganese precipitation and the impact of the presence of aluminium, chromium and magnesium and the other minor impurities (non-valuable or target metals) on the purification of nickel and cobalt are also reviewed. The chemistry of iron in solution is addressed in relation to the hydrolysis of ferrous and ferric ion, the oxidation of ferrous ion, and ferric ion precipitation and phase transformations which is the basis for the application and success of the iron precipitation processes. Lastly, the fundamentals of crystallisation and precipitation theory, particularly the thermodynamic and kinetic properties that significantly impact on the precipitation processes are briefly highlighted.

2.2 Nickel laterite ores and impurities in sulfate leach solutions

2.2.1 Nickel laterite ores

Nickel laterite ores are a product of the weathering of ultramafic rocks rich in ferromagnesian minerals with a primary nickel content of about 0.2 to 0.4% (Golightly, 1981). Typically, three main types of ores are distinguished in nickel laterite deposits: limonite, nontronite and saprolite, and their distribution in an idealised cross-section of a laterite profile is illustrated in Figure 2.1. The ore type classification is based on the relative concentrations of cobalt, iron, magnesia, nickel and silica in the ores as shown in Table 2.1 (Elias, 2002, Dalvi et al., 2004, Wedderburn, 2009).

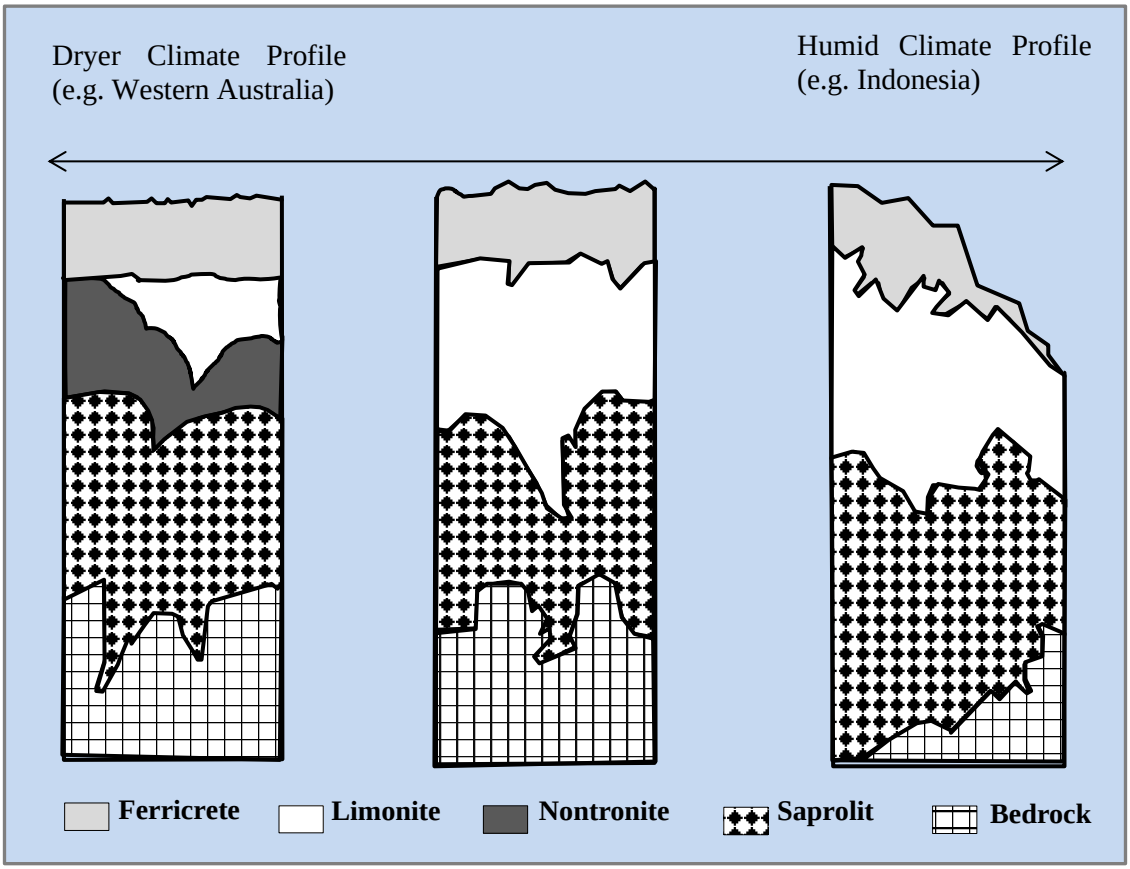

Figure 2.1: Typical nickel laterite profiles for dry and humid climates adapted from Dalvi et al. (2004)

Table 2.1: Typical chemical composition of nickel laterite ores in a profile (Elias, 2002, Dalvi et al., 2004, Wedderburn, 2009)

	Approximate composition (weight %)				
Ore type	Ni	Co	Fe	MgO	SiO2
Limonite	0.8-1.5	0.1-0.2	>40	<5	0-10
Nontronite	1.5-2.0	0.02-0.1	10-30	5-15	10-30
Saprolite	1.5-3.0	0.02-0.1	10-25	15-35	30-50

Limonite ores which occur at the top of the laterite profile are enriched with iron and to a certain extent aluminium, chromium and manganese, but depleted in magnesium and silicon content due to strong leaching. Iron is mainly present as goethite (de Carvalho-e-Silva et al., 2002, Carvalho-e-Silva et al., 2003, Swamy et al., 2003), with some few deposits having haematite as the major iron phase, such as the Greek laterites (Agatzini-Leonardou et al., 2009). Other elements, both impurities and the valuable metals are purported to be associated with the goethite mineral lattice (Georgiou and Papangelakis, 1998). Aluminium and chromium have been found in a

limonite ore as oxides, mainly gibbsite and chromite and also substituting for each other in the oxides to form a minor phase of alumino-chromite (Georgiou and Papangelakis, 1998). Manganese minerals when present in ore deposits are also found intergrown with goethite and concentrated in the interface between the limonite and successive layers (Elias et al., 1981). Most of the nickel in the ores is hosted by goethite (de Carvalho-e-Silva et al., 2002, Carvalho-e-Silva et al., 2003, Swamy et al., 2003), but high nickel and cobalt concentrations are also found in the manganese minerals. The deposits found at Bulong near Kalgoorlie Western Australia had up to 12% Ni and 8.5% Co content in manganese minerals and are a very good example (Elias et al., 1981). A study by Watling et al. (2011) on determining the mineral phases in 50 nickel laterite ores, also confirmed highest nickel and cobalt concentrations in the manganese oxide minerals which constituted less than 10 wt.% of each ore tested. Examples of oxide type deposits are those from Cawse and Ravensthorpe operations in Australia, Goro in New Caledonia, Moa Bay in Cuba, and Ramu River in Papua New Guinea (Brand et al., 1998).

Nontronite ores are found beneath the limonite ores and are dominated by iron-rich and iron-magnesium-rich smectite silicate clay minerals. These ores are prevalent in dry regions where groundwater movement is restricted, limiting silica leaching. The silica combines with iron and aluminium to form the smectite group of minerals, consisting mainly of nontronite and saponite with a mean nickel content of about 1.5 to 2.0 wt.% (Brand et al., 1998). Other minerals such as chromite, magnetite and goethite may be present especially towards the top of the nontronite ore zone (Elias et al., 1981). In saponite and serpentine minerals in nontronite ores, iron is not only in the ferric oxidation state, but a significant amount is present in the ferrous oxidation state, found substituting for magnesium in lattice structures (Rubisov and Papangelakis, 2000, Hernandez et al., 2014). The Australian deposits in Murrin Murrin (Motteram et al., 1996) and Bulong (Elias et al., 1981) are clay-dominated and can be classified as nontronite ores.

Saprolite ores are at the bottom of the laterite profile and consist largely of hydrous magnesium silicates, which mainly consist of serpentines, chlorite, sepiolite, talc, chlorite and garnierite (Brand et al., 1998). At the top of the saprolite zone are minor smectite and secondary silica phases such as opaline and chalcedonic silica formed from excess silica from the nontronite ore zone (Elias et al., 1981). Nickel is enriched

in the hydrous magnesium silicates, and the highest nickel concentrations can be found in saprolite ores. The average nickel concentration in most of the silicate minerals is greater than 1.5 wt.%, especially in amorphous garnierite minerals (Brand et al., 1998). Saprolite deposits from New Caledonia are hydrous magnesium silicates (Golightly, 1981).

Although the mineralogical composition of nickel laterite ores vary considerably (Zhu et al., 2012), two major types of host minerals for nickel and cobalt in almost all nickel deposits have been identified: the oxides and silicates (Berger et al., 2011, Butt and Cluzel, 2013, Brand et al., 1998). Table 2.2 provides a list of minerals and a few Ni and Co analogues of the silicate minerals often found in nickel laterite ores. From the chemical formulae of the minerals and the mineralogy of laterite ores, it is clear that all laterite ores contain iron, magnesium, silicon, manganese aluminium and chromium as impurities. Nickel and cobalt in the ores are not present as discrete phases but in solid solution with the impurity elements that exist in a variety of mineral phases. Ni is mainly contained in iron oxides and silicates (Bernstein and Waychunas, 1987, Reeder et al., 1999, Greegor et al., 1997, Swamy et al., 2003) and cobalt in manganese minerals (Brand et al., 1998, Manceau et al., 2000, Watling et al., 2011). For metals that occur in solid-solution, beneficiation and upgrading are difficult and inherently, hydrometallurgical processing is the only viable option for meaningful nickel and cobalt extraction from the low-grade ores.

Table 2.2: A list of some of the minerals often found in nickel laterite deposits.

Oxides (Brand et al., 1998, Butt and Cluzel, 2013, Elias et al., 1981)		**Silicates** (Brand et al., 1998, Butt and Cluzel, 2013)	
Mineral	**Formula**	**Mineral**	**Formula**
Goethite	α-FeOOH	Nontronite	$Na_{0.3}Fe_2^{3+}Si_3AlO_{10}(OH)_2•n(H_2O)$
Haematite	α-Fe_2O_3	Saponite	$Ca_{0.1}Na_{0.1}Mg_{2.25}Fe^{2+}_{0.75}Si_3AlO_{10}(OH)_2•4(H_2O)$
Magnetite	Fe_3O_4	Lizardite	$Mg_3Si_2O_5(OH)_4$
Lepidocrocite	γ-FeO(OH)	Ni lizardite	$(Mg,Ni)_3Si_2O_5(OH)_4$
Asbolane	$(Co^{3+},Ni^{2+})_{1-y}(MnO_2)_{2-x}(OH)_{2-y+2x}•n(H_2O)$	Cronstedtite	$[(Fe_8^{2+}Fe_4^{3+})(Si_4Fe_4^{3+})O_{20}(OH)_{16}]$,
Lithiophorite	$(Al,Li)MnO_2(OH)_2$	Nimite	$(Ni,Mg,Fe^{2+})_5Al(Si_3Al)O_{10}(OH)_8$
Chalcophanite	$(Zn,Fe^{2+},Mn^{2+})Mn_3^{4+}O_7•3(H_2O)$	Pecoraite	$Ni_3Si_2O_5(OH)_4$
Cryptomelane	$K(Mn^{4+},Mn^{2+})_8O_{16}$	Antigorite	$(Mg,Fe^{2+})_3Si_2O_5(OH)_4$
Todorokite	$(Na,Ca,K)_2Mn_4^{4+}Mn_2^{3+}O_{12}•3(H_2O)$	Sepiolite	$Ni_3Si_2O_5(OH)_4$
Ernienickelite	$NiMn_3^{4+}O_7•3(H_2O)$	Garnierite	Not available
Gibbsite	$Al(OH)_3$	Falcondoite	$(Ni,Mg)_4Si_6AO_{15}(OH)_2.6H_2O$
Boehmite	AlO(OH)	Willemseite	$(Ni,Mg)_3Si_4O_{10}(OH)_4$
Chromite	$Fe^{2+}Cr_2O_4$	Brindleyite	$(Ni,Mg)_3(Si,Al)_2O_5(OH)_2$

Note: The compounds are not neutral as they are variable in composition as substituted compounds in solid solution and the cation charge represent the oxidation state of the element present in the mineral.

2.2.2 Impurities in sulfate leach solutions

In hydrometallurgical processing, nickel laterite ores are leached in strong sulfuric acid solutions by three leaching techniques, one at high temperatures and pressures (HPAL) and two under atmospheric conditions (HL and AL). The extent of nickel and cobalt extraction from the ores depends on the degree of decomposition of the host mineral phases. Nickel and cobalt host minerals are highly soluble in strong sulfuric acid solutions irrespective of the leaching technique, with dissolution of nickel and cobalt of more than 90% achieved in nickel operations (Motteram et al., 1996, Önal and Topkaya, 2014, Carlson and Simons, 1960, White et al., 2006) and laboratory tests (Georgiou and Papangelakis, 1998, Önal and Topkaya, 2014). However, there is no selectivity for nickel and cobalt over the impurities during leaching. Sherrit (Motteram et al., 1996) conducted HPAL testwork on composite ore for Murrin Murrin and obtained metal extractions of 95% Ni and 93% Co at 250 °C and acid addition of 400 kg/t, within 90 mins, but manganese and magnesium extractions were also high at 91% and 94%, respectively. Iron, aluminium and chromium extractions were low at less than 4%, 12% and 5%, respectively. Önal and Topkaya (2014) obtained extractions of 94% Ni and Co, 84% Mg, 82% Mn, 1.7% Fe, 60% Al and 1.9% Cr within 60 mins during HPAL leaching of Caldag limonite ore at optimum conditions of 250 °C and 325 kg/t acid addition. Furthermore, agitation leaching of nontronite and limonite ores from Gordes by Büyükakinci and Topkaya (2009) showed that 99% Ni, 65% Co, 88% Fe and 51% Cr could be extracted from nontronite ore and 93% Ni, 75% Co, 81% Fe and 40% Cr from limonite ore using 2.5 M H_2SO_4 at 95 °C within 24 hours. The leach solution obtained from nontronite ore processing contained 26 g/L Fe, whereas that of the limonite ore contained 45 g/L Fe. Table 2.3 gives the elemental composition of the ores and the composition of the sulfate solutions obtained from operations using the three common leaching techniques, AL, HL and HPAL including the studies discussed above.

The concentration of Fe, Al and Cr are much lower in HPAL than AL or HL solutions because ferric ion is largely precipitated together with a significant portion of the trivalent aluminium and chromium at the high temperatures used in HPAL. AL and HL sulfate solutions, however, have higher concentrations of Fe, Al and Cr because the milder temperatures used do not enhance the subsequent precipitation of the

trivalent ions of Fe, Al and Cr following their dissolution. Often more than 95% of the ore is impurities. Thus, regardless of the selectivity induced by operating at extremely high temperatures in HPAL, the leach solution still contains a significant amount of Fe, Al and Cr together with the other impurities, manganese and trace amounts of copper and zinc. The removal of the impurities is always a challenge in nickel and cobalt purification of the sulfate laterite leach solutions. The trivalent ions of Fe, Al and Cr, are removed first using iron precipitation processes, leaving manganese as the major impurity of concern which is separated from nickel and cobalt solutions using various processes which vary from operation to operation.

2.3 Iron removal by precipitation from acidic sulfate leach solutions

Iron control by precipitation is a preferred and widely used process in processing hydrometallurgical sulfate solutions. The nature and composition of the iron phases formed depend on the kinetics of the precipitation process (nucleation and crystal growth). The driving force of the precipitation process is the supersaturation level which can be manipulated by changing process parameters such as solution pH and temperature (Claassen and Sandenbergh, 2007). The pH and temperature influence the kinetics of the precipitation process and consequently the nature and composition of iron phases. Figure 2.2 shows the relationship between the major equilibrium iron phases formed from ferric sulfate solution (0.5 M) and the process pH and temperature as determined in a study by Babcan (1971). From Figure 2.2, precipitation will occur at lower pH values when the temperature is increased.

Table 2.3: A Comparison of the elemental ore composition and the resultant leach solution composition

	Ore elemental Composition (wt. %)							Processing Technique	Solution Composition (g/L)							
	Ni	Co	Fe	Mn	Mg	Al	Cr		Ni	Co	Fe	Fe(II)	Mn	Mg	Al	Cr
Caldag[1]	1.215	0.078	32.70	0.349	1.62	1.66	1.01	HPAL	4.564	0.294	2.231	NA	1.150	5.460	3.296	0.0648
Gördes[2] (L)	1.28	0.083	29.0	0.46	1.36	3.09	1.36	AL	2.38	0.12	45.48	NA	NA	NA	NA	NA
(N)	1.20	0.044	15.95	0.26	4.17	2.21	0.68	AL	2.30	0.06	25.92	NA	NA	NA	NA	NA
Moa Bay[3]	1.35	0.146	47.5	0.76	1.00	4.5	2.01	HPAL	4.3	0.46	0.58	NA	1.4	2.0	1.7	0.22
Murrin Murrin[4]	1.24	0.09	21.7	0.4	4.0	2.5	0.88	HPAL	3.3	0.18	2.0	NA	0.7	7.5	1.5	0.1
Ravensthorpe[5] (L)	2.17	0.075	27.2	0.40	4.50	1.60	NA	HPAL	11.8	0.41	2.2	1.8	2.2	21	0.055	0.020
(S)	1.40	0.031	11.7	0.23	13.3	0.6	NA	EPAL	13.4	0.48	3.7	2.7	2.5	47	0.56	0.063

Note: NA refers to not available, EPAL is a combination of AL and HPAL, L is limonite, N is nontronite and S is saprolite ore and superscript 1,2,3,4,5 refer to the authors: Önal and Topkaya (2014), Büyükakinci and Topkaya (2009), Carlson and Simons (1960), Motteram et al., 1996 and White et al. (2006), respectively.

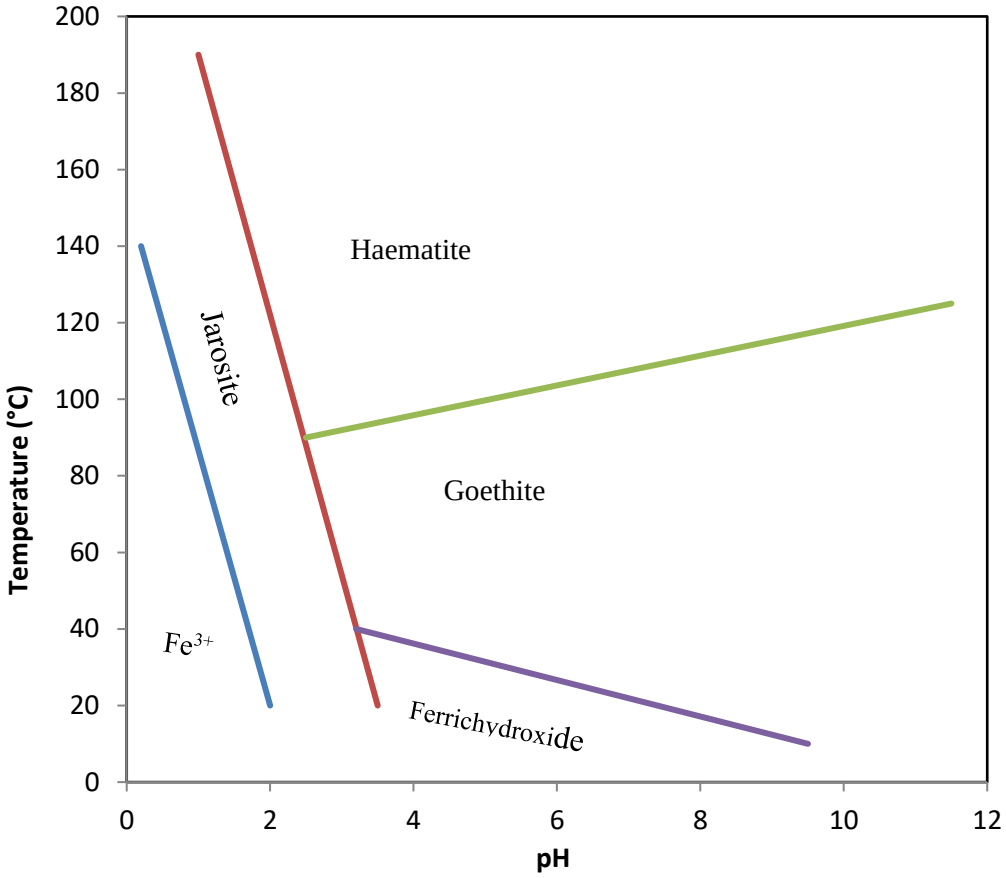

Figure 2.2: Stability regions of the various iron phases usually formed in a sulfate matrix adapted from Babcan (1971)

In industrial solutions containing large amounts of iron, the iron phases shown in Figure 2.2 are not always present in the iron residues, especially when operating in the stability region of goethite (Claassen and Sandenbergh, 2007). The metastable phases ferrihydrite (Jambor and Dutrizac, 1998, Loan et al., 2002) and schwertmannite are usually formed under these conditions instead of goethite (Claassen et al., 2002, Wang et al., 2013, Claassen and Sandenbergh, 2007). Figure 2.3 shows the relationship between the metastable iron phases formed from ferric sulfate solution (≈0.18 M) and the process pH and temperature as determined in a study by Claassen and Sandenbergh (2007). The formation of schwertmannite is favoured at lower pH values, and ferrihydrite formation is preferred in less acidic solutions. The metastable phases tend to transform into more stable and crystalline phases goethite and haematite over time (Blesa and Matijević, 1989, Cornell and Schwertmann, 2003). For example, if working at pH 2 and 65 °C, schwertmannite is mainly precipitated, and then over time, it converts to stable goethite (Figure 2.2).

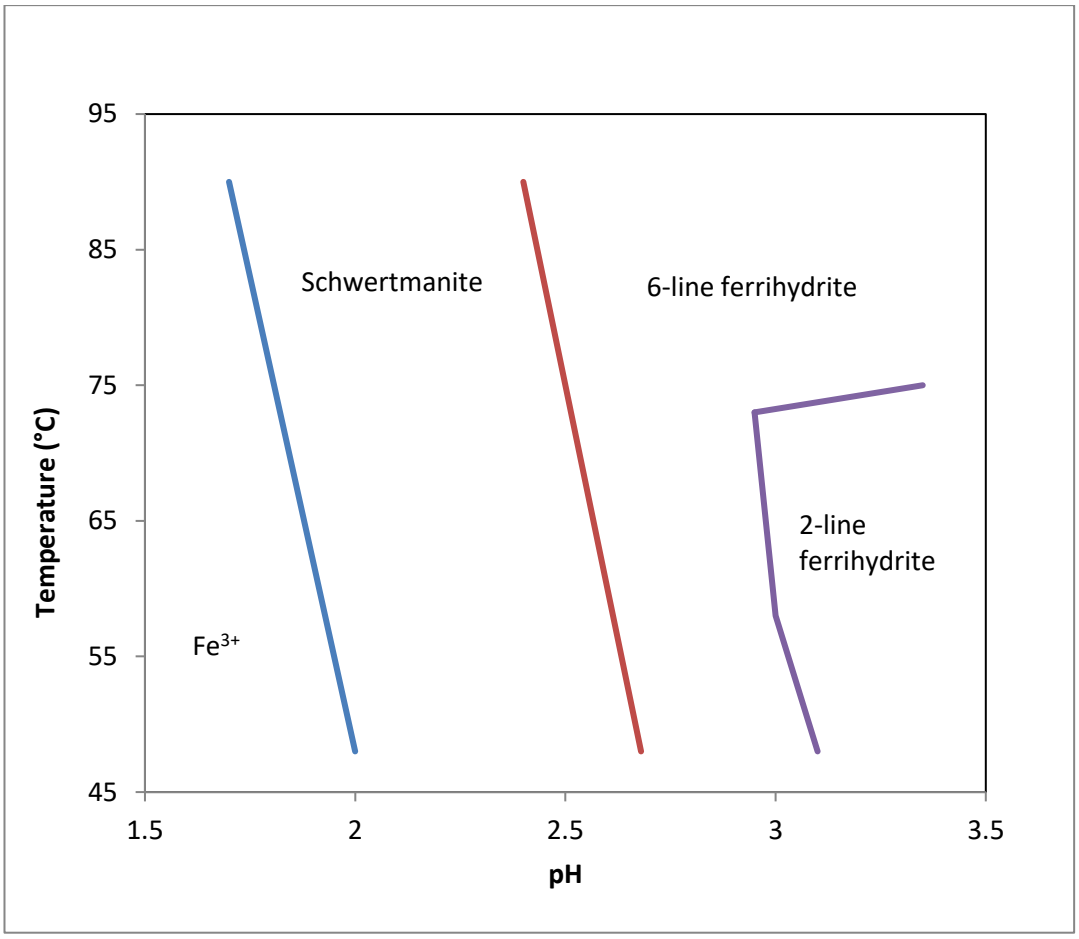

Figure 2.3: Metastability diagram for ferric ion hydrolysis from ferric sulfate solution, adapted from Claassen and Sandenbergh (2007)

Iron control in zinc leaching circuits has led to the development of three popular iron precipitation processes, the Goethite, Jarosite and Haematite and also the less popular Para-Goethite and Zincor Processes, with pH controlled by neutralisation. The names of the three major iron precipitation processes allude to the iron phases expected to form under the given process conditions. Figure 2.4 is a schematic diagram of the three major iron precipitation processes used in iron control mainly in the zinc and nickel laterite industry.

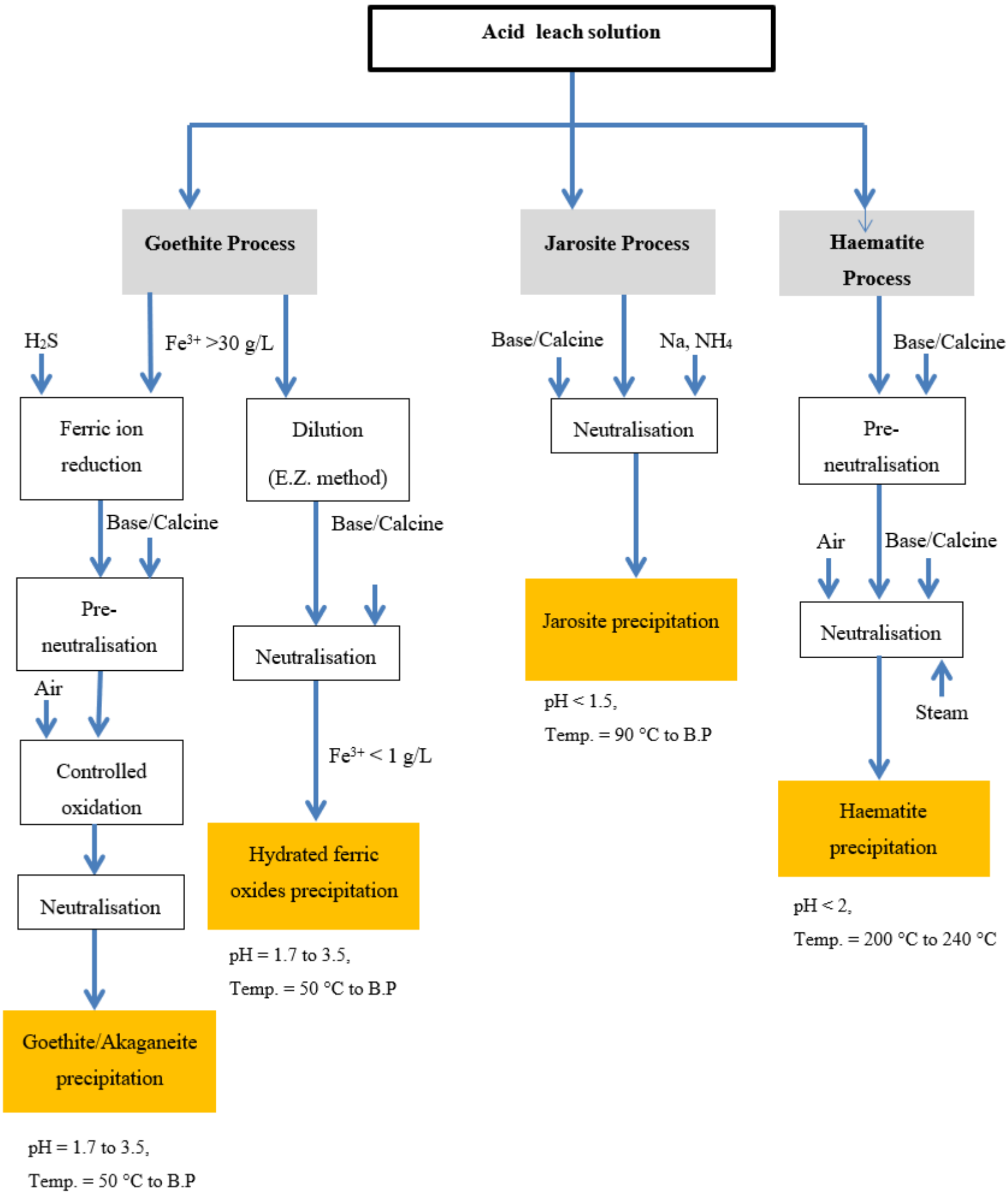

Figure 2.4: A Schematic representation of the major iron precipitation processes adapted from Allan et al. (1970), Gordon and Pickering (1975), Davey and Scott (1976) and Dutrizac (1987).

2.3.1 Goethite (FeOOH) Process

The Goethite Process was developed in the 1960s to process zinc sulfate solutions by the Ballen Plant, Vielle Montagne S.A., Belgium and the Electrolytic Zinc Company (Gupta and Mukherjee, 1990). There are two methods used (Figure 2.4) in the Goethite Process, Vielle Montagne (V.M. method) and the Electrolytic Zinc (E.Z. method) to precipitate goethite. The control of ferric ion concentration in the solution to less than 2 g/L is crucial during goethite precipitation (Dutrizac, 1987, Davey and Scott, 1976). In the V.M. method, all in the hot leach solution is first reduced to ferrous ion followed by slow-controlled oxidation of ferrous to ferric ion by either oxygen or air (Dutrizac, 1987, Allan et al., 1970) at pH 1.7 to 3.5 and 50 °C to 90 °C to precipitate goethite as shown in Equation 2.1 (Davey and Scott, 1976). In the E.Z. method, the highly concentrated ferric ion solution is diluted in a precipitation vessel, maintaining a ferric ion concentration of less than 1 g/L and solution pH of 1.7 to 3.5 by adding a neutralising agent to precipitate goethite according to Equation 2.2 (Dutrizac, 1987). Two more processes, the Para-goethite and the Zincor that follow the same route as the E.Z. method but in a continuous mode emerged in the 1990s and were first implemented at the Enirisorse Porto Vesme Plant (Cubeddu et al., 1996) and the Zinc Corporation of South Africa (Meyer et al., 1996), respectively. The iron residues in the Para-goethite and the Zincor Process were initially identified as amorphous iron phases, but it was realised later on that the residues were mainly the poorly-ordered nanoscale minerals ferrihydrite and schwertmannite (Loan et al., 2006, Claassen et al., 2002). The residues from the Goethite Process in some studies were found to be a mixture of goethite and other iron oxyhydroxides minerals (Davey and Scott, 1976, Wang et al., 2013).

The goethite residues are compact and relatively stable, which is important for process economics taking into account stringent environmental regulations on waste disposal (Torfs and Vliegen, 1996).

V.M. method

$$4FeSO_{4\,(aq)} + 4MgO_{(aq)} + O_{2\,(g)} + 2H_2O_{(l)} \rightarrow 4FeOOH_{(s)} + 4MgSO_{4\,(aq)} \quad 2.1$$

E.Z. method

$$2Fe_2(SO_4)_{3\,(aq)} + 6MgO_{\,(aq)} + 2H_2O_{\,(l)} \rightarrow 4FeOOH_{\,(s)} + 6MgSO_{4\,(aq)} \quad 2.2$$

2.3.2 Jarosite ($MFe_3(OH)_6(SO_4)_2$) Process

The Jarosite Process was developed around the same time as the Goethite Process in the 1960s by the joint effort by three independent companies: Electrolytic Zinc Company of Australasia Ltd, Norske Zinkkompani and Asturiana de Zinc (Dutrizac and Jambor, 2000, Tamargo et al., 1996). It was the first iron removal process in the zinc industry that enabled the production of easily filterable iron residues on a commercial scale and is the most widely used. The Jarosite Process removes high ferric ion and aluminium concentrations in the leach solutions as jarosite and alunite respectively at 90 °C to 100 °C and pH of 1.5 to 1.8 (Dutrizac, 1982, Dutrizac and Jambor, 2000, Dutrizac, 1983). Jarosite formation requires the presence of jarosite-forming cations such as Na^+, K^+, NH_4^+, H_3O^+ and Pb^{2+} and the generalised jarosite precipitation reaction is given by Equation 2.3 where M represents the jarosite-forming cation.

$$3Fe_2(SO_4)_{3\,(aq)} + M_2SO_{4\,(aq)} + 12H_2O_{\,(l)} \rightarrow 2MFe_3(OH)_6(SO_4)_{2\,(s)} + 6H_2SO_{4\,(aq)} \quad 2.3$$

Jarosite precipitation is self-seeding, that is once the jarosite starts to form in the vessel, the particles act as seeds suppressing homogeneous nucleation in the system, and if well suspended by agitation, it enhances the rate of formation and crystallinity of jarosite precipitates (White and Gillaspie, 2015, Gupta and Mukherjee, 1990, Dutrizac, 1999). Any jarosite compound can efficiently act as seeding material for the synthesis of the other jarosite types (Dutrizac, 1999). The Jarosite Process was the most widely used iron removal process in the zinc industry and played a major role in the removal of certain impurities such as fluoride, germanium, antimony and arsenic (Tamargo et al., 1996).

The capital and operational costs are reasonably lower for the Jarosite Process compared to the Goethite and Haematite Processes (Torfs and Vliegen, 1996). However, jarosites are voluminous and are not environmentally stable with high specific volume and permeability coefficients ($\approx 10^{-6}$ m/s) compared to goethite ($\approx 10^{-9}$ m/s) (Torfs and Vliegen, 1996). In wet regions, the heavy metals that can be incorporated during jarosite precipitation can be easily leached thus making further

disposal management practices a necessity (Rosato and Agnew, 1996). For example, the Jarofix process was invented by the Canadian Electrolytic Zinc (CEZinc) company to be used in conjunction with the Jarosite Process to form more stable compounds. In the Jarofix process, jarosite compounds are washed and mixed with an appropriate quantity of cement to stabilise the residue so that it meets the environmental requirements for disposal. The need for secondary processing of the jarosite residue prior to the disposal of residues makes the cost of the Jarosite Process comparable to that of the Goethite Process.

2.3.3 Haematite (Fe_2O_3) Process

In the 1970s, Dowa Mining Company developed the Haematite process for the Akita Zinc Company, Iijima (Onozaki et al., 1986). A sulfide source was used during leaching at mild temperatures to produce a leach solution high in ferrous ion followed by heating of the solution to temperatures more than 200 °C in pressurised autoclaves where simultaneous oxidation and hydrolysis precipitation of haematite occurs (Cheng et al., 2003). In the nickel laterite industry, limonite ores are leached in pressurised autoclaves at high temperatures, and subsequent hydrolysis to haematite takes place (Chou et al., 1977). The composition of the product formed is dependent on the acidity and temperature of the system (Tozawa and Sasaki, 1986, Cheng et al., 2003, Papangelakis et al., 1994). At high acidity, sulfate concentration and temperature (more than 280 °C) the formation of basic ferric sulfate (Equation 2.4) is favoured, whereas haematite formation (Equation 2.5) is favoured at low acidity (Chou et al., 1977, Cheng et al., 2003).

$$Fe_2(SO_4)_{3\,(aq)} + 2H_2O_{\,(l)} \rightarrow 2FeSO_4OH_{\,(s)} + H_2SO_{4\,(aq)} \quad 2.4$$

$$Fe_2(SO_4)_{3\,(aq)} + 3H_2O_{\,(l)} \rightarrow Fe_2O_{3\,(s)} + 3H_2SO_{4\,(aq)} \quad 2.5$$

The haematite residue is chemically stable, low in volume with the highest iron content per mass of residue produced and can be used as raw material for the ceramic and cement industry because of the high iron content (Papangelakis et al., 1994, Rosato and Agnew, 1996). The capital cost and operational costs are extremely high due to the use of the specialised titanium autoclaves and this is to a certain extent the reason for the demise of most laterite operations, especially the second-generation plants of HPAL in Western Australia.

Iron precipitation as a mixture of easily filterable iron residues can be carried out at the Goethite Process conditions without necessarily controlling and maintaining the ferric ion concentration at below 2 g/L (Köse and Topkaya, 2011, Claassen and Sandenbergh, 2007). A dilute neutralising agent is added in a controlled manner to the iron-rich solution resulting in a gradual and controlled pH change to the desired value to control supersaturation of the trivalent ions of iron, aluminium and chromium and allow for the precipitation of ferric ion as easily filterable residue. Although the iron residues from iron precipitation processes at the Goethite Process conditions usually have good filterability, the uptake of nickel and cobalt can be quite high in the poorly ordered iron phases (Davey and Scott, 1976).

2.4 Chemistry of iron in precipitation

The chemistry of iron in aqueous systems involves the ferrous ion [Fe(II)] and ferric ion [Fe(III)] oxidation states which are present in varying amounts in ores and concentrates of valuable metals such as nickel and zinc. Iron is present in significant amounts in all types of nickel laterite ores, chiefly as goethite which assumes the presence of iron as Fe(III). The presence of Fe(II) in nickel laterite ores is generally associated with saprolite ores where ferrous ion is found substituting for magnesium in the serpentine (Rubisov and Papangelakis, 2000, Hernandez et al., 2014) and ores with relatively low manganese content (White et al., 2006). However, there are also a few studies were the presence of ferrous ion in solutions is reported during high pressure acid leaching of limonite ores (White et al., 2006, Loveday, 2008). Iron precipitation is an integral step in the purification of acidic laterite sulfate solutions, where ferric ion is removed from the acidic solution by hydrolysis precipitation. On the contrary, ferrous ion cannot be precipitated at the low acidities necessary for acceptable nickel losses to residues unless it is oxidised to ferric ion leading to precipitation of ferric oxyhydroxides. Thus, the removal of iron from acidic sulfate solutions of laterite ores by precipitation depends on the chemistry of the ferrous ion and ferric ion, that is but not limited to the oxidation of Fe(II) to Fe(III) and the hydrolysis precipitation of ferric ion.

2.4.1 Ferrous ion oxidation

The oxidation of ferrous ion is essential in controlling iron in acidic leach sulfate solutions of nickel laterites by precipitation, with particular reference to its application in the V.M. method and secondary neutralisation stage. Ferrous ion is relatively stable in acidic solutions, and its removal in the acidic medium can only be achieved through first oxidising to ferric ion followed by ferric ion hydrolysis precipitation. The oxidation of ferrous ion can proceed homogeneously in solution and heterogeneously on iron oxyhydroxides or other solid particulates present or formed in solution. Homogeneous oxidation is prevalent in systems were ferrous ion concentrations are very low such as in most natural waters and very acidic solutions. In the processing of hydrometallurgical solutions were ferrous ion concentrations are often high and solids are easily formed, both heterogeneous and homogeneous oxidation are responsible for the depletion of ferrous ion from solution. In industrial systems, air and oxygen are mostly used as oxidants (Davey and Scott, 1976, White et al., 2006, Chang et al., 2010), but the use of hydrogen peroxide is mentioned in Bulong nickel operation (Mayze, 1999, O'Callaghan, 2003) and in a number of studies using the V.M method (Davey and Scott, 1976, Yue et al., 2016).

2.4.1.1 Ferrous ion oxidation with oxygen

Ferrous ion oxidation in acidic environments is not favourable and the rate of oxidation using oxygen proceeds slowly (Stumm and Lee, 1961, Stumm and Morgan, 1996). This could explain the use of less acidic pH values in V.M method (Section 2.3.1) and secondary neutralisation stage despite unacceptable high nickel and cobalt losses at the conditions. The rate at which ferrous ion oxidation proceeds depends on several parameters such as pH, temperature, concentration of oxygen and ferrous ion, the presence of solid material, cations especially, Cu(II)and Mn(II) (Stumm and Lee, 1961, Cher and Davidson, 1955), anions (Tamura et al., 1976a) and micro-organisms such Thiobacillus ferroxidans (Pesic et al., 1989). Different rate laws have been proposed by researchers relating the kinetics of ferrous ion oxidation with air to the various process parameters.

An early study by McBain (1900) investigated the kinetics of ferrous ion oxidation using oxygen in acidic solution, pH less than 2 and reported no dependence on pH but a second order relationship with respect to the concentration of ferrous ion and

first-order dependence on the partial pressure of oxygen. The rate law is shown in Equation 2.6:

$$\frac{-\,d[Fe^{2+}]}{dt} = k\,[Fe^{2+}]^2 P_{O_2} \qquad 2.6$$

where [ ] refers to the concentration (M) of the given species, k is the rate constant ($M^{-1}s^{-1}atm^{-1}$), p is partial pressure (atm), and t is time.

The rate law was later confirmed in sulfate, nitrate and perchlorate solutions by several other researchers (Lamb and Elder, 1931, Sung and Morgan, 1980, Stumm and Lee, 1961). However, under the same acidic conditions in a biotic system, using Thiobacillus ferroxidans, Pesic et al. (1989) established that the reaction was slightly faster depending on the concentration of the micro-organisms.

In less acidic conditions (2< pH < 5), the reaction is more rapid, begins to show dependence on pH and the reaction order changes with respect to hydroxide ions and ferrous ion concentrations with the rate generalised as in Equation 2.7. There are various modified versions of the equation in this pH range as the rate laws vary amongst solutions especially acid mine drainage (Lowson, 1982).

$$\frac{-\,d[Fe^{2+}]}{dt} = k\,[Fe^{2+}][OH^-] P_{O_2} \qquad 2.7$$

In near neutral solutions, pH range of 5 to 8, the reaction rate is much faster and for every unit increase in pH, the rate increases by two orders of magnitude leading to the rate law described by Equation 2.8 (Stumm and Lee, 1961):

$$\frac{-\,d[Fe^{2+}]}{dt} = k\,[Fe^{2+}][OH^-]^2 P_{O_2} \qquad 2.8$$

A hundred-fold increase in the rate of oxidation for every unit pH increment and about 10-fold increase for an increment of 15 °C in alkaline conditions was reported by Stumm and Lee (1961). Since the pH was measured at solution temperature, the temperature dependence could be due to variation in hydroxyl ion activity with the temperature at any given pH. The rate law reported by Stumm and Lee (1961) was later confirmed by Sung and Morgan (1980) using buffered ferrous ion solutions in sodium chlorate, chloride and sulfate media at pH values less than 7.

The strong dependence of oxidation on pH is accredited to ferrous ion speciation, which changes with pH (King, 1998, Stumm and Sulzberger, 1992). In very acidic pH

values less than 3, Fe(II) is unhydrolysed (Davison and Seed, 1983), but as the acidity decreases (5 < pH < 9), Fe(II) is readily hydrolysed (Millero, 1985). In hydrolysed form, the electron density shifts towards the centre of Fe(II) and the species tend to be stronger reductants than the unhydrolysed Fe(II) (Luther, 1990). Thus, an increase in the rate of oxidation is expected when solution pH increases. Additionally, in industrial systems where different acids are used, such as in the leaching of nickel laterite ores, the conjugate base ligands of the acids also react primarily with Fe(II) to give ferrous ion species of the nature FeA^{2-n} according to Equation 2.9 and these species are involved in the oxidation process (Tamura et al., 1976a).

$$Fe^{2+} + A^{n-} \longrightarrow FeA^{(2-n)} \qquad 2.9$$

where A^- is an anion such as OH^-, PO_4^{3-}, SO_4^{2-}, CI^- and FeA^{2-n} is the ferrous-anion complex.

Ferrous ion oxidation becomes the sum of the parallel oxidation reactions of FeA^{2-n} species. The effect of anions including sulfate, nitrate, chloride and carbonate on the oxidation of ferrous ion in natural and synthetic waters has been investigated by several researchers (Tamura et al., 1976a, Davison and Seed, 1983, Millero et al., 1987, Millero, 1985, Sung and Morgan, 1980). The anions with a high complexing affinity for Fe(III) give higher rates of Fe(II) oxidation (Huffman and Davidson, 1956). The rate constant for ferrous ion oxidation of the FeA^{2-n} species is reported to decrease in the order $OH^- > PO_4^{3-} > F^- > ClO_4^- > NO_3^- > Cl^- > H_3SiO_4^- > Br^- > I^- > SO_4^{2-}$ (Tamura et al., 1976a). The different rate constants could be due to the varying competitiveness of the FeA^{2-n} and $Fe(OH)^+$ species for the reactive hydrolysed form of oxygen, O_2OH^- (Equation 2.10).

$$O_2 + OH^- \rightarrow O_2OH^- \qquad 2.10$$

The oxidation is independent of Fe(III) concentration in solution (Cher and Davidson, 1955). However, ferric oxyhydroxides catalyse the Fe(II) oxidation in less acidic to neutral solutions (Tamura et al., 1976b, Tüfekci and Sarikaya, 1996, Jones et al., 2014, Park and Dempsey, 2005). The addition of ferric oxyhydroxide as seeding material and its presence as a precipitation product induces heterogeneous oxidation that occurs parallel to homogeneous oxidation in the solution thereby transforming the rate equation to that given in Equation 2.11:

$$\frac{-d[Fe^{2+}]}{dt} = k\,[Fe^{2+}] + k\,[Fe^{2+}]\{k'\,[\equiv Fe^{3+}]\} \quad 2.11$$

where k is the rate constant for homogeneous oxidation, k′ is the rate constant for heterogeneous oxidation and ≡ is the ferric oxyhydroxide.

When Fe(II) is adsorbed on the oxide surfaces, it is easily hydrolysed by the hydroxyl group making it a better reducing agent, similar to the hydrolysed Fe(II) species in solution (Stumm and Sulzberger, 1992). The adsorption of Fe(II) is affected by pH, and type and concentration of ferric oxyhydroxides in the system (Tamura et al., 1976b, Jones et al., 2014). In a study by (Tamura et al., 1980), it was found that the addition of amorphous ferric hydroxide, goethite, akaganeite and lepidocrocite in neutral solutions enhanced oxidation. The rate constant was found to be approximately 5-times greater when using amorphous ferric hydroxide compared to goethite. Jones et al. (2014) investigated the effect of ferric oxides surfaces, ferrihydrite, Si-ferrihydrite, schwertmannite, lepidocrocite and goethite on Fe(II) oxidation over a pH range of 4 to 5.5. Higher rates of oxidation in the presence of oxide surfaces, 70-fold faster than in homogeneous oxidation at pH 4.5 to 5.5 were observed. They also noted higher rate constants associated with ferrihydrite than goethite and negligible heterogeneous oxidation of Fe(II) with increasing acidity (below pH 4). The high specific surface area in the amorphous ferric oxide and poorly ordered ferrihydrite could be the reason for the increased adsorption and oxidation rate of ferrous ion.

The presence of cations such as cupric ions even at very low concentrations has been reported to catalyse ferrous oxidation in acidic solutions (Cher and Davidson, 1955). The addition of cupric ions as low as 0.02 mg/L had a 5-fold increase on the rate of ferrous oxidation at pH values where oxidation rates are slowest (pH 5 to7) (Stumm and Lee, 1961). Cupric ions are believed to enhance the oxidation rate through the production of oxygen free radicals following reactions that are given in Equation 2.12 and 2.13. The free radicals of oxygen then undergo propagation and chain reactions during ferrous ion oxidation as suggested by (Weiss, 1935).

$$Cu^{2+} + Fe^{2+} \leftrightarrow Cu^{+} + Fe^{3+} \quad 2.12$$

$$Cu^{+} + O_2 \leftrightarrow Cu^{2+} + HO_2^{\cdot} \quad 2.13$$

Although there is lack of solubility data of oxygen in slurries, model results by Kaskiala (2005) showed that the solubility of oxygen decreases as the complexity of

aqueous solutions increase and with increasing temperature under 100 °C at a constant pressure. Slow kinetics can be of great benefit to the nature of the product (crystal formation and filterability); however, it can also be detrimental to plant throughput.

2.4.1.2 Oxidation with hydrogen peroxide

Hydrogen peroxide is a strong oxidant, but its application in iron removal from hydrometallurgical solutions is limited mainly because it is more expensive than oxygen. In addition to being a strong oxidant, hydrogen peroxide solutions are easier to use compared to gaseous oxygen that involves dissolution and transport from the gas-liquid interface to bulk solution. The application of hydrogen peroxide in the removal of iron from sulfate solutions was implemented by Bulong nickel operation (Frampton and Buratto, 1999, O'Callaghan, 2003) (Frampton and Buratto, 1999(O'Callaghan, 2003 #778)and also pilot tested for processing copper-cobalt tailings solutions (Dry et al., 1998). At Bulong, hydrogen peroxide together with air was used in a neutralisation stage at pH range of 4 to 5.8 to lower iron concentrations to below 2 mg/L, a requirement for effective nickel and cobalt purification by solvent extraction in downstream processing. In pilot tests by (Dry et al., 1998), ferrous ion concentrations were reduced to less than 10 mg/L Fe at 80 °C and pH range 3.5 to 4.6 at minimal cobalt loss to the residue (0.85%). The oxidative behaviour of hydrogen peroxide in acidic solutions is based on its reduction given by Equation 2.14 and when oxidising ferrous ion proceeds according to Equation 2.15.

$$H_2O_{2\,(aq)} + 2H^+_{\,(aq)} + 2e^- \rightarrow 2H_2O_{\,(l)} \qquad 2.14$$

$$2Fe^{2+}_{\,(aq)} + H_2O_{2\,(aq)} + 2H^+_{\,(aq)} \rightarrow 2Fe^{3+}_{\,(aq)} + 2H_2O_{\,(l)} \qquad 2.15$$

In contrast to the slow oxidation kinetics of ferrous ion by molecular oxygen, the oxidation of ferrous ion by hydrogen peroxide is rapid even in acidic solutions (Haber and Weiss, 1934, Manchot and Lehmann, 1928). The laboratory study of the V.M. method by (Davey and Scott, 1976) and (Yue et al., 2016) showed that hydrogen peroxide could effectively oxidise ferrous ion in less acidic solutions ($pH \leq 3.5$). The rate of oxidation of Fe(II) by hydrogen peroxide depends on a number of factors such as pH, ferrous ion and hydrogen peroxide concentration, the presence of cations especially Cu(II) and Fe(III) (Medalia and Kolthoff, 1949, Barb et al., 1951b) and temperature (Taylor and Weiss, 1953, Hardwick, 1957).

In strongly acidic solutions containing stable inorganic salts, with either ferrous ion or hydrogen peroxide in excess, the oxidation rate law is independent of the acidity and shows first-order dependence on both ferrous ion and hydrogen peroxide concentration and is expressed by Equation 2.16 (Medalia and Kolthoff, 1949, Barb et al., 1951b). The same rate law applies in less acidic solutions (pH 3) when Fe(II) is in excess. However, the rate law can depart from second order when cupric and ferric ions are present in the system (Barb et al., 1951b). The cupric and ferric ions enhance the decomposition of hydrogen peroxide. In a subsequent study on the kinetics of the decomposition of hydrogen peroxide by Fe(III), it was confirmed that hydrogen peroxide decomposition was dependent on the ferric ion and the hydrogen peroxide concentration and can be expressed by Equation 2.17 (Barb et al., 1951a).

$$\frac{-\,d[Fe^{2+}]}{dt} = 2k\ [Fe^{2+}][H_2O_2] \qquad 2.16$$

$$\frac{-\,d[H_2O_2]}{dt} = 2k_d[Fe^{3+}][H_2O_2] \qquad 2.17$$

where k is the rate constant in $Lmol^{-1}s^{-1}$.

The dependence on acidity occurs when the peroxide to ferric ion ratio is less than 1, modifying Equation 2.17 to Equation 2.18

$$\frac{-\,d[H_2O_2]}{dt} = 2k_d[Fe^{3+}][H_2O_2]^{3/2}[H^+]^{-1} \qquad 2.18$$

The rate constants of ferrous ion oxidation with hydrogen peroxide have been found to increase with an increase in temperature at low temperatures (15 to 40 °C) (Taylor and Weiss, 1953). However, high temperatures above 100°C contribute to the decomposition of hydrogen peroxide (Lin et al., 1991).

Kinetic studies on the oxidation of ferrous ion usually involve natural waters and synthetic solutions with extremely low ferrous ion concentrations, which are not representative of the industrial solutions. In industrial solutions, such as sulfate laterite leach solutions, ferrous and ferric ions and other cations and anions that can have an impact on oxidation are present in considerable amounts. Thus, the effect of the various parameters overlaps, and the rate equations reviewed above cannot adequately describe the oxidation process in the highly supersaturated and complex multicomponent systems.

2.4.2 Ferric ion hydrolysis chemistry

Both Fe(II) and Fe(III) ions form hexa-aquo complexes of the form $[Fe(H_2O)_6]^{z+}$, in which the water molecules are polarised, and the polarisation is dependent on the charge and size of cation (Jolivet et al., 2004). The ferric-aquo complex with a more positive charge and high electronegativity is more acidic than the ferrous-aquo complex. The hexa-aquo ions rapidly undergo deprotonation (hydrolysis) to form charged low molecular weight species (monomers) of the form $[Fe(H_2O)_{6-y}(OH)_y]^{2-y}$ and $[Fe(H_2O)_{6-x}(OH)_y]^{3-x}$ induced by base addition. In the deprotonation process, the hexa-aquo ions are losing H^+ ions. For simplicity, the water molecules are omitted in the chemical formula of the monomers with the monomers represented by $Fe(OH)_y^{2-y}$ and $Fe(OH)_x^{3-x}$.

The net ionic equilibrium hydrolysis reactions for the formation of monomers of Fe(III) and their respective equilibrium constants are given in Table 2. 4. The relative concentration of the different iron complex species at equilibrium with the iron hydroxide at any given pH can be computed using the complex formation equilibrium constants and the solubility product of iron hydroxides as illustrated in Figure 2.5. Ferric ion is easily hydrolysed in acidic conditions, whereas the hydrolysis of Fe(II) is favoured in alkaline conditions (Baes and Mesmer, 1976). In ferrous and ferric ion mixed solutions, the hydrolysis of ferric ion is independent of that of ferrous ion and happens in acidic conditions (pH < 3) while ferrous is favoured at circumneutral pH > 6 (Ruby et al., 2003).

Table 2.4: Equilibrium constants for the net ionic hydrolysis reactions of Fe(III) (Barnum, 1983, Baes and Mesmer, 1976) at 25 °C

Hydrolysis reaction	Log K
$Fe^{3+} + H_2O \leftrightarrow Fe(OH)^{2+} + H^+$	− 2.19
$Fe(OH)^{2+} + H_2O \leftrightarrow Fe(OH)_2^+ + H^+$	− 5.67
$Fe(OH)_2^+ + H_2O \leftrightarrow Fe(OH)_3 + H^+$	− 13.1
$Fe(OH)_3 + H_2O \leftrightarrow Fe(OH)_4^- + H^+$	− 21.6
$2Fe^{3+} + 2H_2O \leftrightarrow Fe_2(OH)_2^{4+} + 2H^+$	− 2.95
$3Fe^{3+} + 4H_2O \leftrightarrow Fe_3(OH)_4^{5+} + 4H^+$	− 6.30

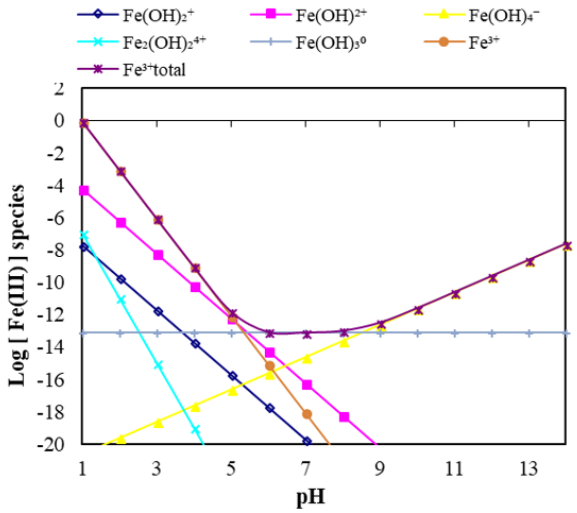

Figure 2.5: Ferric ion speciation at equilibrium with $Fe(OH)_3$ as a function of pH at 25 °C

2.4.3 Precipitation of iron oxyhydroxides and metastable phases

Precipitation of iron phases is a polymerisation reaction occurring upon ferric ion deprotonation. In a homogeneous solution of ferric ion, the monomeric species ($Fe(OH)_x^{3-x}$) interact to form dimers, $Fe_2(OH)_2^{4+}$ and trimers, $Fe_3(OH)_4^{5+}$ and eventually large polycations, red-brown colloids ($Fe_p O_r(OH)_s^{3p-(2r+s)}$). Although there is evidence to support the existence of dimers and trimers in chloride solutions (Bottero et al., 1994), the existence of species beyond trimers is a subject of debate. A polycation of the form of $Fe_{12}(OH)_{34}^{2+}$ together with monomers and dimers was found in nitrate solutions (Daniele et al., 1994). Large polycations are formed at a higher OH^-/Fe ratio where polymerisation proceeds rapidly making it difficult to trace the large polymers (Flynn, 1984). It is the molecular processes involved in the formation of the low weight polycations that govern the morphology of the final product. Two condensation processes, olation (Equation 2.19) and oxolation (Equation 2.20) are involved in the formation of dimers and further polymerisation of the polynuclear species. In olation, aquohydroxo-complexes condense to form hydroxobridges, whereas the condensation of oxohydroxo-complexes by oxolation leads to the formation of oxobridges (Blesa and Matijević, 1989, Jolivet et al., 2004). Oxobridges are not easily reversed by acidification unlike hydroxobridges, and thus the charged polymeric species formed by oxolation are relatively more stable than those formed by olation (Dousma and De Bruyn, 1976).

Olation

$$H_2O - Fe - OH + OH_2 - Fe - OH \rightarrow H_2O - Fe - OH - Fe - OH + H_2O \quad 2.19$$

Oxolation

$$\sim Fe - OH + \sim Fe - OH \rightarrow \sim Fe - O - Fe\sim + H_2O \quad 2.20$$

Further polymerisation of the low molecular weight polycations leads to the formation of higher molecular weight polycations, the red-brown colloids of diameter 3 to 5 nm and amorphous in nature (Cornell et al., 1989). The addition of a base to the red-brown colloids enables instantaneous coagulation to poorly ordered nanosize polymers by deprotonation of co-ordination water molecules. The nanosize polymers are identified as amorphous ferric hydroxide, schwertmannite and ferrihydrite (Jambor and Dutrizac, 1998, Loan et al., 2005), which can be said to be the first residues formed during precipitation.

Ferrihydrite is a poorly ordered iron oxyhydroxide made up of spherical crystals 2 to 5 nm in diameter that rapidly aggregates (up to 300 nm in size) creating internal and inter-particle micro-porosity and a high specific surface area ranging from 220 to 560 m^2/g (Carlson and Schwertmann, 1981). The structure of ferrihydrite is not fully understood and has resulted in ferrihydrite being wrongly identified as amorphous ferric hydroxide (Claassen et al., 2002, Loan et al., 2006, Loan et al., 2005). The compound has been approximated by various chemical formulas, for example, $Fe_5HO_8.4H_2O$ (Towe and Bradley, 1967, Bigham et al., 1996), $Fe_2O_3.2FeOOH.2.6H_2O$ (Russell, 1979) and $5Fe_2O_3.9H_2O$ (Carlson and Schwertmann (1981). Although the structure is almost similar to that of haematite, ferrihydrite is excessively hydrous and has a Fe/O ratio of less than two-thirds. It is suggested that the low degree of order of ferrihydrite is because of vacant Fe sites and the replacement of some oxygen by water and hydroxyl group (Schwertmann and Cornell, 2008). Two forms of ferrihydrite with different degrees of structural order are generally identified, 2-line and 6-line ferrihydrite, with the prefix referring to the number of peaks observed in X-ray diffraction patterns. The former is formed from rapid iron hydrolysis when OH^-/ Fe(III) is greater than 3.0 (Cornell et al. 1988), with more crystalline 6-line ferrihydrite formed at OH^-/ Fe(III) ratio less than 3.0 (Jambor and Dutrizac, 1998, Schwertmann et al., 1999). The 2-line ferrihydrite has disordered planar 4Fe(O,OH)-octahedra units and only two weak broad peaks at 2.74 Å and 1.5 Å (which is a double

line at 1.53 Å and 1.48 Å) (Carlson and Schwertmann, 1981, Feitknecht et al., 1973). Particles of 6-line ferrihydrite consist of hexagonal close-packed oxygen planes with Fe in the tetrahedral sites (Eggleton and Fitzpatrick, 1988) and have five to seven broad peaks at 2.54 Å, 2.25 Å, 1.97 Å, 1.72 Å, 1.53 Å and 1.48 Å (Abdus-Salam and Civer, 2012, Carlson and Schwertmann, 1981).

The hydrolysis of ferric ions is influenced by the presence of other complexing ligands in a solution other than H_2O, OH^- and O_2^- which is an unwritten assumption made in Equations 2.19 and 2.20. The presence of other anions, such as SO_4^{2-} and Cl^- have been found to alter and complicate the hydrolysis process pathway (Schneider, 1984). In a sulfate matrix SO_4^{2-} ions are incorporated as bridging ligand in the polymeric complexes (Equation 2.21), and the process leading to sulfate incorporation competing effectively with olation and oxolation (Blesa and Matijević, 1989). Once the sulfate containing polynuclear species undergo oxolation, the inclusion of sulfate becomes irreversible.

$$\sim Fe - OH + \sim Fe - OH + SO_4^{2-} \rightarrow \sim Fe - O - SO_2 - O - Fe\sim + H_2O \qquad 2.21$$

It has been argued that the morphology of iron phases is primarily directed by the molecular processes involved in the formation of the low nuclearity species (Misawa et al., 1974). The formation of the SO_4^{2-} containing polymers could be an explanation for the formation of schwertmannite in sulfate-rich solutions.

Schwertmannite is a poorly ordered iron oxyhydroxysulfate formed from sulfate-rich solutions at pH range 2.5 to 4 and generally exists in a mixed assemblage with other nanophase iron minerals (Bigham et al., 1990). The structure and sulfate content of schwertmannite is of considerable debate. It has a tunnel structure akin to that of akageneite (Bigham et al., 1990) and maghemite (Loan et al., 2005), with sulfate as the bridging link between the Fe atoms in the tunnel structure instead of chloride, in the akageneite-like structure. Schwertmannite has an ideal formula of $Fe_8O_8(OH)_6SO_4 \cdot nH_2O$ and thus a Fe/S molar ratio of 8 compared to 1.5 for jarosite which is a preferred iron phase at pH below 2 in the presence of jarosite-forming cations (Bigham and Nordstrom, 2000). The sulfate content in schwertmannite somewhat varies with the Fe/S ratio normally in the range of 4.6 to 8 and hence the formula depends upon the degree to which tunnel and surface sites are saturated with sulfate (Bigham et al., 1990, Bigham et al., 1996). The optimal condition for the

formation of schwertmannite is a pH range of 3 to 4.5 and sulfate concentration in the range 1 to 3 g/L (Murad, 1994). Schwertmannite is mostly a product of fast reaction kinetics and hence has low crystallinity and very small particles (nanoparticles) with high sorption capacity due to the high specific surface area (100 to 225 m^2/g) (Bigham et al., 1990, Murad, 1994). The low degree of crystallinity of schwertmannite makes characterisation difficult, especially in mixtures with other iron minerals and it is often wrongly designated for example as dense amorphous basic ferric sulfate and gelatinous precipitates (Flynn, 1990) and ferrihydrite (Loan et al., 2006). Ferrihydrite is normally precipitated together with schwertmannite, and since the former has a high sorption capacity, it can sorb enough sulfate to approximate the structure of schwertmannite making it difficult to distinguish the two minerals. It has eight broad XRD peaks at 4.86, 3.39, 2.55, 2.28, 1.95, 1.66, 1.51 and 1.46 Å.

In zinc hydrometallurgy, especially the Paragoethite and Zincor Process, difficulties in characterising ferrihydrite and schwertmannite produced iron residues designated as a variety of iron phases such as amorphous ferric hydroxide and goethite. The residues were later confirmed to be abundantly poorly crystalline, intermediate iron phases ferrihydrite and schwertmannite and not goethite (Claassen et al., 2002, Loan et al., 2006, Loan et al., 2005). For example, (Claassen et al., 2002) showed that iron residues from Zincor Process were approximately 50% ferrihydrite and schwertmannite, 20% plumbojarosite ($Pb[Fe_3(SO_4)_2(OH)_6]_2$), 25% franklinite ($ZnO \cdot Fe_2O_3$) and 5% unknown phases. Loan et al. (2006) showed that 40 to 50% of the iron residue in the Paragoethite Process was 6-line ferrihydrite and the remainder jarosite phases and poorly crystalline goethite. The disordered structures of ferrihydrite, schwertmannite and amorphous ferric hydroxide are rapidly dissolved in ammonium oxalate at pH 3 which distinguishes these minerals from the crystalline phases such as goethite which is insoluble in the ammonium oxalate solution (Schwertmann, 2000). Ferrihydrite and schwertmannite are thermodynamically unstable and transform into more crystalline iron phases, particularly goethite and haematite (Murad, 1994, Schwertmann and Murad, 1983).

2.4.4 Transformation of metastable phases

The final product of iron precipitation mainly depends on the ageing and transformation of the thermodynamically unstable phases such as amorphous iron

hydroxide, ferrihydrite and schwertmannite. Crystalline phases, however, can be formed directly from a solution of small cationic species without intervention of large polycations at $0.5<OH^-/Fe(III)<1$ (Cornell et al., 1989), and lepidocrocite is suggested to be the only crystalline phase that forms directly from solution (Blesa and Matijević, 1989). The majority and common reaction products goethite and haematite are a result of the transformation of amorphous phases and poorly ordered iron phases. The kinetics of transformation is generally slow, with complete transformation requiring hours to years. For example, the transformation of synthetic schwertmannite in acidic sulfate solutions to goethite is reported to have taken 353 days in one study (Acero et al., 2006) and 543 days in another (Bigham et al., 1996) and 20 to 140 days were required for 2-line ferrihydrite transformation to goethite and haematite (Wang et al., 2015). In hydrometallurgical processing where reaction times are short, most of the precipitate exist as the amorphous iron oxides due to slow transformation kinetics. The transformation of ferrihydrite and schwertmannite to goethite and haematite is by competing mechanisms, and the conditions that favour the formation of one compound are not favourable to the other. Goethite is formed by a dissolution-reprecipitation process whereas haematite is formed by dehydration–internal rearrangement of ferrihydrite (Jolivet et al., 2004).

The preferential formation of ferrihydrite and schwertmannite and their transformation to goethite and haematite follows Stranski's rule. According to Stranski's rule, the least stable phase nucleates first due to lesser activation energy requirements (Söhnel and Garside, 1992). Where various phases are possibly formed for example ferrihydrite (Ft), goethite (Gt) and haematite (Ht), the order of the solubilities directs the rate of precipitation. The solubility of ferrihydrite (pKsp =37 to 39) and schwertmannite (pKsp =28 to 32) is much higher (lower stability) compared to that of goethite and haematite (pKsp = 40 to 44) (Cornell and Schwertmann, 2003). Ferrihydrite and schwertmannite will nucleate first and at higher rates than both goethite and haematite. Once the ferric concentration drops below the solubility of ferrihydrite and the induction related to the nucleation of goethite and haematite is over, schwertmannite and ferrihydrite dissolution become a new source of Fe(III) for the growth of goethite and haematite. Thus, the formation of the stable phases, goethite and haematite from ferrihydrite and schwertmannite can be conceptualised as follows (Blesa and Matijević, 1989):

$Fe^{3+}_{(aq)} \rightarrow Fe_2(OH)_4^{4+}{}_{(aq)} \rightarrow$ Fe(III)oxyhydroxy salts/amorphous $Fe_2O_3.xH_2O_{(s)} \rightarrow$ goethite/haematite $_{(s)}$

The proportion of goethite and haematite is influenced by a number of factors such as pH (Schwertmann and Murad, 1983, Cudennec and Lecerf, 2006), temperature (Chukhov et al., 1974, Johnston and Lewis, 1983) and the presence of other species such as cobalt, copper and manganese (Cornell and Giovanoli, 1989, Cornell et al., 1990, Cornell et al., 1992). The pH of the system affects both the solubility and speciation of ferrihydrite and is the major variable that governs the final product.

Goethite forms from ferrihydrite in both acidic media (pH < 4) and alkaline media (pH > 8) when the solubility of ferrihydrite is higher, that is maximum activity of $Fe(OH)_2^+$ in acidic conditions and Fe $(OH)_4^-$ in alkaline conditions (Schwertmann and Murad, 1983). Haematite formation is maximum at pH between 7 and 8 when ferrihydrite solubility is minimal and is the point of zero charge (pzc) of ferrihydrite. At pzc, aggregation of ferrihydrite is greatest. Cudennec and Lecerf (2006) studied the influence of pH on the relative yields of goethite and haematite, and their results were in agreement with those by Schwertmann and Murad (1983). Goethite formation was high at pH 2 to 5 and 10 to14 and maximum haematite formation at circumneutral pH. An earlier study (Torrent et al., 1982) found that in humid conditions ferrihydrite easily transforms to goethite but dry and warm conditions favoured the formation of haematite. At high temperatures, the rate of transformation of ferrihydrite is much faster and the yield of haematite relative to goethite increases (Johnston and Lewis, 1983). Johnston and Lewis (1983) found that haematite formed directly from ferrihydrite at 92 °C, but at 85 °C, it was formed via goethite. Haematite formation from ferrihydrite was noticeable after 10 minutes ageing time at 92 °C compared to 60 minutes at room temperature. The precipitation of iron is often associated with the co-precipitation of cations, both impurities and metals of value. The presence of species such as cations of Al, Co, Cu, Mn, Ni and Zn have been found to have a marked impact on the rate of formation of goethite and haematite from amorphous ferric hydroxide and ferrihydrite (Cornell and Giovanoli, 1989, Cornell et al., 1990, Cornell et al., 1992).

Lewis and Schwertmann (1979) investigated the influence of aluminium on the conversion of ferrihydrite at room temperature and observed that the rate of transformation of ferrihydrite to goethite decreased with increasing Al concentration

in the residue. In a subsequent study carried out at 45 ℃ and 55 ℃ and varying humidity (Torrent et al., 1982), aluminium was found to inhibit goethite formation completely. Aluminium substituted ferrihydrite has a lower solubility which retards transformation to goethite leads to an increase in the amount of hematite relative to goethite (Schwertmann et al., 2000). In alkaline media, cobalt (Cornell and Giovanoli, 1989), manganese (Cornell and Giovanoli, 1987, Wang et al., 2015) and nickel (Cornell et al., 1992) are reported to retard the formation of crystalline iron phases from ferrihydrite and amorphous ferric hydroxide. Iron and manganese are closely related, with manganese reported to replace as much as 15 mole % of iron in synthetic goethite (Cornell and Giovanoli, 1987). The stabilising ability decreases in the order Ni > Cu > Co > Mn and follows the Irving Williams series (Cornell and Giovanoli, 1989). When metal ions are in excess, spinel phases are formed from ferrihydrite, for example, $NiFe_2O_4$ and jacobsite are formed in nickel and manganese-rich solutions, respectively (Giovanoli and Cornell, 1992). The formation of goethite is inhibited when cations are adsorbed in the precipitates, especially divalent ions (Cornell et al., 1989).

On the contrary, the presence of Fe(II) is found to enhance the transformation of non-crystalline phases to crystalline phases (Burton et al., 2008, Pedersen et al., 2005). When Fe(II) is adsorbed onto the ferrihydrite structure, there is electron exchange between the Fe(II) and Fe(III) in the ferrihydrite structure weakening the structure thus promoting its decomposition and dissolution which supports goethite formation (Chukhov et al., 1974). Similar behaviour of ferrous ion replacing ferric ions was observed when the transformation was investigated using aqueous ferrous ion and ^{55}Fe-labelled iron oxides of ferrihydrite, lepidocrocite and goethite in anoxic conditions. When the ^{55}Fe-labelled iron oxides were added in ferrous solution (0 to 1.0 mM), there was a rapid release of ^{55}Fe, while in the absence of ferrous ion, no release was observed. During the exchange of the two iron species, all ferrihydrite was converted into more crystalline and stable phases of goethite and lepidocrocite. Burton et al. (2008) studied the transformation of schwertmannite to goethite in anoxic conditions and complete transformation of schwertmannite within 3 to 5 hours at a pH greater than 6 was reported.

The various possible iron phases likely to be produced during ferric hydrolysis precipitation and oxidative precipitation of ferrous ion in sulfate medium are aggregated and summarised in Figure 2.6.

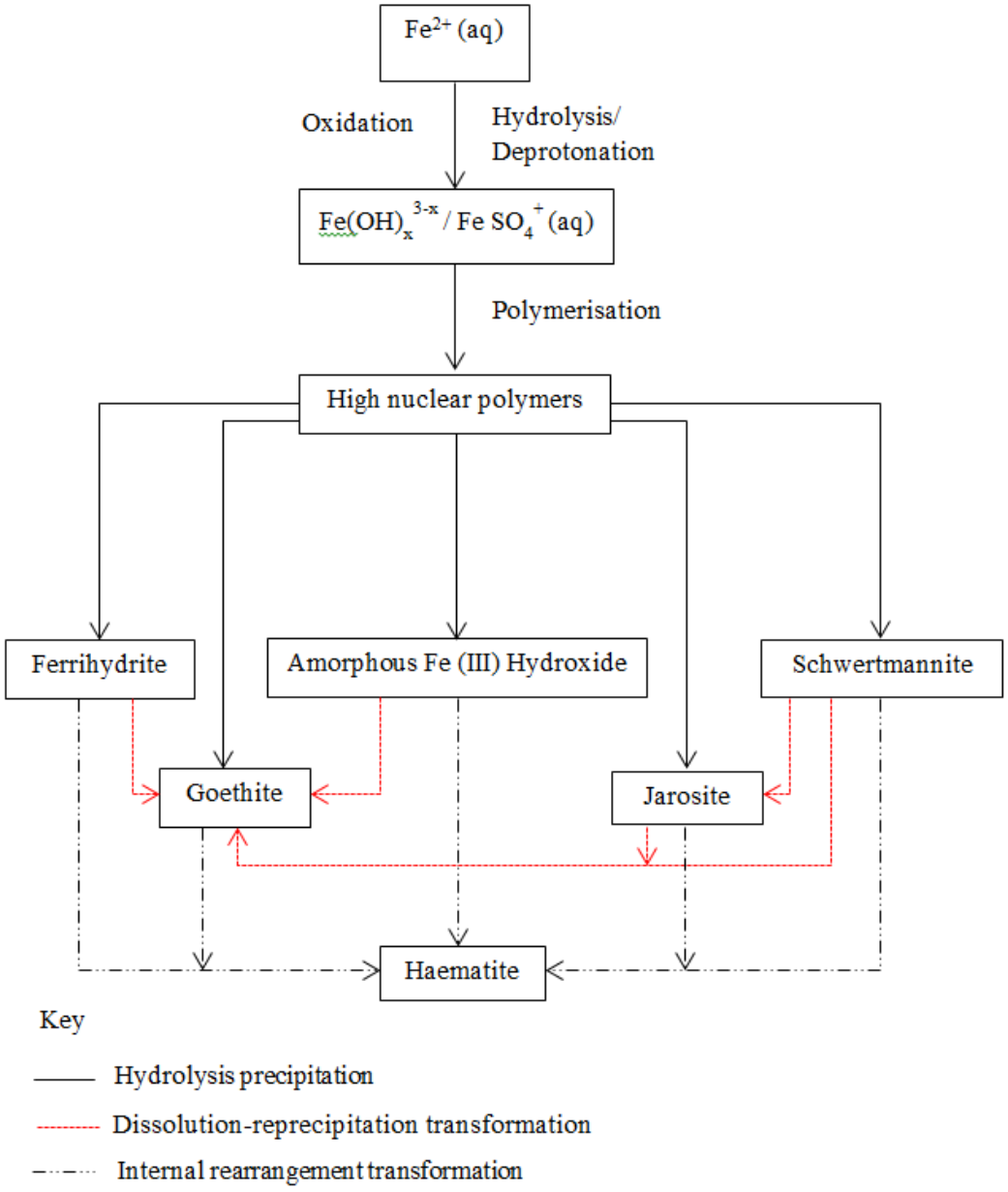

Figure 2.6: A diagrammatic representation of the formation of iron mineral phases in acidic conditions and their transformation modified from (Jambor and Dutrizac, 1998) and (Schwertmann and Cornell, 2008).

Unfortunately, most of the species that influence the transformation of non-crystalline phases to crystalline phases, are present in sulfate leach solutions of laterite ores and therefore the effects of the individual species overlap. The iron residue from the Goethite Process consists mainly of the poorly ordered iron phases due to the slow transformation to ordered iron phases.

2.5 Precipitation of iron, aluminium and chromium from nickel laterite sulfate solutions and the associated nickel and cobalt losses

As highlighted in Section 2.2.2, leach solutions of nickel laterite ores are highly contaminated with iron and significant amounts of other impurities, especially aluminium, chromium and magnesium. Iron precipitation is usually the first step in the purification of the sulfate leach solutions of nickel laterites, which occurs simultaneously with the removal of the trivalent ions of aluminium and chromium. A major weakness of iron removal by precipitation processes is the incorporation of nickel and cobalt in the solid residues. The extent of nickel incorporation in the solid residues is, however, related to precipitation parameters such as pH, temperature and the concentration of ferric ion. Moreover, the co-precipitation of aluminium and chromium during iron precipitation have been found to exacerbate the amount of nickel losses (Guise and Castro, 1996, Wang et al., 2011). The removal of iron, aluminium and chromium from nickel laterite leach solutions is through the well-known hydroxide precipitation process.

2.5.1 Hydroxide precipitation of cations

The removal of both divalent and trivalent cations as metal hydroxides has been reviewed by Monhemius (1977) and occurs according to Equation 2.22.

$$M^{n+}(aq) + n(OH)(aq) \rightarrow M(OH)_n(s) \qquad 2.22$$

, where M is the metal and n is the metal valency.

Thus, the equilibrium constant, K can be expressed as:

$$K = \frac{1}{[M^{n+}][OH^-]^n} = \frac{1}{K_s}, \qquad K_s = [M^{n+}][OH^-]^n \qquad 2.23$$

, where Ks is the solubility product of the metal hydroxide, and n is the valency (ionic charge) of the metal.

Combining the ionic product of water (K_w) and the solubility product expression, the activity of the metal ions as a function of pH can be calculated as follows:

$$\log[M^{n+}] = \log K_{sp} - n\log K_w - npH \quad 2.24$$

From Equation 2.23, the equilibrium concentration of cations in solution depends on pH (hydroxide ion concentration) and is related to individual cation solubility product and valency (Monhemius, 1977). The concentration of the various divalent and trivalent ions at equilibria with their hydroxides can be constructed using Equation 2.24 and is illustrated in Figure 2.7. The trend is the basis for the application of hydroxide precipitation in the separation and recovery of cations in hydrometallurgical processing.

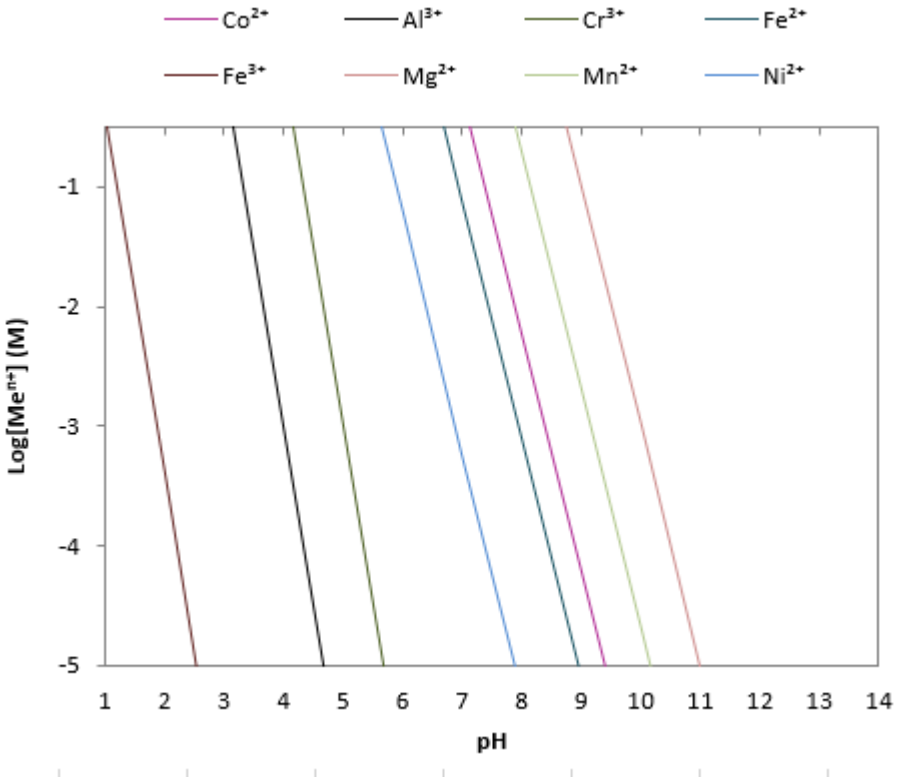

Figure 2.7: Metal ions solubility as a function of pH, after Monhemius (1977)

However, the selectivity of hydroxide ions for the individual cations especially of the same valency is not good. This is evident in iron precipitation processes where the trivalent ions of Fe, Al and Cr cannot be selectively precipitated and also in MHP process were nickel and cobalt are not easily separated from manganese. In iron precipitation, almost complete removal of ferric ion can be accomplished at low pH values of 2.5 to 3.5 and simultaneously significant amounts of Al and Cr are removed but whose complete removal requires slightly higher pH values (Steemson and Smith, 2009). At high pH, nickel and cobalt incorporation in the solids becomes significant and multistage precipitation is used to minimise nickel losses and allow for high

removal of Fe, Al and Cr. At Ravensthorpe nickel operation (RNO), a primary neutralisation stage at pH 2.5 is used for bulk removal of the trivalent ion impurities followed by a secondary neutralisation stage at pH 4 to 5.5 to remove any iron, aluminium and chromium remaining in solution (White et al., 2006). The solids obtained at high pH in the final neutralisation stages are recycled back to the leaching circuit to recover nickel and cobalt though it leads to impurity build-up with time. The impact of iron precipitation on nickel losses is greater during goethite precipitation than in jarosite precipitation possibly due to the high pH values used.

2.5.2 Nickel and cobalt losses during iron precipitation

Iron precipitates are known to remove other metal ions contained in solutions (Dutrizac and Dinardo, 1983, Tamargo et al., 1996), and the level of metal uptake is influenced by precipitate quality. The precipitate quality (particle size distribution and density) is determined by the degree of supersaturation during the time of precipitation in the Goethite Process. Supersaturation control is critical in goethite precipitation but not jarosite and haematite precipitation. Higher levels of supersaturation cause rapid nucleation and the formation of fine particles with large surface area and high sorption capacity. Furthermore, the fine particles which are often gelatinous have poor liquid-solid separation and washing properties which promote the entrainment of considerable amounts of process solution in between particles. Nonetheless, it is critical that the incorporation of nickel and cobalt in the iron phases be kept low in any iron precipitation process for process economics.

Several studies on goethite precipitation have shown pH as the significant factor influencing the amount of nickel losses in the precipitates and Fe/Ni ratio a secondary factor. In a study by Davey and Scott (1976) using both E.Z. and V.M. method to process sulfate and chloride leach solutions, it was found that nickel and cobalt incorporation in solids increased with increasing pH and that lower iron content in the filtrate with the V.M. method than the E.Z. method. Nickel up to 3.6% and cobalt up to 0.37% in the dried residue were obtained at pH range 2 to 3.5 and 85 °C. Increasing pH from 2.0 to 3.5 with V.M. method resulted in nickel losses increasing from 0.3% to 1.7%. When using air as an oxidant in the V.M. method to process sulfate leach solutions Chang et al. (2010), found nickel losses increased with increasing pH and Fe/Ni ratio. At pH range of 2.5 to 3.0, quadrupling the amount of iron with respect to

nickel resulted in an increase in nickel loss from the solution from 1.41 % to 4.12%, with even higher nickel losses of 15.9% at pH range 3.0 to 4.0. A subsequent study using E.Z. method by Wang (2011) confirmed the findings by Chang et al. (2010), that is nickel losses increase with increasing pH and Fe/Ni ratio. At 85 °C and Fe/Ni ratio of 12, nickel losses to solid residue increased from 0.42 % at pH 2.0 to 8.20% at pH 4.0. It was also observed by Wang (2011) that nickel losses increased with temperature and the higher the iron removal, the higher the amount of nickel lost from solution even at the same Fe/Ni ratio, pH and temperature. In a recent study using hydrogen peroxide and sodium hydroxide solution at 85 °C in V.M. method (Yue et al., 2016), the nickel losses were found to increase with pH, from 1.1 % to 5.6 % at pH 2.9 to 3.3 and 3.9 to 4.3, respectively.

In the studies involving jarosite precipitation, when precipitating lead jarosite using two approaches, autoclave synthesis at 130 °C in a pressurised vessel and slow jarosite-cation addition synthesis at 97 °C, the amount of nickel and cobalt co-precipitated was found to largely depend on temperature and the procedure of precipitation (Dutrizac and Dinardo, 1983). The incorporation of cobalt in the residue was more than that of nickel irrespective of the approach used, with 2.92% nickel and 2.94% cobalt incorporated in autoclave synthesis and 0.28% nickel and 1.02% cobalt incorporated in slow-addition synthesis. In a study of nickel and cobalt incorporation in jarosite-type compounds conducted at pH 1.6 and temperature range 60 to 200 °C (Dutrizac and Chen (2004), it was shown that alkali forming cations influenced nickel and cobalt losses. Higher nickel and cobalt (~1%) was incorporated in potassium jarosite compared to sodium jarosite (~0.4%). A laboratory study on the removal of iron, aluminium and chromium as jarosite-alunite compounds (Agatzini-Leonardou et al., 2009) indicated 3.5% nickel and 2.0% cobalt incorporation in the residue at pH 3.5 and 95 °C.

In a study by Köse and Topkaya (2011), were iron precipitation from AL sulfate solutions of nontronite ores was conducted without controlling Fe(III) concentration and adding jarosite-forming cations it was observed that nickel and cobalt losses increased with increasing pH and temperature. At pH 2.5 nickel and cobalt losses were below 1% and at pH 3.5 nickel and losses increased and were above 15%.

2.5.3 Effect of aluminium, chromium and magnesium on nickel and cobalt losses during iron precipitation

The effect of the co-removal of iron, aluminium and chromium on nickel and cobalt losses to solids in a two-stage precipitation process was investigated by Guise and Castro (1996) using synthetic sulfate leach solutions at 90 °C. Higher nickel and cobalt losses from solutions containing aluminium and chromium were found compared to the solution were only iron was present. Nickel and cobalt losses increased in the order (Fe^{3+}+ Ni^{2+}+Co^{2+}) < (Fe^{3+} + Al^{3+} +Ni^{2+}+Co^{2+}) < (Fe^{3+} +Al^{3+} Cr^{3+} +Ni^{2+}+Co^{2+}). At pH 3.5, 13.3% nickel and 10.3% cobalt were lost from the ternary system (Fe^{3+}+ Ni^{2+}+Co^{2+}) compared to 44.4 % nickel and 34.9% cobalt in the quartenary system (Fe^{3+} + Al^{3+} +Ni^{2+}+Co^{2+}) and 62.2% nickel and 67.9% cobalt in the quinary system (Fe^{3+} +Al^{3+} Cr^{3+}+Ni^{2+}+Co^{2+}). High nickel and cobalt co-precipitation in the presence of aluminium is attributed to the formation of amorphous aluminium oxyhydroxides with strong adsorption properties, which predispose nickel and cobalt to high adsorption and incorporation in the residue. It was shown during iron precipitation from heap leach laterite solutions, that the concentration of magnesium oxide slurry aggravated the losses of nickel and cobalt to the solids. At pH 1.5 using 100 g/L, MgO nickel losses were almost comparable to losses obtained at pH 2.5 using 50 g/L MgO. However, when 25 g/L MgO slurry was used at pH 2.5, about 6.7% Ni and 11% Co losses were obtained as compared to 26.2% Ni and 37.1% Co losses with 50 g/L MgO slurry. The study by (Wang, 2011) on the co-removal of Fe, Al and Cr from a binary system [Fe(III) + Ni(II)], ternary systems [Fe(III) + Al(III) +Ni(II)] and [Fe(III) + Cr(III) + Ni(II)] and quaternary system [Fe(III) + Al(III) + Cr(III) + Ni(II)], also revealed an increase in nickel losses with increasing pH and temperature and during co-precipitation of iron, aluminium and chromium. At pH 4 and 85 ºC, nickel loss in the binary system was 7.5% compared to respective 12% and 9.2% in the aluminium and chromium ternary systems. The nickel losses in the quaternary system were more than 10%.

The effect of magnesium on goethite and jarosite precipitation is not known despite the ubiquitous amount of magnesium in leach solutions of saprolite ores. However, at high temperatures in the Haematite Process, iron precipitation has been found to increase with the addition of sulfates of copper, magnesium and zinc. This is because when the sulfates are added in solution, the excess sulfate ion forms bisulfate thereby

decreasing the activity of the hydronium ion (HSO_4^-), which might be the case even during precipitation under atmospheric conditions.

Nickel and cobalt losses to solids at low pH (≤ 2.5) are comparable for all the iron precipitation processes, goethite and jarosite and in those studies were ferric ion concentration was not controlled, and there is no addition of alkali-forming cation. The losses of nickel and cobalt become more significant at higher pH (>2.5) regardless of the iron precipitation process (Chang et al., 2010, Köse and Topkaya, 2011, Guise and Castro, 1996). It has been shown in the Goethite process that rarely is goethite formed during precipitation (Claassen and Sandenbergh, 2007). Although the Goethite Process produces easily filtered slurries, the production of stable goethite for disposal is not always the outcome. The low residual iron, aluminium and chromium concentrations at the high pH values are at the cost of greater nickel and cobalt losses which are comparable to studies where Fe(III) is not controlled. For example, nickel losses in the study by Chang et al. (2010) using the V.M. method and the study by Köse and Topkaya (2011) without Fe(III) concentration control during precipitation were almost similar. Multistage precipitation can be used to minimise nickel and cobalt loss as shown by White et al. (2006) and Köse and Topkaya (2011). Thus, a detailed study on iron precipitation processes at high Fe(III) concentrations and multi-element sulfate laterite solutions is required to understand the relation between iron precipitation and the level of nickel and cobalt losses.

2.5.4 Manganese separation and removal from nickel and cobalt in acidic sulfate leach solutions

There are various routes for the purification of nickel and cobalt solutions following iron precipitation, but so far, no process has emerged as a clear preferred processing route. Following neutralisation stages used to remove iron, aluminium and chromium, process flowsheets differ from one operation to another, ostensibly governed by the method of manganese removal and separation from nickel and cobalt. Manganese concentrations in the laterite solutions are relatively low but are high enough to serve as a secondary manganese source. Mixed hydroxide precipitation (MHP)(White, 2002), mixed sulfide precipitation (MSP) (Kyle, 2010) and solvent extraction (SX) (Donegan, 2006) are among the commercially proven processes for separating and recovering nickel and cobalt from the manganese and the other impurities including,

calcium, copper, magnesium and zinc. The success of the various processes is influenced by a number of factors including selectivity, product quality and reagents costs.

2.5.5 Mixed hydroxide precipitation (MHP)

Hydroxide precipitation is commonly used to quantitatively separate metal ions contained in multi-element systems. As outlined in section 2.5.1, the process is not selective especially for cations of the same valency. The separation of nickel and cobalt from manganese, copper, magnesium, calcium and zinc is difficult because of the narrow pH window for metal hydroxide precipitation. Copper and zinc are minor contaminants, and even if co-precipitated, their levels are tolerable in the MHP product, unlike manganese which is in significant amounts in the process solutions.

In Australia, the MHP process found application in both Ravensthorpe (White, 2002) and Cawse nickel operations (Manson et al., 1997), where it is followed by ammoniacal carbonate re-leach leading to nickel and cobalt separation and recovery by SX and electrowinning in downstream processing. Magnesia is the preferred precipitant compared to the more expensive caustic soda and the calcium-containing bases which result in contamination of the product with gypsum. Manganese is co-precipitated in the process, and the level of manganese co-precipitated is found to depend on Ni/Mn ratio, the number of precipitation stages used (Willis, 2007), temperature (Köse and Topkaya, 2011) and type of neutralising agent (Zhang et al., 2010).

A patent on the application of MHP in leach solution with Ni/Co:Mn ratio of 11.2 from a low manganese containing ore (0.26 wt.%) using magnesia reported recoveries of 80 to 100% for nickel and cobalt, at an optimum temperature of 50 °C and from 5 to 15% Mn co-precipitation (White, 2002). Pilot studies (Adams et al., 2004, Mayhew et al., 2009) and industrial applications (White et al., 2006, Harvey et al., 2011) at higher temperatures using a two-stage precipitation process revealed that nickel content of MHP product could be improved to more than 40 wt.% which corresponds to recoveries of more than 95% nickel and 98% cobalt. High temperatures are beneficial for faster reaction kinetics and not specifically for high percentage recoveries, with high recoveries of 99% for both nickel and cobalt achievable at 25 °C and pH range 8.2 to 9.0 (Oustadakis et al., 2006). Manganese precipitation is very sensitive to change

in pH (Zhang et al., 2010). At pH 7.5 and 60 °C, hydroxide precipitation with sodium hydroxide removed 10 % manganese which increased to 71% at pH to 8.0. In a subsequent study by Köse and Topkaya (2011), it was shown that manganese precipitation at pH 7.5 increases with increasing operating temperature, with the precipitation at 70 °C double that at 50 °C. MHP process is suited to process ores low in manganese content (Mn/Ni ratio <1:3) (Willis, 2007). Although not highly selective, there has been increasing interest in using MHP for newer projects such as Vermelho in Brazil, Ramu in Papua New Guinea and Ambatovy in Madagascar. The reason for its preference is that it is a proven and well-known process without safety concerns.

2.5.6 Mixed sulfide precipitation (MSP)

Selective precipitation of metal ions from weak acidic solutions as metal sulfides is also used as a separation and recovery technique in the hydrometallurgical nickel laterite ore processing. The precipitation is typically carried out using hydrogen sulfide gas at elevated temperatures (90-120 °C) and pressures (1000 kPa), for example at Moa Bay, Murrin Murrin and in the AMAX process (Jha et al., 1978, Motteram et al., 1996). Non-gaseous reagents such as sodium sulfide and sodium hydrogen sulfide are also used under atmospheric conditions though their dosing is difficult and impacts on the reaction kinetics of the process (Veeken and Rulkens, 2003). The separation follows the same principle as hydroxide precipitation and the thermodynamic equilibria involved in metal sulfide precipitation using hydrogen sulfide gas can be expressed using Equation 2.25 to 2.27.

$$H_2S\ (g) \leftrightarrow 2H^+ + S^{2-} \qquad K_{s1} = \frac{[H^+]^2[S^{2-}]}{P_{H_2S}} \qquad 2.25$$

$$\log K_{s1} = -2pH + \log [S^{2-}] - \log P_{H2S} \qquad 2.26$$

$$M^{2+} + S^{2-} \leftrightarrow MS\ (s) \qquad \frac{1}{K_{s2}} = \frac{1}{[M^{2+}][S^{2-}]} \qquad 2.27$$

$$\log K_{s2} = \log [M^{2+}] - \log [S^{2-}] \qquad 2.28$$

A solubility diagram of the metal sulfides can be plotted as a function of pH together with sulfide ion concentration at a given pressure of H_2S using Equation 2.25 and 2.27 as shown in Figure 2.8, after Monhemius (1977).

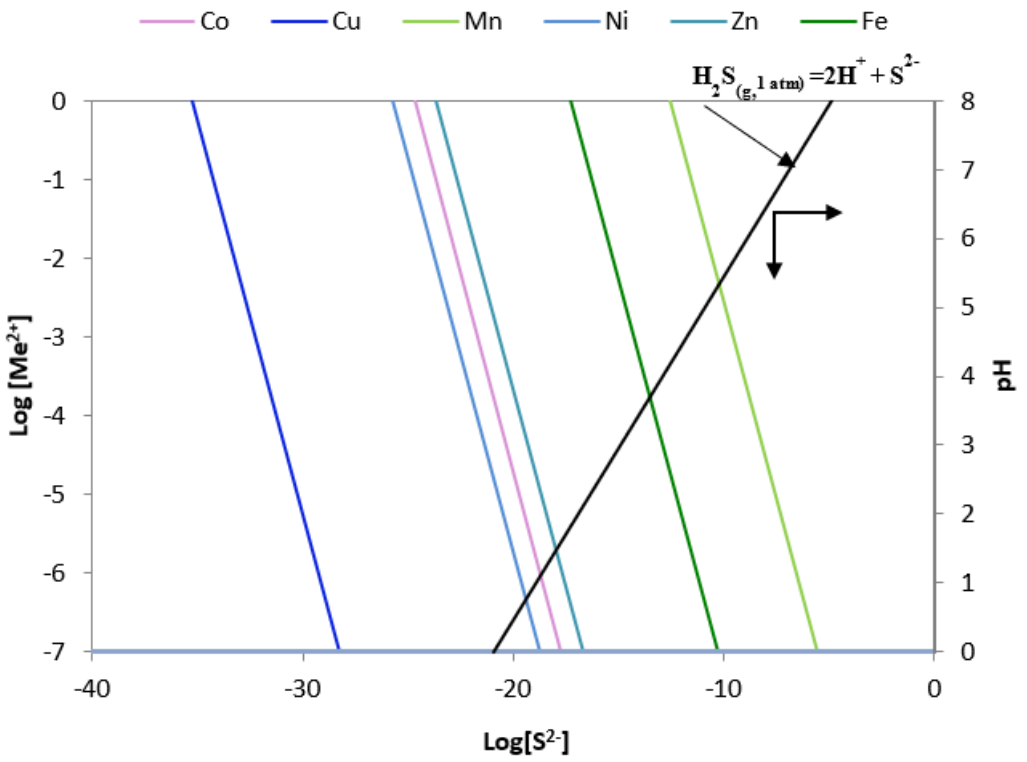

Figure 2.8: The solubility of metal sulfides as a function of pH after Monhemius (1977)

The manganese sulfide line is on the far right and below the hydrogen sulfide line at pH less than 5, which shows that manganese sulfide is more soluble than the sulfides of nickel, cobalt, iron, copper and zinc. The presence of magnesium sulfate during sulfide precipitation benefits the process by buffering against the acid produced from precipitation at the high temperatures (Jha et al., 1978, Motteram et al., 1996).

The Murrin Murrin process uses mixed sulfide precipitation, followed by oxidative pressure leaching of the precipitate and separation of nickel and cobalt by SX. The same process is used at Moa Bay at pH 2.2 to 2.3, 120 ℃ and 1 MPa. The batch tests for Murrin Murrin process by Motteram et al., (1996) indicated 99% Ni and 98% Co precipitated from process solutions at pH 2.5, 90 ℃ and 105 kPa of H_2S. The concentration of manganese and magnesium is very low in mixed sulfide precipitates, and the product is of high purity compared to mixed hydroxide precipitates. However, the use of autoclaves in oxidative pressure leaching is relatively costly, and the use of H_2S is associated with occupational health and safety issues which makes the MSP process difficult compared to MHP. It requires highly trained personnel to avoid safety issues (Willis, 2007).

2.5.7 Direct solvent extraction (DSX)

Solvent extraction is an important unit process in the purification of nickel and cobalt solutions in the hydrometallurgical processing of nickel laterite ores. It is mainly used for the separation and recovery of nickel and cobalt following precipitation processes such as MSP and MHP. The attractiveness of the solvent extraction process was enhanced with the inception of both Cyanex 272 and Cyanex 301 extractants, which can handle solutions with low Co/Ni ratios due to a high separation factor for nickel and cobalt. Both Cyanex 272 and Cyanex 301 found application in direct solvent extraction (DSX) at Bulong nickel project in Australia and Goro nickel project in New Caledonia, respectively.

The Bulong operation consisted of three solvent extraction circuits, Co SX, Ni SX and Zn SX before the production of nickel and cobalt as cathodes (Donegan, 2006, Taylor and Cairns, 1997). Nickel and cobalt and the other impurities are removed from post neutralisation laterite solutions by solvent extraction. In the Co SX circuit, nickel is separated from cobalt, copper, zinc, and manganese using Cyanex 272. Cobalt, copper and zinc are precipitated as sulfides from the strip liquor, followed by re-leaching of the mixed sulfide product to separate zinc by solvent extraction (Zn SX) and copper by ion exchange prior to the recovery of cobalt cathode. The raffinate from the Co SX circuit mainly consisting of nickel, magnesium and calcium is feed to the Ni SX circuit, where nickel is separated from magnesium and calcium using Versatic 10 and nickel solution electronwon to produce nickel cathode. There were several technical and process issues encountered, excessive scaling from gypsum precipitation, extractant and metal entrainment and crud formation, which all contributed to lower recoveries than the design targets (O'Callaghan, 2003, Donegan, 2006). Gypsum precipitation was the major challenge in the project, especially in the Ni SX circuit. Additionally, Cyanex 272 is an effective calcium extractant when used at pH values greater than 6.0 in the Ni SX circuit. Thus, Cyanex 272 entrainment in the Co SX raffinate (Ni SX feed solution) exacerbated the scaling problem by increasing the co-extraction of calcium.

A number of developments and changes were made to reduce and eliminate most of the technical issues experienced in the day to day running of the plant. In the Ni SX circuit, a diluent wash and Jameson flotation cells were incorporated in the process to reduce the amount of entrained Cyanex 272, and almost 99% Cyanex 272 recovery from the Co SX raffinate was achieved at the operating conditions. With the addition

of anti-scalant in the system, gypsum formation was successfully minimised in the circuits (Donegan, 2006, Helm, 2004). At the time of Bulong plant closure in 2003 due to financial pressures, the metallurgical performance of the Bulong plant had been significantly improved with most problems experienced since its commissioning overcome through plant modifications. The process was proficiently producing nickel electrolyte suitable for electrowinning nickel cathodes with purity greater than 99.8% and nickel and cobalt recoveries of 98.2% and 98.5%, respectively (Donegan, 2006).

Goro Nickel project in New Caledonia is the second commercial plant to use solvent extraction techniques and is still running up to date. Two solvent extraction circuits, Ni/Co SX and Co SX are incorporated in the process flowsheet to recover and separate nickel and cobalt from the other impurities (Mihaylov et al., 2000). Cyanex 301 is used to simultaneously extract nickel and cobalt, separating them from Mn and Mg following copper removal by ion exchange in the first circuit (Ni/Co SX). Cyanex 301 selectivity resembles that of mixed sulfide precipitation where both manganese and magnesium are left in solution while nickel, cobalt, zinc and any copper are co-extracted. Zinc is removed from the Ni/Co SX strip solution by ion exchange to produce cobalt-rich feed solution for the Co SX circuit. Cobalt is separated from nickel using tertiary Octyl Amine in the second solvent extraction circuit, leading to nickel pyrohydrolysis and cobalt carbonate precipitation.

The applicability of Cyanex 301 at low pH and the ability to be regenerated makes it more lucrative compared to the other extractants (such as Versatic 10, operating pH of 6.5) as it reduces the cost of neutralising reagent required. The use of highly concentrated acids during stripping is unavoidable. This is as a result of the low dissociation constant (pK_a value) of Cyanex 301 (2.6) compared to other extractants such as Cyanex 302 (5.6) and Cyanex 272 (6.4) and the strong extraction of nickel by the extractant (Rickelton, 1992). Cyanex 301 is not chemically stable in the presence of oxygen and oxidising cations such as ferric ion (Mihaylov, 2003). These impurities can either be removed or excluded ahead of nickel and cobalt recovery or scrubbed if possible, prior to metal value stripping. In general, the pH window for extraction of metal ions is usually narrow making it difficult to achieve good separation. Despite the challenges associated with SX, its use as a separation technique in conjunction with other separation techniques is beneficial and crucial.

2.5.8 Oxidative Precipitation (OP)

Oxidative precipitation is not a very popular separation process in the processing of hydrometallurgical solutions, especially of nickel laterite ores. However, it has found considerable application in the removal of manganese from natural waters and potable water, where the manganous ion is predominantly precipitated as sparingly soluble oxides and oxyhydroxides of MnO_2, MnOOH and Mn_2O_3. Various oxidants can be used for manganese oxidation such as air, ozone, a mixture of SO_2/O_2, chlorine, chlorine dioxide, ammonium peroxy-sulphuric acids and potassium permanganate. The viability of using each oxidising agent is primarily influenced by its cost, efficacy and health and safety considerations. The oxidation of Mn(II) to higher oxidation states Mn(III) and Mn(IV) requires oxidants with strong oxidising power considering the high standard potentials as given in Equation 2.29 and 2.30.

$$MnO_2\,(s) + 4H^+ + 2e^- \leftrightarrow Mn^{2+} + 2H_2O \qquad E^\theta = 1.23\ V \qquad 2.29$$

$$Mn^{3+} + e^- \leftrightarrow Mn^{2+}\ (7.5\ M\ H_2SO_4) \qquad E^\theta = 1.49\ V \qquad 2.30$$

The strong oxidants are costly and often corrosive. However, fast reaction rates and high removal of manganese are easily achieved in acidic conditions. It is essential that the oxidant is easy to use, non-toxic and does not introduce an additional impurity in the system. Thus, potassium permanganate oxidant is suited for manganese oxidation as its reaction results in the formation of manganese oxides.

2.5.8.1 Manganous ions oxidation precipitation with permanganate

The reaction between manganous ions and permanganate ion is given by Equation 2.31.

$$2MnO_4^-{}_{(aq)} + 3Mn^{2+}{}_{(aq)} + 2H_2O_{(l)} \leftrightarrow 5MnO_{2\,(s)} + 4H^+{}_{(aq)} \qquad 2.31$$

Based on Equation 2.31, the removal of Mn(II) from solution by oxidative precipitation is dependent on pH and 2 moles of potassium permanganate is required to oxidise 3.0 moles of Mn(II), which equates to 1.92 mg $KMnO_4$ per mg Mn(II) ions. However, less than 1.92 mg $KMnO_4$ per mg of Mn(II) is often required (Freitas et al., 2013, Van Benschoten et al., 1992, Roccaro et al., 2007) probably because the removal of Mn(II) is a combination of solution phase oxidation, Mn(II) adsorption onto the manganese oxide and surface oxidation (Van Benschoten et al., 1992, Roccaro et al., 2007). When metal oxides are in solutions, a charge develops on the surface; an

electrical double layer is formed from the OH^- and H^+ ions which control the adsorption of inorganic species. The charge changes with pH (that is sign and magnitude) and the pH where the charge changes from positive to negative and vice versa is called the point of zero charge (pzc). The pzc various among the different manganese oxides usually formed from process solutions. The pzc of amorphous manganese dioxide was found to be 2.8 ± 0.3 by Morgan and Stumm (1964), which indicates that the oxide surface is positively charged at pH less than 2.8 and negatively charged at pH values more than 2.8. In a study by Healy et al. (1966), the pzc for a number of manganese dioxides was determined by electrophoresis and coagulation sedimentation techniques and a pzc of pH 1.5 was reported for δ-MnO_2, 1.8 for Mn (II)-manganite, 4.5 for α-MnO_2, 5.5 for γ-MnO_2 and 7.3 for β-MnO_2. The pzc was found to increase with the crystallinity of the oxide. Both cations and anions are adsorbed as counterions, to maintain electroneutrality on the charged oxide surfaces. The adsorption of Mn(II) ions on the oxide surface could be the limiting step to their complete oxidation and it was suggested that the presence of other cations preferentially adsorbed can prevent Mn(II) adsorption (Adams, 1960). Several studies performed on the oxidation of Mn(II) have shown that the process depends on pH, manganese oxides (Van Benschoten et al., 1992), permanganate dose, temperature, and initial Mn(II) concentration (Freitas et al., 2013).

In the early studies on manganese oxidation by potassium permanganate, it was suggested that complete oxidation and precipitation of Mn(II) from aqueous solution could only be achieved at high pH about 8.0 (Hem, 1963, Coughlin and Matsui, 1976). In comparison to other strong oxidants for manganese, potassium permanganate also removes organic compounds responsible for taste and odour in water (Kao et al., 2008). Thus, as studies focused on the application of $KMnO_4$ on the treatment of potable water and AMD, it was also realised that complete removal of Mn(II) could be achieved in slightly acidic conditions (Van Benschoten et al., 1992). The reaction rates of oxidation and precipitation of manganese are more rapid at high pH values than in acidic solutions (Hem, 1963, Van Benschoten et al., 1992). A study on Mn(II) oxidation with permanganate from dilute solutions containing less than 1.25 mg/L Mn(II), at pH range 5.5 to 8.0 and 25 °C by Van Benschoten et al. (1992) has shown that half a minute was required for oxidation and the kinetics increased with an increase in Mn(II) concentration and temperature. Roccaro et al. (2007) studied the

removal of manganese from groundwater at pH 8.5 and found that a retention time of half an hour was required using less than the stoichiometric quantity of $KMnO_4$. Investigations using slightly acidic synthetic Mn(II) solution by Freitas et al., (2013) determined the retention time for equilibrium to be reached at pH 3 was 20 mins compared to 10 mins at pH 5.0 and 7.0. Permanganate less than the stoichiometric value was needed, although the amount varied with pH, more permanganate was consumed with a decrease in pH, and longer retention time at lower pH. At pH 3 and pH ≥ 5, 1.63 mg and 1.54 mg $KMnO_4$ per mg Mn(II) were used, respectively for the oxidative precipitation of more than 99.7% Mn(II). Equilibrium was not attained at pH 3.0, which could be due to pH 3 being within the point of zero charge of manganese dioxide, which is the point of minimum stability where maximum coagulation and solubility of the colloids occurs. Low manganese oxidation in the very acidic medium could be a result of the reduction of permanganate to Mn(II) in accordance to the equilibrium reaction given in Equation 2.32 (Ladbury and Cullis (1958).

$$2MnO_4^- + 6H^+ \leftrightarrow 2Mn^{2+} + 3H_2O + 2.5O_2 \qquad 2.32$$

Studies on Mn(II) oxidation by permanganate pertain mainly to low manganese content solutions, which are typical concentrations in natural and drinking water and acid mine drainage (AMD) (Coughlin and Matsui, 1976, Willey and Jennings, 1963, Adams, 1960, Freitas et al., 2013). In high manganese and other metal ions concentrations, the effect of adsorption is more pronounced due to a larger amount of precipitate (Freitas et al., 2013) and the competitive adsorption of the ions (Murray et al., 1968, Murray, 1975b). It is, therefore, necessary to further investigate the removal of manganese by potassium permanganate especially in multi-element solutions, high in manganous ions such as leach solutions of nickel laterite ores.

2.5.8.2 The uptake of cations by manganese oxides and the effect on the removal of manganese from solution

The co-removal of other metal ions with manganese in oxidative precipitation is a common occurrence, evidenced by the composition of manganese minerals in soils, manganese bearing nodules and synthetic manganese oxides (Taylor et al., 1964, Spencer et al., 1972, Loganathan and Burau, 1973). The enrichment of manganese oxides with other metal ions, (alkali, alkali-earth and transition) is through co-precipitation and adsorption on the charged surface of the hydrous oxides by ion

exchange and surface complex formation (Morgan and Stumm, 1964). The uptake of alkali and alkali-earth metals is often lower than that of transition metals and has been found to be strongly dependent on pH at low concentrations but independent of pH at high concentrations (Murray et al., 1968). It is suggested that at low concentrations cations are adsorbed as counter ions on the oxide surface and at high concentration due to rapid precipitation the ions are incorporated in the lattice. Thus, isotherms such as the Langmuir adsorption isotherm can only describe the uptake of the various metal ions in manganese oxides at low concentrations and not high concentrations. Transition metal ions such as cobalt, copper, nickel and zinc exhibit high specific sorption potential with limited sorption at pzc (Murray, 1975b, Murray, 1975a, Murray et al., 1968, Loganathan and Burau, 1973).

The adsorption potential of ions of Li, Na, K, Ba, Ca, Co, Cu and Ni were investigated at 25 °C and pH values close to the pzc of manganese (II) manganite by Murray et al. (1968). It was noted that at above pH 3.0, the level of Ni(II) adsorption was similar to that of the alkali metal cations and less than a third the amount of Co(II) adsorbed. The sodium and potassium ions were easily desorbed from the manganese oxide at pH below the pzc, but desorption of cobalt, copper and nickel was difficult as they were much more strongly adsorbed. McKenzie (1970) studied the adsorption of cobalt, copper and nickel by synthetic manganese dioxides and found that there is a rapid uptake of the ions initially followed by a slow uptake of the ions with a release of manganese into solution and an excessive uptake of cobalt compared to other ions. In a subsequent study on the sorption of Ca, Co, Na and Zn on δ-MnO_2 at 24 °C and pH 4 by Loganathan and Burau (1973), the higher affinity for transition ions than the alkali and alkali-earth ions by manganese oxides was confirmed. In contrast to the sorption of sodium and calcium, the sorption of cobalt and zinc was accompanied by the release of manganese into solution. In a study on the interaction of various ions and manganese dioxide it was observed that the affinity of the metals for the oxide surface follows the order: Mg < Ca < Sr <Ba <Ni < Zn < Mn ≤ Co < Cu (Murray, 1975b) and readily hydrolysable metal ions are preferentially adsorbed on manganese oxide surfaces (Loganathan and Burau, 1973, Morgan and Stumm, 1964). In a recent study on the removal of Mn(II) and Fe(II) from synthetic ternary system [Fe(II)+Mn(II)+Ca(II)] and [Fe(II)+Mn(II)+Mg(II)] at pH 8.0 (Phatai et al., 2014), it was realised that the presence of Ca(II) and Mg(II) resulted in a decrease in the percent removal of Mn(II).

In general, the uptake of the other cations on manganese oxides reduces the percent removal of manganese It is suggested that the high sorption capacity of cupric ions is due to cupric ion hydrolysis and the formation of complexes which is known to enhance metal ion adsorption (Stumm and O'Melia, 1968, Murray, 1975b). For the marked sorption of cobalt at low pH values, significantly lower than those for significant divalent cobalt precipitation in bulk solution, it is argued by several authors that in addition to interchanging with the surface bound hydronium and manganous ion in the lattice structure, cobalt also interchanges with Mn(III) in the disordered layers of the oxide. Co(II) is oxidised to Co(III) at the water-solid interface by nearby Mn(IV) (Burns, 1976, Loganathan and Burau, 1973, McKenzie, 1970, Murray, 1975b, Murray, 1975a, Murray et al., 1968, Murray and Dillard, 1979), and the low spin Co(III) ions formed replaces the Mn(III) in the lattice structure according to crystal field theory (Murray and Dillard, 1979, Burns, 1976). Manganese ion in the oxide lattice structure is octahedrally coordinated by six negatively charged anions (Burns, 1976). Repulsion of the electrons in two of the five d-orbitals by the negatively charged anions excites them while the energy of the electrons in the other three orbitals is reduced. The electrons with higher energy destabilise the ion whereas those with reduced energy stabilise the ion (crystal field stabilisation energy). The crystal field stabilisation energies of Mn(III), Mn(II), Co(III), Co(II), Ni(II) and Cu(II) as calculated by McKenzie (1970) were found to be 35.9, 0, 45, 17.1, 29.3, and 22.2 kcal mol^{-1}, respectively. If divalent Mn is substituted by divalent ions of Co, Cu and Ni, there is a gain in crystal field stabilisation energy in the lattice as is also the case when trivalent Co is substituted for trivalent Mn. The cation-substituted crystal lattice with reduced total energy is more stable than the unsubstituted manganese oxides. Also, comparing the ionic radii of Co(III) (0.53 Å), Mn(II) (0.82 Å), Mn(III) (0.65 Å) and Mn(IV) (0.54 Å), isomorphous substitution is favourable for Co^{3+} and Mn^{4+} ions. The highly plausible explanation for the Mn(III) substitution with cobalt is that the adsorbed Co(II) is oxidised to Co(III) by electron transfer to Mn(IV) in the lattice.

The low levels of cobalt make it a challenge to investigate the nature and mechanism of cobalt removal from solution using routine techniques such as X-Ray Diffraction (XRD) and Scanning Electron Microscopy (SEM). During investigations using X-ray photoelectron spectroscopy (XPS) (Murray and Dillard, 1979) and X-ray absorption near-edge structure (XANES) (Kay et al., 2001) to analyse the surface of manganese

oxide and distinguish the oxidation state of the metals it was found that adsorbed cobalt was oxidised to trivalent cobalt. Considering the high sorption tendency of cobalt by manganese oxides, oxidative precipitation of manganese can be used similarly as the DSX process used in Bulong refinery plant to separate nickel and cobalt ahead of their recovery from the other impurities contained in solution downstream.

2.6 Precipitation (reactive crystallisation) theory

Precipitation is the reactive form of crystallisation, widely used as a separation and purification technique in the chemical industry (Mullin, 1972). During precipitation, solids are formed from solution and the precipitate quality, expressed in terms of particle size, purity and density are critical for the economics of the process. The quality of the product is largely dependent on the control of supersaturation, nucleation, crystal growth and secondary processes such as aggregation and agglomeration (Ajinkya and Ray, 1974).

2.6.1 Supersaturation

When the concentration of a solute in a solution is more than its equilibrium concentration (solubility limit), a solution is said to be supersaturated and such a state of the system can result in precipitation. Thus, supersaturation is the driving force for the precipitation process and is usually expressed as the supersaturation ratio (S) given by Equation 2.33.

$$S = \frac{\alpha}{\alpha^*} \qquad 2.33$$

, where α is the activity of the solute and α^* is the solute activity at equilibrium.

For solute A reacting with B to form compound A_aB_b according to Equation 2.34, the expression for the supersaturation ratio for this reaction is given by Equation 2.35. The activities of solutes are usually used for sparingly soluble compounds and are estimated using different procedures such as the Debye-Hückel method or the Pitzer model.

$$aA\ (aq) + bB\ (aq) \leftrightarrow AaBb\ (s) \quad (2.34)$$

$$S = \frac{\alpha_A^a \times \alpha_B^b}{\alpha_{A_{eq}}^a \times \alpha_{B_{eq}}^b} = \frac{\alpha_A^a \times \alpha_B^b}{K_{sp}} \quad (2.35)$$

, where K_{sp} is the solubility product of compound A_aB_b.

As the reaction given by Equation 2.34 proceeds, more of A_aB_b is formed and consequently clusters of A_aB_b are formed.

2.6.2 Nucleation

Nucleation according to the commonly used classical nucleation theory, is the process were molecules in a supersaturated solution interact to form a thermodynamically stable cluster of molecules referred to as nucleus or embryo. The formation of the nucleus from a clear solution is known as primary homogeneous nucleation and occurs in highly supersaturated solutions when the thermal equilibrium of a system is disturbed. The formation of a nucleus leads to a change in Gibbs free energy (ΔG) and the expression during homogeneous nucleation of a spherical nucleus with n molecules and radius, r is given by Equation 2.36.

$$\Delta G = -n\,kT\ln S + A\sigma \qquad z = \frac{4\pi r^3}{3v} \quad (2.36)$$

, where k is the Boltzmann constant (1.381×10^{-23} J K^{-1}), T is the temperature (K), S is the supersaturation ratio, A is the area of the cluster of molecules (m^2), and σ is the specific surface energy (Jm^{-2}). The first term is the volume free energy which is the drop in energy upon phase transition from liquid to solid and the second term is the free energy associated with the creation of a new surface. The Gibbs free energy passes a maximum, ΔG* at a critical cluster size z* (Figure 2.9), which is the nucleation barrier for solid formation.

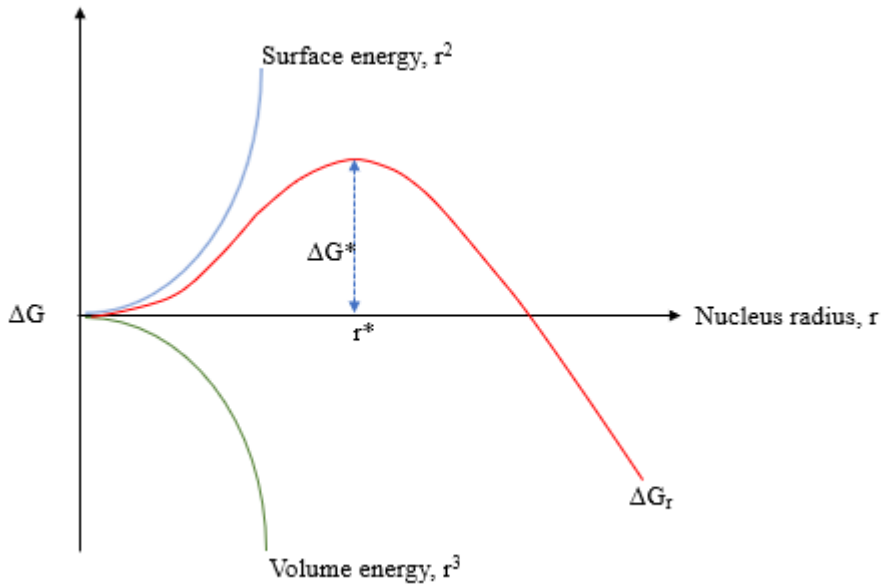

Figure 2.9: Change in Gibbs free energy during homogeneous nucleation (Mullin, 2001)

The critical cluster size is a metastable phase in equilibrium with the liquid phase, and when the nucleus grows through the addition of molecules, Gibbs free energy decreases, and the nuclei become more viable. The total number of nuclei formed in homogeneous nucleation depends on the rate of nucleation (J), defined as the number of new clusters formed per unit time per unit volume, calculated using the Arrhenius Equation 2.37, which gives the change in Gibbs free energy.

$$J = A \exp\left[\frac{-\Delta G^*}{kT}\right] \qquad \Delta G^* = \frac{16\pi\sigma^3\upsilon^2}{3(kT)^2 \ln S^2} \text{ (Gibbs Thompson equation)} \qquad 2.37$$

, where A is the pre-exponential kinetic factor ($m^{-3}s^{-1}$), ΔG* is the Gibbs free energy for the formation of the critical nucleus for spherical particles according to the Gibbs Thompson equation (Mullin, 1972). In industrial applications, homogeneous nucleation is rare due to the presence of solid surfaces, in the form of the wall of the container, process equipment and foreign particles which induces heterogeneous nucleation. The foreign surfaces reduce the energy barrier for the formation of the critical nucleus, which means that it occurs at a lower supersaturation than homogeneous nucleation as illustrated by Figure 2.10. Heterogeneous nucleation is somewhat almost similar to secondary nucleation which occurs in solutions containing the precipitating compound (seeding) (Mersmann, 2001; Stumm, 1992; Mullin, 1972). Seeding is used to suppress homogeneous nucleation and control product quality from supersaturated solutions in industry. It is fair to say that homogeneous nucleation and

heterogeneous nucleation cannot be isolated in industrial processes due to the inevitable presence of foreign bodies in the systems especially the equipment.

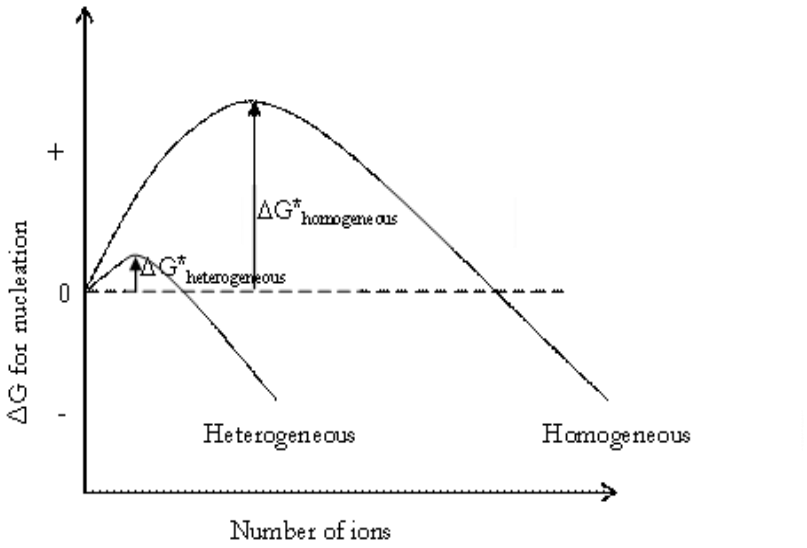

Figure 2.10: Change in Gibbs free energy for nucleation in the presence of solid (Stumm, 1992)

2.6.3 Crystal growth

Once thermodynamically stable nuclei are formed, the incorporation of ions or molecules on the existing crystal creates even bigger particles. The process involves the transport of growth units from the bulk solution through the diffusion layer, surface diffusion and integration of the units on the crystal faces. Thus, crystal growth can be diffusion or surface integration controlled depending on which step is the slowest (Mersmann, 2001). When growth is controlled by diffusion, the building blocks (growth units) diffuse from the bulk solution to the particle surface and are then incorporated into the crystal structure. For surface integration controlled growth, the mechanism of crystal enlargement depends on supersaturation and interface structure, which can be spiral, two-dimensional nucleation and rough growth on the steps and kinks found on crystal faces (Giulietti et al., 2001). At low supersaturation and smooth surfaces, growth units are incorporated at the steps created by dislocations on the crystal faces following a spiral pattern (Cubillas and Anderson, 2010). However, when supersaturation is increased to the critical value for nucleation, growth on smooth surfaces is by birth and spread (two-dimensional nucleation) which occurs through the formation of crystals on the crystal surface creating the steps and edges necessary for growth. At high supersaturations, rough growth takes over as the surface becomes

rough producing rounded surfaces. Secondary processes especially aggregation and breakage are involved in crystal growth and determine the particle size distribution of the final product.

Aggregation is prominent in systems with metal ions that undergo hydrolysis and polymerisation such as the formation of iron oxyhydroxides. When suspended in solution, iron oxide particles have a surface charge (electrical double layer) created by the hydroxide and hydrogen ion bound on the oxide surface. Cations and anions are sorbed onto the surface to maintain electroneutrality. The hydroxyl group on the surfaces of two polymers can undergo oxolation (Equation 2.32) to form bigger crystals and in the process hydrogen ions are released. The hydrogen ion released can reduce the surface charge of the particles to zero point of charge where particle repulsion is at its lowest favouring agglomeration of colloids (Cölfen and Mann, 2003).

2.6.4 Particle formation process

Particle formation processes can be inferred by tracking the evolution of the particle size using a number density n(L) function. Particle number density can be obtained from volume histogram particle distribution for a batch system using Equation 2.38 (Randolph and Larson, 1988).

$$n(L)dL = \sum_i \frac{(\%\,\text{Volume})_i \times \text{Concenstration}}{100} \times \frac{1}{k_v L^3} \qquad 2.38$$

,where k_v is the shape factor ($\pi/6$) when the particles are assumed spherical.

Precipitation is a complex process, especially when used in hydrometallurgical solutions where supersaturation control is difficult. Depending on the free energy of precipitation (that is nucleation, growth and transformation), the formation of precipitates can follow a one-step route or may proceed by a sequence of intermediate precipitates before reaching the most thermodynamically stable phase as shown in Figure 2.11 (Cölfen and Mann, 2003). When kinetic control dominates as is the case with most systems, based on Stranski's rule and the Ostwald ripening, phases with the closest free energy to the initial state are formed first and are usually the amorphous phases (Karthika et al., 2016). The precipitation of ferric ion from laterite leach solutions is a typical example of a kinetically controlled process. Amorphous ferric hydroxide is often formed first followed by transformation to more crystalline phases as depicted in the following sequence (Blesa and Matijević, 1989).

$Fe^{3+} \rightarrow (Fe_pO_r(OH)_s^{3p-(2r+s)})/ (Fe_p(OH)_q^{3p-q} \rightarrow$ Ferrihydrite/Amorphous $Fe(OH)_3 \rightarrow$ Goethite

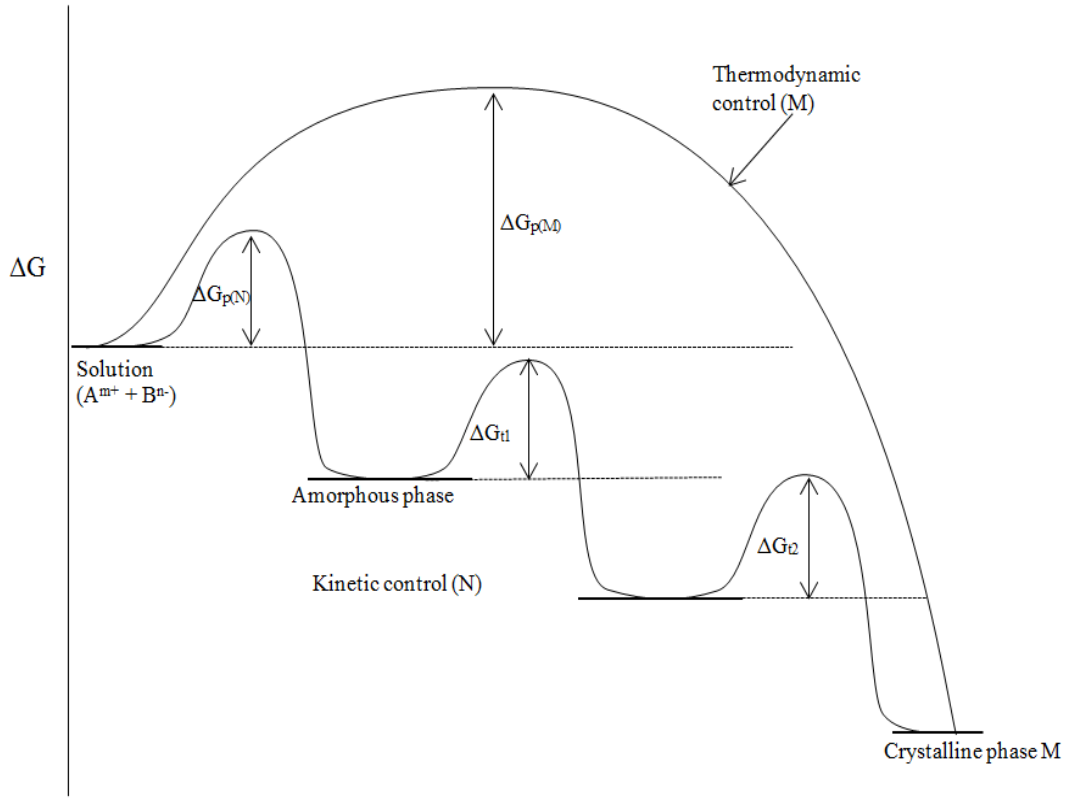

Figure 2.11: Precipitation routes for the precipitation of crystalline compound M under thermodynamic and kinetic control. Precipitation (p) of M in one step is route M while route N is precipitation of M via the initial formation of amorphous phase N and its transformation (t) to crystalline phase M after Cölfen and Mann (2003).

2.7 Summary

The future of the nickel industry is in the hydrometallurgical processing of low-grade nickel laterite ores using AL, HP and HPAL, given that high grade nickel sulfide and laterite ores are fast depleting. Nickel laterite sulfate leach solutions contain various other metal ions as impurities which must be removed preceding the recovery of nickel and cobalt in downstream processing. Although all impurities must be removed and separated from nickel and cobalt, the removal of iron, aluminium chromium and manganese is arguably the most crucial and challenging steps in the purification of nickel and cobalt solutions.

Iron, aluminium and chromium are removed from solution ahead of all the other impurities by hydroxide precipitation following leaching of the ore. Iron precipitation

processes, Goethite, Jarosite and Haematite Process are used, which offer varying advantages. Both jarosite and goethite precipitation have lower capital expenditure compared to haematite precipitation. The advantage of using Goethite to Jarosite Process is allegedly the production of stable and low volume goethite. The literature review indicated that iron residue formed during the processing of laterite solutions using the Goethite Process are rarely goethite but instead are often a mixture of amorphous iron oxyhydroxide and poorly ordered metastable phases, ferrihydrite and schwertmannite. Even without the control of ferric ion concentration and the addition of jarosite-forming cations, effective iron removal is achieved under atmospheric conditions through goethite and jarosite precipitation. The removal of iron, aluminium and chromium by precipitation is associated with nickel and cobalt losses in the different iron precipitation processes. Nickel and cobalt losses and the nature of the precipitates is related to factors affecting iron precipitation such as pH, temperature, co-existence of the impurities and the concentration of iron.

The extent of nickel and cobalt losses can be minimised through manipulating the precipitation parameters and using a multistage precipitation process with the right combination of process parameters. The use of high pH during precipitation is inevitable because of aluminium even when all iron in solution is in the ferric ion state. Ferrous ion is effectively removed by oxidative precipitation at the favourable conditions for aluminium precipitation when using air and oxygen. The removal of ferrous ion can be easily achieved in acidic conditions using hydrogen peroxide were nickel, and cobalt incorporation in the precipitate is minimal.

Once iron, aluminium and chromium are removed from laterite leach solutions, the removal and separation of manganese from nickel and cobalt is the major challenge, signified by the absence of a clear preferred processing route. Different processes including MHP, MSP and SX are used, with the choice of the process influenced by the desired end product and process factors such as selectivity, cost of operation, personnel safety and environmental concerns. Precipitation is a straightforward process unlike solvent extraction, which explains the wide application of both MSP and MHP. MSP has high selectivity for nickel and cobalt over manganese, and the capital and operational cost are comparable to that of MHP. The use of hydrogen sulfide is associated with safety and environmental concerns making the process less attractive. The selectivity of MHP is relatively low. The literature review indicated

that manganese removal and separation from nickel and cobalt solutions could be effected using oxidative precipitation. However, cobalt is co-precipitated and incorporated in significant amounts.

Based on the literature review findings, it is clear that there is a need to study further, iron precipitation in multi-element sulfate solutions simulating real nickel laterite sulfate leach solutions and the associated nickel and cobalt losses. This must include solutions containing both ferrous and ferric ion, which means the investigation into oxidative precipitation using different oxidants. Secondly, there is a need to study the applicability of oxidative precipitation as an alternative downstream process for separating nickel, cobalt and manganese following iron, aluminium and chromium precipitation.

References

ABDUS-SALAM, N. & CIVER, F. 2012. Synthesis, Characterization and Application of 2-Line and 6-Line Ferrihydrite to Pb(II) Removal from Aqueous Solution. *Journal of Applied Science & Environmental Management,* 16**,** 327-336.

ACERO, P., AYORA, C., TORRENTÓ, C. & NIETO, J.-M. 2006. The behavior of trace elements during schwertmannite precipitation and subsequent transformation into goethite and jarosite. *Geochimica et Cosmochimica Acta,* 70**,** 4130-4139.

ADAMS, M., VAN DER MEULEN, D., CZERNY, C., ADAMINI, P., TURNER, J., JAYASEKERA, S., AMARANTI, J., MOSHER, J., MILLER, M. & WHITE, D. Piloting of the beneficiation and EPAL circuits for Ravensthorpe nickel operations. International Laterite Nickel Symposium 2004(as held during the 2004 TMS Annual Meeting), 2004. 193-202.

ADAMS, R. B. 1960. Manganese removal by oxidation with potassium permanganate. *Journal (American Water Works Association),* 52**,** 219-228.

AGATZINI-LEONARDOU, S., TSAKIRIDIS, P. E., OUSTADAKIS, P., KARIDAKIS, T. & KATSIAPI, A. 2009. Hydrometallurgical process for the separation and recovery of nickel from sulphate heap leach liquor of nickeliferrous laterite ores. *Minerals Engineering,* 22**,** 1181-1192.

AJINKYA, M. B. & RAY, W. H. 1974. ON THE OPTIMAL OPERATION OF CRYSTALLIZATION PROCESSES. *Chemical Engineering Communications,* 1**,** 181-186.

ALLAN, R., HAIGH, C. & HAMDORF, C. 1970. An improved method of removing dissolved ferric iron from iron-bearing solutions. *Australian Patent,* 424.

BABCAN, J. 1971. Synthesis of jarosite, KFe3 (SO4) 2 (OH) 6. *Geol. Zb,* 22**,** 299-304.

BAES, C. F. & MESMER, R. E. 1976. *Hydrolysis of cations,* Wiley.

BARB, W., BAXENDALE, J., GEORGE, P. & HARGRAVE, K. 1951a. Reactions of ferrous and ferric ions with hydrogen peroxide. Part II.—The ferric ion reaction. *Transactions of the Faraday Society,* 47**,** 591-616.

BARB, W. G., BAXENDALE, J. H., GEORGE, P. & HARGRAVE, K. R. 1951b. Reactions of ferrous and ferric ions with hydrogen peroxide. Part I.-The ferrous ion reaction. *Transactions of the Faraday Society,* 47**,** 462-500.

BARNUM, D. W. 1983. Hydrolysis of cations. Formation constants and standard free energies of formation of hydroxy complexes. *Inorganic Chemistry,* 22**,** 2297-2305.

BERGER, V. I., SINGER, D. A., BLISS, J. D. & MORING, B. C. 2011. *Ni-Co laterite deposits of the world: Database and grade and tonnage models,* US Department of the Interior, Geological Survey.

BERNSTEIN, L. R. & WAYCHUNAS, G. A. 1987. Germanium crystal chemistry in hematite and goethite from the Apex Mine, Utah, and some new data on germanium in aqueous solution and in stottite. *Geochimica et Cosmochimica Acta,* 51**,** 623-630.

BIGHAM, J. & NORDSTROM, D. K. 2000. Iron and aluminum hydroxysulfates from acid sulfate waters. *Reviews in mineralogy and geochemistry,* 40**,** 351-403.

BIGHAM, J., SCHWERTMANN, U., CARLSON, L. & MURAD, E. 1990. A poorly crystallized oxyhydroxysulfate of iron formed by bacterial oxidation of Fe (II) in acid mine waters. *Geochimica et Cosmochimica Acta,* 54**,** 2743-2758.

BIGHAM, J. M., SCHWERTMANN, U., TRAINA, S. J., WINLAND, R. L. & WOLF, M. 1996. Schwertmannite and the chemical modeling of iron in acid sulfate waters. *Geochimica et Cosmochimica Acta,* 60**,** 2111-2121.

BLESA, M. A. & MATIJEVIĆ, E. 1989. Phase transformations of iron oxides, oxohydroxides, and hydrous oxides in aqueous media. *Advances in Colloid and Interface Science,* 29**,** 173-221.

BOTTERO, J.-Y., MANCEAU, A., VILLIERAS, F. & TCHOUBAR, D. 1994. Structure and mechanisms of formation of FeOOH (Cl) polymers. *Langmuir,* 10**,** 316-319.

BRAND, N., BUTT, C. & ELIAS, M. 1998. Nickel laterites: classification and features.

BURNS, R. G. 1976. The uptake of cobalt into ferromanganese nodules, soils, and synthetic manganese (IV) oxides. *Geochimica et Cosmochimica Acta,* 40**,** 95-102.

BURTON, E. D., BUSH, R. T., SULLIVAN, L. A. & MITCHELL, D. R. 2008. Schwertmannite transformation to goethite via the Fe (II) pathway: reaction rates and implications for iron–sulfide formation. *Geochimica et Cosmochimica Acta,* 72**,** 4551-4564.

BUTT, C. R. & CLUZEL, D. 2013. Nickel laterite ore deposits: weathered serpentinites. *Elements,* 9**,** 123-128.

BÜYÜKAKINCI, E. & TOPKAYA, Y. A. 2009. Extraction of nickel from lateritic ores at atmospheric pressure with agitation leaching. *Hydrometallurgy,* 97**,** 33-38.

CARLSON, E. & SIMONS, C. 1960. Acid leaching Moa Bay's nickel. *JOM,* 12**,** 206-213.

CARLSON, L. & SCHWERTMANN, U. 1981. Natural ferrihydrites in surface deposits from Finland and their association with silica. *Geochimica et Cosmochimica Acta,* 45**,** 421-429.

CARVALHO-E-SILVA, M. L., RAMOS, A. Y., TOLENTINO, H. C. N., ENZWEILER, J., NETTO, S. M. & DO CARMO MARTINS ALVES, M. 2003. Incorporation of Ni into natural goethite: An investigation by X-ray absorption spectroscopy. *American Mineralogist,* 88**,** 876-882.

CHANG, Y., ZHAI, X., LI, B. & FU, Y. 2010. Removal of iron from acidic leach liquor of lateritic nickel ore by goethite precipitate. *Hydrometallurgy,* 101**,** 84-87.

CHENG, T. C., DEMOPOULOS, G. P., SHIBACHI, Y. & MASUDA, H. 2003. The precipitation chemistry and performance of the Akita hematite process—an integrated laboratory and industrial scale study. *Electrometallurgy and Environmental Hydrometallurgy, Volume 2***,** 1657-1674.

CHER, M. & DAVIDSON, N. 1955. The Kinetics of the Oxygenation of Ferrous Iron in Phosphoric Acid Solution. *Journal of the American Chemical Society,* 77**,** 793-798.

CHOU, E. C., QUENEAU, P. B. & RICKARD, R. S. 1977. Sulfuric acid pressure leaching of nickeliferous limonites. *Metallurgical Transactions B,* 8**,** 547-554.

CHUKHOV, F., ZVYAGIN, B., GORSHKOV, A., YERMILOVA, L. & BALASHOVA, V. 1974. Ferrihydrite. *International Geology Review,* 16**,** 1131-1143.

CLAASSEN, J. O., MEYER, E. H. O., RENNIE, J. & SANDENBERGH, R. F. 2002. Iron precipitation from zinc-rich solutions: defining the Zincor Process. *Hydrometallurgy,* 67**,** 87-108.

CLAASSEN, J. O. & SANDENBERGH, R. F. 2007. Influence of temperature and pH on the quality of metastable iron phases produced in zinc-rich solutions. *Hydrometallurgy,* 86**,** 178-190.

CÖLFEN, H. & MANN, S. 2003. Higher‐order organization by mesoscale self‐assembly and transformation of hybrid nanostructures. *Angewandte Chemie International Edition,* 42**,** 2350-2365.

CORNELL, R. & GIOVANOLI, R. 1987. Effect of manganese on the transformation of ferrihydrite into goethite and jacobsite in alkaline media. *Clays and Clay Minerals,* 35**,** 11-20.

CORNELL, R. & GIOVANOLI, R. 1989. Effect of cobalt on the formation of crystalline iron oxides from ferrihydrite in alkaline media. *Clays and Clay Minerals,* 37**,** 65-70.

CORNELL, R., GIOVANOLI, R. & SCHNEIDER, W. 1990. Effect of cysteine and manganese on the crystallization of noncrystalline iron (III) hydroxide at pH 8. *Clays and Clay Minerals,* 38**,** 21-28.

CORNELL, R. M., GIOVANOLI, R. & SCHNEIDER, W. 1989. Review of the hydrolysis of iron (III) and the crystallization of amorphous iron (III) hydroxide hydrate. *Journal of Chemical Technology and Biotechnology,* 46**,** 115-134.

CORNELL, R. M., SCHNEIDER, W. & GIOVANOLI, R. 1992. The Effect of Nickel on the Conversion of Amorphous Iron(III) Hydroxide into more Crystalline Iron Oxides in Alkaline Media. *Journal of Chemical Technology & Biotechnology,* 53**,** 73-79.

CORNELL, R. M. & SCHWERTMANN, U. 2003. *The iron oxides: structure, properties, reactions, occurrences and uses,* John Wiley & Sons.

COUGHLIN, R. W. & MATSUI, I. 1976. Catalytic oxidation of aqueous Mn(II). *Journal of Catalysis,* 41**,** 108-123.

CUBEDDU, F., PIASENTIN, M., REILLY, F., MEREGALLI, L. & TOLOMIO, M. 1996. The paragoethite process at the ENIRISORSE--Porto Vesme plant. *Iron Control and Disposal***,** 147-161.

CUBILLAS, P. & ANDERSON, M. W. 2010. Synthesis mechanism: crystal growth and nucleation. *Zeolites and Catalysis: Synthesis, Reactions and Applications***,** 1-55.

CUDENNEC, Y. & LECERF, A. 2006. The transformation of ferrihydrite into goethite or hematite, revisited. *Journal of Solid State Chemistry,* 179**,** 716-722.

DALVI, A. D., W., G. B. & OSBORNE, R. C. 2004. The Past and the Future of Nickel Laterites. *PDAC 2004 International Convention.*

DANIELE, P. G., RIGANO, C., SAMMARTANO, S. & ZELANO, V. 1994. Ionic strength dependence of formation constants—XVIII. The hydrolysis of iron(III) in aqueous KNO3 solutions. *Talanta,* 41**,** 1577-1582.

DAVEY, P. T. & SCOTT, T. R. 1976. Removal of iron from leach liquors by the "Goethite" process. *Hydrometallurgy,* 2**,** 25-33.

DAVISON, W. & SEED, G. 1983. The kinetics of the oxidation of ferrous iron in synthetic and natural waters. *Geochimica et Cosmochimica Acta,* 47**,** 67-79.

DE CARVALHO-E-SILVA, M. L. M., PARTITI, C. S. M., ENZWEILER, J., PETIT, S., NETTO, S. M. & DE OLIVEIRA, S. M. B. 2002. Characterization of Ni-Containing Goethites by Mössbauer Spectroscopy and Other Techniques. *Hyperfine Interactions,* 141**,** 559-576.

DONEGAN, S. 2006. Direct solvent extraction of nickel at Bulong operations. *Minerals Engineering,* 19**,** 1234-1245.

DOUSMA, J. & DE BRUYN, P. L. 1976. Hydrolysis-precipitation studies of iron solutions. I. Model for hydrolysis and precipitation from Fe(III) nitrate solutions. *Journal of Colloid and Interface Science,* 56**,** 527-539.

DRY, M., IRIO, G., JACOBS, D., COLE, P., FEATHER, A., SOLE, K., ENGELBRECHT, J., MATCHETT, K., CILLIERS, P. & O'KANE, P. Cu/Co Tailings Treatment Project, Democratic Republic of Congo. ALTA Nickel/Cobalt Conference, 1998.

DUTRIZAC, J. Jarosite-type compounds and their application in the metallurgical industry. JOURNAL OF METALS, 1982. MINERALS METALS MATERIALS SOC 420 COMMONWEALTH DR, WARRENDALE, PA 15086, A70-A70.

DUTRIZAC, J. 1987. An overview of iron precipitation in hydrometallurgy. *Crystallization and Precipitation, Eds., GL Strathdee, MO Klein and LA Melis***,** 259-283.

DUTRIZAC, J. & CHEN, T. 2004. Factors affecting the incorporation of cobalt and nickel in jarosite-type compounds. *Canadian metallurgical quarterly,* 43**,** 305-319.

DUTRIZAC, J. & DINARDO, O. 1983. The co-precipitation of copper and zinc with lead jarosite. *Hydrometallurgy,* 11**,** 61-78.

DUTRIZAC, J. E. 1983. Factors affecting alkali jarosite precipitation. *Metallurgical Transactions B,* 14**,** 531-539.

DUTRIZAC, J. E. 1999. The effectiveness of jarosite species for precipitating sodium jarosite. *JOM,* 51**,** 30-32.

DUTRIZAC, J. E. & JAMBOR, J. L. 2000. Jarosites and their application in hydrometallurgy. *Reviews in Mineralogy and Geochemistry,* 40**,** 405-452.

EGGLETON, R. A. & FITZPATRICK, R. W. 1988. NEW DATA AND A REVISED STRUCTURAL MODEL FOR FERRIHYDRITE. *Clays and Clay Minerals,* 36**,** 111-124.

ELIAS, M. 2002. Nickel laterite deposits-geological overview, resources and exploitation. *Giant ore deposits: Characteristics, genesis and exploration. CODES Special Publication,* 4**,** 205-220.

ELIAS, M., DONALDSON, M. & GIORGETTA, N. 1981. Geology, mineralogy, and chemistry of lateritic nickel-cobalt deposits near Kalgoorlie, Western Australia. *Economic Geology,* 76**,** 1775-1783.

FEITKNECHT, W., GIOVANOLI, R., MICHAELIS, W. & MÜLLER, M. 1973. Über die Hydrolyse von Eisen(III)Salzlösungen. I. Die Hydrolyse der Lösungen von Eisen(III)chlorid. *Helvetica Chimica Acta,* 56**,** 2847-2856.

FLYNN, C. M. 1984. Hydrolysis of inorganic iron(III) salts. *Chemical Reviews,* 84**,** 31-41.

FLYNN, C. M. 1990. Dense hydrolysis products from iron (III) nitrate and sulfate solutions. *Hydrometallurgy,* 25**,** 257-270.

FRAMPTON, G. & BURATTO, R. 'Experiences during early commissioning of the Bulong nickel operation. Proceedings ALTA 1999 Nickel/Cobalt Pressure Leaching and Hydrometallurgy Forum, 1999.

FREITAS, R. M., PERILLI, T. A. & LADEIRA, A. C. Q. 2013. Oxidative Precipitation of Manganese from Acid Mine Drainage by Potassium Permanganate. *Journal of Chemistry,* 2013.

GEORGIOU, D. & PAPANGELAKIS, V. G. 1998. Sulphuric acid pressure leaching of a limonitic laterite: chemistry and kinetics. *Hydrometallurgy,* 49**,** 23-46.

GIOVANOLI, R. & CORNELL, R. M. 1992. Crystallization of Metal Substituted Ferrihydrites. *Zeitschrift für Pflanzenernährung und Bodenkunde,* 155**,** 455-460.

GIULIETTI, M., SECKLER, M., DERENZO, S., RÉ, M. & CEKINSKI, E. 2001. Industrial crystallization and precipitation from solutions: state of the technique. *Brazilian Journal of Chemical Engineering,* 18**,** 423-440.

GOLIGHTLY, J. 1981. Nickeliferous laterite deposits. *Economic Geology,* 75**,** 710-735.

GORDON, A. R. & PICKERING, R. W. 1975. Improved leaching technologies in the electrolytic zinc industry. *Metallurgical and Materials Transactions B,* 6**,** 43-53.

GREEGOR, R. B., PINGITORE, N. E. & LYTLE, F. W. 1997. Strontianite in coral skeletal aragonite. *Science,* 275**,** 1452-1454.

GUISE, L. & CASTRO, F. 1996. Iron, aluminum and chromium co-elimination by hydrolytic precipitation from nickel and cobalt containing sulphuric acid solutions. *Iron Control and Disposal***,** 275-286.

GUPTA, C. K. & MUKHERJEE, T. 1990. *Hydrometallurgy in extraction processes,* CRC press.

HABER, F. & WEISS, J. 1934. The Catalytic Decomposition of Hydrogen Peroxide by Iron Salts. *Proceedings of the Royal Society of London A: Mathematical, Physical and Engineering Sciences,* 147**,** 332-351.

HARVEY, R., HANNAH, R. & VAUGHAN, J. 2011. Selective precipitation of mixed nickel–cobalt hydroxide. *Hydrometallurgy,* 105**,** 222-228.

HEALY, T. W., HERRING, A. P. & FUERSTENAU, D. W. 1966. The effect of crystal structure on the surface properties of a series of manganese dioxides. *Journal of Colloid and Interface Science,* 21**,** 435-444.

HELM, D. J. 2004. *Surface and interfacial precipitations in the direct solvent extraction of nickel and cobalt / Daniel John Helm.* Thesis (Ph. D.)--Curtin University of Technology.

HEM, J. D. 1963. Chemical equilibria and rates of manganese oxidation. *Water Supply Paper.* - ed.

HERNANDEZ, O. Y. C., MULLER, H., REYNOLDS, G. & LIU, H. 2014. Nickel recovery from a high ferrous content laterite ore. Google Patents.

HUFFMAN, R. E. & DAVIDSON, N. 1956. Kinetics of the ferrous iron-oxygen reaction in sulfuric acid solution. *Journal of the American Chemical Society,* 78**,** 4836-4842.

JAMBOR, J. L. & DUTRIZAC, J. E. 1998. Occurrence and constitution of natural and synthetic ferrihydrite, a widespread iron oxyhydroxide. *Chemical Reviews,* 98**,** 2549-2586.

JHA, M. C., WICKER, G. R. & MEYER, G. A. 1978. Selective precipitation of nickel and cobalt sulfides from acidic sulfate solution. Google Patents.

JOHNSTON, J. H. & LEWIS, D. G. 1983. A detailed study of the transformation of ferrihydrite to hematite in an aqueous medium at 92°C. *Geochimica et Cosmochimica Acta,* 47**,** 1823-1831.

JOLIVET, J.-P., CHANÉAC, C. & TRONC, E. 2004. Iron oxide chemistry. From molecular clusters to extended solid networks. *Chemical Communications***,** 481-483.

JONES, A. M., GRIFFIN, P. J., COLLINS, R. N. & WAITE, T. D. 2014. Ferrous iron oxidation under acidic conditions–The effect of ferric oxide surfaces. *Geochimica et Cosmochimica Acta,* 145**,** 1-12.

KAO, C., HUANG, K., WANG, J., CHEN, T. & CHIEN, H. 2008. Application of potassium permanganate as an oxidant for in situ oxidation of trichloroethylene-contaminated groundwater: a laboratory and kinetics study. *Journal of Hazardous Materials,* 153**,** 919-927.

KARTHIKA, S., RADHAKRISHNAN, T. & KALAICHELVI, P. 2016. A review of classical and nonclassical nucleation theories. *Crystal Growth & Design,* 16**,** 6663-6681.

KASKIALA, T. 2005. *Studies on gas-liquid mass transfer in atmospheric leaching of sulphidic zinc concentrates,* Helsinki University of Technology.

KAY, J. T., CONKLIN, M. H., FULLER, C. C. & O'DAY, P. A. 2001. Processes of Nickel and Cobalt Uptake by a Manganese Oxide Forming Sediment in Pinal Creek,

Globe Mining District, Arizona. *Environmental Science & Technology,* 35**,** 4719-4725.

KING, D. W. 1998. Role of Carbonate Speciation on the Oxidation Rate of Fe(II) in Aquatic Systems. *Environmental Science & Technology,* 32**,** 2997-3003.

KÖSE, C. H. & TOPKAYA, Y. A. 2011. Hydrometallurgical processing of nontronite type lateritic nickel ores by MHP process. *Minerals Engineering,* 24**,** 396-415.

KYLE, J. 2010. Nickel laterite processing technologies – where to next? . *ALTA 2010 Nickel/Cobalt/Copper Conference,*. Perth, Western Australia.

LADBURY, J. & CULLIS, C. 1958. Kinetics and mechanism of oxidation by permanganate. *Chemical Reviews,* 58**,** 403-438.

LAMB, A. B. & ELDER, L. W. 1931. The electromotive activation of oxygen. *Journal of the American Chemical Society,* 53**,** 137-163.

LEWIS, D. & SCHWERTMANN, U. 1979. The influence of Al on iron oxides. Part III. Preparation of Al-goethites in KOH. *Clay Miner,* 14**,** 115-126.

LIN, C., SMITH, F., ICHIKAWA, N., BABA, T. & ITOW, M. 1991. Decomposition of hydrogen peroxide in aqueous solutions at elevated temperatures. *International journal of chemical kinetics,* 23**,** 971-987.

LOAN, M., NEWMAN, O. M. G., COOPER, R. M. G., FARROW, J. B. & PARKINSON, G. M. 2006. Defining the Paragoethite process for iron removal in zinc hydrometallurgy. *Hydrometallurgy,* 81**,** 104-129.

LOAN, M., PIERRE, T. S., PARKINSON, G., NEWMAN, O. & FARROW, J. 2002. Identifying nanoscale ferrihydrite in hydrometallurgical residues. *JOM,* 54**,** 40-43.

LOAN, M., RICHMOND, W. R. & PARKINSON, G. M. 2005. On the crystal growth of nanoscale schwertmannite. *Journal of Crystal Growth,* 275**,** e1875-e1881.

LOGANATHAN, P. & BURAU, R. 1973. Sorption of heavy metal ions by a hydrous manganese oxide. *Geochimica et Cosmochimica Acta,* 37**,** 1277-1293.

LOVEDAY, B. K. 2008. The use of oxygen in high pressure acid leaching of nickel laterites. *Minerals Engineering,* 21**,** 533-538.

LOWSON, R. T. 1982. Aqueous oxidation of pyrite by molecular oxygen. *Chemical reviews,* 82**,** 461-497.

LUTHER, G. 1990. The frontier-molecular-orbital theory approach in geochemical processes.

MANCEAU, A., SCHLEGEL, M. L., MUSSO, M., SOLE, V. A., GAUTHIER, C., PETIT, P. E. & TROLARD, F. 2000. Crystal chemistry of trace elements in natural and synthetic goethite. *Geochimica et Cosmochimica Acta,* 64**,** 3643-3661.

MANCHOT, W. & LEHMANN, G. 1928. Über die Einwirkung von Hydroperoxyd auf Ferrosalz (Studien über die Oxydationsvorgänge). *Justus Liebigs Annalen der Chemie,* 460**,** 179-201.

MANSON, P., GROUTSCH, J., MAYZE, R. & WHITE, D. 1997. Process development and plant design for the Cawse nickel project. *ALTA Metallurgical Service, Perth, Western Australia*.

MAYHEW, K., MEAN, R., O'CONNOR, L. & WILLIAMS, T. 2009. Nickel and cobalt recovery from Mesaba concentrate. *Proceedings ALTA 2009 Nickel Cobalt*.

MAYZE, R. An engineering comparison of the three treatment flowsheets in WA nickel laterite projects. Proceedings ALTA Nickel/Cobalt Pressure Leaching & Hydrometallurgy Forum, 1999.

MCBAIN, J. W. 1900. Oxidation of Ferrous Solutions by Free Oxygen. *The Journal of Physical Chemistry*, 5**,** 623-638.

MCKENZIE, R. 1970. The reaction of cobalt with manganese dioxide minerals. *Soil Research,* 8**,** 97-106.

MEDALIA, A. I. & KOLTHOFF, I. M. 1949. Redox recipes. I. Reaction between ferrous iron and peroxides. General considerations. *Journal of Polymer Science*, 4**,** 377-398.

MERSMANN, A. 2001. *Crystallization technology handbook,* CRC Press.

MEYER, E. H. O., HOWARD, G., HEAGELE, R. & BECK, R. D. 1996. Iron control and removal at the Zinc Corporation of South Africa. *Iron Control and Disposal***,** 163 - 182.

MIHAYLOV, I. 2003. Solvent extractants for nickel and cobalt: new opportunities in aqueous processing. *JOM,* 55**,** 38-42.

MIHAYLOV, I., KRAUSE, E., COLTON, D., OKITA, Y., DUTERQUE, J.-P. & PERRAUD, J.-J. 2000. The development of a novel hydrometallurgical process for nickel and cobalt recovery from Goro laterite ore. *CIM bulletin,* 93**,** 124-130.

MILLERO, F. J. 1985. The effect of ionic interactions on the oxidation of metals in natural waters. *Geochimica et Cosmochimica Acta*, 49**,** 547-553.

MILLERO, F. J., SOTOLONGO, S. & IZAGUIRRE, M. 1987. The oxidation kinetics of Fe(II) in seawater. *Geochimica et Cosmochimica Acta,* 51**,** 793-801.

MISAWA, T., HASHIMOTO, K. & SHIMODAIRA, S. 1974. The mechanism of formation of iron oxide and oxyhydroxides in aqueous solutions at room temperature. *Corrosion Science,* 14**,** 131-149.

MONHEMIUS, A. 1977. Precipitation diagrams for metal-hydroxides, sulfides, arsenates and phosphates. *Transactions of the Institution of Mining and Metallurgy Section C-Mineral Processing and Extractive Metallurgy,* 86**,** C202-C206.

MORGAN, J. J. & STUMM, W. 1964. Colloid-chemical properties of manganese dioxide. *Journal of Colloid Science,* 19**,** 347-359.

MOTTERAM, G., RYAN, M., BEREZOWSKY, R. & RAUDSEPP, R. Murrin-Murrin Nickel/Cobalt Project-Project Development Overview. Nickel and Cobalt Pressure Leaching and Hydrometallurgy Forum, Alta Metallurgical Service, Perth, Western Australia, 1996.

MULLIN, J. W. 1972. *Crystallisation,* CRC press.

MULLIN, J. W. 2001. *Crystallization*, Elsevier.

MURAD, E. 1994. Schwertmannite, a new iron oxyhydroxy-sulphate from Pyhasalmi, Finland, and other localities. *Mineralogical Magazine,* 58**,** 641-648.

MURRAY, D., HEALY, T. & FUERSTENAU, D. 1968. The adsorption of aqueous metal on colloidal hydrous manganese oxide. ACS Publications.

MURRAY, J. W. 1975a. The interaction of cobalt with hydrous manganese dioxide. *Geochimica et Cosmochimica Acta,* 39**,** 635-647.

MURRAY, J. W. 1975b. The interaction of metal ions at the manganese dioxide-solution interface. *Geochimica et Cosmochimica Acta,* 39**,** 505-519.

MURRAY, J. W. & DILLARD, J. G. 1979. The oxidation of cobalt(II) adsorbed on manganese dioxide. *Geochimica et Cosmochimica Acta,* 43**,** 781-787.

O'CALLAGHAN, J. Process improvements at Bulong Operations Pty Ltd. Proceedings of the ALTA Nickel/Cobalt Conference 2003, 2003.

ÖNAL, M. A. R. & TOPKAYA, Y. A. 2014. Pressure acid leaching of Çaldağ lateritic nickel ore: An alternative to heap leaching. *Hydrometallurgy,* 142**,** 98-107.

ONOZAKI, A., SATO, K. & KURAMOCHI, S. 1986. Effect of some impurities on iron precipitation at the Iijima Zinc Refinery. *Iron Control in Hydrometallurgy***,** 742-752.

OUSTADAKIS, P., AGATZINI-LEONARDOU, S. & TSAKIRIDIS, P. E. 2006. Nickel and cobalt precipitation from sulphate leach liquor using MgO pulp as neutralizing agent. *Minerals Engineering,* 19**,** 1204-1211.

PAPANGELAKIS, V., BLAKEY, B. & LIAO, H. 1994. Hematite solubility in sulphate process solutions. *Hydrometallurgy'94.* Springer.

PARK, B. & DEMPSEY, B. A. 2005. Heterogeneous oxidation of Fe (II) on ferric oxide at neutral pH and a low partial pressure of O2. *Environmental science & technology,* 39**,** 6494-6500.

PEDERSEN, H. D., POSTMA, D., JAKOBSEN, R. & LARSEN, O. 2005. Fast transformation of iron oxyhydroxides by the catalytic action of aqueous Fe(II). *Geochimica et Cosmochimica Acta,* 69**,** 3967-3977.

PESIC, B., OLIVER, D. & WICHLACZ, P. 1989. An electrochemical method of measuring the oxidation rate of ferrous to ferric iron with oxygen in the presence of Thiobacillus ferrooxidans. *Biotechnology and Bioengineering,* 33**,** 428-439.

PHATAI, P., WITTAYAKUN, J., CHEN, W.-H., FUTALAN, C. M., GRISDANURAK, N. & KAN, C.-C. 2014. Removal of manganese(II) and iron(II) from synthetic groundwater using potassium permanganate. *Desalination and Water Treatment,* 52**,** 5942-5951.

RANDOLPH, A. D. & LARSON, M. A. 1988. *Theory of particulate process: analysis and techniques of continuous crystallization*, Academic Press.

REEDER, R. J., LAMBLE, G. M. & NORTHRUP, P. A. 1999. XAFS study of the coordination and local relaxation around Co2+, Zn2+, Pb2+, and Ba2+ trace elements in calcite. *American Mineralogist,* 84**,** 1049-1060.

RICKELTON, W. 1992. Novel uses for thiophosphinic acids in solvent extraction. *JoM,* 44**,** 52-54.

ROCCARO, P., BARONE, C., MANCINI, G. & VAGLIASINDI, F. G. A. 2007. Removal of manganese from water supplies intended for human consumption: a case study. *Desalination,* 210**,** 205-214.

ROSATO, L. & AGNEW, M. 1996. Iron disposal options at Canadian electrolytic zinc. *Iron Control and Disposal***,** 77-89.

RUBISOV, D. H. & PAPANGELAKIS, V. G. 2000. Sulphuric acid pressure leaching of laterites - speciation and prediction of metal solubilities `at temperature'. *Hydrometallurgy,* 58**,** 13-26.

RUBY, C., GÉHIN, A., ABDELMOULA, M., GÉNIN, J.-M. R. & JOLIVET, J.-P. 2003. Coprecipitation of Fe(II) and Fe(III) cations in sulphated aqueous medium and formation of hydroxysulphate green rust. *Solid State Sciences,* 5**,** 1055-1062.

RUSSELL, J. 1979. Infrared spectroscopy of ferrihydrite: evidence for the presence of structural hydroxyl groups. *Clay Miner,* 14**,** 109-114.

SCHNEIDER, W. 1984. Hydrolysis of Iron (III)… Chaotic Olation Versus Nucleation. *Comments on Inorganic Chemistry,* 3**,** 205-223.

SCHWERTMANN, U. 2000. *Iron oxides in the laboratory : preparation and characterization / U. Schwertmann, R.M. Cornell,* Weinheim

New York, Weinheim

New York : Wiley-VCH.

SCHWERTMANN, U. & CORNELL, R. M. 2008. *Iron oxides in the laboratory: preparation and characterization,* John Wiley & Sons.

SCHWERTMANN, U., FRIEDL, J. & STANJEK, H. 1999. From Fe(III) Ions to Ferrihydrite and then to Hematite. *Journal of Colloid and Interface Science,* 209**,** 215-223.

SCHWERTMANN, U., FRIEDL, J., STANJEK, H. & SCHULZE, D. G. 2000. The effect of Al on Fe oxides. XIX. Formation of Al-substituted hematite from ferrihydrite at 25 C and pH 4 to 7. *Clays and Clay Minerals,* 48**,** 159-172.

SCHWERTMANN, U. & MURAD, E. 1983. Effect of pH on the formation of goethite and hematite from ferrihydrite. *Clays and Clay Minerals,* 31**,** 277-284.

SÖHNEL, O. & GARSIDE, J. 1992. *Precipitation: basic principles and industrial applications,* Butterworth-Heinemann.

SPENCER, D. W., BREWER, P. G. & SACHS, P. L. 1972. Aspects of the distribution and trace element composition of suspended matter in the Black Sea. *Geochimica et Cosmochimica Acta,* 36**,** 71-86.

STEEMSON, M. & SMITH, M. The development of nickel laterite heap leach projects. Proceedings of ALTA 2009 Nickel/Cobalt conference, 2009.

STUMM, W. 1992. *Chemistry of the solid-water interface: processes at the mineral-water and particle-water interface in natural systems,* John Wiley & Son Inc.

STUMM, W. & LEE, G. F. 1961. Oxygenation of ferrous iron. *Industrial & Engineering Chemistry,* 53**,** 143-146.

STUMM, W. & MORGAN, J. 1996. *Aquatic Chemistry, Chemical Equilibria and rates in natural waters,* New York

John Wiley & Sons.

STUMM, W. & O'MELIA, C. R. 1968. Stoichiometry of coagulation. *Journal (American Water Works Association),* 60**,** 514-539.

STUMM, W. & SULZBERGER, B. 1992. The cycling of iron in natural environments: Considerations based on laboratory studies of heterogeneous redox processes. *Geochimica et Cosmochimica Acta,* 56**,** 3233-3257.

SUNG, W. & MORGAN, J. J. 1980. Kinetics and product of ferrous iron oxygenation in aqueous systems. *Environmental Science & Technology,* 14**,** 561-568.

SWAMY, Y. V., KAR, B. B. & MOHANTY, J. K. 2003. Physico-chemical characterization and sulphatization roasting of low-grade nickeliferous laterites. *Hydrometallurgy,* 69**,** 89-98.

TAMARGO, F., MARTIN, F. S. & VALCARCEL, M. Asturiana de Zinc: more than thirty years of experience with the jarosite process. *In:* DUTRIZAC, J. E. & HARRIS, G. B., eds. Iron Control and Disposal, 1996 Canada. Second International Symposium on Iron Control in Hydrometallurgy, 93-100.

TAMURA, H., GOTO, K. & NAGAYAMA, M. 1976a. Effect of anions on the oxygenation of ferrous ion in neutral solutions. *Journal of Inorganic and Nuclear Chemistry,* 38**,** 113-117.

TAMURA, H., GOTO, K. & NAGAYAMA, M. 1976b. The effect of ferric hydroxide on the oxygenation of ferrous ions in neutral solutions. *Corrosion Science,* 16**,** 197-207.

TAMURA, H., KAWAMURA, S. & HAGAYAMA, M. 1980. Acceleration of the oxidation of Fe2+ ions by Fe(III)-oxyhydroxides. *Corrosion Science,* 20**,** 963-971.

TAYLOR, A. & CAIRNS, D. Technical development of the Bulong laterite treatment project. Nickel and Cobalt Pressure Leaching and Hydrometallurgy Forum. ALTA Metallurgical Services, Melbourne, Australia, 1997.

TAYLOR, R., MCKENZIE, R. & NORRISH, K. 1964. The mineralogy and chemistry of manganese in some Australian soils. *Soil Research,* 2**,** 235-248.

TAYLOR, W. & WEISS, J. 1953. The Rate Constant of the Reaction between Hydrogen Peroxide and Ferrous Ions. *The Journal of Chemical Physics,* 21**,** 1419-1420.

TORFS, K. & VLIEGEN, J. 1996. The Union Miniere Goethite process: plant practice and future prospects. *Iron Control and Disposal***,** 135-146.

TORRENT, J., GUZMAN, R. & PARRA, M. 1982. Influence of relative humidity on the crystallization of Fe (III) oxides from ferrihydrite. *Clays and clay minerals,* 30**,** 337-340.

TOWE, K. M. & BRADLEY, W. F. 1967. Mineralogical constitution of colloidal "hydrous ferric oxides". *Journal of Colloid and Interface Science,* 24**,** 384-392.

TOZAWA, K. & SASAKI, K. 1986. Effect of coexisting sulphates on precipitation of ferric oxide from ferric sulphate solutions at elevated temperatures. *Iron Control in Hydrometallurgy***,** 454-476.

TÜFEKCI, N. & SARIKAYA, H. Z. 1996. Catalytic effects of high Fe(III) concentrations on Fe(II) oxidation. *Water Science and Technology,* 34**,** 389-396.

VAN BENSCHOTEN, J. E., LIN, W. & KNOCKE, W. R. 1992. Kinetic modeling of manganese (II) oxidation by chlorine dioxide and potassium permanganate. *Environmental science & technology,* 26**,** 1327-1333.

VEEKEN, A. & RULKENS, W. 2003. Innovative developments in the selective removal and reuse of heavy metals from wastewaters. *Water Science and Technology,* 47**,** 9-16.

WANG, K. 2011. *Impurity rejection in the nickel laterite leach system.* 109.

WANG, K., LI, J., MCDONALD, R. & BROWNER, R. 2011. The effect of iron precipitation upon nickel losses from synthetic atmospheric nickel laterite leach solutions: statistical analysis and modelling. *Hydrometallurgy,* 109**,** 140-152.

WANG, K., LI, J., MCDONALD, R. G. & BROWNER, R. E. 2013. Characterisation of iron-rich precipitates from synthetic atmospheric nickel laterite leach solutions. *Minerals Engineering,* 40**,** 1-11.

WANG, X., ZHU, M., LAN, S., GINDER-VOGEL, M., LIU, F. & FENG, X. 2015. Formation and secondary mineralization of ferrihydrite in the presence of silicate and Mn (II). *Chemical Geology,* 415**,** 37-46.

WATLING, H. R., ELLIOT, A. D., FLETCHER, H. M., ROBINSON, D. J. & SULLY, D. M. 2011. Ore mineralogy of nickel laterites: controls on processing characteristics under simulated heap-leach conditions. *Australian Journal of Earth Sciences,* 58**,** 725-744.

WEDDERBURN, B. Nickel laterite processing: a shift towards heap leaching. ALTA Nickel/Cobalt Conference, May, Perth, 2009.

WEISS, J. 1935. Investigations on the radical HO2 in solution. *Trans. Faraday Soc.,* 31**,** 668-681.

WHITE, D., MILLER, M. & NAPIER, A. 2006. Impurity disposition and control in the Ravensthorpe acid leaching process. *Iron Control Technologies—3rd International Symposium on Iron Control in Hydrometallurgy, Canadian Inst. Min. Metall. & Petroleum.*

WHITE, D. T. 2002. Selective precipitation of nickel and cobalt. Google Patents.

WHITE, D. T. & GILLASPIE, J. D. 2015. Atmospheric leaching of nickel laterites with iron precipitation *Nickel-Cobalt-Copper Proceedings.* Perth, Australia: ALTA Metallurgical Services.

WILLEY, B. F. & JENNINGS, H. 1963. Iron and Manganese Removal With Potassium Permanganate. *Journal (American Water Works Association),* 55**,** 729-734.

WILLIS, B. Downstream processing options for nickel laterite heap leach liquors. ALTA Conference Ni/Co, Proceedings, 2007.

YUE, T., HAN, H., SUN, W., HU, Y., CHEN, P. & LIU, R. 2016. Low-pH mediated goethite precipitation and nickel loss in nickel hydrometallurgy. *Hydrometallurgy*.

ZHANG, W., CHENG, C. Y. & PRANOLO, Y. 2010. Investigation of methods for removal and recovery of manganese in hydrometallurgical processes. *Hydrometallurgy,* 101**,** 58-63.

ZHU, D.-Q., CUI, Y., HAPUGODA, S., VINING, K. & PAN, J. 2012. Mineralogy and crystal chemistry of a low grade nickel laterite ore. *Transactions of Nonferrous Metals Society of China,* 22**,** 907-916.

CHAPTER 3
EFFECT OF VARIOUS FACTORS ON IRON PRECIPITATION AND THE ASSOCIATED NICKEL AND COBALT LOSSES

3.1 Introduction

As reviewed in Chapter 2, iron is the major impurity followed by magnesium in nickel laterite leach solutions. Also, present in the sulfate leach solutions in significant amounts is aluminium and chromium. The removal of iron, aluminium and chromium from solution is usually carried out in a series of hydroxide precipitation steps, which are customarily referred to as primary and secondary neutralisation steps in the hydrometallurgical processing of nickel laterite solutions (White et al., 2006). The primary neutralisation step is used to remove the bulk of the trivalent ions of iron, aluminium and chromium while the secondary neutralisation step removes any ferric ion, aluminium, chromium and ferrous ion remaining in solutions following the primary neutralisation step. The precipitation of iron, aluminium and chromium is notorious for the associated nickel and cobalt losses to the residues, especially in the Goethite Process.

In goethite precipitation, maintaining a low ferric ion concentration (below 2 g/L) in solution during precipitation and the control of operating variables such as pH and temperature is crucial for the control of supersaturation and the production of the desired product. As reviewed in Chapter 2, even when ferric ion concentration is maintained below 2 g/L, the iron precipitates formed are usually found to be chiefly a mixture of poorly ordered ferrihydrite and schwertmannite, amorphous iron phases with minor quantities of goethite (Claassen et al., 2002, Loan et al., 2006, Wang et al., 2013). The nature of precipitate formed have a profound effect on the liquid-solid separation process which impacts profoundly on nickel and cobalt losses to the precipitates. Therefore, the purpose of Chapter 3 was to study the effect of operating variables (factors) and the presence of other impurities on the nature of precipitates and nickel and cobalt losses when iron precipitation is carried out under high ferric ion concentration in solution above 2 g/L used in goethite precipitation.

Chapter 3 consists of five sections. The first section (Section 3.6.1) involved modelling of a quinary sulfate system [Fe(III)+Al(III)+Cr(III)+Ni(II)+Co(II)] using a freeware chemical equilibrium model, Visual MINTEQ (version 3.1) for the initial design and

development of the precipitation process and for analysis of the experimental results. The second section (Section 3.6.2) was preliminary experiments carried out to determine the effects of using various neutralising agents on the removal of iron by precipitation and the level of nickel and cobalt losses to the precipitates. The third section (Section 3.6.3) was aimed at investigating the effect of the presence of impurities other than iron in sulfate solutions during iron precipitation on the amount of nickel and cobalt losses and the nature of precipitate formed. In the fourth section (Section 3.6.4), the effect of the controllable factors, temperature, pH and neutralising agent concentration on the removal of the trivalent ions of Fe, Al and Cr from multi-element synthetic sulfate laterite solutions simulating real laterite leach solutions were investigated, using design of experiment (DOE) and statistical analysis to evaluate the significance of the factors on the process. Lastly, the significant factors were optimised using one variable at a time approach (Section 3.6.5).

3.2 Materials and methods

3.2.1 Reagents

The following analytical grade chemicals were used to prepare synthetic sulfate solution of different metal combinations during the experimental work: nickel (II) sulphate hexahydrate ($NiSO_4.6H_2O$) (99%Chem-Supply), cobalt (II) sulphate heptahydrate ($CoSO_4.7H_2O$) (99%, Chem-Supply), manganese (II) sulphate monohydrate ($MnSO_4.H_2O$) (98.5%, Chem-Supply), aluminium sulphate octadecahydrate ($Al_2(SO_4)_3.18H_2O$) (98%, Chem-Supply), magnesium sulphate heptahydrate ($MgSO_4.7H_2O$) (98%, Chem-Supply), calcium sulphate dihydrate ($CaSO_4.2H_2O$) (98%, Chem-Supply), copper sulphate pentahydrate ($CuSO_4.5H_2O$) (98%, Chem-Supply), zinc sulphate heptahydrate ($ZnSO_4.7H_2O$) (99%, Chem-Supply), iron (II) sulphate heptahydrate ($FeSO_4.7H_2O$) (99.5%, Chem-Supply), sulphuric acid (H_2SO_4) (98%, EMSURE®), sodium hydroxide (NaOH) pellets (99%, Rowe Scientific), calcium carbonate ($CaCO_3$) (99%, Chem-Supply), light magnesium carbonate and magnesium oxide (95%, Chem-Supply). In addition, the following laboratory grade reagents were used: chromium (III) chloride hexahydrate ($CrCl_3.6H_2O$) (97.5%, Chem-Supply) and iron (III) sulphate heptahydrate ($Fe_2(SO_4)_3.7H_2O$) (21% metal assay, Chem-Supply). All solutions and slurries of the neutralising agents were made by adding the respective reagents to deionised water.

3.2.2 Preparation of test solutions

Nickel laterite ore was initially leached in sulfuric acid and the solution analysed for elemental composition. The metal ion concentrations of the leach solution together with those reported in previous studies (White et al., 2006, Agatzini-Leonardou et al., 2009, Büyükakinci and Topkaya, 2009, Köse and Topkaya, 2011, Önal and Topkaya, 2014) were used to approximate the composition and relative metal ion concentration to make synthetic sulfate solutions to be used in this study. Synthetic sulfate solution that simulated the leach solution usually produced during leaching of low-grade laterite ores were prepared by dissolving the pre-determined amounts of the metal salts in a minimum volume of deionised water in a beaker. The solution pH was adjusted to less than 1.0 using concentrated sulfuric acid and the volume of the solution made to that of the volumetric flasks as determined during concentration calculations. The synthetic sulfate solution was deoxygenated by bubbling nitrogen gas to prevent the oxidation of ferrous ions from any dissolved oxygen. The deoxygenation of the solution was done following the procedure by Rollie et al. (1987). The target metal ion concentrations in the synthetic sulfate solution are given in Table 3.1.

Table 3.1: Target composition of the synthetic sulfate solution.

Element	Ni	Co	Fe	Fe(III)	Al	Cr	Mn	Mg	Ca	Cu	Zn
Concentration (g/L)	4.50	0.35	37.0	35.0	4.00	1.00	0.90	13.0	0.50	0.10	0.25

The slurries of the neutralising agents were prepared by adding $CaCO_3$, $MgCO_3$ or MgO in deionised water while sodium hydroxide solution was made by dissolving NaOH pellets in deionised water.

3.2.3 Experimental set-up and general procedure

The precipitation experiments were carried out in a five-neck 500 mL flat bottom glass reactor seated in a water bath to allow for temperature control. The neck openings were used for the impeller, thermometer, neutralising agent addition, gas sparger and pH probe. A mounted overhead stirrer (Heidolph RZR 2020 Mixer System) fitted with a pitch-blade turbine impeller was used, and the neutralising agent added directly above the impeller for better mixing during the reaction at the rate of 0.5 – 1.5 mL/min. The stirring speed was set at 500 rpm or more to allow for efficient mixing and keeping the

solids in suspension. The pH of the suspension was measured at temperature (automatically compensated by the instrument) using a Mettler Toledo® Inlab Versatile pH probe with a working temperature ranging from 0 to 100 °C. The pH meter also measured the temperature in the test solution and was used in combination with a thermometer immersed in the solution throughout the experiments. The experimental set up is as shown in Figure 3.1.

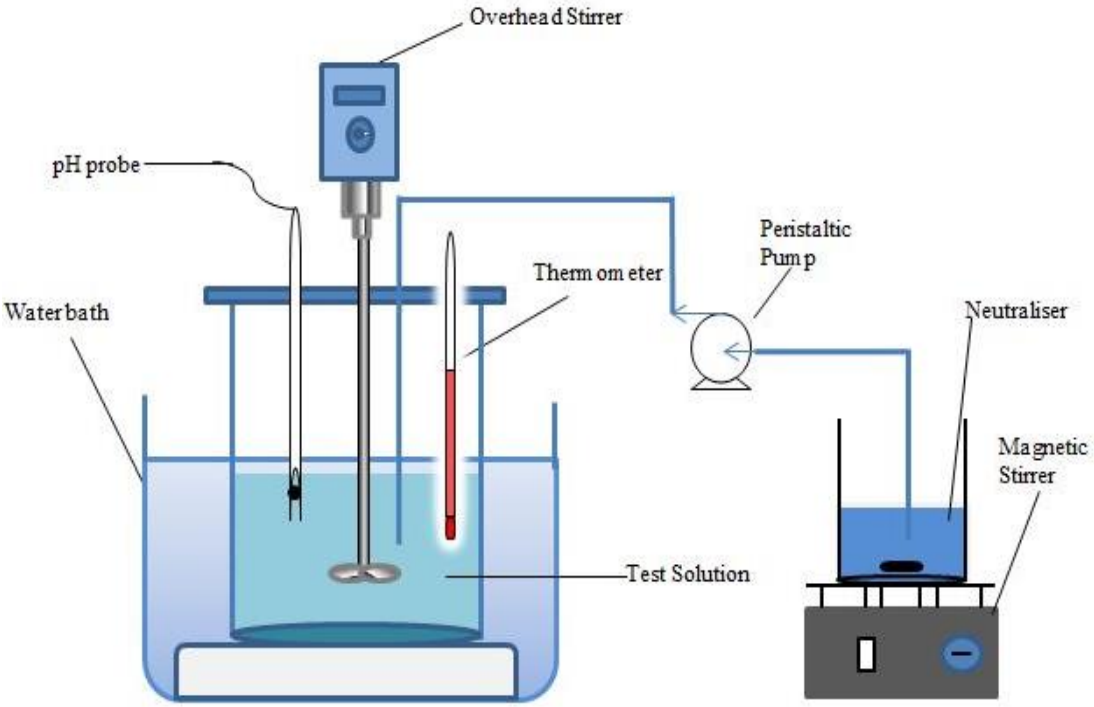

Figure 3.1: Schematic diagram of the experimental set-up.

Semi-batch mode experimental set-up was used for the precipitation experiments using a similar process as given by Kose and Topkaya (2011). The precipitation experiments were carried out by transferring 100 mL of the test solution into the reactor, followed by adjusting the temperature to the desired value, ranging from 55 to 90 °C using the water bath while the solution was under continuous stirring. The temperature was controlled within 1°C of the desired value. When the desired temperature was attained, the pH was adjusted by pumping the neutralising agent into the reactor at a slow controlled flow rate ranging from 0.5 to 1.0 mL/min, changing the solution pH gradually until the target pH value was reached under continuous stirring and maintained at the setpoint. At the completion of the reaction, the slurry was cooled, and vacuum filtered using a circular hardened ashless filter paper (Whatman No

542/110 mm) on a Buchner funnel with a 1000 mL flask. The precipitate was thoroughly washed with acidified deionised water (at pH equivalent to target pH during precipitation) to recover the nickel and cobalt entrained filtrate in the filter cake (precipitate). The filtrate and wash liquor were analysed for the respective metal ions while a sample of the wet solid was mixed with distilled water and examined for particle size distribution using a Malvern Mastersizer 3000 Hydro EV. The rest of the precipitate produced was dried at 105 ℃ overnight. The mineralogy of the precipitates was determined by powder X-Ray Diffraction (XRD) using a Bruker D8 Discover diffractometer with a Co-Kα radiation source operated at 40kV and 40 mA and equipped with a LynxEye detector, at step scan of 0.014° and time/step of 0.8 seconds. The chemical composition analysed using a Rigaku Advanced Supermini200 X-Ray Fluorescence (XRF) Spectrometer and particle size distribution by Malvern Mastersizer 3000 Hydro EV. The chemical composition of the recovered filtrate and wash liquor were determined using Inductively Coupled Plasma Optic Emission Spectroscopy (ICP-OES) (Agilent 5100 Synchronous Vertical View-SVDV). The filtrate and wash liquor volumes were measured and together with the measured respective elemental concentrations were used to calculate the percentage metal removal using Equation 3.1.

$$\%\ \text{Metal removal}\ (R_M) = \frac{[C_{initial}.V_{initial} - (C_{filtrate}.V_{filtrate} + C_{wash}.V_{wash})]}{C_{initial}.V_{initial}} \text{ x } 100 \qquad 3.1$$

, where M is metal, $C_{initial}$, and $C_{fitlrate}$ and C_{Wash} are the test solution, filtrate and wash liquor concentrations (mg/L) of the individual element and $V_{initial}$, $V_{fitrate}$ and V_{Wash} are the test solution, filtrate and wash liquor volume (L), respectively.

3.3 Modelling of sulfate solutions using Visual MINTEQ (version 3.1)

Chemical process modelling is used as a tool to predict and understand the behaviour of complex aqueous systems (Liu and Papangelakis, 2005). The Visual MINTEQ software can calculate the relative concentration and distribution of the species and the saturation index of minerals as a function of process parameters such as pH and temperature. The speciation of metal ions in solution has been found to influence hydrolysis precipitation (Schneider, 1984). Knowledge on the speciation can, therefore, be used to explain the formation of the different iron oxyhydroxides and sulfates in the complex aqueous systems (Sapieszko et al., 1977) such as that of nickel laterite leaching solutions. Also, the saturation index which is the difference between

the logarithms of the ion activity products (IAP) and the solubility product (K_s) and its value is a measure of the stability of the solution. A negative, zero and positive saturation index value indicates that the solution is undersaturated, at equilibrium and oversaturated with respect to individual minerals, respectively (Allison et al., 1991). The calculated saturation index (SI) values predict the pH range for recovery of the cations by precipitation. Therefore, in this study, the simulation was used to evaluate the potential selective simultaneous precipitation of the hydroxides of Fe, Al and Cr from the nickel laterite sulfate solutions, especially the pH range. The pH range was evaluated using synthetic sulfate solutions simulating real nickel laterite leach solutions.

The speciation of the trivalent ions of Fe, Al and Cr and the divalent ions of Ni and Co in dilute sulfate solutions as a function of pH (0 to 4.5) was simulated using Visual MINTEQ (version 3.1). The concentrations of the metal ions in the dilute solutions used in the simulation were kept at similar ratios as in the synthetic sulfate leach solutions used in the iron precipitation experiments throughout Chapter 3 (Table 3.1). A quinary sulfate solution containing 0.01 M Fe^{3+}, 0.0022 M Al^{3+}, 0.0003 M Cr^{3+},0.0012 M Ni^{2+}, 0.09 mM Co^{2+} and 0.02 M SO_4^{2-} was used. The divalent ions of copper, calcium, magnesium, manganese and zinc were not included since their presence in nickel laterite leach solutions has not been reported to impact on nickel and cobalt losses during iron precipitation processes. The speciation of the cations as a function of pH was evaluated at 25 ℃ and 40 ℃ using the dilute quinary sulfate solutions. The letters L and M were used in the graphs to denote the operating temperatures 25 ℃ and 40 ℃, respectively. The Y axis in the speciation diagrams is the mole fraction of the individual metal species in solution as a function of the total individual species in solution. The water molecules coordinated with the metal ions were omitted in the chemical formula of the species. For example, the hexacoordinated aquo complex $[Fe(H_2O)_6]^{3+}$ was abbreviated as Fe^{3+} and $[Fe(H_2O)_5OH]^{2+}$ as $Fe(OH)^{2+}$. The pH of the modelled solution was adjusted using hydroxide concentration.

3.4 Preliminary Experiments

Preliminary experiments were carried out to determine the effect of using different neutralising agents on the removal of iron and the amount of nickel and cobalt losses to the precipitate. The neutralising agents investigated were calcium carbonate (10 wt.

%), magnesium carbonate (7.5 wt. %) and magnesium oxide (7.5 wt. %) slurries and sodium hydroxide solution (1.0 M). The experiments were carried out using both [Fe(III)+Ni(II)+Co(II)] ternary system and multi-element system (with elemental composition as shown in Table 3.1), with the concentration of iron, nickel and cobalt kept comparable in both synthetic sulfate solutions. The dilute neutralising agent was added slowly into the iron-rich synthetic sulfate solution to gradually change and control pH and regulate supersaturation of iron, aluminium and chromium and minimise the formation of amorphous precipitates at experimental temperature. A high temperature of 85 °C was used during the experiments because the formation of precipitates with better properties is favoured at high temperatures (Claassen and Sandenbergh, 2007).

3.5 Full factorial design experiments

Factorial designs are a more effective and economical technique for investigating the effect of multiple factors on the dependent variable(s) during experiments in comparison to a one variable at a time approach. The advantage of full factorial designs is that they measure responses at all combinations of the factor levels and enables the evaluation of the interactions between factors.

A full factorial design with all factors, evaluated at two levels, low (-) and high (+) was used to determine the significant factors and interaction effects on the response variables. The factors investigated were pH, temperature and base concentration (calcium carbonate slurry), with the low (-) and high (+) levels selected for each factor as shown in Table 3.2.

Table 3.2: Factors and the ranges used for a 2^3 full factorial design.

Factor	Low level (-)	High Level (+)	Units
A=pH	2.5	4.0	-
B=Temperature	55	85	° C
C=$CaCO_3$ concentration	10	25	% w/v

The responses measured were percentage removal of iron, aluminium and chromium and the percentage loss of nickel and cobalt. The levels of pH (factor A) were set at 2.5 and 4.0 which is a commonly used pH range for the effective removal of the trivalent ions of iron, aluminium and chromium from zinc and nickel leach solutions

with minimal zinc and nickel losses in multi-stage precipitation (Köse and Topkaya, 2011). The low level of temperature (Factor B) was set at 55 ℃ and the high level at 85 ℃, which is the typical working temperature range for the goethite precipitation (Claassen and Sandenbergh, 2007). At the high ferric ion concentrations used, which are not the preferred for iron precipitation, the concentration of calcium carbonate slurry (factor C) would significantly affect the degree of supersaturation and homogeneity in pH and ultimately the properties of the precipitate. The minimum concentration of calcium carbonate slurry was set at 10% w/v and the maximum at 25% w/v, despite the use of 25% w/w calcium carbonate slurry was found to have insignificant effect on the iron precipitation and nickel losses during precipitation (Wang et al., 2011). However, in this study, due to the absence of process solution dilution, the concentration of the neutralising agent could be a significant factor. Minitab 18 program was used to generate the experimental matrix and for the statistical analysis of the experimental results obtained. The two-replicate experimental design matrix for the three factors is given in Table 3.3, and the concentration of the trivalent ions in the filtrate at the completion of the experiment is provided in Table 3.4. The significant factors were optimised using one variable at a time approach.

Table 3.3: A 2^3 full factorial design matrix.

Run	A	B	C
1	+	-	-
2	+	-	+
3	+	+	-
4	-	+	-
5	-	-	-
6	+	+	+
7	-	+	-
8	-	+	+
9	+	-	+
10	+	+	+
11	-	-	+
12	-	-	-
13	+	+	-
14	+	-	-
15	-	+	+
16	-	-	+

Table 3.4: Metal ion concentration (mg/L) in filtrate after precipitation experiments (two replicates).

Run	Ni(II)	Co(II)	Fe(III)	Al(III)	Cr(III)
1	2.45	0.225	BDL	0.013	BDL
2	2.30	0.192	0.022	0.092	BDL
3	2.13	0.200	0.013	BDL	BDL
4	3.65	0.313	0.188	2.250	0.075
5	4.10	0.350	0.338	3.450	0.138
6	1.74	0.167	0.006	0.003	BDL
7	3.73	0.313	0.300	2.150	0.050
8	2.61	0.222	0.203	1.490	0.033
9	2.30	0.192	0.022	0.092	BDL
10	2.27	0.224	0.002	0.011	BDL
11	4.58	0.375	0.613	3.675	0.113
12	2.96	0.251	0.294	2.580	0.091
13	2.96	0.254	0.204	1.870	0.055
14	2.06	0.183	0.003	0.032	BDL
15	2.27	0.224	0.002	0.011	BDL
16	3.03	0.249	0.374	2.440	0.067

Note BDL stands for Below Detection Limit

3.6 Results and Discussions

3.6.1 Modelling of quinary sulfate solutions using Visual MINTEQ (version 3.1)

3.6.1.1 Speciation of the trivalent ions of iron, aluminium and chromium and divalent ions of nickel and cobalt

Figure 3.2 shows the calculated equilibrium concentration distribution of the various aqueous iron species in the pH range 0 to 4.5 and temperature 25 °C and 40 °C for a dilute quinary system with the initial composition given in Section 3.3. The proportion of the individual impurities, Fe, Al and Cr to the divalent cations of nickel and cobalt in the dilute quinary system used for simulation is comparable to that in the synthetic multi-element sulfate system investigated in chapter 3. The ratio of Fe/(Ni+Co), Al/(Ni+Co) and Cr(Ni+Co) is 8, 1.8 and 0.23, respectively in both the quinary and multi-element sulfate systems. The results in Figure 3.2 show that the concentration

distribution of the iron species is highly dependent on pH and an increase in temperature from 25 °C to 40 °C had a minimal effect on the concentration distribution of the species. In highly acidic conditions (pH < 2), iron existed predominantly as Fe^{3+} and $FeSO_4^+$ species, which is reasonable as ferric hydrolysis is a function of pH. Increasing pH from 0, the amount of Fe^{3+} decreased rapidly with increase in pH while the amount of $FeSO_4^+$ steeply increased, reaching a maximum around pH 2. Above pH 2, the amount of $FeSO_4^+$ quickly decreased and that of the hydrolysed ferric species, $FeOH^{2+}$, $Fe(OH)_2^+$ and the dimer, $Fe_2(OH)_2^{4+}$ and trimer $Fe_3(OH)_4^{5+}$ ions increased. The monomeric hydrolysed ferric ion species in aqueous solution have been found to form in acidic pH range (Baes and Mesmer, 1976). The formation of the monomeric ferric species occurs according to the reactions given in Table 2.4 in Section 2.4.2, with protons released during hydrolysis. The loss of protons is sequential, that is $FeOH^{2+}$ is formed first as a result of the loss of a proton (H^+ ion) from the unhydrolysed hexa-aquo ferric ion. As pH increases, the amount of $FeOH^{2+}$ in solution increases until it reaches a maximum and begins to drop and more $Fe(OH)_2^+$ forms from the successive loss of a second proton. The dimer ($Fe_2(OH)_2^{4+}$) and trimer ($Fe_3(OH)_4^{5+}$) are predicted and are formed as a result of the interaction of the monomeric species ($FeOH^{2+}$) (Cornell et al., 1989) as shown in Equation 3.2.

$$Fe(OH)^{2+} + FeOH^{2+} \rightarrow Fe_2(OH)_2^{4+} + Fe(OH)^{2+} + H_2O \rightarrow Fe_3(OH)_4^{5+} + H^+ \quad 3.2$$

Further polymerisation of the low molecular weight polycations (monomers, dimers and trimers) lead to the formation of higher molecular weight polycations, the red-brown colloids (Cornell et al., 1989) and consequently the precipitation of the various iron oxyhydroxides such as ferrihydrite ($5Fe_2O_3 \cdot 9H_2O$) and goethite (FeOOH) (Cornell and Schwertmann, 2003). In the sulfate solutions, depending on pH not only the monomer species, $FeOH^{2+}$ and $Fe(OH)_2^+$ are formed but also significant amounts of the ferric sulfate species, $FeSO_4^+$ and $Fe(SO_4)_2^-$. The sulfate species, $FeSO_4^+$, is suggested to interact with the $Fe(OH)^{2+}$ species to form iron oxyhydroxysulfates according to Equation 3.3 (Sapieszko et al., 1977).

$$FeOH^{2+} + 2FeSO_4^+ + 6H_2O \rightarrow Fe_3(SO_4)_2(OH)_5.2H_2O + 4H^+ \quad 3.3$$

The $FeSO_4^+$ species is predominant in acidic sulfate solution and has been found to suppress the formation of oxyhydroxides (Matijević et al., 1975, Sapieszko et al.,

1977), which could be the reason for AMD iron precipitates mainly consisting of schwertmannite and jarosite (Bigham et al., 1996).

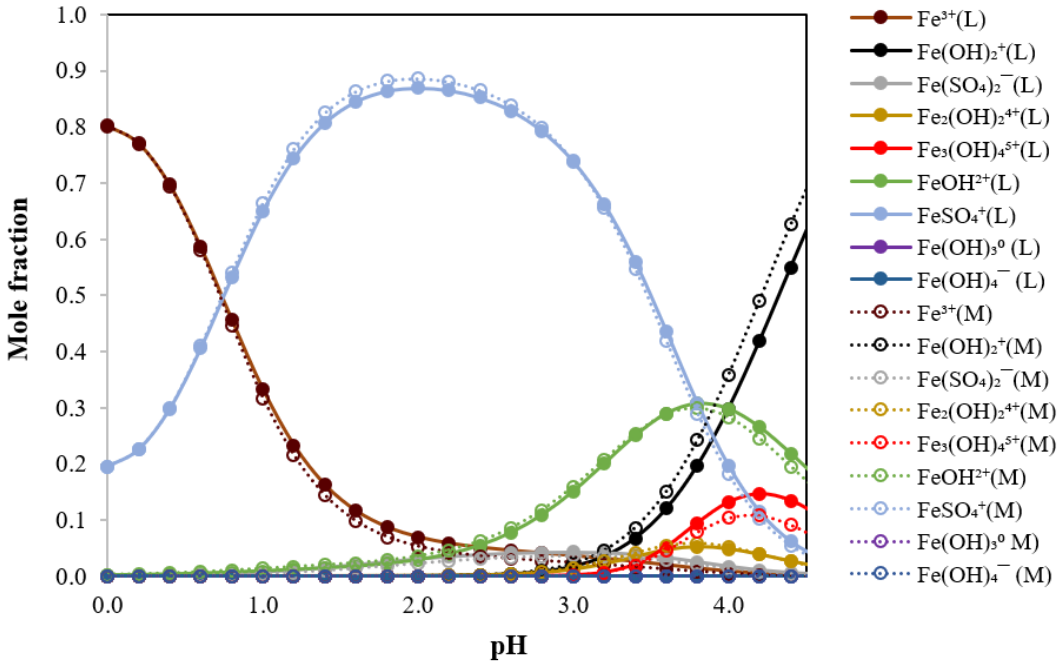

Figure 3.2: Iron speciation as a function of pH in a quinary solution containing 0.01 M Fe^{3+}, 0.0022M Al^{3+}, 0.0003M Cr^{3+},0.0012 M Ni^{2+}, 0.09 mM Co^{2+} and 0.02 SO_4^{2-} at 25 °C (L) and 40 °C (M).

The speciation of aluminium is given in Figure 3.3, and the concentration of the aqueous aluminium hydrolysis complexes is highly dependent on pH and temperature. At pH values below 3.4, aluminium ions existed mainly in the form Al^{3+}, $AlSO_4^+$ and $Al(SO_4)_2^-$. At pH above 3.4, the fraction of the hydrolysed aluminium species $AlOH^{2+}$ and $Al(OH)_2^+$ increases. The trend in their formation is probably a successive deprotonation steps like the trend in ferric hydrolysis species formation with increasing pH. The concentration distribution of the aluminium sulfate species shows more dependence on temperature than ferric ion speciation. The dimer, $Al_2(OH)_2^{4+}$ and trimer, $Al_3(OH)_4^{5+}$ at the pH values modelled do not occur to any significant extent as reported by (Martin, 1991). In general, Al^{3+} and the aluminium sulfate complexes dominate at the pH range.

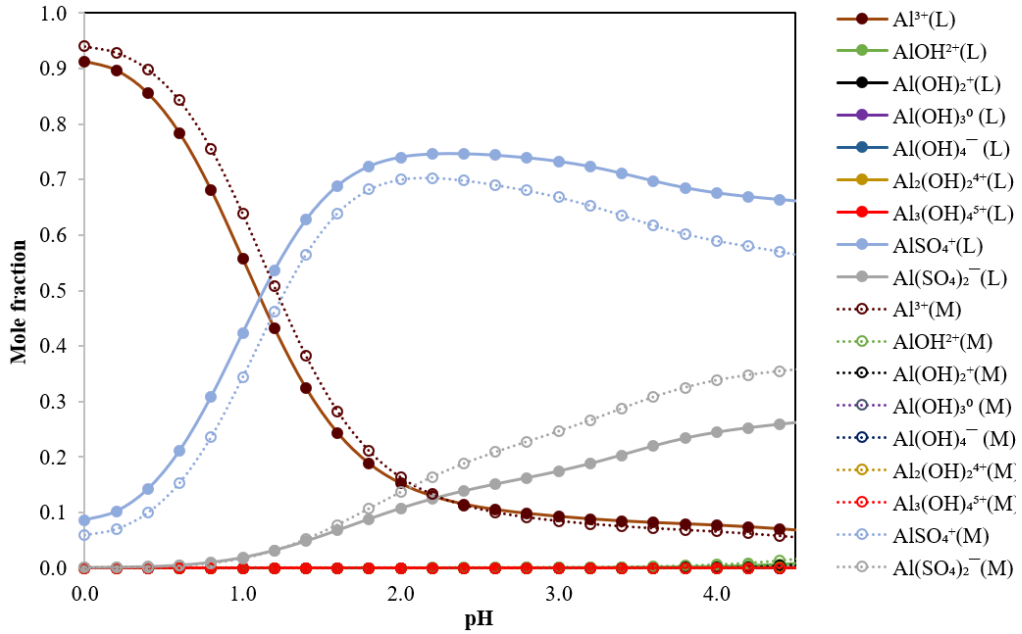

Figure 3.3: Aluminium speciation as a function of pH for a quinary solution containing 0.01 M Fe^{3+}, 0.0022 M Al^{3+}, 0.0003M Cr^{3+},0.0012 M Ni^{2+}, 0.09 mM Co^{2+} and 0.02 SO_4^{2-} at 25 °C (L) and 40 °C (M).

The relative amounts and distribution of chromium species in solution are shown in Figure 3.4, and the speciation is influenced mainly by pH and temperature. As shown in the distribution diagram (Figure 3.4), Cr^{3+} and the chromium sulfate species, $CrSO_4^+$ are dominant in a highly acidic solution. As pH increases (0 to 3), the amount of Cr^{3+} drops rapidly as chromium sulfate species ($CrSO_4^+$ and $CrOHSO_4^0$) and hydrolysed chromium species ($CrOH^{2+}$) are formed. The dimeric species ($Cr_2(OH)_2^{4+}$) is predicted in a significant amount similar to the speciation of ferric ion but not the aluminium ion speciation. The formation of the hydrolysed species shifts to lower pH with increasing temperature.

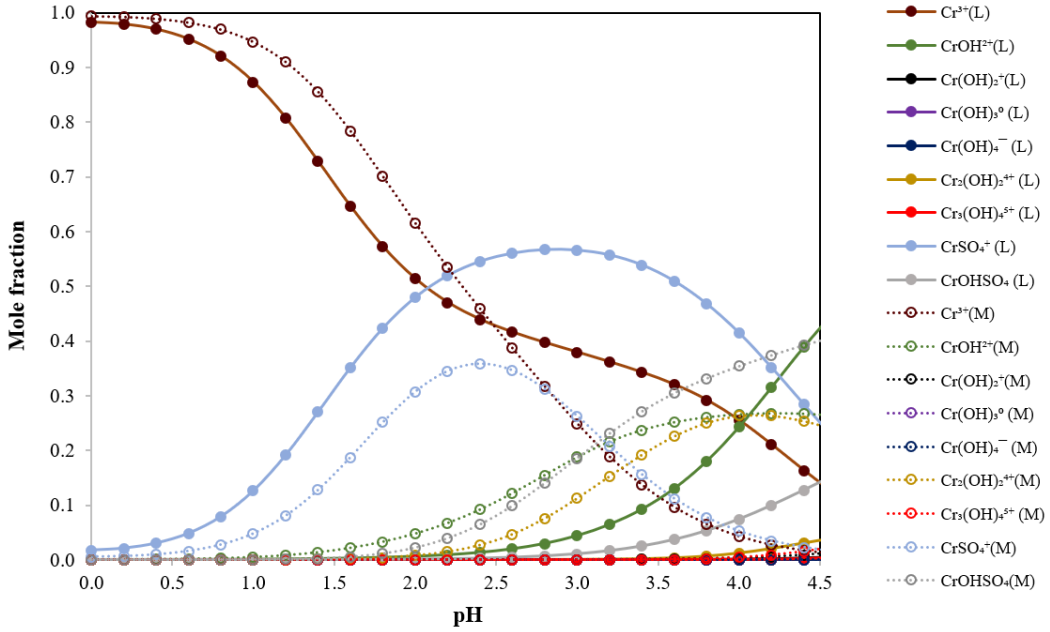

Figure 3.4: Chromium speciation as a function of pH for a quinary solution containing 0.01 M Fe^{3+}, 0.0022 M Al^{3+}, 0.0003M Cr^{3+},0.0012 M Ni^{2+}, 0.09 mM Co^{2+} and 0.02 SO_4^{2-} at 25 ℃ (L) and 40 ℃ (M).

Figure 3.5a and Figure 3.5b show the speciation of nickel and cobalt, respectively as a function of pH at 25 ℃ and 40 ℃. The trend in the speciation of nickel is almost identical to that of cobalt ions in the pH range. The dominant nickel species at the pH range used are Ni^{2+} and $NiSO_4^0$ (Figure 3.5a) and Co^{2+} and $CoSO_4^0$ as the equivalent species for cobalt ion speciation (Figure 3.5b) and the other species are negligible at the pH range. With increasing pH, the amount of Ni^{2+} and Co^{2+} species in aqueous solution decrease gradually as the respective metal sulfate species $NiSO_4^0$ and $CoSO_4^0$ increase in concentration. Nickel and cobalt ions complex strongly with sulfate ion in acidic pH values.

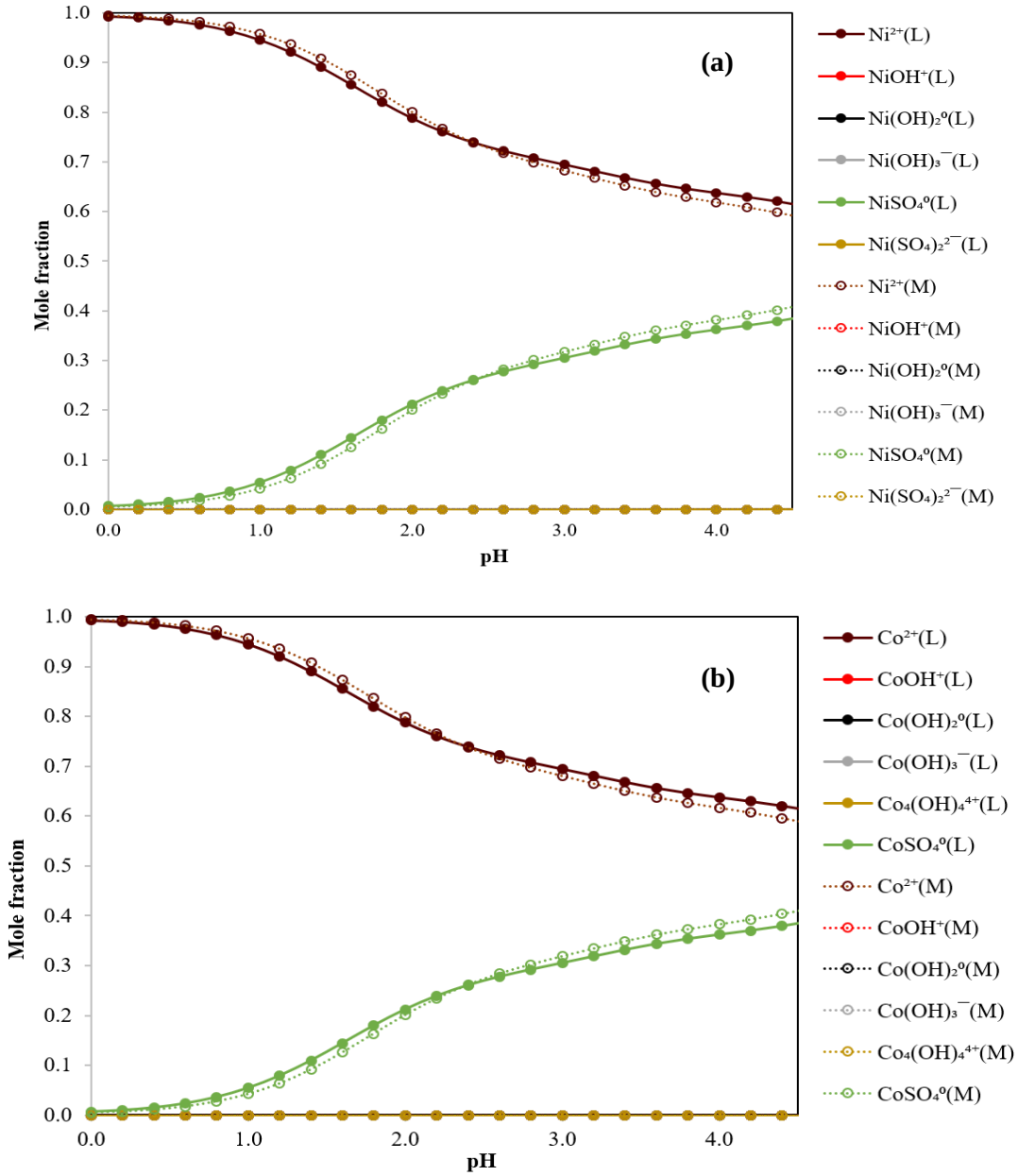

Figure 3.5: (a) Nickel speciation and (b) cobalt speciation as a function of pH and temperature for a quinary solution containing 0.01 M Fe^{3+}, 0.0022 M Al^{3+}, 0.0003M Cr^{3+},0.0012 M Ni^{2+}, 0.09 mM Co^{2+} and 0.02 SO_4^{2-} at 25 ℃ (L) and 40 ℃ (M).

2.7.1.1 Saturation index

In Figure 3.6a is shown the plots of the saturation index values (Section 3.3) with respect to ferrihydrite, goethite, haematite and jarosite as a function of pH in the dilute quinary sulfate solution at 25 ℃ and 40 ℃, calculated using the Visual MINTEQ software. The results (Figure 3.6a) indicate that the saturation index values for the individual mineral phases are influenced by pH and temperature. The calculated SI values increase with increasing pH, and the curves shift to lower pH values with increasing temperature. The solubility of iron phases decreases with increasing

solution pH and temperature values. The saturation index of ferrihydrite, goethite, haematite and jarosite are positive at pH above 2.4, which means that the solution is saturated with respect to the iron phases. The saturation index of haematite and goethite are positive at lower pH values compared to jarosite and ferrihydrite. The SI calculations support the experimental finding for acidic sulfate solutions in that, amorphous ferric hydroxide (Park et al., 2015) and metastable phases, ferrihydrite and schwertmannite (Lee et al., 2002) are the dominant phases and not goethite and haematite. The model assumes chemical equilibrium for all thermodynamically favoured phases not considering the kinetics of formation. Haematite and goethite are not kinetically favoured in acidic sulfate solutions but are a product of the transformation of the metastable phases as expected from Stranski's rule (Söhnel and Garside, 1992). The metastable phases, ferrihydrite for example easily undergo dissolution to monomeric species, $FeOH^{2+}$ and $Fe(OH)_2^{+}$ (Schwertmann and Murad, 1983), which creates a new supersaturation. Goethite formation is favoured at pH below 4 and above 8 when the solubility of ferrihydrite is high while haematite is formed at pH range 5 to 8 when ferrihydrite solubility is low (Schwertmann and Murad, 1983, Combes et al., 1989). The saturation index and the speciation results suggest that ferric ion in sulfate solutions could be precipitated as a mixture of iron oxyhydroxides and oxyhydroxysulfates and since ferrihydrite is the kinetically and thermodynamically favoured iron phase, the best condition for its iron removal is probably at a pH above 2.4.

As pH increases to more than 3.2 the solution become saturated with respect to aluminium minerals, amorphous aluminium hydroxide, diaspore and jurbanite ($AlOHSO_4$) indicated by positive saturation index values (Figure 3.6b). Similar to ferric ion precipitation, oxyhydroxides and oxyhydroxysulfates of aluminium are predicted to precipitate.

The plot in Figure 3.6c shows that the saturation index with respect to chromium hydroxide and oxide is negative at pH 4.5 and below. The saturation of the solution with respect to chromium hydroxide and oxide is at higher pH values than 4.5 despite the hydrolysis species of chromium, $CrOH^{2+}$ and the dimer, $Cr_2(OH)_2^{4+}$ and trimer $Cr_3(OH)_4^{5+}$ being dominant at low pH below 4 (Figure 3.4), which supports the suggested high stability of the complexes in acidic solutions by Stuenzi and Marty (1983). In solutions of ferric ion and chromium, chromites are known to form easily

under laboratory conditions (Richard and Bourg, 1991). Therefore chromium would be expected to precipitate as chromite and amorphous (Fe(III), Cr(III)] hydroxide.

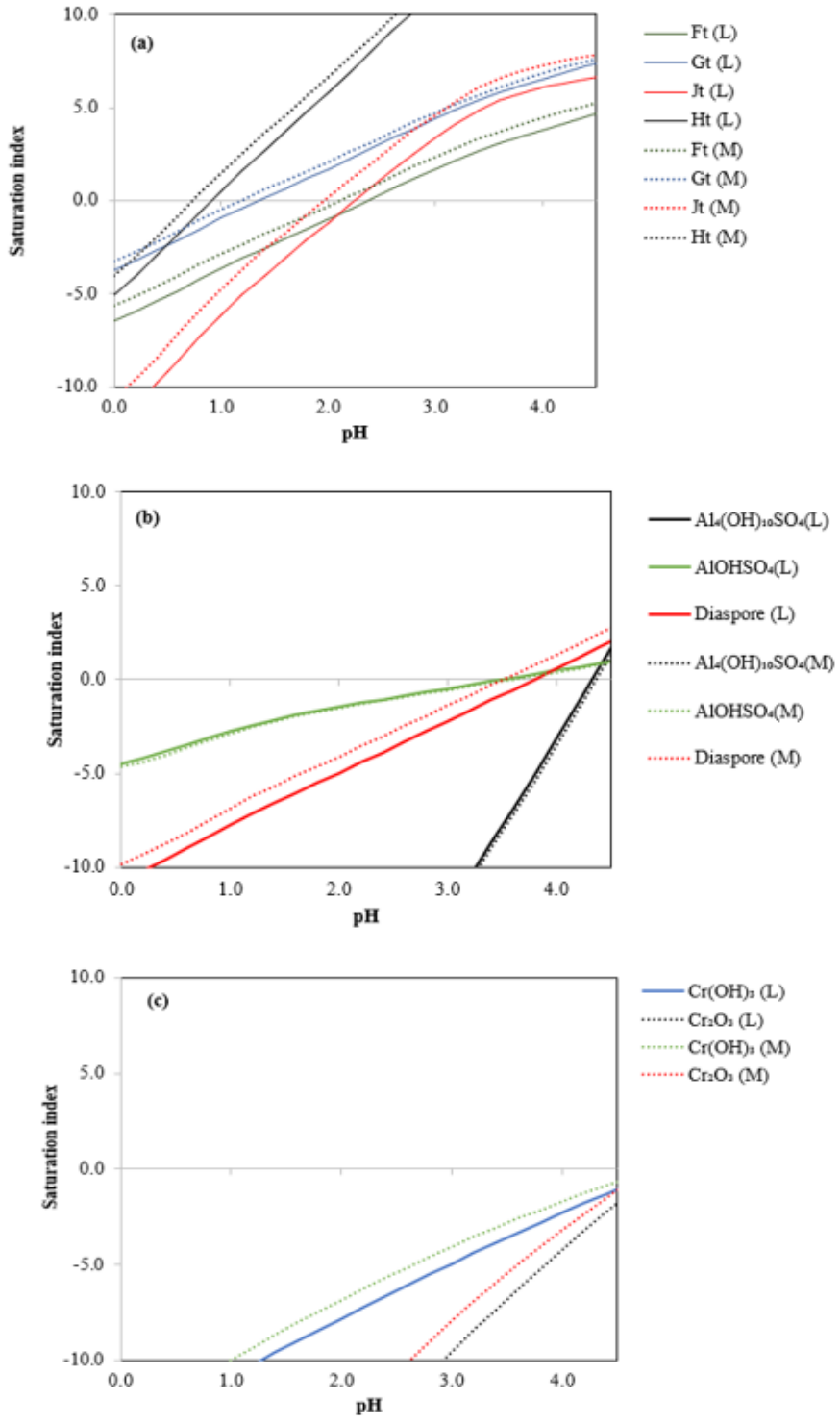

Figure 3.6: (a) Saturation index for ferrihydrite (Ft), goethite (Gt), haematite (Ht) and jarosite (Jt), (b) amorphous aluminium hydroxide ($Al(OH)_3$), $AlOHSO_4$ and diaspore and (c) amorphous chromium hydroxide ($Cr(OH)_3$) and chromium oxide (Cr_2O_3) as a function of pH for a quinary solution at 25 °C (L) and 40 °C (M).

The stability of the quinary sulfate solution with respect to nickel phases (nickel hydroxide) and cobalt phases (cobalt hydroxide and $CoFe_2O_4$) is shown in Figure 3.7a and Figure 3.7b, respectively, as plots of the SI of the mineral phases as a function of pH. The solution is undersaturated with respect to nickel and cobalt hydroxide phases at pH 4.5 and below, indicated by the negative SI values, but $CoFe_2O_4$ is predicted to form at pH less than 1. Depending on the kinetics of the formation of $CoFe_2O_4$, the separation of divalent ions of Co from the trivalent ions of Fe, Al and Cr by manipulating pH could be more difficult compared to the separation of Ni.

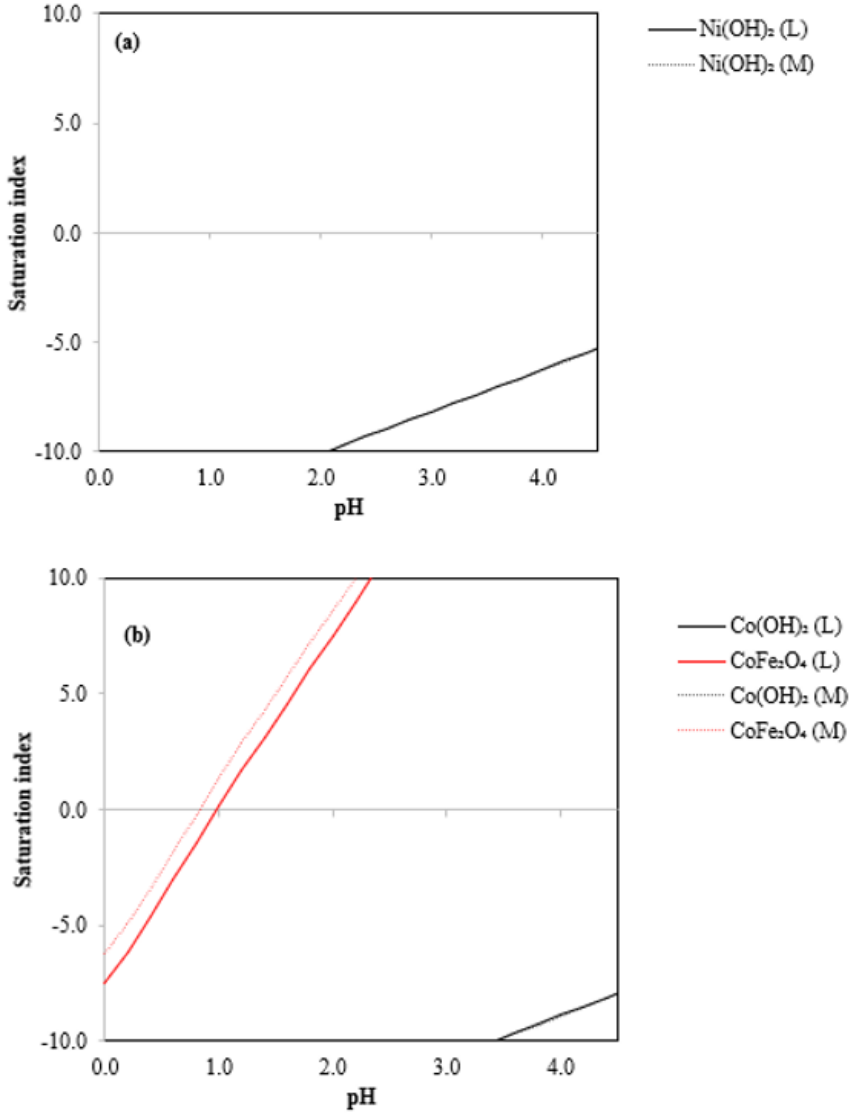

Figure 3.7: (a) Saturation index for nickel hydroxide ($NiOH_2$) and (b) cobalt hydroxide ($Co(OH)_2$) and $CoFeO_4$ as a function of pH for a quinary solution at 25 °C (L) and 40 °C (M).

The simulation results showed that the behaviour of the cations in solution and the stability of the sulfate solution is influenced by both pH and temperature. The results

of the simulation assisted in estimating the operating conditions in the design of the experiments in the subsequent sections, investigating the removal of iron, aluminium and chromium from synthetic sulfate solutions simulating real leach solutions from leaching nickel laterite ores.

3.6.2 Preliminary Experiments

3.6.2.1 The effect of using different neutralising agent during iron precipitation on nickel and cobalt losses

Calcium carbonate is a common neutralising agent used in the processing of solutions highly contaminated with iron such as nickel laterite sulfate leach solutions because it is cost-effective. Gypsum, a secondary mineral is formed when calcium carbonate slurry is used to neutralise acid sulfate solutions. The formation of gypsum causes severe scaling of plant equipment and the production of bulky precipitates for waste disposal and management. The use of magnesium and sodium containing neutralising agents, on the other hand, will minimise the scaling problem and produce less bulky precipitates since no gypsum or any other secondary mineral is formed. In addition, the choice of the neutralising agent to use in the processing of nickel laterite sulfate leach solutions largely depends on the removal efficiency of iron and the level of nickel and cobalt losses incurred when using the neutralising agent. Therefore, preliminary experiments were carried out to determine the effect of using $MgCO_3$, MgO, NaOH and $CaCO_3$ neutralising agents on the level of iron removal and the amount of nickel and cobalt losses from solution. The experiments were carried out using the experimental setup and general procedure described in Section 3.2.3 at pH 2.5, temperature 85 °C, using synthetic ternary sulfate solution [Fe(III)+Ni(II)+Co(II)] and a more complex synthetic multi-element sulfate solution (elemental composition as given in Table 3.1) containing about 37 g/L Fe(III), 4.5 g/L Ni(II) and 0.35 g/L Co(II). The results are given in Table 3.5.

Table 3.5: Effect of using various neutralising agents on the removal of iron and the amount of nickel and cobalt losses at 85 °C and pH 2.5, from solutions containing 35 g/L Fe (III), Fe/(Ni+Co) = 7.6 and 2 hours reaction time.

ID	Neutralising Agent	Metal in the dried precipitate (weight %)				Iron removal (%)	Ni loss (%)	Co los (%)
		Fe	Mg	Ca	Ni			
T1	$MgCO_3$ slurry	29.55	0.23		0.12	96.12	3.80	3.33
T2	MgO slurry	29.42	0.38		0.56	95.95	7.36	6.37
T3	NaOH solution	28.66			0.08	90.27	2.23	2.26
T4	$CaCO_3$ slurry	11.73		18.45	0.05	97.88	0.23	0.50
M1	$MgCO_3$ slurry	29.89	0.42		1.54	97.88	21.49	18.84
M2	NaOH solution	29.24			1.14	97.82	15.92	13.64
M3	$CaCO_3$ slurry	12.83		19.34	0.11	99.11	1.74	2.02

The results labelled T1 to T4 were obtained using ternary sulfate solution [Fe(III)+Ni(II)+Co(II)] while M1 to M3 were obtained using multi-element sulfate solution [Fe(III)+Al(III)+Cr(III)+Mg(II)+Mn(II)+Ca(II)+Cu(II)+Zn(II)+Ni(II)+Co(II)]. The results labelled T1 to T4 show that the percentage iron removal is higher when using neutralising agents in the slurry form than when using sodium hydroxide solution. The removal of iron was quite low approximately 90% with sodium hydroxide solution compared to more than 95% obtained with the slurries of $MgCO_3$, MgO and $CaCO_3$. The nickel and cobalt losses varied with the different neutralising agents and the affinity for nickel and cobalt uptake by the precipitates produced is in the following order: MgO > $MgCO_3$ > NaOH > $CaCO_3$. The uptake of base metal ions in iron precipitates is influenced by the properties of the iron precipitates formed (Claassen and Sandenbergh, 2007). Highly reactive neutralising agents cause rapid hydrolysis precipitation and the production of fine and amorphous precipitates with high adsorbent properties which promote high nickel and cobalt losses. NaOH solution is dissociated with the OH^- ready to react and is, therefore, more reactive than the slurry neutralising agents which must undergo decomposition to release the OH^- ions. From the experimental results, nickel and cobalt losses were lesser with NaOH

solution than with MgO and $MgCO_3$ slurries neutralising agents which is not in support of the reactivity of the neutralising agents. This could be because the introduction of Na^+ ions from the sodium hydroxide solution at 85 °C, low pH values and high ferric ion concentration causes jarosite precipitation (Dutrizac and Jambor, 2000), a precipitate with lower adsorption affinity for divalent metal ions. Comparison of the results obtained in the ternary system (T1 to T4) and those of the multi-element system (M1 to M3) shows that more nickel and cobalt is lost during the processing of multi-element sulfate solutions. The finding agrees with the observations made in studies on the co-removal of Fe, Al and Cr (Wang et al., 2011, Guise and Castro, 1996), where the level of nickel loss was found to increase with increase in the number of impurities in solution in the order [Fe(III)+Ni(II)]<[Fe(III)+Al(III)+Ni(II]<[Fe(III)+Al(III)+ Cr(III)+Ni(II)]. A reason for the increased nickel loss has not been advanced in the literature, however, increase in nickel and cobalt could be due to high adsorption properties of aluminium and chromium oxyhydroxides which are also formed during iron precipitation.

3.6.2.2 Analysis of the precipitates

The elemental composition of the precipitates (Table 3.5) indicates that % iron content is high in the precipitates formed from non-calcium containing neutralising agents which suggest less bulky precipitates are obtained. A lower % iron content in the precipitates when using calcium carbonate slurry is because of gypsum formation, a secondary product which dilutes the concentrations. Additionally, the amount of nickel and cobalt losses to the precipitate varied significantly among the precipitate samples, probably due to the difference in precipitate quality. The quality of precipitate, especially the particle size distribution impacts on liquid-solid separation processes and nickel and cobalt uptake by the precipitates. The slurries obtained from processing the ternary synthetic sulfate solution, at pH 2.5, 85 °C, using $CaCO_3$, $MgCO_3$, MgO and NaOH neutralising agents were analysed for particle size distribution. The % volume and number density distribution of the particles when using the different neutralising agents in the ternary synthetic sulfate solution is shown in Figure 3.8a and Figure 3.8b, respectively.

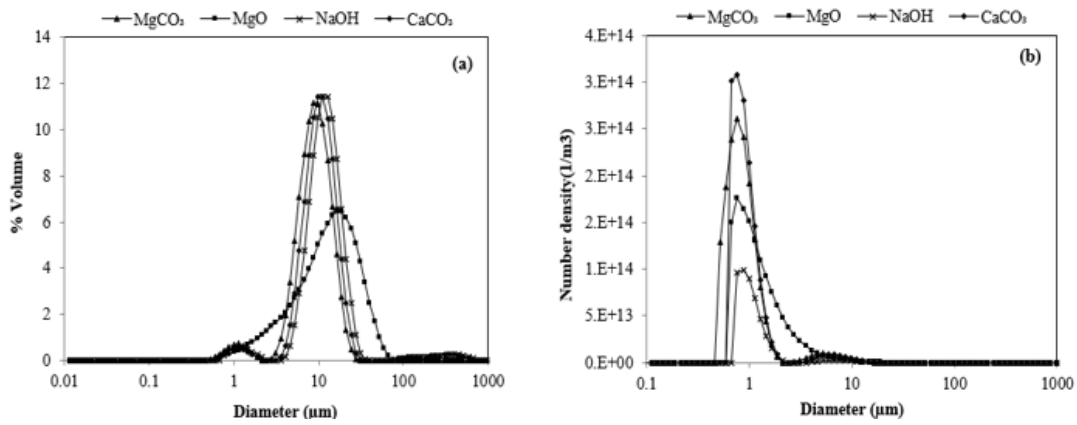

Figure 3.8: Particle size distribution (PSD) for different neutralising agents for iron precipitation. (a) % volume and (b) number density distribution.

The results show bimodal distributions when neutralising the acid sulfate solution with $MgCO_3$, NaOH and $CaCO_3$ and unimodal when using MgO (Figure 3.8a and Figure 3.8b). The bimodal distributions had peaks with maximum at 0.68 and 5.21 µm with $CaCO_3$, 0.77 and 5.21 µm with $MgCO_3$ and 0.68 and 5.9 µm with NaOH solution. When using MgO the single peak was maximum at 0.77 µm. The number density distribution shows the formation of a large number of fine particles (Figure 3.8b). At the high initial ferric ion concentration, supersaturation levels are high which suggests high primary nucleation rates evidenced by the formation of many small particles, red-brown colloids. The wide span particle distribution with all neutralising agents supports the precipitation mechanism of nucleation and crystal growth which occurs through the formation of monomers which condense to polymers (red-brown colloids) and nanoparticles (Dousma and De Bruyn, 1976). The bimodal distribution obtained could be due to aggregation of smaller particles and growth of particles promoted at lower ferric ion concentration as the reaction proceeds. Also, the bimodal distribution could be an indication of the presence of more than one mineral formed in the system, which is a common phenomenon in iron precipitation processes (Park et al., 2013, Park et al., 2015). Although the use of different neutralising agents affects the level of nickel and cobalt losses and iron removal, there was no substantial difference on the particle size distribution of the precipitates to support the observed difference in nickel and cobalt losses. This was also evident during filtration with the filtration properties of the slurries from the ternary sulfate solutions not sensitive to the type of neutralising agent. The filtrates were recovered in less than a minute by vacuum filtration. On the contrary, the slurries obtained from processing multi-element sulfate solutions were

very fine and difficult to filter, and when filtered and washed, the precipitate had a clay-like (muddy) consistency and dried into a very hard lump. Excessive nickel and cobalt losses (Table 3.5) were observed when processing multi-element synthetic sulfate solution for all neutralising agents except calcium carbonate slurry.

The precipitates obtained from the processing of ternary sulfate solution were also analysed using SEM (Figure 3.9) and EDS (Figure 3.10). SEM images of the precipitates revealed different morphologies (Figure 3.9) for the different neutralising agent used. The SEM micrographs T1 and T4 showed web-like structures, which closely resemble those of schwertmannite particles (Dold, 2003). Sample T2 which was formed when using magnesium oxide formed aggregates of particles irregular in shape which is possibly the amorphous iron oxyhydroxides. In comparison, the precipitates formed while neutralising with sodium hydroxide solution consisted of bigger and smooth, regular shaped particles with some aggregates of fine particles which could be an indication of the formation of a crystalline iron phase, jarosite which is pseudocubic in structure (Wagner et al., 1982).

The SEM micrographs of the precipitates T1 to T4 were analysed for elemental content using EDS area analysis. The results are given in Figure 3.10. The results show that the precipitates consisted mainly of iron, sulfur and oxygen and trace amounts of aluminium and the cation from the neutralising agent that is Mg for sample T1 and T2, Na for sample T3 and Ca for T4. There was no noticeable change in elemental composition during the analysis of different crystals within the same precipitate in samples T1 to T3. Sample T4, a precipitate obtained using calcium carbonate consisted of needle-like crystals similar in structure to those of gypsum (Wagner et al., 1982) and aggregates of smaller particles like those in T1 and T3. The needle-like crystals (spectrum 20) consisted mainly of Ca, S and O and minor Fe which supports the presence of the calcium mineral, gypsum while the aggregates (spectrum 23) were composed mainly of Fe, S and O and minor Ca, Ni and other trace elements. The detection of Ni in the aggregates suggests that nickel losses are mainly associated with the iron phases and not gypsum which agrees with findings by Wang (2012), where no nickel was detected when gypsum was precipitated from a nickel sulfate solution. Nickel losses incurred during iron precipitation may occur through adsorption on the minerals, or co-precipitation (Beukes et al., 2000). The SI index calculated for nickel hydroxide (Figure 3.7a) indicated that nickel hydroxide would not form below pH 4.5

and Ramesh and Kamath (2006) indicates that it only forms above pH 5.0. This implies that nickel losses incurred at pH 2.5 could be because nickel is substituting for iron in the lattice through isomorphous substitution due to analogous ionic radius, nickel (0.69 Å) and iron (0.64 Å) as suggested in the model by (Carvalho-e-Silva et al., 2003) or the nickel is adsorbed on the mineral surface. Nickel was not detected in samples T1 to T3 most likely because of low nickel content of the precipitate below the detection limits of the analytical instrument.

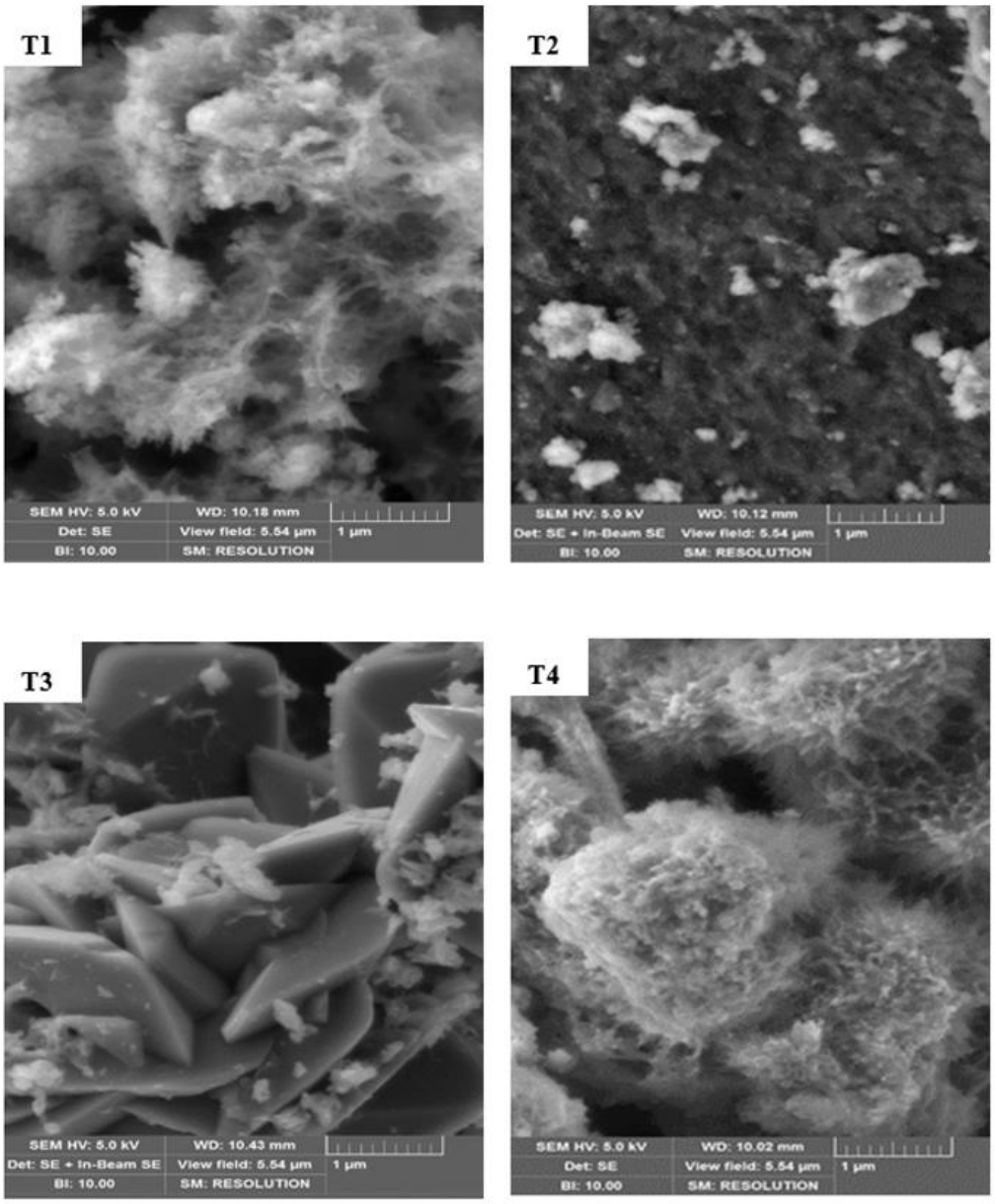

Figure 3.9: Scanning electron micrographs (high magnification) of iron precipitates from a ternary sulfate solution [Fe(III)+Ni(II)+Co(III)] at pH 2.5 and 85 °C using four different neutralising agents:T1 - magnesium carbonate slurry, T2 - magnesium oxide slurry, T3 - sodium hydroxide solution and T4 - calcium carbonate slurry.

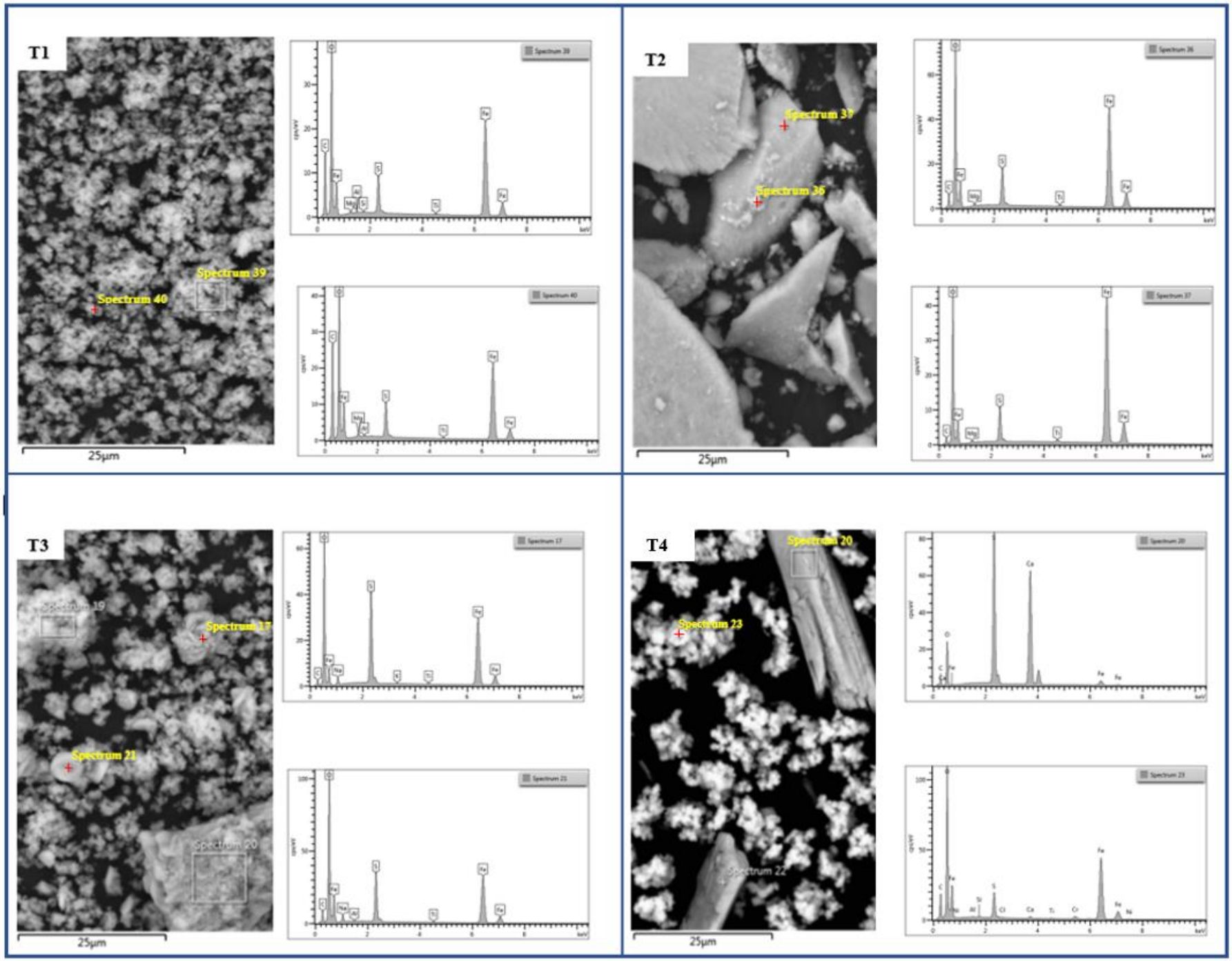

Figure 3.10: Low magnification SEM micrographs of precipitates and EDS area analysis: T1 - magnesium carbonate slurry, T2 - magnesium oxide slurry, T3 - sodium hydroxide solution and T4 - calcium carbonate slurry.

The precipitation of iron in this study is carried out at temperature and pH values mainly used for goethite precipitation (Allan et al., 1970) but without Fe^{3+} concentration kept at 2 g/L during precipitation (uncontrolled ferric concentrations) as in the Jarosite Process (Dutrizac, 1983). The goethite and jarosite precipitates from the processing of acidic iron sulfate solution using precipitation processes are often a mixed assemblage of poorly and highly ordered iron minerals (Section 2.3.1). XRD analysis was used in an attempt to identify the minerals present in each precipitate sample (T1 to T4), and the XRD patterns obtained are given in Figure 3.11a and b.

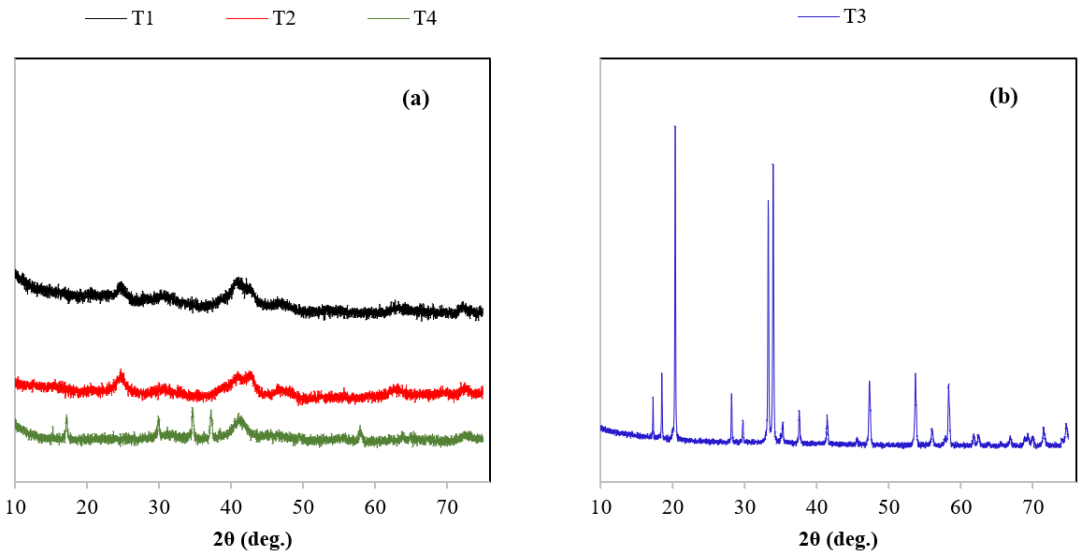

Figure 3.11: (a) X-ray diffraction patterns of the precipitate samples T1- magnesium carbonate slurry, T2 - magnesium oxide and T4 calcium carbonate slurry (T4) and (b) T3 - sodium hydroxide solution in processing the ternary synthetic sulfate solution at pH 2.5 and 85 °C.

The XRD patterns of samples T1, T2 and T4 given in Figure 3.11a shows weak and broad XRD peaks indicative of a mixed assemblage of amorphous and poorly ordered iron phases, which supports the observed non-crystalline structure in Figure 3.9. The amorphous nature of the precipitate makes it difficult to identify the phases with certainty. XRD peaks at around 25°, 41°, 63° and 72° 2θ can be identified in precipitates obtained using magnesium carbonate and magnesium oxide slurries as neutralising agents. When using calcium carbonate slurry, although the sample was physically washed using deionised water to remove gypsum by scrapping the white flakes of separated gypsum, some crystalline gypsum remained entrained, and the sharp peaks for gypsum continue to mask iron phases, and the only iron phase peak that can be identified is at 41° 2θ. Schwertmannite and ferrihydrite have been found to exhibit peaks that correlate with the observed peaks at 2-theta angle of 41°, 63° and

72° while the peak at around 25° 2θ could be that of goethite when using Co-Kα radiation (Bigham et al., 1990). Goethite could have been formed by transformation of the initially formed poorly ordered and amorphous iron phases. The observed XRD patterns are to some extent similar with those identified during iron precipitation using E.Z. goethite process at 85 °C in acidic sulfate solutions (Wang et al., 2013), and this is regardless of the high ferric iron concentration (> 2 g/L) during precipitation in this study.

On the contrary, sharp XRD patterns were obtained when analysing the precipitates formed from the acidic ternary sulfate solution when neutralising with sodium hydroxide solution, which is indicative of the formation of a more crystalline phase. This is in support of the well-defined crystal structure of sample T3 observed in Figure 3.9. The XRD patterns of T3 matched those of jarosite, which was formed because of sodium hydroxide solution supplying sodium ion a jarosite-forming cation at the high ferric ion concentration. At lower ferric ion concentrations (<2 g/L) generated using V.M. method, at the same temperature of 85 °C and pH value, goethite was reported to form and not jarosite when a binary sulfate solution [Fe(II)+Ni(II)] was neutralised with sodium hydroxide solution (Yue et al., 2016), which suggests that for goethite to form, ferric ion concentration must be low (<2 g/L) during precipitation. In all the samples (T1 to T4), there were no nickel and cobalt phases detected which is probably attributed to the low nickel and cobalt content in the precipitate as can be seen from Table 3.5.

Overall, better iron removal and selectivity for iron over nickel were obtained when neutralising with $CaCO_3$ slurry than when using the other neutralising agents in both the ternary and multi-element sulfate solutions. The difference in the filtration properties of the slurries and the increase in the amount of nickel and cobalt losses during processing the multi-element sulfate solution could have been influenced by the foreign metal ions. Therefore, it is necessary to investigate the effect the presence of the major foreign metal ions have on the amount of nickel and cobalt losses to the precipitates and the nature of iron precipitates formed. The multi-element sulfate solution is a better simulation of real nickel laterite leach sulfate solutions and therefore better suited for further investigations to understand the behaviour of real nickel laterite sulfate leach solutions. The main objective of this study is to effectively co-remove iron, aluminium and chromium at minimal nickel and cobalt losses. In

addition to calcium carbonate being widely used and of relatively low cost, the lowest nickel and cobalt losses are incurred compared to when using magnesium carbonate and magnesium oxide slurries and sodium hydroxide solution. Therefore, calcium carbonate slurry was used in subsequent experiments carried out to investigate the effect of the major foreign metal ions present in the multi-element sulfate solution on nickel and cobalt losses and the factorial design experiments.

3.6.3 Effect of the presence of aluminium, chromium and magnesium on nickel and cobalt losses during iron precipitation

The filtration properties of the precipitates were poor, and the level of nickel and cobalt losses increased when more impurity elements were in solution in the multi-element sulfate solution during iron precipitation (Section 3.6.2). In the multi-element sulfate solution, there are significant amounts of aluminium, chromium, magnesium and manganese and low levels of copper and zinc in solution with nickel and cobalt. This section was carried out to estimate the effect of the presence of aluminium, chromium and magnesium during iron precipitation on nickel and cobalt losses and the nature of the precipitates. A set of experiments were carried out using the procedure described in Section 3.2.3 at pH 4.0 and temperature 85 °C using synthetic sulfate solutions with various combinations of metal ions and calcium carbonate slurry neutralising agent. A pH value of 4 is a typical pH for the precipitation of aluminium (Steemson and Smith, 2009). The following metal combinations were used: FNC [Fe(III)+Ni(II)+Co(II)], ANC [Al(III)+Ni(II)+Co(II)], CrNC [Cr(III)+Ni(II)+Co(II)], FANC[Fe(III)+Al(III)+ Ni(II)+Co(II)], FCrNC [Fe(III)+Cr(III)+Ni(II)+Co(II)], FMNC [Fe(III)+Mg(II)+ Ni(II)+Co(II)], FACrNC [Fe(III)+Al(III)+Cr(III)+Ni(II)+Co(II)] and a multi-element sulfate solution with composition as given in Table 3.1. Table 3.6 shows the metal removal from the various synthetic sulfate solutions.

Table 3.6: Metal removal (%) obtained from the different synthetic sulfate solutions with various combinations of metal ions at pH 4.0 and temperature 85℃, using calcium carbonate slurry as neutralising agent .

ID	Metal removal (%)					
	Fe	Al	Cr	Mg	Ni	Co
FNC	99.16				7.47	2.32
ANC		98.08			6.37	3.79
CrNC			98.26		7.03	4.49
FANC	99.93	94.67			12.08	7.93
FCrNC	99.53		99.42		11.04	7.24
FMNC	99.27			0.00	8.60	10.46
FACrNC	99.97	97.45	99.76		11.00	7.03
Multi	99.95	99.26	99.90		27.59	11.70

The results show that the removal of iron, aluminium and chromium is high at the conditions used but at the cost of more nickel and cobalt losses from solution. Nickel and cobalt losses were reasonably lower in the ternary systems, FNC, ANC and CrNC compared to when using quaternary and higher systems. Higher nickel and cobalt losses were observed (Table 3.6) during the co-removal of iron, aluminium and chromium, with the highest losses in the multi-element sulfate solution. This is somewhat in agreement with the observations of Guise and Castro (1996) and Wang et al. (2011) who studied the co-removal of iron, aluminium and chromium from binary, ternary and quaternary nickel sulfate solutions. They found that nickel losses were higher during the co-removal of iron, aluminium and chromium. The increase in nickel losses could be due to high adsorption properties of aluminium and chromium oxyhydroxides which are also formed during iron precipitation The nickel losses in FNC, FANC, FCrNC and FACrNC in the present study are comparable to those obtained by Wang (2012) at the same pH value of 4 and temperature of 85 ℃ in the respective systems but without cobalt. The almost similar results in nickel loss are

irrespective of the high metal concentrations of the metal ions during precipitation in the present study compared to the iron concentrations kept below 2 g/L with E.Z. method in Wang (2012). The use of E.Z method is meant to improve precipitate quality and reduce the uptake of nickel by the precipitates. Comparison of the nickel loss results obtained in the quaternary system FMNC and those of FANC and FCrNC shows that less nickel is lost during the processing of sulfate solutions with magnesium in comparison to both aluminium and chromium. With respect to cobalt, comparison of FNC and FMNC indicated an 8% increase in cobalt loss. However, no magnesium is precipitated out as it was not detected in the precipitate. A review of Table 3.5 indicates greater cobalt losses when magnesium containing neutralizing agents were used. This suggests that magnesium both from the leach solution and from magnesium neutralising agents increases the cobalt losses probably through its influence of the nature of precipitate formed.

The precipitates produced from processing FMNC and multi-element sulfate solution had a different texture to those obtained when processing iron solutions without magnesium. The presence of magnesium in the iron sulfate solutions resulted in the production of clay-like (ultra-fine) precipitates and not the fluffy precipitate obtained in the other systems without magnesium. The clay-like precipitates were difficult to filter taking more than 30 minutes compared to the other precipitates which were instantaneously filtered. Furthermore, gypsum could not be washed from the clay-like precipitates as was the case in the fluffy precipitates formed in the absence of magnesium in solution during precipitation. The precipitates obtained when processing the FNC, FANC, FCrNC, FMNC and the multi-element sulfate systems were analysed using SEM and XRD. The SEM micrographs and the results are shown in Figure 3.12.

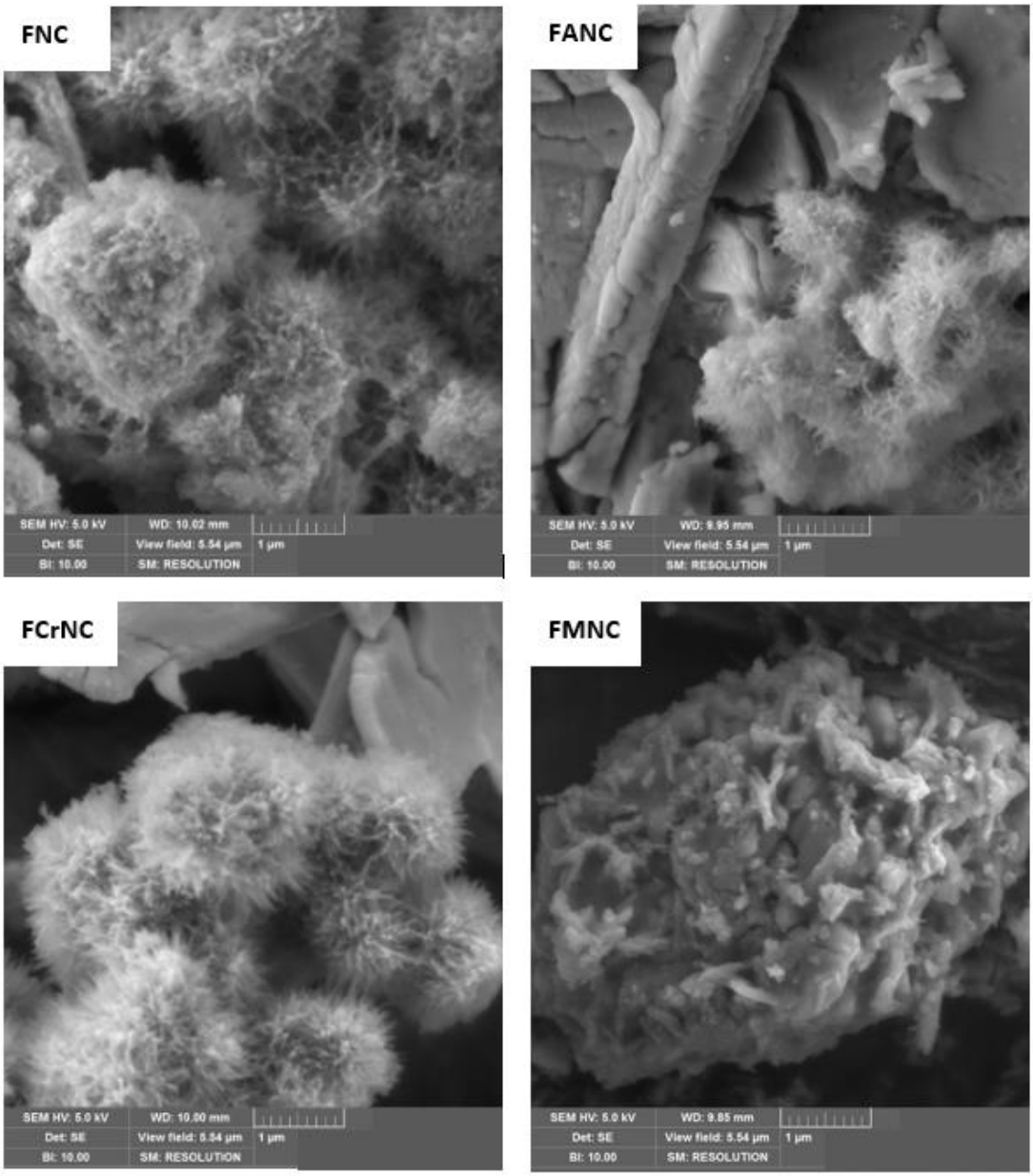

Figure 3.12: Scanning electron micrographs of iron precipitates sulfate solutions of various combinations of metal ions, [Fe(III)+Ni(II)+Co(III)], [Fe(III)+Al(III)+Ni(II) +Co(III)], [Fe(III)+Cr(III)+Ni(II)+Co(III)] an [Fe(III)+Mg(II)+Ni(II)+Co(III)] at pH 4 and 85 ℃ using calcium carbonate slurry.

There are some noticeable similarities in particle morphology and crystallinity among samples FNC, FANC and FCrNC but not FMNC based on the SEM and XRD analysis results. The SEM micrographs of samples FNC, FANC and FCrNC showed web-like structures, which visually closely resemble the structure of schwertmannite (Dold, 2003) and a broad peak identified at around 41° 2θ similar to that observed in sample T4 (Section 3.6.2.2). It is evident that the structure was affected differently by the presence of magnesium, with the precipitate FMNC consisting of aggregates of

particles which produced an uneven surface. The concentration of magnesium in the magnesium-containing sulfate solution was high (>13 g/L) which could be the reason for highly amorphous iron precipitates compared to those when using magnesium-containing neutralising agents in processing ternary system in Section 3.6.2, where magnesium concentration is very low. This suggests that magnesium concentration during precipitation influence the nature of precipitates. The observations are supported by the XRD analysis results given in and Figure 3.13.

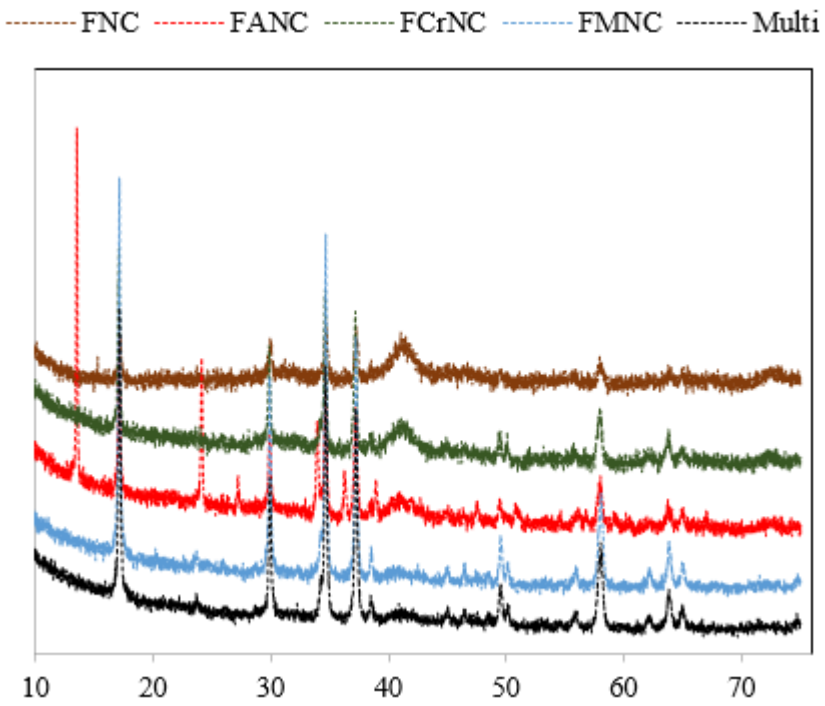

Figure 3.13: X-ray diffraction patterns of the precipitate samples FNC, FANC, FCrNC and FMNC produced at pH 4 and 85 ℃.

In Figure 3.13, broad peaks at around 41° 2θ were only identified in samples FNC, FANC and FCrNC and not FMNC and multi-element system were only peaks of gypsum are identified. Iron phases are masked by crystalline gypsum, and this is more profound in the precipitates formed from solutions containing a significant amount of magnesium. It was very difficult to separate gypsum by washing the clay-like consistency precipitates of magnesium-containing solutions. The gypsum particles and the iron precipitates were very fine and formed an almost perfect mixture. The presence of magnesium in nickel sulfate solution during precipitation influences the nature of precipitates which directly impacts on liquid-solid separation processes (such as filtration) and indirectly on the amount of nickel and cobalt losses. In the presence

of magnesium in solution during iron precipitation, the precipitates formed are slimes (clay in nature) which could be as a result of magnesium ions influencing the precipitation mechanism. It is an interesting observation considering that also higher nickel and cobalt losses are observed when using magnesium containing neutralising agents (Section 3.6.2.1).

3.6.4 Full factorial design

Full factorial design experiments were carried out using the procedure described in Section 3.2.3 to evaluate the significance of the three selected factors: pH, temperature and concentration of the calcium carbonate slurry. The experimental results of the full factorial design are given in Table 3.7. The significant variables were screened using graphical analysis, by plotting half-normal probability plots, typically used to screen the factors to be kept in the model for unreplicated experiments (Box and Meyer, 1986). In half-normal probability plots, the standardised values of the effects, are plotted against the normal distribution fit line to the data. It is assumed that only the main effects and low order interactions dominate the process and the high order interactions are negligible. The significant effects deviate from the normal distribution line. That is they fall off the line while the non-significant and less significant effects follow the normal distribution line. Similarly, the statistical significance of the different variables and their interactions can be identified using analysis of variation (ANOVA) at a given significance level (α), normally at 0.05 (95% confidence interval). When the p-value of the variable is less than or equal to the significance level (0.05), this demonstrates that the variable is of a statistical significance on the response variable while a p-value more than 0.05 suggests statistical insignificance.

Table 3.7: The calculated percentage metal loss and metal removal of the full factorial design experiments.

Run	Responses				
	Metal loss (%)		Metal removal (%)		
	Ni	Co	Fe	Al	Cr
1	4.60	4.59	100.00	99.02	100.00
2	3.57	3.39	99.89	94.66	100.00
3	27.59	11.70	99.93	99.60	99.90
4	0.69	0.61	99.23	33.84	91.92
5	0.15	0.01	98.98	16.90	84.96
6	34.02	21.53	99.96	99.70	100.00
7	1.74	2.02	99.11	36.21	91.77
8	3.19	3.74	99.64	44.84	96.72
9	9.77	5.82	99.98	97.51	100.00
10	38.72	26.80	100.00	99.41	100.00
11	0.01	0.42	98.41	23.47	88.77
12	0.01	0.01	98.84	13.87	86.29
13	22.25	10.30	99.95	99.40	100.00
14	5.15	5.64	100.00	97.76	100.00
15	4.13	3.32	98.90	42.85	94.64
16	0.21	1.02	98.53	20.08	89.76

Figure 3.14 to Figure 3.18 are the half-normal plots for the % iron, % aluminium and % chromium removal and the log (% nickel loss) and log (% cobalt loss) obtained during precipitation. Log transformation was used to describe nickel and cobalt losses because the ratio of the maximum response to the minimum response is large. Box-Cox analysis was used to determine whether a transformation is necessary for describing the results in an appropriate form for statistical analysis and stabilising the variance of the response and improve the fit of the model for the data. The transformation in the family $y^* = y^{\lambda}$, where λ is the parameter defining the transformation was used. For theoretical analysis, standard analysis is usually performed using various values of λ on the preferred form:

$$y^{\lambda} = \frac{y^{\lambda}-1}{\lambda} \ (\lambda \neq 0), \ y^{\lambda} = \log y \ (\lambda = 0)$$

The transformation applies to response values (y) more than 0. The estimation for λ can be found by plotting a graph of standard deviation versus λ, and for the fitted model, the maximum likelihood value for λ occurs at the lowest point in the graph. Furthermore, the values of λ at a given confidence interval can be determined from the plots and are the values where the graph cuts the critical standard deviation (limit). In this study, the plots of the standard deviation for the various values of λ for % nickel and cobalt losses and % aluminium removal and a 95% confidence interval were carried out and Table 3.8 gives the respective optimum, low and high values of λ obtained for the % Ni and Co loss and % Al removal. For both % nickel and cobalt losses, the optimum value for λ and zero falls in the 95% confidence limit, which means that the log transformation can be used to adequately process the results (Figure 3.17 and Figure 3.18). When the confidence limit for λ value includes 1, it is equivalent to using the original data. Since the confidence interval for the optimal λ includes 1 for % aluminium removal, then no transformation is necessary (Figure 3.15) despite the large range in the response values.

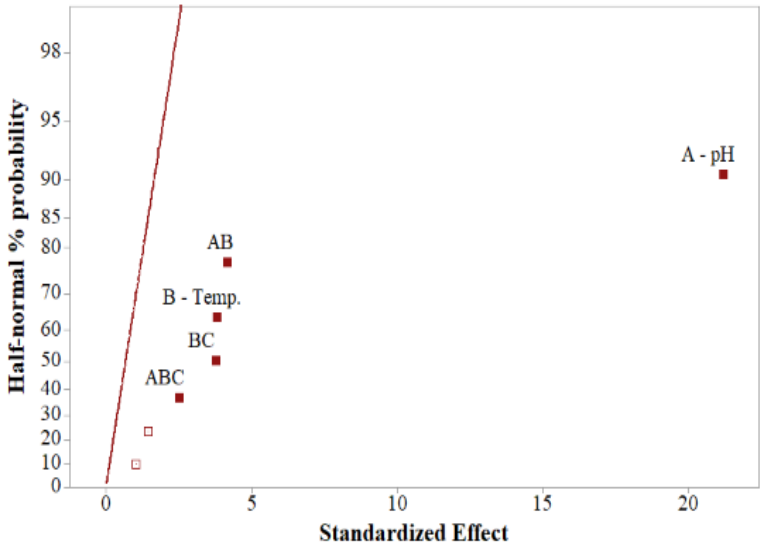

Figure 3.14: Half-normal plot of the standardised effects for iron removal (%) showing significant effects and interactions as filled labelled squares.

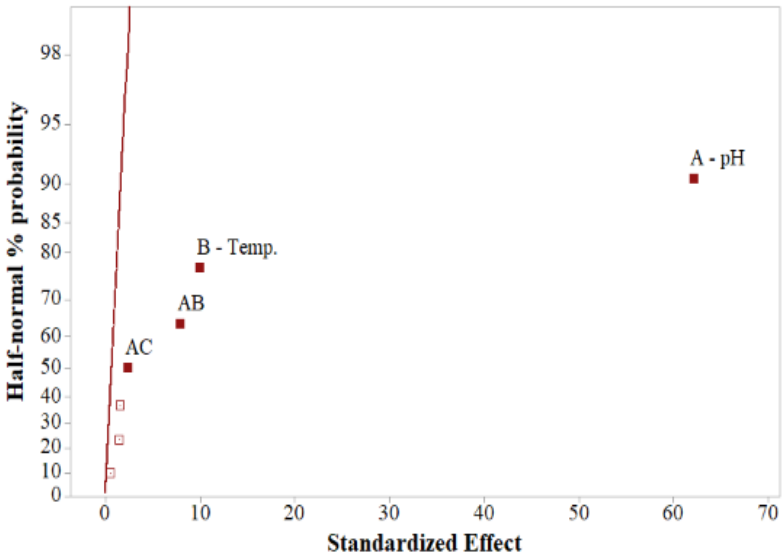

Figure 3.15: Half-normal plot of the standardised effects for aluminium removal (%) (%) showing significant effects and interactions as filled labelled squares.

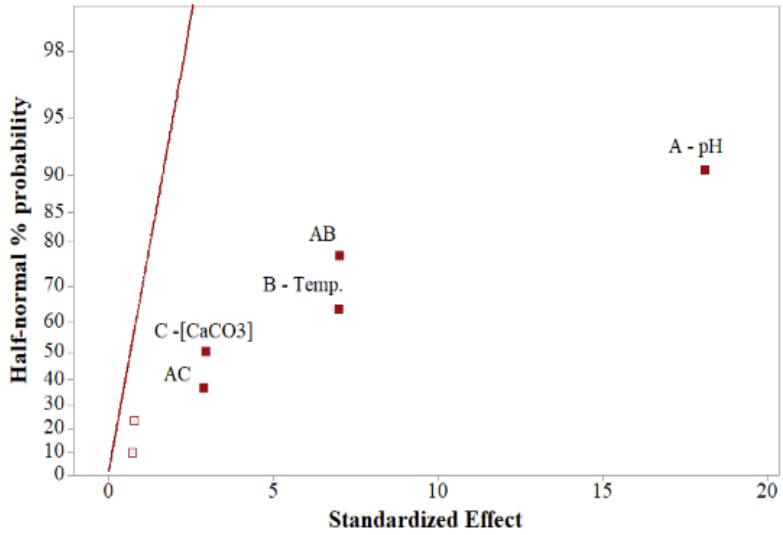

Figure 3.16: Half-normal plot of the standardised effects for chromium removal (%), (%) showing significant effects and interactions as filled labelled squares.

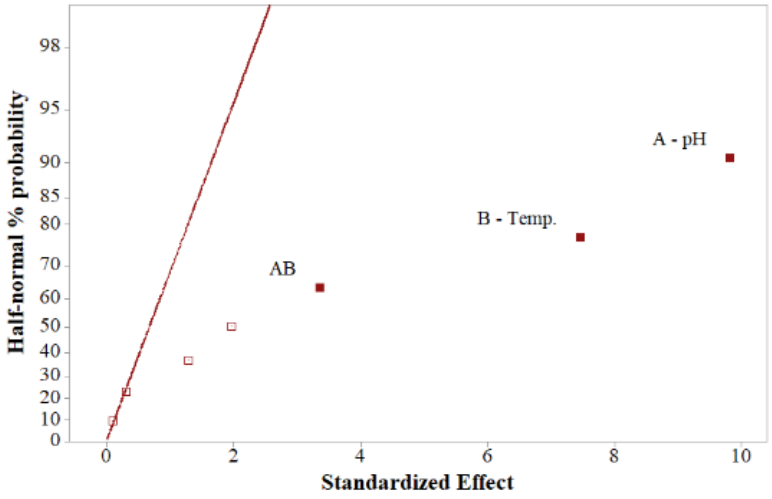

Figure 3.17: Half-normal plot of the standardised effects for log (% nickel loss), (%) showing significant effects and interactions as filled labelled squares.

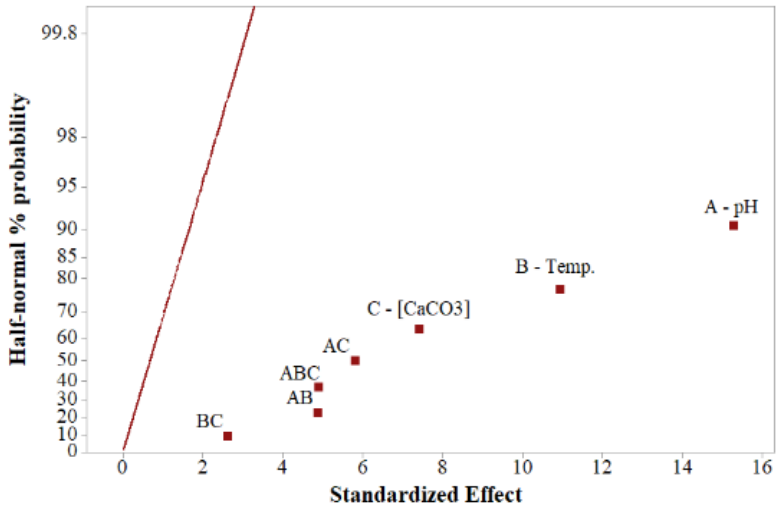

Figure 3.18: Half-normal plot of the standardised effects for log (% cobalt loss), (%) showing significant effects and interactions as filled labelled squares.

Table 3.8: λ-values obtained from the Box-Cox plots of % Ni, Co and Al removal at 95% confidence interval.

Response	λ-value		
(%)	Optimum	Low	High
Ni	0.10	-0.12	0.34
Co	0.17	-0.02	0.47
Al	0.65	-0.30	1.52

Figure 3.14 to Figure 3.18 show that variables A (pH) and B (temperature) have significant effects on the removal of iron, aluminium and chromium and nickel and

cobalt losses from the system while variable C ($CaCO_3$ concentration) show a substantial effect on the removal of chromium and cobalt loss. Both pH and temperature have a large effect on nickel loss while pH and $CaCO_3$ concentration have a significant effect on cobalt loss. However, pH has the largest effect on the removal of all metal ions from the solution shown by the very small p-value (<0.0001) in Table 3.9 and Table 3.10. The interactions of pH and temperature (AB) and, pH and calcium carbonate concentration (AC) are of statistical significance to the removal of iron, aluminium and chromium as well as cobalt loss, but temperature and calcium carbonate concentration (BC) interaction and the 3-way interaction of the variables (ABC) have a significant effect on the removal of iron and cobalt loss. The removal of the trivalent ions of iron, aluminium and chromium from solution increases with increasing pH and temperature, but at the expense of more nickel and cobalt losses. The results are in agreement with the results obtained by Wang et al. (2011) who observed greater iron removal and nickel loss when pH increased from 2.0 to 4.0 and temperature increased from 25 to 85 °C. At high pH and temperature, the equilibrium concentration of the metal ions (M^{z+}) in solution decreases resulting in more precipitation of the trivalent ions of iron, aluminium and chromium in accordance with the solubility products of the metal hydroxides ($K_{sp_{(M(OH)z)}} = [M^{z+}][OH\text{-}]^{z}$). Calcium carbonate slurry concentration, on the other hand, is not a significant factor on nickel loss but using low concentration can regulate the level of supersaturation. At low level of supersaturation, there is reduced nucleation rate and the precipitation of bigger particles with better liquid-solid separation properties and relatively lower adsorbent properties and solution entrainment which influence the loss of base metal ions (Claassen and Sandenbergh, 2007).

When quantitative variables such as pH, temperature and concentration of species are investigated, it is necessary to use more than two levels of each factor to obtain meaningful information on the effect of the variables on the responses in the form of curves. From the factorial experiments, almost complete removal of iron is possible at pH 2.5 (greater than 98%), but the removal of aluminium and chromium requires operating at higher pH values and temperature values. Thus, a more detailed study on the effect of pH and temperature using one variable at a time approach was carried out using low $CaCO_3$ concentration to estimate the optimal conditions required for the removal of iron, aluminium and chromium.

Table 3.9: Analysis of variance for the 6-parameter model (three main effects and three two-factor interaction terms).

Source	% Nickel loss					% Cobalt loss					% Iron removal				
	Degrees of Freedom	Adjusted Sum of squares	Adjusted Mean squares	F-Value	p-value	Degrees of Freedom	Adjusted Sum of squares	Adjusted Mean squares	F-Value	p-value	Degrees of Freedom	Adjusted Sum of squares	Adjusted Mean squares	F-Value	p-value
Model	7	22.4025	3.2004	24.07	<0.0001	7	15.2920	2.1846	70.70	<0.0001	7	5.2083	0.744	71.8045	<0.0001
Linear	3	20.6805	6.8935	51.84	<0.0001	3	12.5808	4.1936	135.72	<0.0001	3	4.8103	1.6034	154.7423	<0.0001
A-pH	1	12.7881	12.7881	96.17	<0.0001	1	7.2002	7.2002	233.03	<0.0001	1	4.6417	4.6417	447.9493	<0.0001
B- Temperature	1	7.3806	7.3806	55.50	<0.0001	1	3.6936	3.6936	119.54	<0.0001	1	0.1478	0.1478	14.2641	0.0054
C- Base Conc.	1	0.5119	0.5119	3.85	0.0854	1	1.6871	1.6871	54.60	<0.0001	1	0.0209	0.0209	2.0138	0.1936
2-Way interactions	3	1.7096	0.5699	4.29	0.0440	3	1.9765	0.6588	21.32	0.0004	3	0.3332	0.1111	10.7186	0.0036
AB	1	1.4918	1.4918	11.22	0.0100	1	0.7308	0.7308	23.65	0.0013	1	0.1775	0.1775	17.1317	0.0033
AC	1	0.2168	0.2168	1.63	0.2374	1	1.0359	1.0359	33.53	0.0004	1	0.0103	0.0103	0.9909	0.3487
BC	1	0.0009	0.0009	0.01	0.9371	1	0.2098	0.2098	6.79	0.0313	1	0.1454	0.1454	14.0333	0.0057
3-Way interactions	1	0.0124	0.0124	0.09	0.7677	1	0.7347	0.7347	23.78	0.0012	1	0.0647	0.0647	6.2485	0.0370
ABC	1	0.0124	0.0124	0.09	0.7677	1	0.7347	0.7347	23.78	0.0012	1	0.0647	0.0647	6.2485	0.0370
Error	8	1.0638	0.1330			8	0.2472	0.0309			8	0.0829	0.0104		
Total	15	23.4664				15	15.5392				15	5.2912			

Table 3.10: Analysis of variance for the 6-parameter model (three main effects and three two-factor interaction terms) continued.

Source	% Aluminium removal					% Chromium removal				
	Degrees of Freedom	Adjusted Sum of squares	Adjusted Mean squares	F-Value	p-value	Degrees of Freedom	Adjusted Sum of squares	Adjusted Mean squares	F-Value	p-value
Model	7	20343.4	2906.2	574.2	<0.0001	7	443.1	63.3	63.2	<0.0001
Linear	3	19987.8	6662.6	1316.3	<0.0001	3	384.5	128.2	127.9	<0.0001
A-pH	1	19480.2	19480.2	3848.7	<0.0001	1	327.4	327.4	326.8	<0.0001
B- Temperature	1	498.3	498.3	98.5	<0.0001	1	48.6	48.6	48.5	0.0001
C- Base Conc.	1	9.3	9.3	1.8	0.2118	1	8.6	8.6	8.6	0.0192
2-Way interactions	3	344.0	114.7	22.7	0.0003	3	58.0	19.3	19.3	0.0005
AB	1	314.8	314.8	62.2	0.0000	1	49.3	49.3	49.2	0.0001
AC	1	28.1	28.1	5.5	0.0463	1	8.3	8.3	8.3	0.0207
BC	1	1.1	1.1	0.2	0.6589	1	0.5	0.5	0.5	0.4973
Error	1	11.5	11.5	2.3	0.1700	1	0.6	0.6	0.6	0.4683
Lack of fit	1	11.5	11.5	2.3	0.1700	1	0.6	0.6	0.6	0.4683
Pure Error	8	40.5	5.1			8	8.0	1.0		
Total	15	20383.8				15	451.1			

3.6.5 Optimisation of the iron precipitation process

Both temperature and pH were identified in factorial design experiments as important factors for the removal of iron, aluminium and chromium and the amount of nickel and cobalt losses during precipitation. Furthermore, the co-removal of the trivalent ions of Fe, Al and Cr were found to influence the amount of nickel and cobalt losses in Section 3.6.2.3. The effect of pH and temperature on the removal of Fe, Al and Cr removal together with the associated nickel and cobalt loss from the system was therefore further investigated using one variable at a time approach. This was aimed at determining optimum conditions for maximum Fe, Al and Cr removal at acceptable nickel and cobalt losses. During the experiments, one factor was varied while keeping the other constant. The same experimental procedure (Section 3.2.3) used in the factorial design experiments and synthetic sulfate solutions of comparable composition except that total dissolved iron was either Fe(III) only or a mixture of 5% Fe(II), and 95% Fe(III) was used. Both ferrous and ferric ion were used because acidic leach solutions, particularly those generated by means of atmospheric leaching of laterite ores, contain substantial amounts of both Fe (III) and Fe (II) ions (Arroyo and Neudorf, 2001, White et al., 2006, Hernandez et al., 2014).

The effect of equilibrium pH at various operating temperature values on the removal of iron, aluminium and chromium where the iron in solution was a mixture of 5% Fe(II) and 95% Fe(III) is summarised in Figure 3.19, Figure 3.20 and Figure 3.21, respectively.

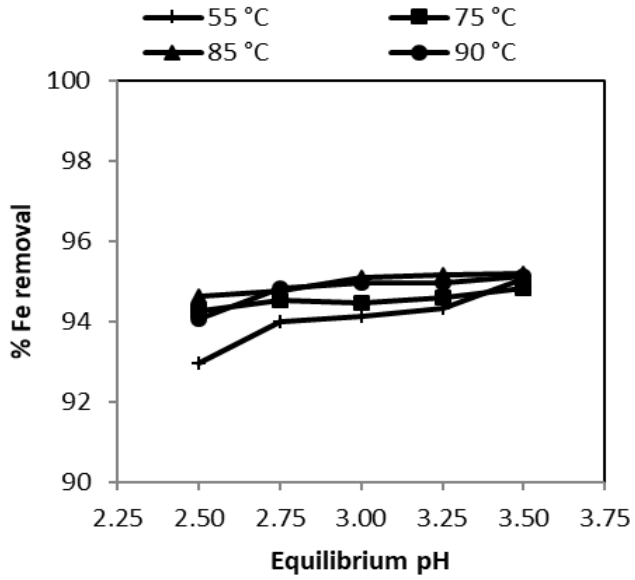

Figure 3.19: Percentage iron removal as a function of equilibrium pH at various temperatures (°C) from synthetic sulfate solution containing Fe (II) and Fe (III) during precipitation.

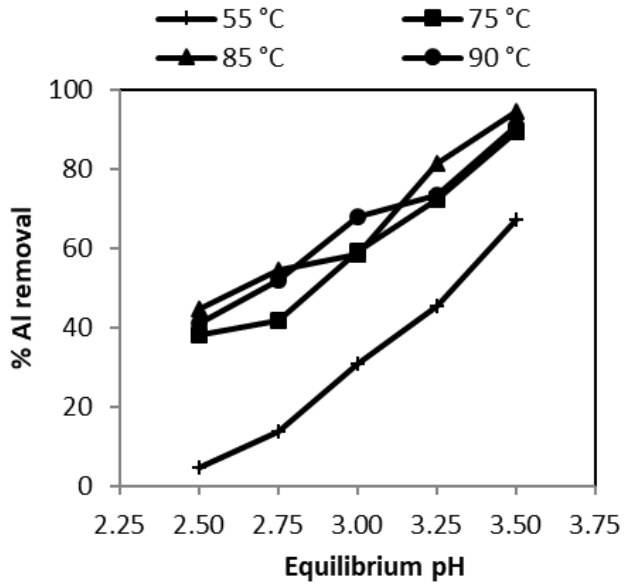

Figure 3.20: Percentage aluminium removal as a function of equilibrium pH at various temperatures (°C) from synthetic sulfate solution containing Fe (II) and Fe (III) during precipitation.

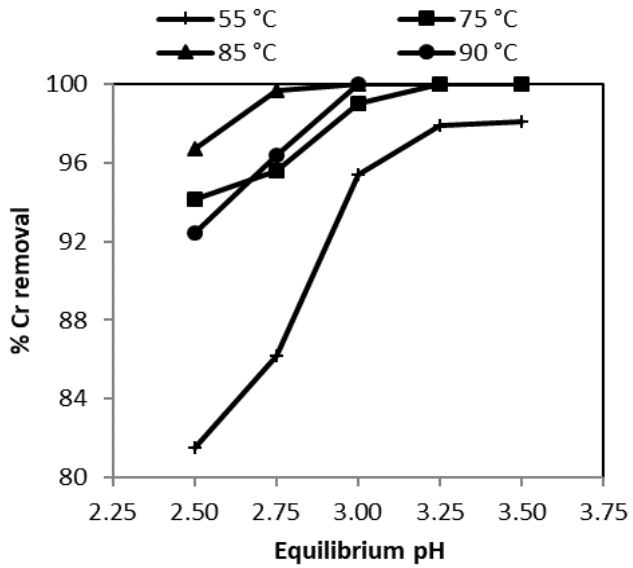

Figure 3.21: Percentage chromium removal as a function of equilibrium pH at various temperatures (°C) from synthetic sulfate solution containing Fe (II) and Fe (III) during precipitation.

The results given in Figure 3.19 to Figure 3.21 show that both temperature and pH had a marked effect on iron, aluminium and chromium removal. In Figure 3.19, the optimum iron removal was approximately 95%. This is because 5% of ferrous ion initially present in the multi-element solution remained in solution and only ferric ion was precipitated at pH value 3.5 and below. The removal of ferrous ion in acidic conditions can only be achieved by oxidising ferrous ion to ferric ion with an oxidant followed by precipitation of ferric oxyhydroxides. As shown in Figure 3.20 and Figure 3.21, aluminium and chromium removal is favoured at high pH values and high temperature values. At 55 °C, for example, increasing pH value from 2.5 to 3.5 resulted in an increase in the removal of aluminium from 4.6% to 67.4% and chromium from 81.5% to 98.1%. Similar behaviour was observed by Wang (2012) during investigations on the co-removal of iron, aluminium and chromium in the E.Z. method. They found that aluminium and chromium removal is favoured at higher pH values even at low temperature values. At constant pH value of 3.5 and different temperatures (Figure 3.22), increasing temperature from 55 °C to at least 75 °C resulted in substantial increase in the removal of aluminium (from 67 % to 95 %) and chromium (from 96 % to 100 %). High aluminium and chromium removal at pH 3.5 and high temperatures (85 and 90 °C) are at the expense of more nickel and cobalt losses (Figure 3.22). A similar trend was observed in studies by Davey and Scott (1976), who observed an increase in the loss of nickel during investigations on the effect of

temperature on the loss of base metals, zinc and nickel, respectively. In the present study, it was also noted during the experiments that high temperatures resulted in less viscous slurries and the residues were easy to filter and wash. Almost similar percentages of precipitation of the metals were obtained at 85 °C and 90 °C and thus, 85 °C was chosen as the optimum temperature for the obvious practical advantage of energy savings and was used in the succeeding experiments.

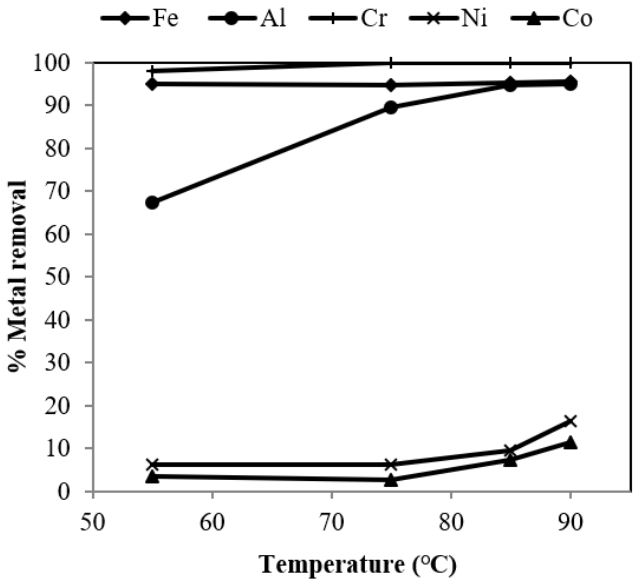

Figure 3.22: Percentage metal removal as a function of temperature at equilibrium pH value 3.5 from synthetic sulfate solution containing both ferrous ion and ferric ion.

For the experiments with only Fe(III), Figure 3.23 shows the percentage removal of metals from solution at 85 °C as a function of equilibrium pH during precipitation. The results show that iron removal of greater than 99 % with < 0.5 % of both nickel and cobalt losses was achieved at pH 2.5 in the absence of ferrous iron in the synthetic sulfate solution. Higher pH values favoured the removal of Cr and Al with 99 % Cr and Al removed at pH 3.25 and 3.5 respectively but with more than 3 % nickel and cobalt losses. The results are in good agreement with a similar study that also used ferric ion only (Kose and Topkaya, 2011).

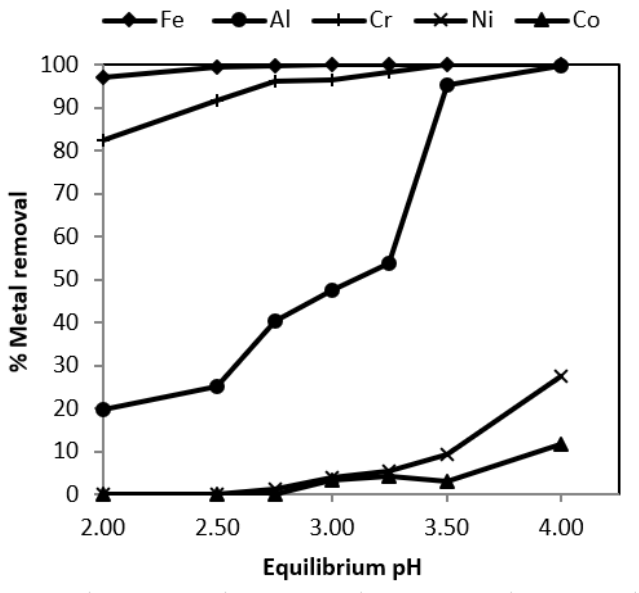

Figure 3.23: Percentage metal removal as a function of pH at 85 ºC as a function of equilibrium pH from synthetic sulfate solution containing iron as ferric ion only.

In the present study, experiments were conducted where 5 % of the total dissolved iron in solution was Fe (II), and 95 % was Fe (III), corresponding to 35 g/L and 2 g/L respectively, and where 100% of the iron was Fe (III). Comparison of the percentage iron removal for the precipitation in the absence and presence of Fe (II) in solution is shown in Figure 3.24. The percentage iron removal obtained from a mixture of Fe (II) and Fe (III) revealed that pH 2.5 was almost ~99 % while when Fe (II) is present iron removal was about 95%. The difference in removal corresponds to the amount of ferrous ions in solution indicating that ferrous ions are not removed from solution by precipitation at pH values up to 3.5. Hence, the high pH values used in White et al. (2006) and Kose and Topkaya (2011), of up to 5.5 and 4.25 respectively can only be justified for aluminium and chromium removal and iron in the divalent form and not the trivalent form. The results indicate that an investigation on the oxidation of ferrous iron at low pH values ($\leq$ 3.5), where the losses of both nickel and cobalt due to co-precipitation are minimal, is of practical importance.

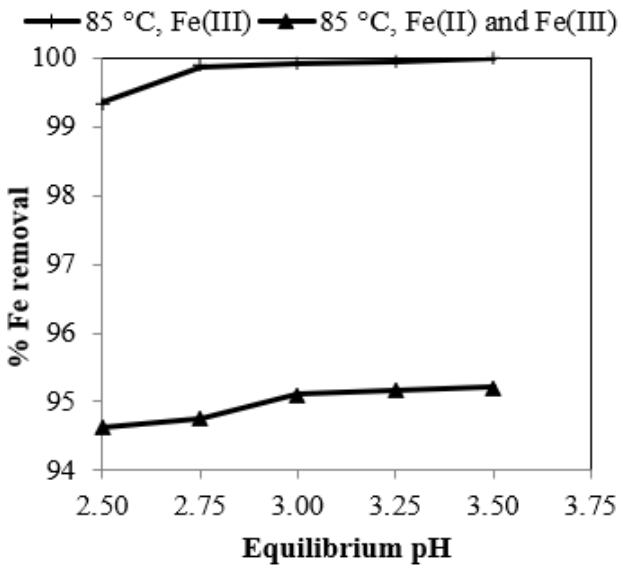

Figure 3.24: Percentage iron removal in the presence and absence of ferrous iron at 85 °C as a function of equilibrium pH.

The analysis of the precipitates by XRD revealed the presence of gypsum and amorphous iron phases, as shown in Section 3.6.2. Unlike most studies, wherein the iron phases were identified using the XRD technique, it was difficult in the present study to identify the phases of iron formed during precipitation using multi-element sulfate solution. This difficulty was owing to the greater portion of the precipitate being crystalline gypsum, which masked the iron phases. Also, the co-precipitation of other metal ions such as Al and Cr might be through their incorporation in the iron phase lattice making it difficult to identify the iron phases formed distinctively.

It is apparent that the removal of iron, aluminium and chromium can be optimised by operating at high pH values and temperature, but this is at the expense of high nickel and cobalt losses. Therefore, the use of precipitation requires a compromise on whether the main goal is the optimisation of the removal of Fe, Al and Cr or the minimisation of nickel and cobalt losses as achieving both at the same time is very difficult. The choice is difficult considering that the removal of Al and Cr is critical as these can have detrimental effects on downstream processes while high nickel and cobalt losses reduce process profitability. For example, aluminium in the MHP process reduces the leachability of the MHP product ahead of nickel and cobalt recovery (White et al., 2006).

3.7 Conclusions

The precipitation of dissolved iron, aluminium and chromium and the level of nickel and cobalt losses from sulfate solutions that simulated pregnant leach solution generated by leaching nickel laterite ores under atmospheric conditions were investigated. Initially, simulation using Visual MINTEQ software was used to investigate the possibility of selective separation of trivalent ions of Fe, Al and Cr from divalent ions of Ni and Co from multi-element sulfate solutions by adjusting pH. Visual MINTEQ can simulate the multi-element solutions and produce the speciation diagram of the cations contained in the solution and predict the precipitation of the various minerals. The simulation results showed that the behaviour of the cations in solution and the stability of the sulfate solution is influenced by both pH and temperature. The metal ions in sulfate solutions exist as a mixture of metal sulfate species and metal hydroxo species.

In highly acidic conditions (pH <2), the metal ions in the quinary sulfate solutions exist predominantly as the unhydrolysed metal ion, M^{z+} together with metal sulfate species, $M(SO_4)_n^{+(z-2n)}$, where z is the valency of the ion and n is the number of sulfate ions in coordination with the cation. As pH increases (> 2), there is an increase in the amount of the trivalent metal ions monomers, hydroxo species, MOH^{2+} and $M(OH)_2^{+}$ and nickel and cobalt exist in the form M^{z+} and MSO_4^{0}. The pH value for significant hydroxo species varies for the cations, but significant amounts of hydroxo species of Fe and Cr exist at pH < 4.5 compared to those of aluminium. Increasing temperature shifts the speciation curves of the monomers to lower pH values.

The stability of solutions which is expressed by the calculated SI values with respect to the minerals linked speciation of the metal ions to mineral precipitation. In sulfate solutions where both metal sulfate species and hydroxo species co-exist, the precipitates were predicted to be a mixture of metal oxyhydroxides and oxyhydroxysulfates. The trivalent ions of Fe, Al and Cr, form monomeric hydroxo species in acidic conditions, and the solutions were saturated with the minerals of the trivalent ions and no Ni and Co minerals, which supports that precipitation occurs through polymerisation of the monomers of the cations. The sulfate solution was saturated with respect to iron minerals (haematite, goethite, ferrihydrite and jarosite), aluminium minerals (diaspore, jurbanite and aluminium hydroxide) and chromium minerals (chromium hydroxide and chromium oxide) at pH below 4.5 and

undersaturated with respect to nickel and cobalt minerals. The saturation index calculations indicated that the trivalent ions of Fe, Al and Cr could be selectively precipitated from nickel and possibly cobalt by pH adjustment. Iron, aluminium and chromium are expected to precipitate at pH 4.5 leaving nickel and cobalt in a solution whose precipitation is predicted at higher pH values. The kinetics of haematite and goethite formation in sulfate solution is slow, and thus ferric ion is expected to precipitate as a mixture of ferrihydrite and jarosite at pH above 2.4, which was realised during iron precipitation from synthetic sulfate solutions. Aluminium and chromium are precipitated as amorphous aluminium and chromium hydroxide at high temperature and pH range 3 to 5. The solubility of the minerals of iron, aluminium and chromium decreases with increasing pH and temperature.

Results of the preliminary experiments showed that the reactivity of the neutralising agent is crucial in controlling supersaturation. The benefit of using lesser reactive $CaCO_3$ slurry compared to using more reactive MgO, $MgCO_3$ and NaOH were apparent in multi-element sulfate solutions. The nature of the slurries and the filtration properties in iron precipitation is dependent on the complexity of the solution (that is the number and type of individual cations in solution). Nickel and cobalt losses increase as the individual cations in solution increase. In general, calcium carbonate is a better neutralising agent than MgO, $MgCO_3$ and NaOH shown by the lower amount of nickel and cobalt losses with $CaCO_3$.

The experiments carried out using FNC [Fe(III)+Ni(II)+Co(II)], ANC[Al(III)+Ni(II) +Co(II)], CrNC [Cr(III)+Ni(II)+Co(II)], FANC [Fe(III)+Al(III)+Ni(II)+Co(II)], FCrNC [Fe(III)+Cr(III)+Ni(II)+Co(II)], FMNC [Fe(III)+Mg(II)+Ni(II)+Co(II)], FACrNC [Fe(III)+Al(III)+Cr(III)+Ni(II)+Co(II)] systems and a more complex multi-element sulfate solution with composition as given in Table 3.1 shows greater loss of nickel and cobalt to the solids is associated with iron, aluminium and chromium co-precipitation. In a more complex multi-element sulfate solution, the level of nickel and cobalt losses was exacerbated by the presence of magnesium. The presence of magnesium in the sulfate solutions influences the characteristics of the precipitates in iron precipitation. Magnesium resulted in the formation of slimy slurries and with a clayey consistency and poor filtration properties resulting in more nickel and cobalt losses probably from solution entrainment. Although greater losses of nickel and cobalt to the precipitates occurred in the presence of aluminium and chromium, the

slurries were easily filtered and not clayey but rather fluffy in the absence of magnesium in solution.

Full factorial design experiments combined with ANOVA were used to determine the factors with a significant effect on the desired responses when using multi-element sulfate solutions. It was found that pH and temperature have significant effects on the removal of iron, aluminium and chromium and nickel and cobalt losses. $CaCO_3$ concentration showed a significant impact on the removal of chromium and cobalt loss. Two-way and there-way interactions were of statistical significance to the impurity removal efficiency and the loss of nickel and cobalt.

Systematic variation of the variables that affect the process in factorial design experiments revealed that the equilibrium pH of the solution influenced the removal of Fe, Al and Cr by precipitation and the level of nickel and cobalt losses to the precipitates. The operating temperature had minimal effect on the removal of ferric iron but a marked effect on the apparent rates of the removal of aluminium and chromium and the filterability of the precipitate. That is at a given pH value, increases in temperature resulted in higher removal of aluminium and chromium and the formation of more easily filterable solids. The removal of ferric ion could be easily achieved by simply raising the pH to at least 2.5, but higher pH values are required for the removal of the trivalent ions of aluminium and chromium. The optimum condition realised as a result of the investigation was a pH value of 3 for chromium removal and pH of at least 4 for aluminium removal. The experimental finding for chromium removal is in disagreement with the pH conditions predicted from the SI index values. Nickel and cobalt losses to the precipitate increase with an increase in equilibrium pH and temperature.

The changes in the percentage of metal removal with a step change in equilibrium pH value illustrate the viability of using multi-stage precipitation in minimising nickel and cobalt losses. The conditions, pH 3.5 and 85 ℃ were found to be the optimum conditions for removal of ferric ion, aluminium and chromium with minimal nickel and cobalt losses. At pH 3.5 and 85 ℃, more than 99% ferric ion and chromium and 95% aluminium were removed from solution with less than 10% nickel and cobalt losses. A pH value of 3.5 can be used as the maximum pH for a first precipitation stage, with the remaining iron (both divalent and trivalent), aluminium and chromium removed in a second precipitation stage at slightly high pH values. The use of multi-

stage precipitation can minimise nickel and cobalt losses as the small amount of solid residue in the second stage can be recycled to the leaching circuit to recover the nickel and cobalt lost to the precipitate.

The precipitates formed consisted mainly of amorphous phases of iron with some poorly ordered iron phases, schwertmannite and jarosite. The formation of goethite is unlikely at the high ferric ion concentrations used during precipitation, and it is also possible that the presence of other cations inhibits its formation. The effect of ferric ion concentration can be assessed by using low iron concentration during precipitation. Chapter 4 will provide some insight into whether the absence of goethite in precipitates was mainly because of high ferric ion concentration during precipitation or was a combination of factors.

References

AGATZINI-LEONARDOU, S., TSAKIRIDIS, P. E., OUSTADAKIS, P., KARIDAKIS, T. & KATSIAPI, A. 2009. Hydrometallurgical process for the separation and recovery of nickel from sulphate heap leach liquor of nickeliferrous laterite ores. *Minerals Engineering,* 22**,** 1181-1192.

ALLAN, R., HAIGH, C. & HAMDORF, C. 1970. An improved method of removing dissolved ferric iron from iron-bearing solutions. *Australian Patent,* 424.

ALLISON, J. D., BROWN, D. S. & NOVO-GRADAC, K. J. 1991. *MINTEQA2/PRODEFA2, A geochemical assessment model for environmental systems: Version 3.0 User's Manual*, Environmental Research Laboratory, Office of Research and Development, US Environmental Protection Agency.

ARROYO, J. C. & NEUDORF, D. A. 2001. Atmospheric leach process for the recovery of nickel and cobalt from limonite and saprolite ores. Google Patents.

BABCAN, J. 1971. Synthesis of jarosite, KFe3 (SO4) 2 (OH) 6. *Geol. Zb,* 22**,** 299-304.

BEUKES, J. P., GIESEKKE, E. W. & ELLIOTT, W. 2000. Nickel retention by goethite and hematite. *Minerals Engineering,* 13**,** 1573-1579.

BIGHAM, J., SCHWERTMANN, U., CARLSON, L. & MURAD, E. 1990. A poorly crystallized oxyhydroxysulfate of iron formed by bacterial oxidation of Fe (II) in acid mine waters. *Geochimica et Cosmochimica Acta,* 54**,** 2743-2758.

BIGHAM, J. M., SCHWERTMANN, U., TRAINA, S. J., WINLAND, R. L. & WOLF, M. 1996. Schwertmannite and the chemical modeling of iron in acid sulfate waters. *Geochimica et Cosmochimica Acta,* 60**,** 2111-2121.

BOX, G. E. P. & COX, D. R. 1964. An Analysis of Transformations. *Journal of the Royal Statistical Society. Series B (Methodological),* 26**,** 211-252.

BOX, G. E. P. & MEYER, R. D. 1986. An Analysis for Unreplicated Fractional Factorials. *Technometrics,* 28**,** 11-18.

BÜYÜKAKINCI, E. & TOPKAYA, Y. A. 2009. Extraction of nickel from lateritic ores at atmospheric pressure with agitation leaching. *Hydrometallurgy,* 97**,** 33-38.

CARVALHO-E-SILVA, M. L., RAMOS, A. Y., TOLENTINO, H. C. N., ENZWEILER, J., NETTO, S. M. & DO CARMO MARTINS ALVES, M. 2003. Incorporation of Ni into natural goethite: An investigation by X-ray absorption spectroscopy. *American Mineralogist,* 88**,** 876-882.

CLAASSEN, J. O., MEYER, E. H. O., RENNIE, J. & SANDENBERGH, R. F. 2002. Iron precipitation from zinc-rich solutions: defining the Zincor Process. *Hydrometallurgy,* 67**,** 87-108.

CLAASSEN, J. O. & SANDENBERGH, R. F. 2007. Influence of temperature and pH on the quality of metastable iron phases produced in zinc-rich solutions. *Hydrometallurgy,* 86**,** 178-190.

COMBES, J., MANCEAU, A., CALAS, G. & BOTTERO, J. 1989. Formation of ferric oxides from aqueous solutions: A polyhedral approach by X-ray absorption spectroscdpy: I. Hydrolysis and formation of ferric gels. *Geochimica et Cosmochimica Acta,* 53**,** 583-594.

CORNELL, R. M., GIOVANOLI, R. & SCHNEIDER, W. 1989. Review of the hydrolysis of iron (III) and the crystallization of amorphous iron (III) hydroxide hydrate. *Journal of Chemical Technology and Biotechnology,* 46**,** 115-134.

CORNELL, R. M. & SCHWERTMANN, U. 2003. *The iron oxides: structure, properties, reactions, occurrences and uses*, John Wiley & Sons.

DANIEL, C. 1959. Use of Half-Normal Plots in Interpreting Factorial Two-Level Experiments. *Technometrics,* 1**,** 311-341.

DAVEY, P. T. & SCOTT, T. R. 1976. Removal of iron from leach liquors by the "Goethite" process. *Hydrometallurgy,* 2**,** 25-33.

DOLD, B. 2003. Dissolution kinetics of schwertmannite and ferrihydrite in oxidized mine samples and their detection by differential X-ray diffraction (DXRD). *Applied Geochemistry,* 18**,** 1531-1540.

DOUSMA, J. & DE BRUYN, P. L. 1976. Hydrolysis-precipitation studies of iron solutions. I. Model for hydrolysis and precipitation from Fe(III) nitrate solutions. *Journal of Colloid and Interface Science,* 56**,** 527-539.

DUTRIZAC, J. E. 1983. Factors affecting alkali jarosite precipitation. *Metallurgical Transactions B,* 14**,** 531-539.

DUTRIZAC, J. E. & JAMBOR, J. L. 2000. Jarosites and their application in hydrometallurgy. *Reviews in Mineralogy and Geochemistry,* 40**,** 405-452.

GUISE, L. & CASTRO, F. 1996. Iron, aluminum and chromium co-elimination by hydrolytic precipitation from nickel and cobalt containing sulphuric acid solutions. *Iron Control and Disposal***,** 275-286.

HERNANDEZ, O. Y. C., MULLER, H., REYNOLDS, G. & LIU, H. 2014. Nickel recovery from a high ferrous content laterite ore. Google Patents.

KÖSE, C. H. & TOPKAYA, Y. A. 2011. Hydrometallurgical processing of nontronite type lateritic nickel ores by MHP process. *Minerals Engineering,* 24**,** 396-415.

LEE, G., BIGHAM, J. M. & FAURE, G. 2002. Removal of trace metals by coprecipitation with Fe, Al and Mn from natural waters contaminated with acid mine drainage in the Ducktown Mining District, Tennessee. *Applied Geochemistry,* 17**,** 569-581.

LIU, H. & PAPANGELAKIS, V. G. 2005. Chemical modeling of high temperature aqueous processes. *Hydrometallurgy,* 79**,** 48-61.

LOAN, M., NEWMAN, O. M. G., COOPER, R. M. G., FARROW, J. B. & PARKINSON, G. M. 2006. Defining the Paragoethite process for iron removal in zinc hydrometallurgy. *Hydrometallurgy,* 81**,** 104-129.

MARTIN, R. B. 1991. Fe3+ and Al3+ hydrolysis equilibria. Cooperativity in Al3+ hydrolysis reactions. *Journal of inorganic biochemistry,* 44**,** 141-147.

MATIJEVIĆ, E., SAPIESZKO, R. S. & MELVILLE, J. B. 1975. Ferric hydrous oxide sols I. Monodispersed basic iron(III) sulfate particles. *Journal of Colloid and Interface Science,* 50**,** 567-581.

ÖNAL, M. A. R. & TOPKAYA, Y. A. 2014. Pressure acid leaching of Çaldağ lateritic nickel ore: An alternative to heap leaching. *Hydrometallurgy,* 142**,** 98-107.

PARK, S.-M., YOO, J.-C., JI, S.-W., YANG, J.-S. & BAEK, K. 2015. Selective recovery of dissolved Fe, Al, Cu, and Zn in acid mine drainage based on modeling to predict precipitation pH. *Environmental Science and Pollution Research,* 22**,** 3013-3022.

PARK, S. M., YOO, J. C., JI, S. W., YANG, J. S. & BAEK, K. 2013. Selective recovery of Cu, Zn, and Ni from acid mine drainage. *Environmental Geochemistry and Health,* 35**,** 735-743.

RAMESH, T. & KAMATH, P. V. 2006. Synthesis of nickel hydroxide: effect of precipitation conditions on phase selectivity and structural disorder. *Journal of power sources,* 156**,** 655-661.

RICHARD, F. C. & BOURG, A. C. 1991. Aqueous geochemistry of chromium: a review. *Water research,* 25**,** 807-816.

SAPIESZKO, R. S., PATEL, R. C. & MATIJEVIC, E. 1977. Ferric hydrous oxide sols. 2. Thermodynamics of aqueous hydroxo and sulfato ferric complexes. *The Journal of Physical Chemistry,* 81**,** 1061-1068.

SCHNEIDER, W. 1984. Hydrolysis of Iron (III)… Chaotic Olation Versus Nucleation. *Comments on Inorganic Chemistry,* 3**,** 205-223.

SCHWERTMANN, U. & MURAD, E. 1983. Effect of pH on the formation of goethite and hematite from ferrihydrite. *Clays and Clay Minerals,* 31**,** 277-284.

SÖHNEL, O. & GARSIDE, J. 1992. *Precipitation: basic principles and industrial applications,* Butterworth-Heinemann.

STEEMSON, M. & SMITH, M. The development of nickel laterite heap leach projects. Proceedings of ALTA 2009 Nickel/Cobalt conference, 2009.

STUENZI, H. & MARTY, W. 1983. Early stages of the hydrolysis of chromium (III) in aqueous solution. 1. Characterization of a tetrameric species. *Inorganic Chemistry,* 22**,** 2145-2150.

WAGNER, D., FANNING, D., FOSS, J., PATTERSON, M. & SNOW, P. 1982. Morphological and Mineralogical Features Related to Sulfide Oxidation under Natural and Disturbed Land Surfaces in Maryland 1. *Acid sulfate weathering***,** 109-125.

WANG, K. 2012. *Impurity rejection in the nickel laterite leach system.* Curtin University.

WANG, K., LI, J., MCDONALD, R. & BROWNER, R. 2011. The effect of iron precipitation upon nickel losses from synthetic atmospheric nickel laterite leach solutions: statistical analysis and modelling. *Hydrometallurgy,* 109**,** 140-152.

WANG, K., LI, J., MCDONALD, R. G. & BROWNER, R. E. 2013. Characterisation of iron-rich precipitates from synthetic atmospheric nickel laterite leach solutions. *Minerals Engineering,* 40**,** 1-11.

WHITE, D., MILLER, M. & NAPIER, A. 2006. Impurity disposition and control in the Ravensthorpe acid leaching process. *Iron Control Technologies—3rd International Symposium on Iron Control in Hydrometallurgy, Canadian Inst. Min. Metall. & Petroleum.*

YUE, T., HAN, H., SUN, W., HU, Y., CHEN, P. & LIU, R. 2016. Low-pH mediated goethite precipitation and nickel loss in nickel hydrometallurgy. *Hydrometallurgy*.

CHAPTER 4
OXIDATIVE PRECIPITATION OF FERROUS ION FROM ACIDIC SULFATE SOLUTION

4.1 Introduction

The review of impurities in nickel laterite ores highlight that although iron is mainly present as Fe(III) in the ores, some ores also contain Fe(II), which is leached with the other impurities into solution. The pH window for the precipitation of the divalent ions of nickel, cobalt and iron as metal hydroxides is narrow (Monhemius, 1977). Ferrous ion reporting in nickel laterite leach solutions is usually removed as ferric hydroxide by oxidative precipitation at lower pH values than those required for ferrous hydroxide precipitation at reasonable nickel and cobalt losses. At RNO, for example, the oxidation of ferrous ion and precipitation as ferric oxyhydroxides and the co-removal of any aluminium and chromium remaining in solution following the primary neutralisation stage is carried out at pH range 4 to 5.5 (White et al., 2006). The effect of pH and temperature on ferric ion removal and nickel and cobalt losses has been discussed in Chapter 3. The oxidation of ferrous ions in solution is also influenced by several parameters including pH, temperature, dissolved oxygen level and Fe (II) concentration (Stumm and Lee, 1961, Agatzini et al., 1986). Chapter 4 presents an experimental investigation on the removal of Fe(II) and the remaining Al and Cr from synthetic sulfate solutions comparable to the discharge liquors following first partial neutralisation stage of laterite leach solutions. The aims of the chapter were to study: (i) the effect of using air, oxygen and hydrogen peroxide on Fe(II) removal efficiency, and (ii) the effect of Fe, Al and Cr co-removal on nickel and cobalt losses and develop a multistage oxidative precipitation process for effective impurity removal at reasonable Ni and Co losses.

4.2 Materials and methods

4.2.1 Reagents

All reagents except for $Fe_2(SO_4)_3.7H_2O$ used in the preparation of multi-element sulfate solution in Chapter 3 were used in preparing the test solutions used for oxidative precipitation. In addition, the following reagents were used: hydrogen peroxide (H_2O_2) (30% w/v, Chem-Supply) and industrial air, oxygen and nitrogen.

4.2.2 Preparation of test solutions

Multi-element synthetic sulfate solution containing significant ferrous ion (1 to 5 g/L) was prepared by dissolving the required masses of the respective analytical grade salts in deionised water. The concentration of the other metal elements contained were the residual concentrations obtained from the iron precipitation process at pH 3 and 85 °C in Chapter 3. The solution pH was adjusted using sulfuric acid solution (1 to 5 M) and the solution made to predetermined volume in a volumetric flask. The synthetic sulfate solution was deoxygenated by bubbling nitrogen gas to prevent the oxidation of ferrous ions from any dissolved oxygen. The deoxygenation of the solution was done following the procedure by Rollie et al. (1987). Table 4.1 gives the approximate elemental composition of the synthetic sulfate solutions used in this section.

Table 4.1: Elemental composition of the synthetic test solution.

Element	Ni	Co	Fe^{2+}	Al	Cr	Mn	Mg	Ca	Cu	Zn
Concentration (g/L)	3.50	0.25	1.0-5.0	1.50	0.10	0.90	10.0	0.50	0.06	0.20

Slurries of calcium carbonate and magnesium carbonate and sodium hydroxide solution used as neutralising agents were prepared using the respective analytical grade reagents and deionised water.

4.2.3 Experimental set-up and procedures

4.2.4 Oxidative precipitation of iron with air and oxygen

The oxidative precipitation experiments were carried out in the glass reactor used for hydrolysis precipitation experiments shown in Figure 3.1. The reactor has openings

used for a thermometer, pH probe, gas sparger and neutralising agent addition and condenser that is also used for sample collection. The reactor is seated on a water bath to allow for temperature control and a magnetic stirrer used for mixing. The pH of the mixture was measured at temperature and monitored using a Mettler Toledo® Inlab Versatile pH probe. For each experiment, a volume of 100 mL of multi-element synthetic sulfate solution, containing 1 to 5 g/L Fe(II) with the other elemental composition as given in Table 4.1, was transferred into the reactor and deoxygenated by bubbling nitrogen gas. Under stirring, the temperature was attained, and the pH adjusted to the desired value by dropwise addition of neutralising agent (base) or 0.1 to 0.05 M sulfuric acid solution. When the solution pH and temperature were stable, oxygen or air was introduced into the reactor using a sparger at a flow rate of 3 L/min. When the supply of oxygen or air was stopped, this marked the end of reaction. Liquid samples were collected for assaying using a syringe at the start and predetermined time intervals and immediately filtered through a 0.45 µm syringe filter and quenched by dilution using concentrated H_2SO_4 solution. At the completion of the reaction, the slurry was vacuum filtered using a circular hardened ashless filter paper (Whatman No 542/110 mm) on a Buchner funnel with a 1000 mL flask. The precipitate was washed with acidified deionised water to recover both nickel and cobalt adsorbed on the solid residue and entrained solution. The precipitates were analysed using XRF Spectrometer and XRD while the liquid samples were analysed for metal concentrations using ICP-OES.

4.2.5 Oxidative precipitation with hydrogen peroxide

A similar experimental setup and procedure used for oxidative precipitation with oxygen were used with hydrogen peroxide solution (6% w/v). The difference was that ferrous ion concentration in the test solution was varied and in addition to using calcium carbonate slurry (10 %w/v), magnesium carbonate slurry (7.5 %w/v) and sodium hydroxide solutions (0.05 to 0.5 M) were also used as neutralising agents. Secondly, the reaction time during oxidative precipitation of ferrous ion with hydrogen peroxide consisted of the period for which hydrogen peroxide was added (first stage) and an ageing time (second stage). The combination of the two stages is referred to as a multistage oxidative precipitation process. The ageing time refers to the retention time after complete addition of hydrogen peroxide into the system at the desired

equilibrium pH value. During ageing, the precipitate is kept suspended by stirring at the experimental temperature allowing continuing oxidation and precipitation of iron, aluminium and chromium. The first stage is mainly for the oxidative precipitation of ferrous ion and the precipitation of the majority aluminium and chromium. The remaining iron, aluminium and chromium are expected to be removed in the second stage. The samples were collected and assayed similarly to the oxidation with oxygen and air experiments.

4.3 Results and discussions

4.3.1 Effect of pH on the oxidative precipitation of ferrous ion with oxygen and air

A set of oxidative precipitation experiments was carried out using the procedure outlined in Section 4.2.3.1 under comparable conditions: initial ferrous ion concentration of 2 g/L, temperature 85 ℃ and oxygen with a flow rate of 3 L/min, except that pH was varied from 3.0 to 3.5. From the initial iron in solution and that remaining at the sampling times, the iron oxidatively precipitated was calculated. The results are summarised in Figure 4.1.

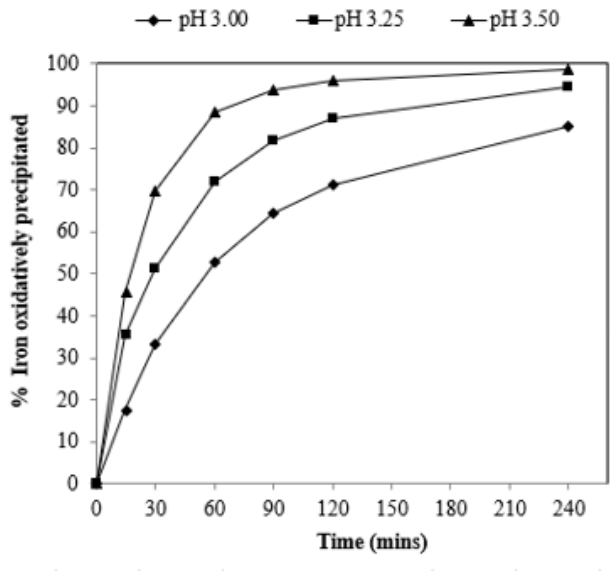

Figure 4.1: Percent iron oxidatively precipitated as a function of time at comparable initial ferrous ion concentration of 2 g/L, temperature of 85 ℃ and various pH values using calcium carbonate slurry.

Figure 4.1 shows the percentage of iron precipitated as a function of time and various equilibrium pH values. The amount of iron precipitated increases with an increase in equilibrium pH, with the highest amount at pH 3.5. The synthetic sulfate solution was greenish at the start of the experiments, and no colour change was observed upon the addition of calcium carbonate slurry when adjusting solution pH to the desired operating pH value. When oxygen was added into solution while controlling pH, the mixture turns brown, and a brownish precipitate is formed. The brown precipitate is indicative of the precipitation of compounds of iron in the trivalent oxidation state. Ferric oxyhydroxide is less soluble with a very low solubility product (10^{-39}) (Vlek et al., 1974) and therefore easily precipitated compared to a more soluble ferrous hydroxide with a solubility product of about 10^{-14} (Arden, 1950).

In this study, at the investigated pH values (3 to 3.5) and the addition of oxygen, iron precipitation from the acidic solution was due to oxidative precipitation. Oxidative precipitation of iron can be considered as a two-step process. First, the ferrous ion is oxidised to ferric ion (Equation 4.1), and then the ferric ion undergoes precipitation according to the generalised Equation 4.2.

$$2Fe^{2+}_{(aq)} + 0.5O_{2\,(g)} + 2H^{+}_{\,(aq)} \leftrightarrow 2Fe^{3+}_{\,(aq)} + H_2O_{\,(l)} \qquad 4.1$$

$$Fe^{3+}_{(aq)} + 3H_2O_{\,(l)} \leftrightarrow Fe(OH)_{3\,(s)} + 3H^{+}_{\,(aq)} \qquad 4.2$$

The precipitate is represented as ferric hydroxide ($Fe(OH)_3$) in Equation 4.2 which is a simplification, but in reality, the precipitates formed in sulfate solutions are a mixture of ferric oxyhydroxysulfates and ferric oxyhydroxides. For instance, ferrihydrite and schwertmannite are found to be the dominant phases in the metastability diagram for ferric ion hydrolysis from iron sulfate solutions at a temperature range 50 to 90 °C and pH range 1.95 to 3.25 (Claassen and Sandenbergh, 2007). Also, in this study (Section 3.6.3), both ferrihydrite and schwertmannite were found to form during iron precipitation. Acid is generated regardless of the iron phase formed, and the addition of a neutralising agent is therefore required to consume the acid produced and for continued iron precipitation.

Figure 4.1 also shows that the incremental percentage of iron oxidatively precipitated decreases over time and the small amount oxidatively precipitated between 120 and 240 minutes indicates that the reaction may be approaching equilibrium after 240 minutes. The % iron oxidatively precipitated after 240 minutes was 71%, 87% and

99% at pH 3.0, 3.25 and 3.5, respectively. This increase in the overall amount of iron oxidative precipitation with an increase in pH (Figure 4) can be explained using the equilibrium constant (K) for the precipitation of the iron compounds. According to Equation 4.2, K can be expressed as ($[H+]^3/[Fe^{3+}]$) and depends on the concentration of acid and ferric ion. At high pH (low acid concentration), the equilibrium ferric ion concentration decreases to maintain the equilibrium, which results in the formation of ferric hydroxides at low ferric ion concentration. When pH is maintained at 3.5, the equilibrium ion concentration is lower than that at pH 3.0, and therefore a higher overall percentage iron precipitation is obtained compared to that at pH 3.0. A similar relationship in the increase in percentage iron precipitation with an increase in operating pH value was observed by Yue et al. (2016) during iron precipitation using the V.M. goethite process in a binary sulfate solution [Fe(II)+Ni(II)] over the pH range 2.0 to 4.3 at 85 ℃.

Iron oxidative precipitation was faster at higher pH values which can be interpreted as oxidation occurring at a faster rate with an increase in pH since iron precipitation at the investigated conditions could only occur if the ferrous ion is oxidised to ferric ion prior ferric hydroxide precipitation. The apparent rates of oxidative precipitation during the first two hours were found to be 9.58 $mgL^{-1}min^{-1}$, 15.51 $mgL^{-1}min^{-1}$ and 18.44 $mgL^{-1}min^{-1}$ at pH 3.00, 3.25 and 3.50, respectively. A similar trend in the increase in the apparent oxidation rate with increase in pH, although at higher initial ferrous ion concentrations has been reported by Chang et al. (2010) who studied the removal of iron from laterite sulfate leach solution using the V.M. goethite process over a pH range of 2.4 to 8.0 at 90 ℃. Since oxidative precipitation is a two-step process, oxidation of ferrous to ferric ion and precipitation of ferric hydroxides, the overall rate of oxidative precipitation will depend on the slow step. Holluta and Koelle (1964) studied the kinetics of ferrous ion oxidation and found that between pH values 2 and 5, the rate of oxidation depends on the hydroxide concentration (pH), as was also found in this study.

The presence of iron oxides have been found to catalyse ferrous ion oxidation in less acidic solutions (Tamura et al., 1976b, Tüfekci and Sarikaya, 1996, Jones et al., 2014, Park and Dempsey, 2005), however, the influence was found to be minor at pH values below 4 (Jones et al., 2014). Furthermore, in ferrous ion oxidation studies carried out between pH 4 and 9, the strong dependence of oxidation on pH is accredited to iron

speciation, that is the dominance of the highly reducing $Fe(OH)_2^0$ species in that pH range (Stumm and Sulzberger, 1992, Morgan and Lahav, 2007). From the study by Jones et al., (2014), the apparent high oxidation rates obtained at pH 3.5 and below in this study, are not due to the catalytic effect of the formed ferric oxyhydroxides, and similarly they are not a result of the influence by ferrous ion speciation, as $Fe(OH)_2^0$ is dominant at pH values above 4.0 (Morgan and Lahav, 2007). The observed apparent rates of iron oxidation precipitation can, therefore, be attributed to the effect of hydroxide ion concentration in solution (pH).

A few additional experiments were carried out using the procedure outlined in section 4.3.1 at the same temperature of 85 ℃, pH 3.5 and solution composition as used for oxygen sparging experiments except that air which contains about 21% oxygen was sparged at the same flow rate as was the oxygen. These were carried out to compare the effect of oxygen concentration (100 % vs 21 %) on the oxidative precipitation of iron.

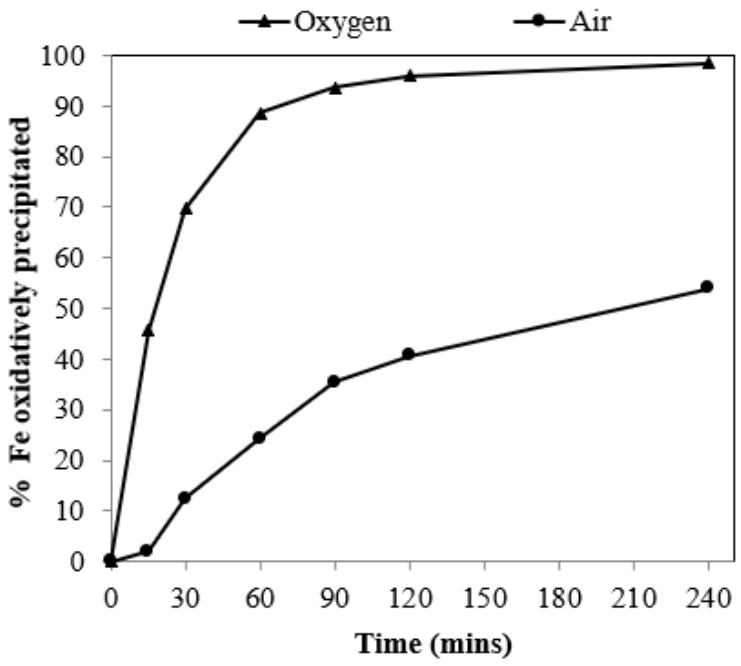

Figure 4.2: A comparison of % iron oxidatively precipitated using air and oxygen at pH 3.5, 85 ℃ and constant oxidant flow rate.

The comparative percent iron oxidatively precipitated against time for air and oxygen is shown in Figure 4.2. The oxidative precipitation curves of iron assume a similar trend with fast initial precipitation and the incremental precipitate amount decreasing over time. Oxidative precipitation of ferrous ion is significantly higher at any given

sampling time with oxygen than with air sparging. Although the results show the influence of oxygen concentration on oxidative precipitation of ferrous ions, there was no direct correlation between the percentage iron oxidatively precipitated and percent oxygen in the sparge gas. The incremental increase in the percentage iron oxidation precipitation is almost negligible with oxygen in the second 2 hours of reaction, while larger with air. This indicates that the reaction is far from reaching equilibrium with air after 4 hours of reaction time. The results can therefore only be interpreted in terms of the rate of reaction and not recovery.

Ferrous ion oxidation rate has been shown to depend on oxygen concentration (Stumm and Lee, 1961, Stumm and Morgan, 1996) and is expressed using different rate laws (Section 2.4.1.1) given from low to high pH values. Comparison of the overall oxidative precipitation results when using air and oxygen indicates that ferrous ion oxidation depends on oxygen concentration and is the rate determining step during the oxidative precipitation process.

Oxidative precipitation with air is very slow at low pH values (3.5) resulting in longer reaction times for the process, however, at the same pH value, oxygen can be used effectively.

4.3.2 Effect of temperature on the oxidative precipitation of ferrous ion

The baseline temperature in the oxidative precipitation experiments (Section 4.4.1) was set at 85 °C, a favourable temperature for the precipitation of both goethite and jarosite (Section 2.3). To investigate the influence of temperature on the oxidative precipitation of ferrous ion with oxygen, an additional set of experiments were carried out at lower temperatures. The experiments were conducted at comparable initial ferrous ion concentration of 2 g/L, pH 3.5, at temperatures of 55 °C and 70 °C and 120 minutes reaction time. The effect of temperature on percent ferrous ion oxidatively precipitated as a function of time is illustrated in Figure 4.3.

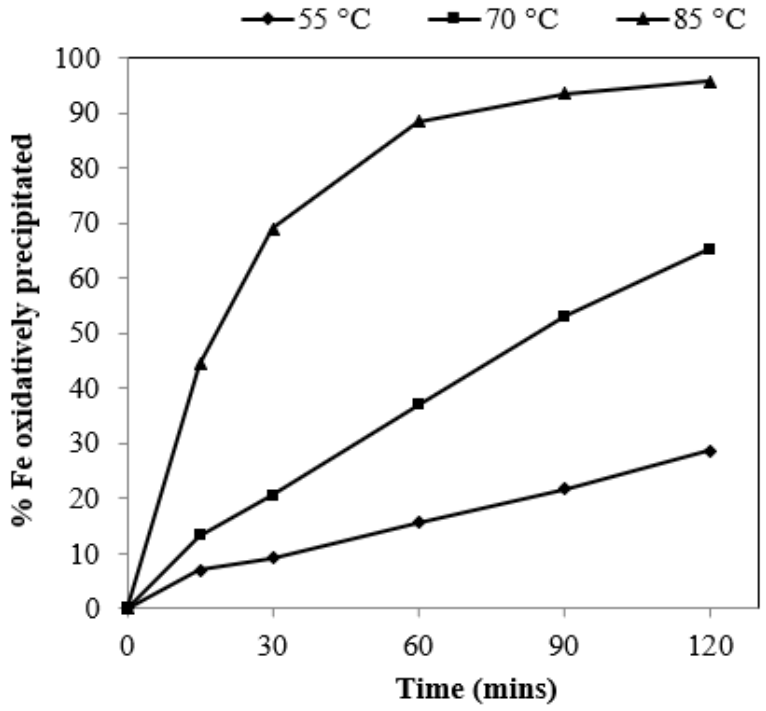

Figure 4.3: Percent iron oxidatively precipitated as a function of time at pH 3.5 and various temperatures using calcium carbonate slurry.

The results show that ferrous ion oxidative precipitation dependence on temperature is significant. As the temperature increased, the percent iron oxidatively precipitated at any given sampling time also increased. The apparent rates of oxidative precipitation of approximately 4.65 $mgL^{-1}min^{-1}$, 10.59 $mgL^{-1}min^{-1}$ and 16.25 $mgL^{-1}min^{-1}$ were obtained at 55℃, 70 ℃ and 85 ℃, respectively. The percent ferric ion removal was found optimal in Section 3.6.4 at pH value 3.5 and the temperature values under investigation. Therefore, the decrease in % iron oxidatively precipitated with decrease in temperature is possibly due to slower oxidation rates of ferrous ion to ferric ion. Since pH was measured at solution temperature, the temperature dependence of the reaction could be due to the variation in hydroxide ion activity with temperature as found by Stumm and Lee (1961) during ferrous ion oxidation, where it was observed that at constant pH value and different temperatures, the activation energy is constant. The dependence of the oxidative precipitation of ferrous ion on temperature could therefore be as a result of the influence of hydroxide ion activity on the precipitation of ferric oxyhydroxides, which is lower at low temperatures. The reaction approaches equilibrium in the first hour at 85 ℃ and longer reaction times are required before the precipitation of iron approach equilibrium at lower temperatures of 55 ℃ and 70 ℃.

In this study, the rate and equilibrium amount of iron oxidation precipitation with oxygen were influenced by pH value, oxygen concentration and temperature. Under the experimental condition, the oxidation of ferrous ion is assumed to occur through homogeneous oxidation. The rate laws for ferrous ion oxidation with oxygen show dependence on ferrous ion concentration and oxygen concentration, with the dependence on hydroxide ion concentration reported at above pH value of 2.0 (Lowson, 1982). The rate law can be generalised using Equation 4.3, with m and n as the order of reaction with respect to Fe(II) and OH^- concentrations.

$$\frac{-\,d[Fe^{2+}]}{dt} = k\,[Fe^{2+}]^m[OH^-]^n P_{O_2} \qquad 4.3$$

At constant oxygen concentration and constant pH value, the oxidation of ferrous ion becomes a function of the ferrous ion concentration only. Plots of the natural logarithm of ferrous ion concentration and the inverse of ferrous ion concentration (assuming that before equilibrium was reached all the iron remaining in solution was in the ferrous oxidation state) versus time were used to determine the order of reaction with respect to Fe(II) concentration at a given pH value. The graph with the largest R^2 values was ln[Fe] versus time, the results of which are presented in Figure 4.4. The linear plots suggest that the oxidation of ferrous ion is first order with respect to Fe(II) concentration at the pH values investigated in this study. This is in agreement with the rate law given in Lowson (1982), despite the high sulfate concentration in the synthetic leach solution used in these experiments which have been found to influence the rate of reaction (Tamura et al., 1976a). The rates of ferrous ion oxidation should be considered as indicative only.

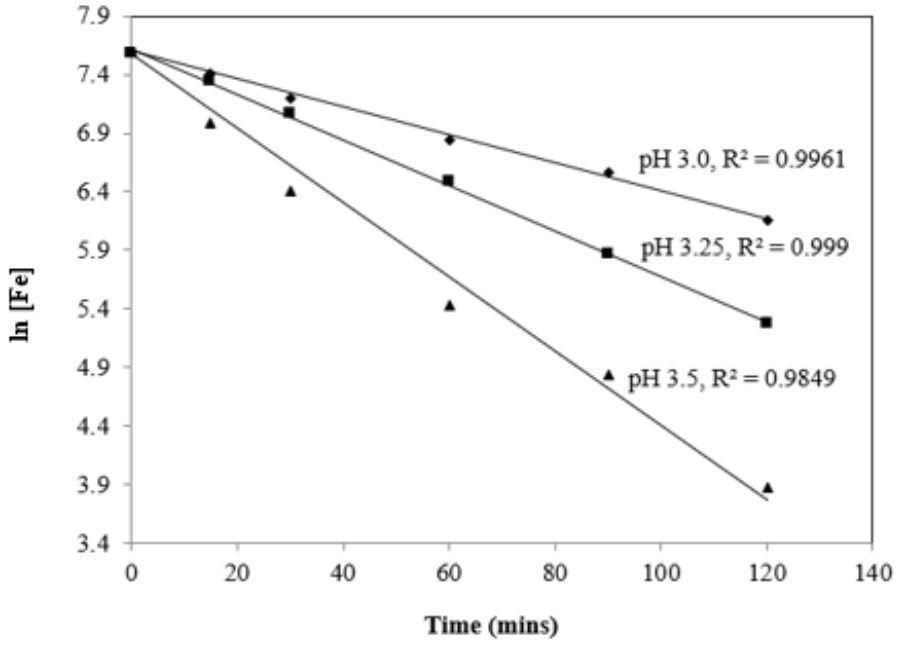

Figure 4.4: A plot of the natural logarithm of iron concentration as a function of time at various pH values at 85 °C and a constant oxygen flow rate.

4.3.3 The co-removal of iron, aluminium and chromium and the associated nickel and cobalt losses

Iron precipitation is used for the removal of aluminium and chromium from leach solutions. However, the loss of nickel and cobalt from the solution during the co-removal of the metal ions is an issue of concern. The co-removal of aluminium and chromium was also investigated during the iron oxidative precipitation experiments carried out under comparable conditions: initial ferrous ion concentration of 2 g/L, temperature 85 ℃ and oxygen with a flow rate of 3 L/min, except that pH was varied from 3.0 to 3.5.

Figure 4.5 illustrates the percentage removal of aluminium and chromium as a function of pH and the iron oxidatively precipitated. The corresponding Fe, Al and Cr concentration in the filtrate and the associated nickel and cobalt losses incurred during oxidative precipitation are given in Table 4.2.

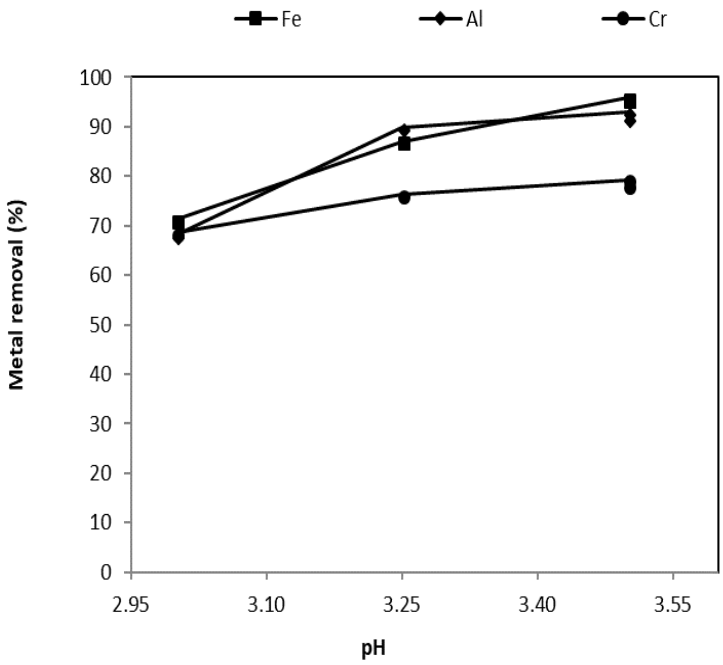

Figure 4.5: Effect of pH on % iron, aluminium and chromium precipitation. Percentage of metal removal by oxidative precipitation as a function of pH at 85 ℃ using oxygen and 120 minutes reaction time.

Table 4.2: Effect of pH on metal removal during the oxidative precipitation process.

Run	pH value	Reaction time (mins)	Filtration time of slurry (min)	Average ferrous oxidation rate $mgL^{-1}min^{-1}$	Metal concentration in filtrate gL^{-1}			Metal losses (%)	
					Fe	Al	Cr	Ni	Co
O1	3.00	120	<1	9.58	0.57	0.50	0.016	0.00	0.00
O2	3.25	120	<1	15.51	0.26	0.23	0.080	0.64	0.81
O3	3.50	120	<1	18.44	0.13	0.10	0.044	2.56	2.22
O4	3.50	240	<1	-	0.03	0.10	0.036	5.74	3.21

The removal of aluminium and chromium during oxidative precipitation increased with increasing pH from 3 to 3.5 (Figure 4.6). As pH increased from 3 to 3.5,

aluminium and chromium removal increased from 68% to 92% and 66% to 71%, respectively. Both trivalent ions of Al and Cr undergo hydrolysis like ferric ion leading to the precipitation of metal hydroxides. At higher pH values the equilibrium solubility of the trivalent ions of Al and Cr decrease resulting in more precipitation of the metal hydroxides. Although Fe, Al and Cr are quantitatively precipitated from solution, their concentration in the filtrate was still high and could disrupt downstream processes. In mixed hydroxide precipitation (MHP), for example, the co-precipitation of iron and aluminium reduces the leachability of the MHP precipitate in ammoniacal ammonium carbonate solution (White et al., 2006). Comparison of O3 and O4 shows that increasing the reaction time from 2 to 4 hours further reduced the iron concentration in the filtrate but had little effect on the Al and Cr concentration. This is due to continued oxidative precipitation of ferrous ion. At the same time, nickel and cobalt losses increased as pH and reaction time increased (Table 4.2). Similar trends were observed during the precipitation process in Chapter 3 and studies by Köse and Topkaya (2011) and Wang (2012), where nickel losses increased with increase in pH and reaction time during the iron precipitation process.

4.3.4 Analysis of the precipitates

Precipitates obtained during oxidative precipitation of ferrous ion with oxygen were fluffy, consisting of slow settling particles (fines) and fast settling particles (coarse). The dried precipitates were analysed by XRD (Figure 4.6) and XRF (Table 4.3). The XRD analysis showed that the precipitates are dominated by gypsum. Gypsum exhibit strong peaks around 17.2°, 30°, 34.6° and 37.3° 2θ. The large quantities of gypsum masked the iron phases formed especially in coarse and homogenised samples. XRD patterns of the fines samples had additional broad peaks detected around 21°, 23° and 32° 2θ which could be goethite and schwertmannite (Wang et al., 2013). It is difficult to identify the iron phases formed during precipitation in a mixed assemblage of phases of iron, aluminium and chromium co-removed and significant quantities of crystalline gypsum. Goethite is a product of the transformation of the amorphous and poorly ordered iron phases. Its formation from metastable ferrihydrite and schwertmannite is very slow normally requiring several days to months (Bigham et al., 1996, Acero et al., 2006). Considering, the short reaction time used in this study, it is most likely that the observed additional peaks could be mainly schwertmannite whose formation is

thermodynamically favoured over that of ferrihydrite in sulfate solutions and pH values in the range 2.8 to 4.5 (Majzlan et al., 2004, Bigham et al., 1996). The oxidative precipitation process used in this study is similar to the V.M. goethite process used by Chang et al. (2010). The presence of minor amounts of goethite with low crystallinity cannot be ruled out at the low ferrous ion oxidation rates with oxygen, considering that goethite was the dominant iron phase in the study by Chang et al. (2010) at higher ferrous ion oxidation rates. The low amount of goethite in the precipitates could have been caused by retarded transformation kinetics of amorphous and metastable iron phases initially formed in the presence of other cations. In a study by Cornell and Giovanoli (1987), the presence of divalent cations of Co, Cu, Mn, Ni and Zn and high Al/Fe ratio have been found to have significant effects on the kinetics of ferrihydrite transformation to goethite. It is clear from the XRD patterns obtained when using high and low Fe(III) concentrations in Chapter 3 and this section, respectively, that the iron phases formed were influenced by ferric ion concentration and the presence of other cations in solution.

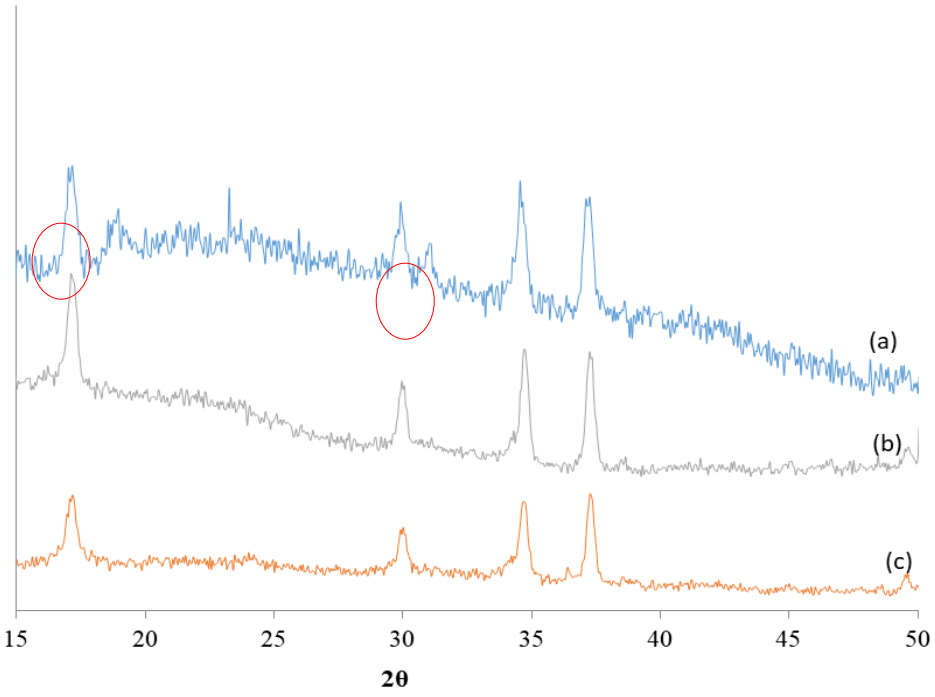

Figure 4.6: X-ray diffraction patterns of the iron residues obtained from oxidative precipitation (a) the fines iron residues, (b) coarse iron residues consisting mainly of bassanite and gypsum and (c) homogenised residue (well-mixed fines and coarse iron residues).

Elemental composition of the precipitates from oxidative precipitation was analysed using XRF and the results are shown in Table 4.3. The coarse material contained smaller amounts of Fe, Al, Cr and Ni, but substantialy greater amounts of Ca and S compared to the fine material. This is an indication for the dominance of gypsum in the coarse material. High nickel content in the fines shows that nickel loss is mainly associated with the Fe, Al and Cr which are predominant in the fine material. The nickel incorporation in the precipitates can be through adsorption and co-precipitation as suggested by Carvalho-e-Silva et al. (2003).

To estimate the effect of gypsum formation on nickel and cobalt losses, a sulfate solution containing nickel and cobalt with no iron was neutralised with calcium carbonate slurry at pH 3.5 and pH 4.5 and 85 ℃. There were no nickel and cobalt losses recorded at pH 3.5, however losses of approximately 0.98% were recorded at pH value 4.5. This is not in agreement with the observations by Wang et al. (2011), who found that no nickel was lost during gypsum precipitation at pH 2 and 4 at 85 ℃. It is possible that pH value 4.5 is high enough to induce nickel and cobalt hydroxide precipitation at the high nickel and cobalt concentrations in solution.

Table 4.3: Elemental analysis of the iron residues obtained during oxidative precipitation using oxygen

Iron residue	Elemental analysis of solids (weight %)					
	Fe	Al	Cr	Ca	S	Ni
(a)	35.94	8.55	0.76	1.05	8.69	2.92
(b)	8.93	2.21	0.20	22.06	19.76	0.78
(c)	11.73	6.99	0.54	17.83	17.22	0.39

4.3.5 Hydrogen peroxide dose for ferrous ion oxidation

It has been explained earlier in section 2.4.1.2 that hydrogen peroxide is a stronger oxidising agent than oxygen with fast reaction kinetics, which could be a potential oxidant for trivalent ions of chromium. However, the application of hydrogen peroxide as an oxidant in the processing of nickel laterite leach solutions is not common.

Experiments were carried out to study the effect of using hydrogen peroxide on the oxidative precipitation of ferrous ion, co-removal of trivalent ions of aluminium and chromium and the associated nickel and cobalt losses. To achieve this, a series of oxidative precipitation experiments were carried out using the procedure outlined in 4.3.2 using multi-element sulfate solution and one variable at a time approach. The variables studied were hydrogen peroxide dose, reaction time, temperature, multistage precipitation, type of neutralising agent and initial ferrous ion concentration.

Initially, the dose of hydrogen peroxide (6% w/v) required for oxidative precipitation of Fe(II) from multi-element sulfate solution with initial Fe(II) concentration of 2 g/L and other cations as given in Table 4.1 was determined at pH 3.5, 85 ℃ and 2 hours reaction time using $CaCO_3$ slurry. A baseline temperature of 85 ℃ and pH value 3.5 were used as they were optimal conditions for iron hydrolysis precipitation in Chapter 3 and ferrous ion oxidation with oxygen.

The oxidation of ferrous ion with hydrogen peroxide can be represented by Equation 4.4. Theoretically, two moles of ferrous ion requires one mole of hydrogen peroxide, provided there are no side reactions.

$$2Fe^{2+}_{(aq)} + H_2O_{2\,(l)} + 2H^{+}_{(aq)} \leftrightarrow 2Fe^{2+}_{(aq)\,)} + 3H_2O_{\,(l)} \qquad 4.4$$

The percent Fe(II) oxidatively precipitated as a function of the percentage of stoiciometric hydrogen peroxide required is given in Figure 4.7. Calculation of percent hydrogen peroxide was carried out using Equation 4.5 which is based on the hydrogen peroxide added relative to stoichiometric amount required according to Equation 4.4.

$$\%\ \text{Hydrogen peroxide} = \frac{\text{Moles of } H_2O_2 \text{ added}}{\text{Stoichiometric moles of } H_2O_2} \times 100\% \qquad 4.5$$

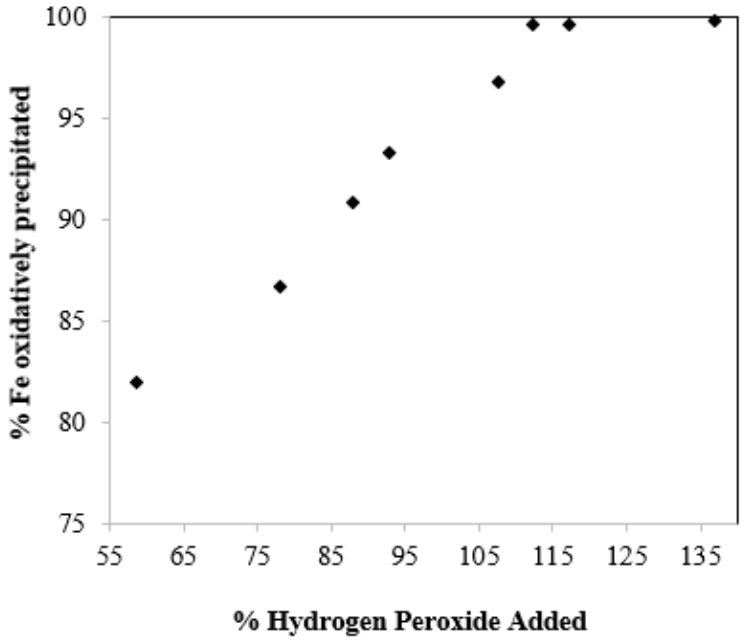

Figure 4.7: The dependence of iron removal on % hydrogen peroxide added in solution during oxidative precipitation at pH 3.5 and 85 °C, 2 hours contact time in a solution containing 2g/L ferrous ion using calcium carbonate slurry.

The results indicate that quantitative oxidative precipitation of Fe(II) from solution is strongly dependent on the amount of hydrogen peroxide added. At the process conditions, more hydrogen peroxide than the stoichiometric amount was required for complete iron removal from solution by oxidative precipitation. At least 12% excess hydrogen peroxide (112% H_2O_2) is required to achieve more than 99.5% ferrous ion removal corresponding to less than 10 mg/L Fe remaining in solution. The addition of more than 12% excess hydrogen peroxide did not improve iron removal. A similar observation, although in a ternary system [(Fe(II)+Ni(II)+Co(II)] has been reported by Agatzini et al. (1986) who studied the removal of iron by oxidative precipitation. They found that 16% excess hydrogen peroxide is required to achieve 20 to 50 mg/L Fe in the filtrate at pH 3.0 and temperature range 70 ℃ to 90 ℃. In contrast, the stoichiometric amount was found adequate to completely remove iron in a binary system [(Fe(II)+Ni(II)] at pH 2.9 to 4.3 using the V.M. goethite process (Yue et al., 2016). It is possible that the high hydrogen peroxide amounts required in this study are caused by the presence of other cations such as cupric ions which have been found to catalyse the decomposition of peroxide (Barb et al., 1951). Maximum iron removal when at least 12% excess hydrogen peroxide is added is probably because the system is at equilibrium.

Ferrous ion oxidation with hydrogen peroxide is rapid and in less acidic conditions is accompanied by the precipitation of ferric oxyhydroxides and oxyhydroxysulfates. Therefore, it is necessary to investigate the effect of time on the oxidative precipitation process. Iron remaining in solution as a function of time at 58%, 92% and 112% peroxide addition are shown in Figure 4.8. The dropwise addition of hydrogen peroxide was complete in less than 15 mins, and the first sample was collected at 15 mins reaction time. The degree of ferrous ion removal by oxidative precipitation depends largely on hydrogen peroxide dose. The plots show that oxidative precipitation of ferrous ion is almost instantaneous and prolonging the contact time has minimal influence on iron removal, although it could promote the formation of solids with better characteristics through transformation (Cornell and Schwertmann, 2003).

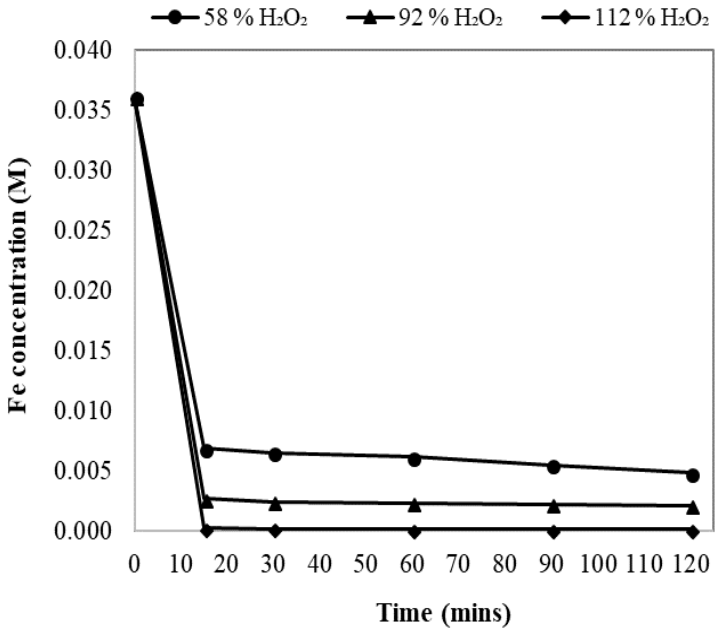

Figure 4.8: Effect of time on iron concentration for various hydrogen peroxide addition at pH 3.5 and 85 °C using calcium carbonate slurry during oxidative precipitation. Effect of temperature

A baseline temperature of 85 ℃ was selected for oxidative precipitation with hydrogen peroxide as it was found optimal in the impurity removal process (iron hydrolysis precipitation) in Chapter 3 and also in ferrous ion oxidation with oxygen. Some experiments were however carried out at 55 ℃ and 70 ℃ to evaluate the influence of temperature on oxidative precipitation process. These experiments were carried out

using the procedure outlined in section 4.3.2. Table 4.4 shows the % Fe, Al and Cr removal, and the corresponding concentration of the elements in the filtrate solutions after ageing the slurry for one hour. The results indicate that increasing temperature, pH and the hydrogen peroxide dose favour the removal of Fe, Al and Cr. At the end of the experiments at 55 ℃ and ageing pH value of 3.5, the filtrate was brownish indicating the presence of a significant concentration of ferric ion. Metal removal of approximately 92% Fe, 44% Al and 81% Cr were obtained. The precipitation of Fe, Al and Cr become faster at higher temperatures and pH values. Increasing temperature to 70 ℃ resulted in more than 96% Fe, 66% Al and 89% removed at ageing pH value 3.5, while increasing ageing pH to 4.5 at 55 ℃, more than 97 % Fe, and 99.5 % Al and Cr were removed. With an adequate amount of hydrogen peroxide, optimal ferrous ion removal (>99%) can be achieved at pH 3.5. Optimal removal of aluminium and chromium from solution is favoured at pH values more than 3.5. The influence of temperature on hydrogen peroxide dose was negligible, hence satisfactory metal ion removal from the system at 85 ℃ can be achieved by optimising the oxidative precipitation and ageing pH values. Hydrogen peroxide dose of 8% in excess stoichiometry was used in the subsequent sections.

Table 4.4: The removal of iron, aluminium and chromium during oxidative precipitation with hydrogen peroxide when temperature was increased from 55 ℃ to 85 ℃ with the slurry aged for 1 hour.

Run	% H_2O_2	Temp. °C	pH		Final Concentrations (g/L)			Metal removal (%)		
			Oxidation	Ageing 1 hour	Fe	Al	Cr	Fe	Al	Cr
T1	108	55	3.5	3.5	0.140	0.83	0.019	92.91	43.89	80.57
T2	108	55	3.5	3.5	0.213	0.77	0.018	92.11	44.63	81.33
T3	108	55	3.5	4.5	0.044	<0.01	<0.001	97.74	99.84	99.90
T4	108	70	3.5	3.5	0.065	0.47	0.010	96.68	66.33	89.33
T5	108	85	3.5	3.5	0.083	0.27	0.008	95.75	80.64	91.80
T6	117	70	3.5	3.5	0.010	0.45	0.010	99.48	68.02	89.33
T7	117	85	3.5	3.5	0.006	0.14	0.005	99.68	89.75	94.56

4.3.6 Multistage oxidative precipitation experiments

As noted in previous sections, pH is the most significant variable in the removal of the trivalent ions of iron, aluminium and chromium. Higher pH values favour the removal of iron, aluminium and chromium. This is however at the expense of greater nickel

and cobalt losses to the precipitate. The study on iron, aluminium and chromium removal from both synthetic and real laterite leach solutions by Wang (2012) showed that a multistage precipitation process at an optimum pH and temperature combination could minimise nickel losses. It is therefore desirable to develop a multistage oxidative precipitation process to minimise nickel and cobalt losses. Experiments were carried out as described in Section 4.3.2 at a temperature of 85 °C and different oxidative precipitation and ageing pH combinations. A multi-element sulfate solution containing 2 g/L Fe(II) and $CaCO_3$ slurry was used for a 1-hour reaction time. The oxidative precipitation pH was varied from 2.5 to 4.5 while ageing was carried out at pH values of either 3.5 or 4.5. Figure 4.9 shows the % iron, aluminium and chromium removal and Figure 4.10 shows the % nickel and cobalt losses from solution.

The results given in Figure 4.9 indicate that the removal efficiency of ferrous ion, aluminium and chromium at 8% excess hydrogen peroxide is dependent on ageing pH value. As can be seen from Figure 4.10, more than 99% Fe, Al and Cr can be removed at an ageing pH value of 4.5. This corresponds to Fe, Al and Cr concentrations in the filtrate solution of less than 20 mg/L, 10 mg/L and 2 mg/L, respectively. These results indicate that pH had little effect on the oxidation of ferrous ion with hydrogen peroxide since comparable amounts of ferrous ion were removed in the oxidative precipitation pH range of 2.5 to 4.5. There was a decrease in the % iron, aluminium and chromium removal at ageing pH 3.5, which is expected as the equilibrium metal ion concentrations increases at lower pH values.

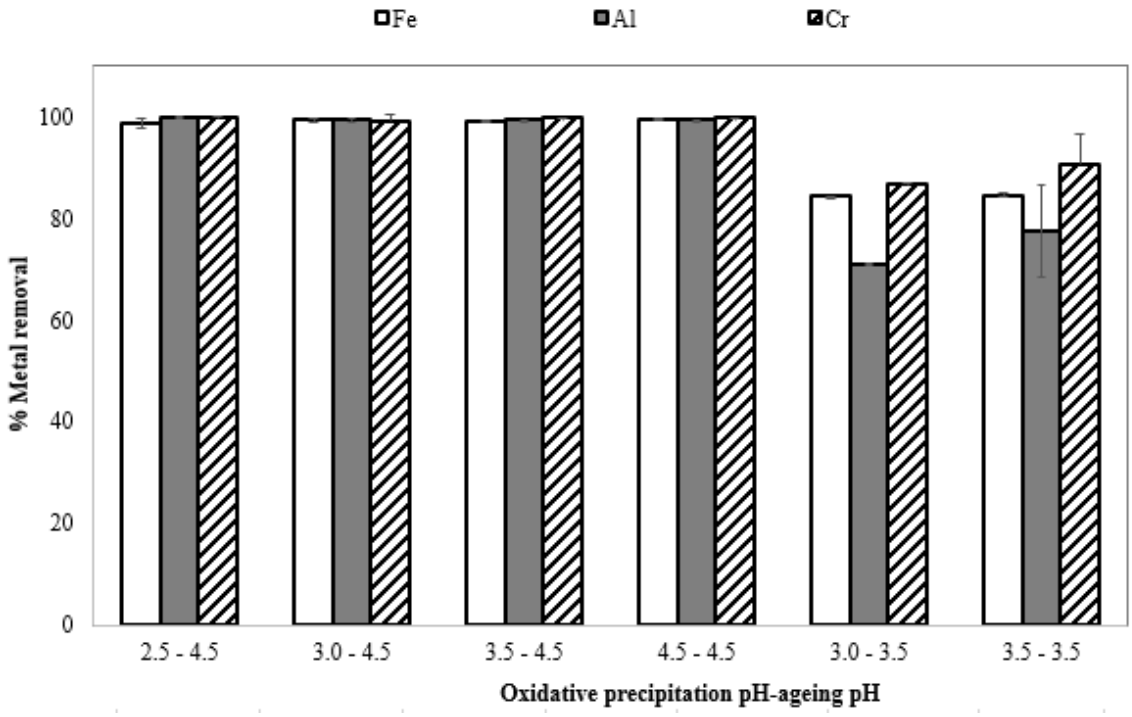

Figure 4.9: Effect of various pH combinations on metal recoveries at 8% excess H_2O_2, 85 °C and 1 hour reaction time

Although high pH values are required for the effective removal of iron, aluminium and chromium (Figure 4.9), this is at the cost of high nickel and cobalt losses (Figure 4.10). The amount of nickel and cobalt losses, however, can be reduced by using certain pH combinations during multistage oxidative precipitation. The optimum pH combination, with regard to significant iron, aluminium and chromium removal, resulting in approximately 11% nickel and 2% cobalt losses was oxidative precipitation and ageing pH values of 3.5 and 4.5 respectively. This is almost half the values observed during oxidative precipitation at pH values of 2.5, 3.0 and 4.5 and ageing at a pH value of 4.5. Ferrous ion oxidation to ferric ion using hydrogen peroxide is rapid in acidic solutions while precipitation of the trivalent ions of Fe, Al and Cr is slow at low pH values. This creates a highly supersaturated solution. When the solution pH is increased by adding neutralising agents, this creates high molar ratios of OH^-/Fe(III) resulting in fast nucleation rate (Van Der Woude et al., 1983) and the formation of small particles with large surface area and higher adsorption capacity for divalent ions of nickel and cobalt (Claassen and Sandenbergh, 2006). Although nickel losses in the present study were higher than those found in binary systems of Fe(II)+Ni(II) when using hydrogen peroxide by Agatzini et al. (1986) and Yue et al. (2016), they were lower than those reported by Chang et al. (2010) when using air at

almost the same pH values. The higher nickel losses in the present study and that by Chang et al. (2010) could be due to the presence of aluminium and chromium, whose co-precipitation increases the level of nickel and cobalt losses (Section 3.6.2.3). The use of pH values of about 3.5 or higher and the significant nickel and cobalt losses in iron precipitation of nickel laterite sulfate solutions are inevitable. This is the case even in the absence of ferrous ion because aluminium is always present in nickel laterite leach solutions and its complete removal requires higher pH values (≥3.5).

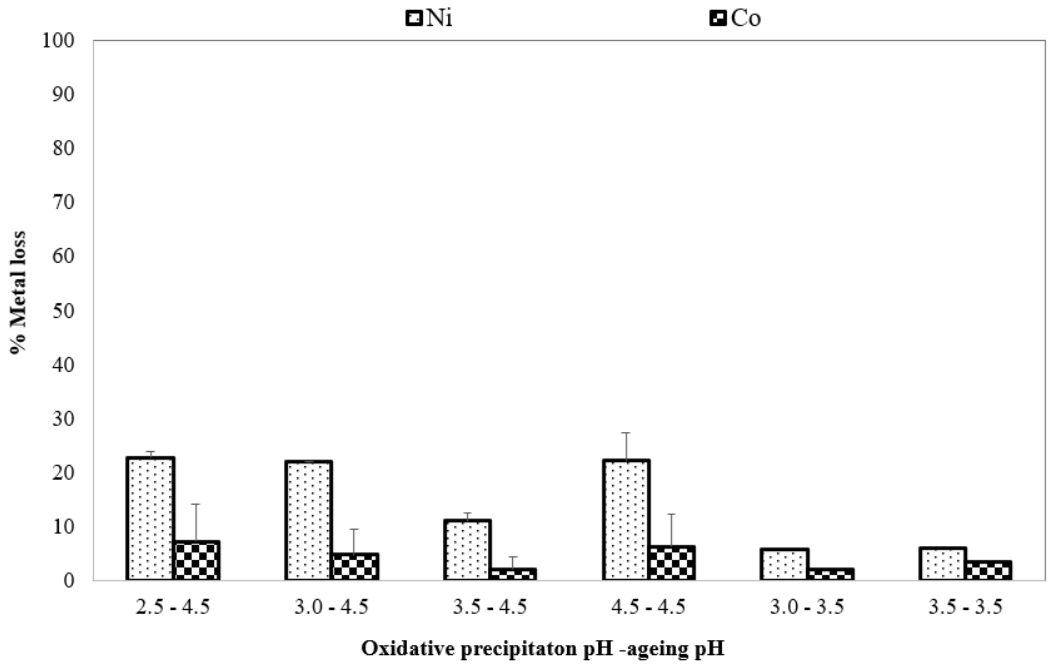

Figure 4.10: Effect of various pH combinations on nickel and cobalt losses at 8% H_2O_2 excess, 85 °C and 1 hour reaction time.

To provide insight into the effect of pH on the particle size distribution during precipitation, the volume-based particle size distribution of the precipitates formed at the oxidation precipitation pH – ageing pH: 3.0 – 3.5, 3.0 – 4.5, 3.5 – 4.5 was determined. Results of the analysis are given in Figure 4.11 and they show a bimodal particle size distribution, with modal peaks for extremely fine particles and coarse particles. The fast oxidation of ferrous ion with hydrogen peroxide creates a high supersaturation level, which leads to faster nucleation and the formation of small particles of iron phases. The bigger particles are mostly gypsum which is formed when using $CaCO_3$ slurry as neutralising agent in a sulfate system (as found in Section 4.4.4).

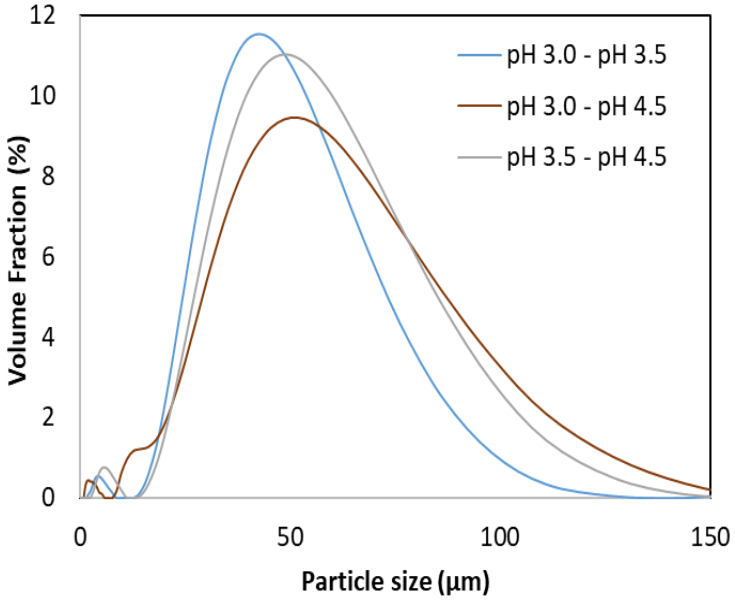

Figure 4.11: Particle size distribution of the precipitates formed during multistage oxidative precipitation with hydrogen peroxide and calcium carbonate slurry for neutralising at 85 °C different pH combination levels.

Settling rate tests were performed on the slurries produced at an oxidative precipitation pH value of 3.0 and ageing pH values of 3.5 and 4.5. The slurries were cooled to room temperature, transferred into a 100 mL graduated measuring cylinder, then thoroughly mixed by inverting the cylinder several times. After setting the cylinder upright, the settling rate was recorded, by noting the height of the mudline as a function of time. The ratio of the height of the mud-line at time t=t and t=0 (h_t/h_o) was plotted versus time and the results are shown in Figure 4.12. Two mud-lines were observed, the slow settling fine particles (Mud line 1) and the fast settling large particles (Mud line 2) which supports the bimodal particle size distribution (Figure 4.11). As can be seen, the settling rates of the coarse material (Mud line 2) in the two experiments were comparable while the settling rate of the fine particles (Mud line 2) was faster at the higher ageing pH of 4.5 compared to pH 3.5. This indicates that the particles at ageing pH 4.5 are bigger probably due to particle growth dominating at the reduced supersaturation level as precipitation continues to reach the lower equilibrium solubilities at higher pH values.

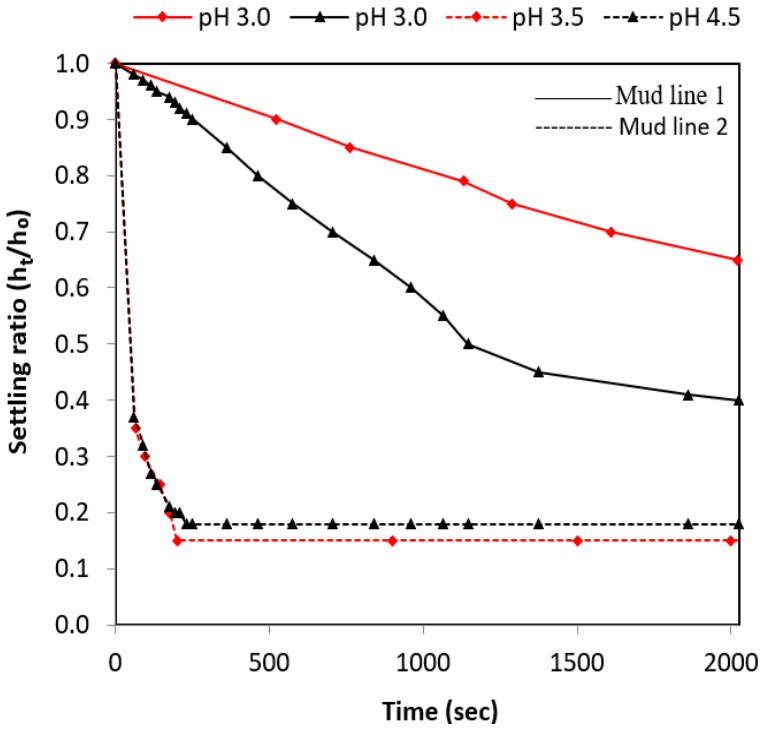

Figure 4.12: Comparison of settling rates of iron precipitates produced at 85 °C using calcium carbonate slurry at oxidation pH 3.5 and ageing pH 3.5 and 4.5: Mud line 1 represents the slow settling solid and mud line 2 represents the fast settling solids.

4.3.7 Effect of type of neutralising agent

In chapter 3, higher nickel and cobalt losses in the processing of high-iron content sulfate solutions were found using $MgCO_3$ and MgO slurries and NaOH solution than when using $CaCO_3$ slurry. The use of non-calcium containing neutralising agents, also, has an advantage of lower precipitate mass and the absence of gypsum scaling. The impurity removal process in this chapter was designed to simulate the secondary neutralisation stage as used in RNO, where any remaining Fe, Al and Cr in solution after the primary neutralisation stage must be removed. The process is carried out at high pH values where nickel and cobalt losses are significant. To recover nickel and cobalt lost, the precipitates from this stage are usually recycled to upstream processes in industrial practice. Less bulky precipitates obtained using non-calcium containing neutralising agents can be better suited for recycling compared to those obtained with $CaCO_3$ slurry, especially if nickel and cobalt losses are reasonably low. This makes it worthwhile to investigate the effect of using non-calcium containing neutralising agents in a multistage oxidative precipitation process with regard to impurity removal efficiency and nickel and cobalt losses.

The multistage oxidative precipitation experiments were carried out using the same procedure and conditions used with $CaCO_3$ slurry. Nickel losses were reasonably low ($\leq 5\%$) at ageing pH value 3.5, irrespective of the neutralising agent used (Figure 4.13) but increased when ageing pH increased to 4.5. As expected, Fe, Al and Cr removal was favoured at a higher final pH value of 4.5 as shown in Figure 4.14, Figure 4.15 and Figure 4.16, respectively. This was, however, at the expense of high nickel losses. Further results comparison with different neutralising agents suggests higher nickel losses with NaOH compared to $CaCO_3$ and $MgCO_3$ slurries. There is better control of pH and supersaturation with $CaCO_3$ and $MgCO_3$ slurries as the hydroxide is slowly released following decomposition of the solid unlike with NaOH where the hydroxide is already dissociated and ready to react. The use of NaOH, which is more reactive leads to faster nucleation and production of smaller particles with higher surface area and adsorption capacity for nickel ions. Although the type of neutralisation agent influences the level of nickel losses, no difference in the filtration rate was observed, and the precipitates were vacuum filtered in less than one minute. The main concern of this chapter was to remove almost all the iron, aluminium and chromium remaining in solution at minimal nickel losses. The optimum pH conditions for multistage oxidative precipitation were 3.5 and pH 4.5 for oxidative precipitation and ageing respectively, using either $MgCO_3$ or $CaCO_3$ slurry at 85°C. These conditions resulted in more than 99% iron, aluminium and chromium removal from synthetic multi-element sulfate solutions, with resultant nickel losses below 11%.

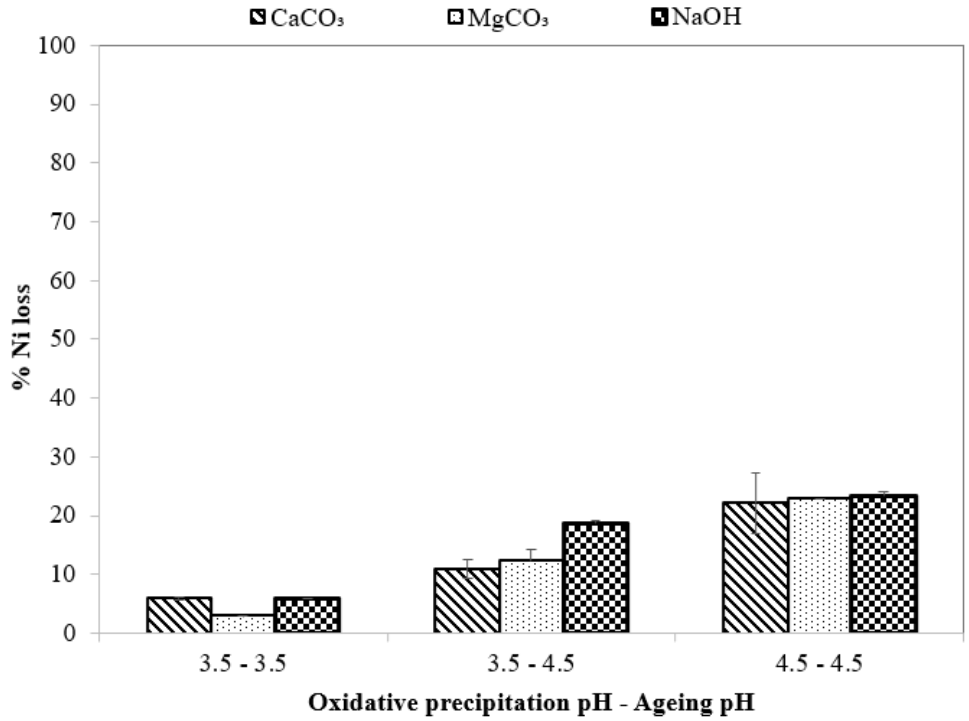

Figure 4.13: Effect of using different neutralising agents on nickel losses at 85 °C, 8% excess hydrogen peroxide and varying oxidative precipitation and ageing pH values.

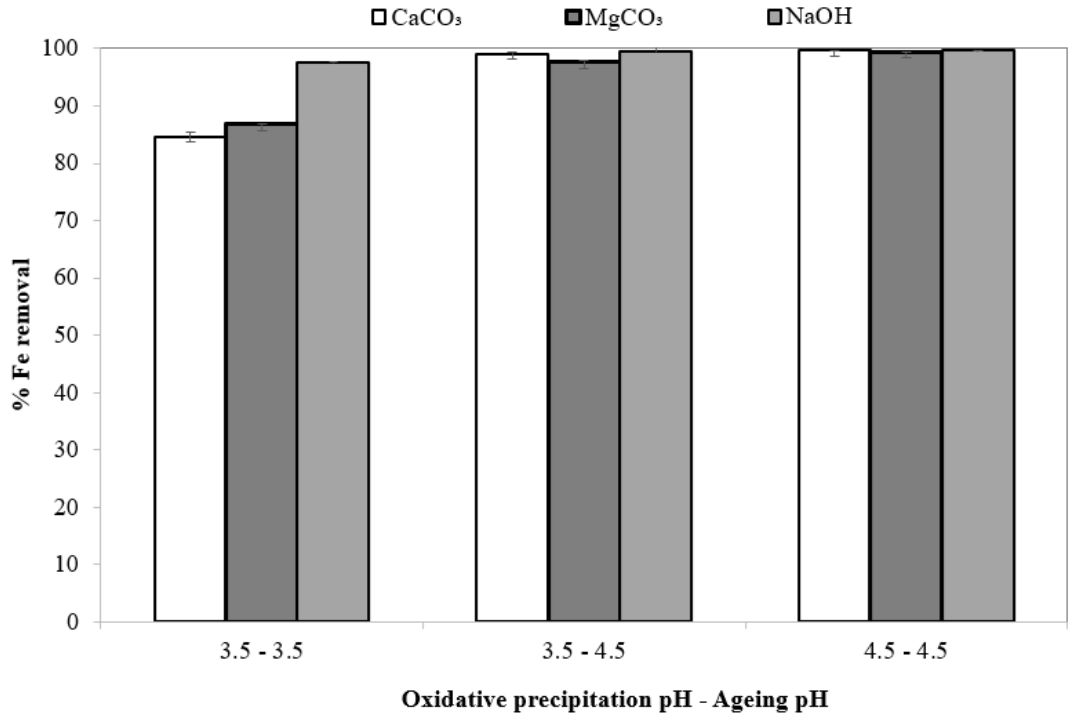

Figure 4.14: Effect of using different neutralising agents on iron removal at 85 °C, 8% excess hydrogen peroxide and varying oxidative precipitation and ageing pH values.

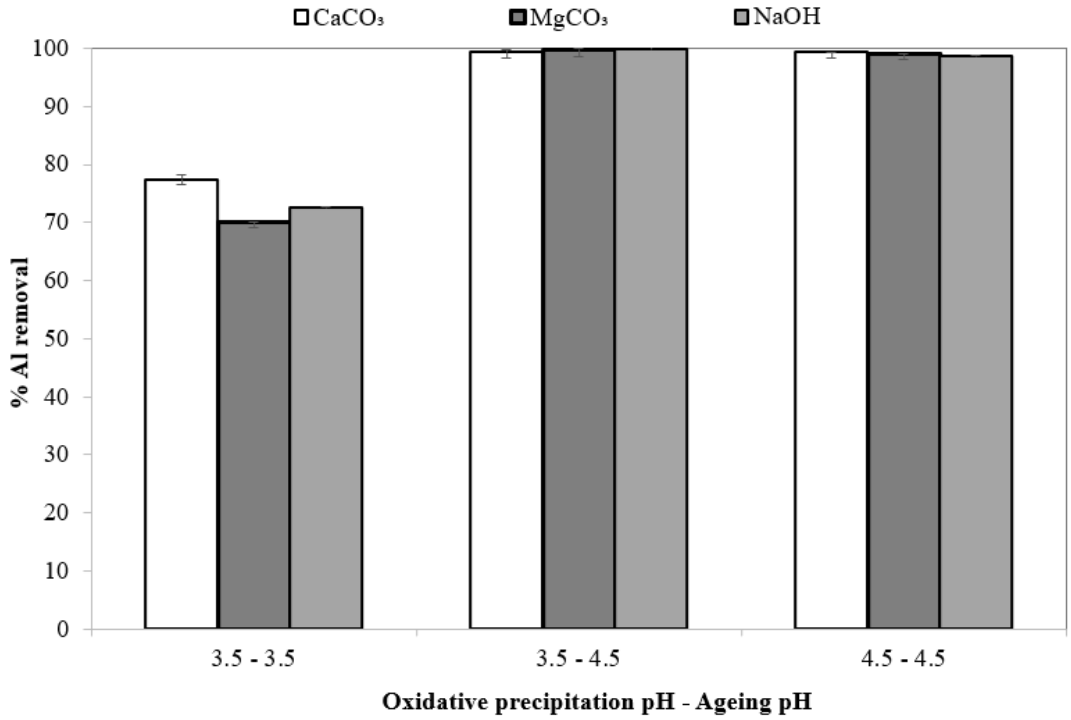

Figure 4.15: Effect of using different neutralising agents on aluminium removal at 85 °C, 8% excess hydrogen peroxide and varying oxidative precipitation and ageing pH values.

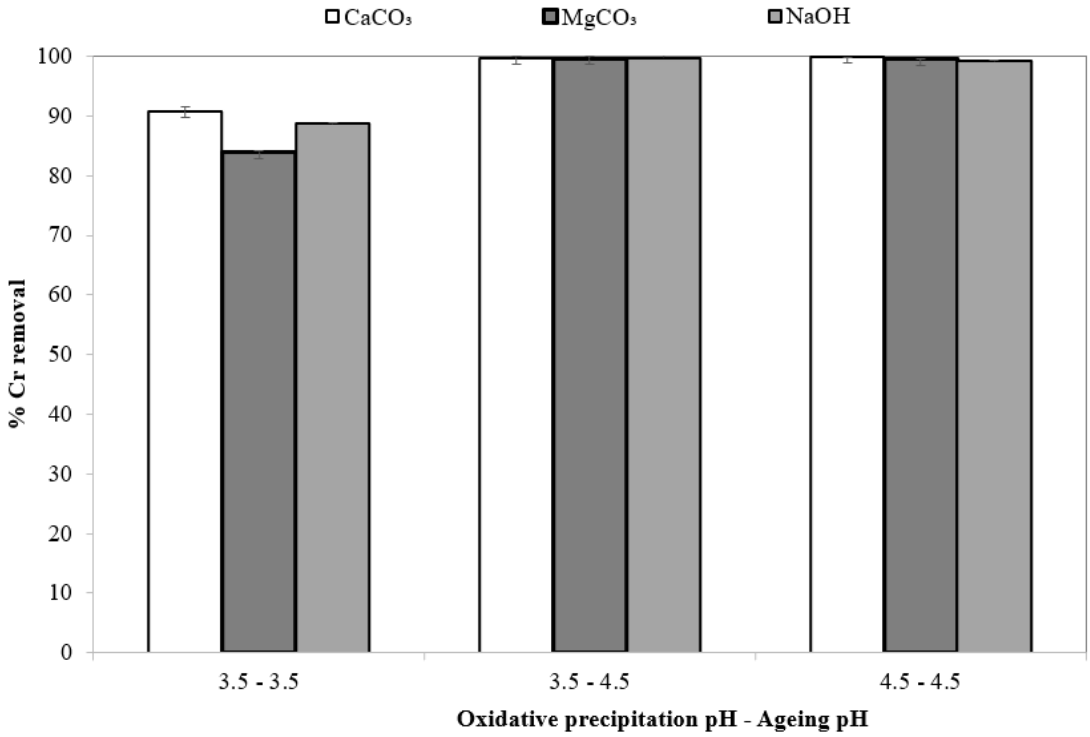

Figure 4.16: Effect of using different neutralising agents on chromium removal at 85 °C, 8% excess hydrogen peroxide and varying oxidative precipitation and ageing pH values.

4.3.8 Analysis of the precipitates

The precipitates obtained by oxidative precipitation with ageing and pH values of 3.5 and 4.5, respectively at 85 ℃ with $CaCO_3$ and $MgCO_3$ slurry and NaOH solution were anlaysed using XRD. The results of this analysis are given inFigure 4.17. The peaks were broad and not well defined indicative of amorphous precipitates. The precipitates of iron, aluminium and chromium phases are in a mixed assemblage which makes the identification of individual metal phases with certainty difficult. When calcium carbonate slurry is used as a neutralising agent, strong peaks of crystalline gypsum are always present, and they tend to mask the peaks of the poorly ordered iron phases. Despite the strong peaks of gypsum, there were characteristic peaks of iron phases observed at about 19°, 23° and 31° 2θ which could be those of schwertmannite and some minor low crystalline goethite. The XRD patterns of the precipitates obtained using magnesium carbonate slurry and sodium hydroxide solution show that the precipitates were extremely amorphous, with weak peaks identified at around 21°, 31° and 41° 2θ. The peaks mirrored those of ferrihydrite and schwertmannite found in a previous study by Wang et al. (2013) during the processing of ferric ion sulfate solutions in a binary system [Fe(III)+Ni(II)] and quaternary system [Fe(III)+Al(III)+Cr(III)+Ni(II)] with the E.Z. goethite method. Both schwertmannite and ferrihydrite have a poorly ordered structure and consist of small particle sizes of less than 10 nm (Murad, 2004). The fine particles result in poor diffracting lines and broad peaks making it difficult to distinguish the two iron phases in a mixed assemblage using XRD analysis. Also, no sharp peaks of jarosite were detected in precipitates obtained using NaOH solution to neutralise acid multi-element sulfate solutions with low ferric ion concentration (≤2 g/L). This contrasts with the observations at very high ferric ion concentrations (≈ 35 g/L) and pH 2.5 (Section 3.6.2.2) in a ternary sulfate system [Fe(III)+Ni(II)+Co(II)]. This shows that jarosites are formed at high ferric ion concentrations during precipitation, but insufficient amounts are formed at low iron concentrations to be detected.

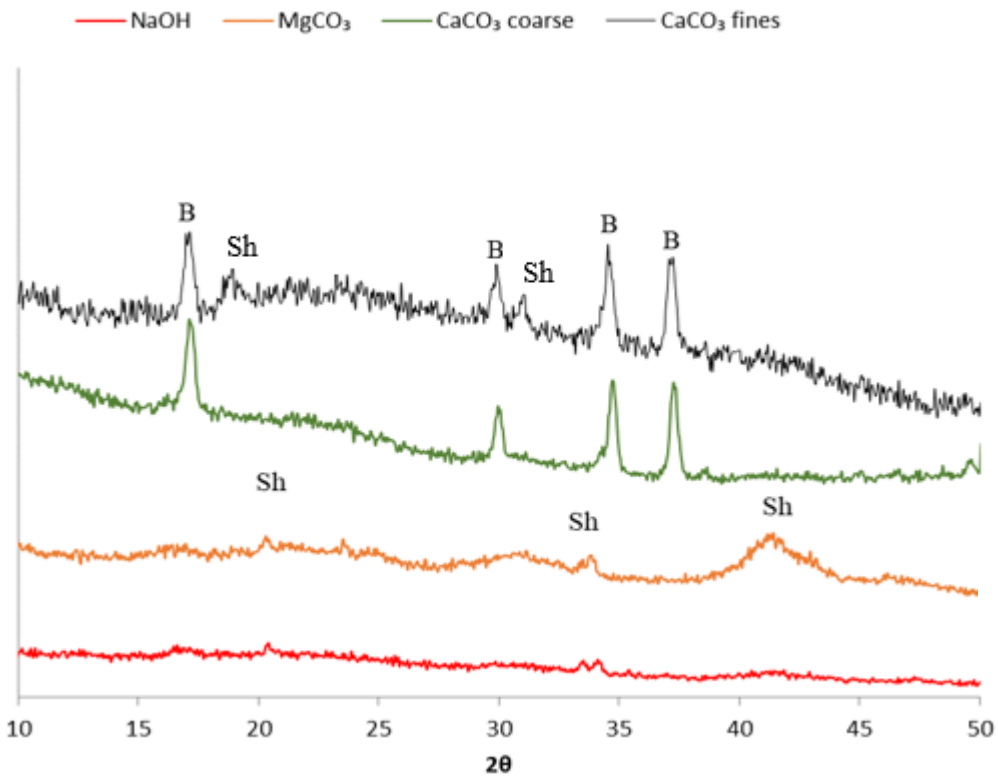

Figure 4.17: X-ray diffraction patterns of the iron residues: gypsum (B), and schwertmannite (Sh) produced using different neutralising agents and Co kα radiation.

The elemental composition of the precipitates produced with $CaCO_3$ and $MgCO_3$ slurry and NaOH solution, determined by XRF, is given in Table 4.5. Sulfur is a common element in all the precipitates including where calcium carbonate is not used as a neutralising agent and where gypsum is not formed. The presence of a significant amount of sulfur in precipitates from $MgCO_3$ and NaOH neutralising agents could be a result of the precipitation of sulfate compounds such as schwertmannite. It is also possible that the sulfur is present as sulfate adsorbed on iron oxyhydroxides as it has been found that ferrihydrite can adsorb adequate sulfate to approximate the composition of schwertmannite (Bigham and Nordstrom, 2000). This makes it difficult to distinguish the iron phases from the elemental composition.

Table 4.5: Elemental analysis for the iron residues for the different neutralising agents.

Neutralising agent	Elemental composition in the solid product (weight %)						
	Fe	Al	Cr	S	Ca	Mg	Ni
NaOH	50.18	3.01	1.47	7.71			0.22
$MgCO_3$	48.11	3.92	1.40	7.35		0.94	0.42
$CaCO_3$	18.79	1.48	0.55	17.21	18.65		0.14

In this study, the precipitates were predominantly amorphous regardless of the low ferric ion concentration (<2 g/L) in solution during precipitation. This is probably because the transformation of amorphous and metastable iron phases into goethite is inhibited by the presence of the divalent ions, Co, Cu, Mn, Ni and Zn (Cornell and Giovanoli, 1989). The cations stabilise the amorphous and poorly ordered iron phases against dissolution which retards goethite formation. Selective dissolution by acidified ammonium oxalate (AAO) solution at pH 2.5 to 3.0 and temperature of 25 ℃ in the absence of light can be used to confirm the presence of goethite in a mixed assemblage precipitate (Cornell and Schwertmann, 2003). The amorphous and poorly ordered iron phases, ferrihydrite and schwertmannite, are easily and to a certain extent selectively dissolved by AAO solution compared to goethite.

4.3.9 Dissolution of the iron-rich precipitates with AAO solution

The dissolution behaviour of the precipitates obtained using $CaCO_3$ and $MgCO_3$ slurry as neutralising agents for the acid multi-element sulfate solution were examined using AAO and the results are given in Figure 4.18.

The percentage of iron dissolved over time curves show that the rate of dissolution is rapid in the first 40 minutes, decreases thereafter and then plateaus after 2 hours reaction time. The overall iron dissolved after 2 hours reaction time was 78% and 97% for the precipitates obtained after neutralising with $MgCO_3$ and $CaCO_3$ slurry, respectively.

The residue from AAO dissolution showed no iron phases but only gypsum when using calcium carbonate slurry neutralising agent. Similar dissolution curves of iron were obtained during AAO dissolution of bi-metallic precipitates of Fe and Ni (Wang, 2012), where the iron dissolution curves of multi-metallic precipitates were almost

linear. When other metal ions are present in solution during iron precipitation, spinel iron phases are formed through isomorphous substitution of Fe^{3+} by cations of similar size, especially Al^{3+}, Cr^{3+}, Mn^{3+} and Ni^{2+} (Cornell, 1996). The substitution of ferric ion by the other metal ions stabilises the minerals against dissolution (Cornell and Giovanoli, 1989, Cornell et al., 1990, Cornell et al., 1992). Aluminium and chromium, for example, were found to retard the dissolution of nickeliferous goethite in strong sulfuric acid solution (2 M H_2SO_4) by Landers et al. (2009) while Al substituted goethite was found to have slow dissolution rate in AAO solution (Cornell and Schindler, 1987). Both aluminium and chromium seem to have a stabilising effect on the dissolution of iron precipitates. In this study, the dissolution rates of the multi-metallic precipitates were relatively fast probably because the precipitates consisted of highly soluble disordered and amorphous iron oxyhydroxide and oxyhydroxysulfate.

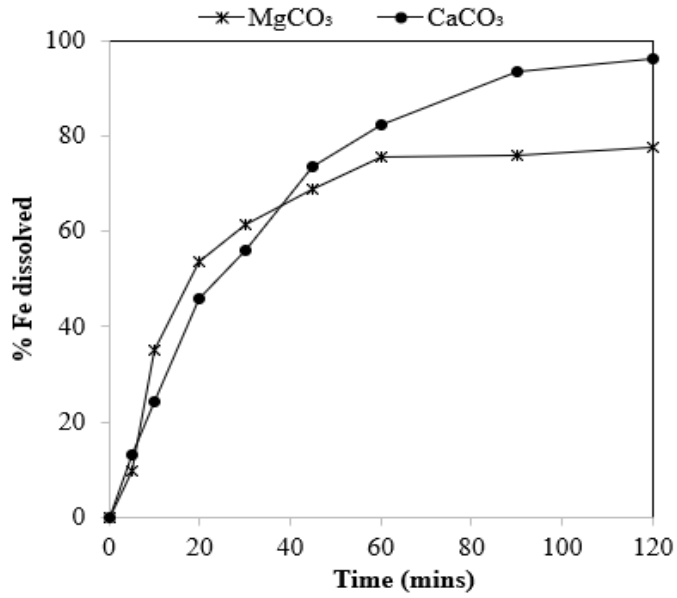

Figure 4.18: The dissolution behaviour of precipitates obtained using slurries of calcium and magnesium carbonate to neutralise multi-element sulfate solution during oxidative precipitation in AAO solution at 25 °C.

The congruency of metal dissolution can be used as an indirect way to establish the distribution of the co-removed metals in relation to the iron minerals (Singh and Gilkes, 1992). If the iron and the other metals dissolve at identical rates (expressed as % metal dissolved as a function of % Fe dissolved), this is evidence that the metals are uniformly distributed in the crystals of the iron minerals. On the contrary, in the absence of congruency in the dissolution rate of iron and the other metals, it can be assumed that the metals and iron are not uniformly distributed in iron mineral crystals,

but they exist as discrete metal phases. The plots showing the relationship between the % Al, Cr and Ni dissolved as a function of % Fe dissolved for the precipitates produced with $CaCO_3$ and $MgCO_3$ slurry are given in Figure 4.19.

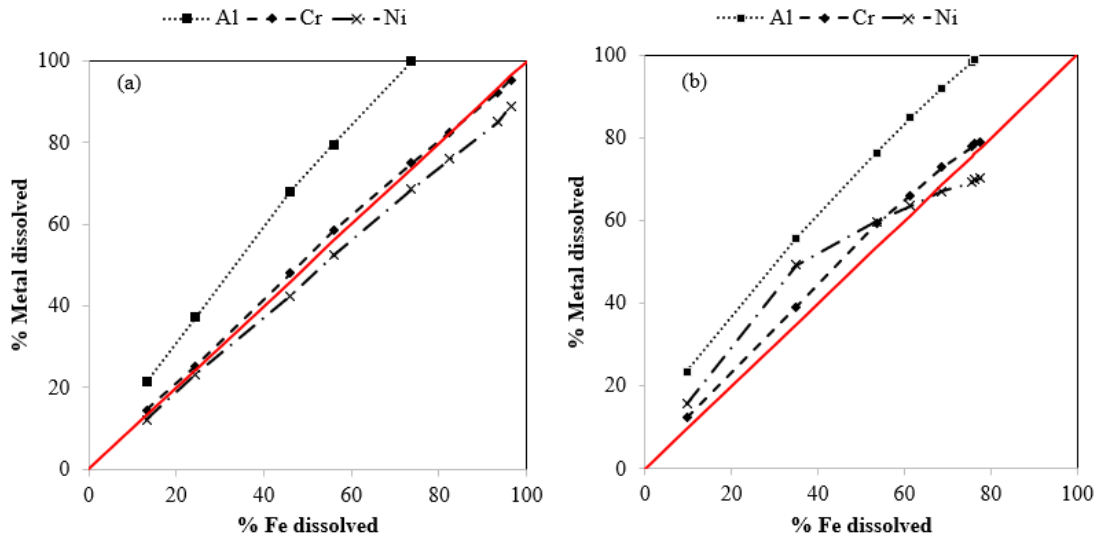

Figure 4.19: The dissolution of the metals (Al, Cr and Ni) plotted against the iron dissolved: (a) – precipitates obtained using calcium carbonate slurry and (b) - precipitates from using magnesium carbonate slurry neutralising agents. The continuous red line indicates congruent dissolution of the metals and iron.

The dissolution of chromium and nickel is approximately congruent to iron dissolution, indicating that both chromium and nickel are largely associated with the iron minerals, probably incorporated and uniformly distributed in the lattices. Aluminium dissolution curve is displaced more to the left of the congruency line because aluminium dissolution is faster than that of iron for both precipitates. The faster dissolution of aluminium is probably due to the presence of discrete aluminium phases which are amorphous since they are not detected in the XRD analyses (Figure 4.17). The dissolution behaviour is in support of the observations during characterisation of limonite ores (Georgiou and Papangelakis, 1998, de Carvalho-e-Silva et al., 2002), where aluminium, chromium and nickel are usually found incorporated in iron minerals, especially goethite. Nickel loss during impurity removal is likely by adsorption and inclusion in the impurity mineral lattices.

4.3.10 Effect of initial ferrous ion concentration on oxidant amount

A series of experiments was carried out to evaluate the effect of initial Fe(II) concentration on the hydrogen peroxide dosage required to achieve iron filtrate

concentrations of less than 20 mg/L. These experiments were carried out at oxidative precipitation and ageing pH values of 3.5 and 4.5, respectively and at 85 ℃. The initial ferrous ion concentration in synthetic multi-element sulfate solution was varied at 1, 3.5 and 5 g/L. Figure 4.20 shows the variation in the filtrate iron concentration as a function of percentage hydrogen peroxide addition where 100% is the stoichiometric required amount. The amount of ferrous ion remaining in solution decreases with increasing hydrogen peroxide dose. At least 12% excess H_2O_2 was required to achieve less than 10 mg/L Fe at 5 g/L initial ferrous ion concentration compared to more than 16% excess H_2O_2 at 1 g/L. It is possible that a large amount of iron oxides at high iron concentrations present an increased surface area for adsorption of any iron remaining in solution (Park and Dempsey, 2005). Despite the solutions in the present study containing other species such as Cu(II) which catalyse the decomposition of hydrogen peroxide (Barb et al., 1951), the amount of hydrogen peroxide needed to achieve 20 mg/L Fe was comparable to 16 % excess found in the binary system [Fe(II)+Ni(II)] by (Agatzini et al., 1986). At the low metal concentration analysed, it is also possible that the differences are due to analytical variation and thus these should be taken as indicative only.

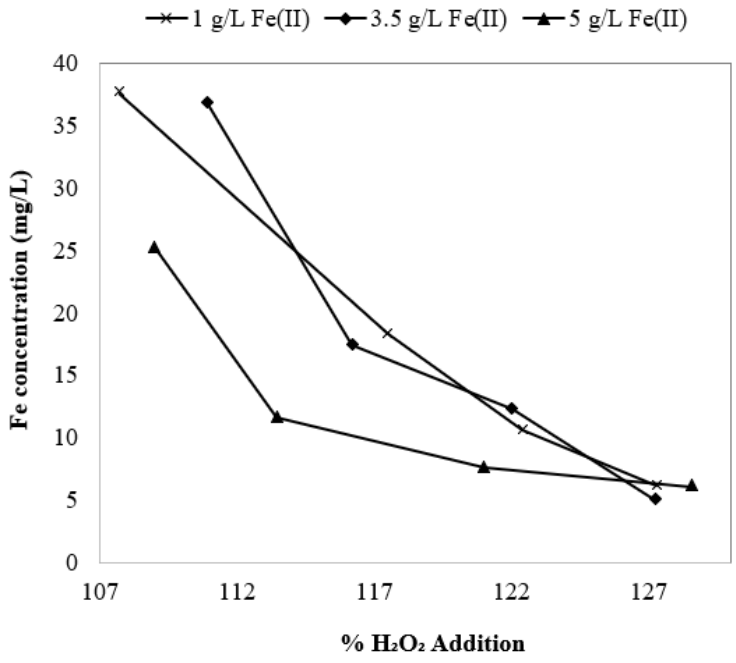

Figure 4.20: Plots of iron concentration in solution as a function of the amount of hydrogen peroxide addition at oxidation pH 3.5 and precipitation/ageing pH 4.5, temperature 85 ℃ using 6 % vol H_2O_2 and calcium carbonate slurry.

4.4 Conclusions

The removal of ferrous ion from synthetic multi-element sulfate solutions by oxidative precipitation using air, oxygen and hydrogen peroxide was investigated. Oxidative precipitation of ferrous ion and the co-removal of aluminium and chromium from synthetic solution was studied as a secondary impurity removal process following the first impurity removal process.

The results showed that ferrous ion could be effectively removed by oxidative precipitation at low pH values where nickel and cobalt losses are reasonably low. The oxidative precipitation of ferrous ion largely depends on the type of oxidant, pH and temperature. Higher apparent rates of ferrous ion oxidation were obtained with pure oxygen than with air indicating the influence of oxygen concentration on the process. Longer reaction times are required for higher % iron oxidative precipitation with oxygen. Iron removal increased from 45% to 96% at 15 minutes and 120 minutes reaction times, respectively at pH 3.5 and 85 °C. A comparison of the oxidative precipitation results using pure oxygen and hydrogen peroxide shows that hydrogen peroxide can be utilised for faster oxidative precipitation of ferrous ion. At the investigated pH range, the oxidative precipitation of ferrous ion is virtually instantaneous with hydrogen peroxide with % iron removal largely dependent on hydrogen peroxide dose and not reaction time. However, hydrogen peroxide consumption during oxidative precipitation of Fe(II) is slightly more than the stoichiometric amount. When using hydrogen peroxide, pH and temperature do not have a profound effect on the apparent rate of ferrous ion oxidation compared to when using air and oxygen. Increasing pH value and temperature favours the removal of the trivalent ions of iron, aluminium and chromium during oxidative precipitation but at the cost of more nickel and cobalt losses.

Further oxidative precipitation experiments carried out using calcium carbonate and magnesium carbonate slurries and sodium hydroxide solution and hydrogen peroxide as oxidant showed that the level of nickel and cobalt losses to the precipitate is also dependent on the type of neutralising agent. Lower nickel and cobalt losses occur when using neutralising agents in the slurry form compared to the use of NaOH solution. Multistage oxidative precipitation can be used to allow for the satisfactory removal of aluminium and chromium while at the same time minimising nickel and cobalt losses

to the precipitate. The losses are lowered by carrying out oxidative precipitation at lower pH followed by ageing at a slightly higher pH value. The results suggest that optimum conditions for multistage oxidative precipitation are oxidative precipitation and ageing pH values of 3.5 and 4.5, respectively at 85 ℃ using 12% excess hydrogen peroxide and either calcium carbonate or magnesium carbonate slurry. Low filtrate concentration of iron, below 20 mg/L at pH 3.5 and less than 10 mg/L aluminium and 1 mg/L chromium in filtrate solutions can only be achieved at pH 4.5 but at the expense of greater nickel and cobalt losses. Although hydrogen peroxide is a strong oxidising agent, it can be concluded from the results that it could not oxidise Cr(III) and Mn(II), considering that chromium removal was almost complete.

The iron precipitates were a mixture of amorphous and metastable iron phases formed during oxidative precipitation despite using low ferric ion concentration during precipitation. It is likely that the final iron product (mineral phases) formed is largely influenced by the elemental composition of the system.

This study demonstrated that ferrous ion removal at low pH values (pH 3.5) is practical, but the use of high pH values associated with greater nickel losses is inevitable as it is necessary mainly for the removal of aluminium. Also, the present study provides insight into the merits of using different reagents (oxidants and neutralising agents) on the processing of nickel laterite sulfate solutions. A better process must balance different factors such as plant throughput, metal recoveries and the precipitate characteristics for separation and disposal. From an operational point of view, using hydrogen peroxide as an oxidant and magnesium carbonate slurry neutralising agent in secondary neutralisation is more practical for tenable plant throughput and less bulky precipitates for recycling.

The measurement of the kinetics of oxidation is difficult in highly contaminated and multi-element solutions and there is no simple heuristic description of the oxidation kinetics in such systems. This is because of the interplay of several factors that influence oxidation such as pH, temperature, other ionic species in solution and iron oxyhydroxides formed. The removal of ferrous ion in less acidic solution could be occurring as a combination of oxidative precipitation in solution and adsorption of the iron on the precipitates.

References

ACERO, P., AYORA, C., TORRENTÓ, C. & NIETO, J.-M. 2006. The behavior of trace elements during schwertmannite precipitation and subsequent transformation into goethite and jarosite. *Geochimica et Cosmochimica Acta,* 70**,** 4130-4139.

AGATZINI, S., KONTOPOULIS, A., MARABOUTIS, P. & XENIDIS, A. 1986. REMOVAL OF IRON FROM IRON-NICKEL-COBALT SOLUTIONS BY PRECIPITATION AND SOLVENT-EXTRACTION TECHNIQUES.

ARDEN, T. 1950. 179. The solubility products of ferrous and ferrosic hydroxides. *Journal of the Chemical Society (Resumed)***,** 882-885.

BARB, W., BAXENDALE, J., GEORGE, P. & HARGRAVE, K. 1951. Reactions of ferrous and ferric ions with hydrogen peroxide. Part II.—The ferric ion reaction. *Transactions of the Faraday Society,* 47**,** 591-616.

BIGHAM, J. & NORDSTROM, D. K. 2000. Iron and aluminum hydroxysulfates from acid sulfate waters. *Reviews in mineralogy and geochemistry,* 40**,** 351-403.

BIGHAM, J. M., SCHWERTMANN, U., TRAINA, S. J., WINLAND, R. L. & WOLF, M. 1996. Schwertmannite and the chemical modeling of iron in acid sulfate waters. *Geochimica et Cosmochimica Acta,* 60**,** 2111-2121.

CARVALHO-E-SILVA, M. L., RAMOS, A. Y., TOLENTINO, H. C. N., ENZWEILER, J., NETTO, S. M. & DO CARMO MARTINS ALVES, M. 2003. Incorporation of Ni into natural goethite: An investigation by X-ray absorption spectroscopy. *American Mineralogist,* 88**,** 876-882.

CHANG, Y., ZHAI, X., LI, B. & FU, Y. 2010. Removal of iron from acidic leach liquor of lateritic nickel ore by goethite precipitate. *Hydrometallurgy,* 101**,** 84-87.

CLAASSEN, J. O. & SANDENBERGH, R. F. 2006. Particle growth parameters in the precipitation of metastable iron phases from zinc-rich solutions. *Hydrometallurgy,* 84**,** 165-174.

CLAASSEN, J. O. & SANDENBERGH, R. F. 2007. Influence of temperature and pH on the quality of metastable iron phases produced in zinc-rich solutions. *Hydrometallurgy,* 86**,** 178-190.

CORNELL, R. & GIOVANOLI, R. 1987. Effect of manganese on the transformation of ferrihydrite into goethite and jacobsite in alkaline media. *Clays and Clay Minerals,* 35**,** 11-20.

CORNELL, R. & GIOVANOLI, R. 1989. Effect of cobalt on the formation of crystalline iron oxides from ferrihydrite in alkaline media. *Clays and Clay Minerals,* 37**,** 65-70.

CORNELL, R., GIOVANOLI, R. & SCHNEIDER, W. 1990. Effect of cysteine and manganese on the crystallization of noncrystalline iron (III) hydroxide at pH 8. *Clays and Clay Minerals,* 38**,** 21-28.

CORNELL, R. & SCHINDLER, P. 1987. Photochemical dissolution of goethite in acid/oxalate solution. *Clays Clay Miner,* 35**,** 347-352.

CORNELL, R. M. 1996. *The iron oxides : structure, properties, reactions, occurrence and uses / R.M. Cornell, U. Schwertmann,* New York, New York : VCH.

CORNELL, R. M., GIOVANOLI, R. & SCHNEIDER, W. 1989. Review of the hydrolysis of iron (III) and the crystallization of amorphous iron (III) hydroxide hydrate. *Journal of Chemical Technology and Biotechnology,* 46**,** 115-134.

CORNELL, R. M., SCHNEIDER, W. & GIOVANOLI, R. 1992. The Effect of Nickel on the Conversion of Amorphous Iron(III) Hydroxide into more Crystalline Iron Oxides in Alkaline Media. *Journal of Chemical Technology & Biotechnology,* 53**,** 73-79.

CORNELL, R. M. & SCHWERTMANN, U. 2003. *The iron oxides: structure, properties, reactions, occurrences and uses,* John Wiley & Sons.

DE CARVALHO-E-SILVA, M. L. M., PARTITI, C. S. M., ENZWEILER, J., PETIT, S., NETTO, S. M. & DE OLIVEIRA, S. M. B. 2002. Characterization of Ni-Containing Goethites by Mössbauer Spectroscopy and Other Techniques. *Hyperfine Interactions,* 141**,** 559-576.

GEORGIOU, D. & PAPANGELAKIS, V. G. 1998. Sulphuric acid pressure leaching of a limonitic laterite: chemistry and kinetics. *Hydrometallurgy,* 49**,** 23-46.

HOLLUTA, J. & KOELLE, W. 1964. Oxidation of ferrous ion by air oxygen. *GWF, das Gas-und Wasserfach,* 105**,** 471-474.

JONES, A. M., GRIFFIN, P. J., COLLINS, R. N. & WAITE, T. D. 2014. Ferrous iron oxidation under acidic conditions–The effect of ferric oxide surfaces. *Geochimica et Cosmochimica Acta,* 145**,** 1-12.

KÖSE, C. H. & TOPKAYA, Y. A. 2011. Hydrometallurgical processing of nontronite type lateritic nickel ores by MHP process. *Minerals Engineering,* 24**,** 396-415.

LANDERS, M., GILKES, R. J. & WELLS, M. 2009. Dissolution kinetics of dehydroxylated nickeliferous goethite from limonitic lateritic nickel ore. *Applied Clay Science,* 42**,** 615-624.

LOWSON, R. T. 1982. Aqueous oxidation of pyrite by molecular oxygen. *Chemical reviews,* 82**,** 461-497.

MAJZLAN, J., NAVROTSKY, A. & SCHWERTMANN, U. 2004. Thermodynamics of iron oxides: Part III. Enthalpies of formation and stability of ferrihydrite (∼Fe(OH)3), schwertmannite (∼FeO(OH)3/4(SO4)1/8), and ε-Fe2O311Associate editor: D. Wesolowski. *Geochimica et Cosmochimica Acta,* 68**,** 1049-1059.

MISAWA, T., HASHIMOTO, K. & SHIMODAIRA, S. 1974. The mechanism of formation of iron oxide and oxyhydroxides in aqueous solutions at room temperature. *Corrosion Science,* 14**,** 131-149.

MONHEMIUS, A. 1977. Precipitation diagrams for metal-hydroxides, sulfides, arsenates and phosphates. *Transactions of the Institution of Mining and Metallurgy Section C-Mineral Processing and Extractive Metallurgy,* 86**,** C202-C206.

MORGAN, B. & LAHAV, O. 2007. The effect of pH on the kinetics of spontaneous Fe(II) oxidation by O2 in aqueous solution – basic principles and a simple heuristic description. *Chemosphere,* 68**,** 2080-2084.

MURAD, E. 2004. Jarosite, schwertmannite, goethite, ferrihydrite and lepidocrocite: the legacy of coal and sulfide ore mining.

PARK, B. & DEMPSEY, B. A. 2005. Heterogeneous oxidation of Fe (II) on ferric oxide at neutral pH and a low partial pressure of O2. *Environmental science & technology,* 39**,** 6494-6500.

ROLLIE, M. E., PATONAY, G. & WARNER, I. M. 1987. Deoxygenation of solutions and its analytical applications. *Industrial & engineering chemistry research,* 26**,** 1-6.

SINGH, B. & GILKES, R. 1992. Properties and distribution of iron oxides and their association with minor elements in the soils of south-western Australia. *Journal of soil Science,* 43**,** 77-98.

STUMM, W. & LEE, G. F. 1961. Oxygenation of ferrous iron. *Industrial & Engineering Chemistry,* 53**,** 143-146.

STUMM, W. & MORGAN, J. 1996. *Aquatic Chemistry, Chemical Equilibria and rates in natural waters,* New York

John Wiley & Sons.

STUMM, W. & SULZBERGER, B. 1992. The cycling of iron in natural environments: Considerations based on laboratory studies of heterogeneous redox processes. *Geochimica et Cosmochimica Acta,* 56**,** 3233-3257.

TAMURA, H., GOTO, K. & NAGAYAMA, M. 1976a. Effect of anions on the oxygenation of ferrous ion in neutral solutions. *Journal of Inorganic and Nuclear Chemistry,* 38**,** 113-117.

TAMURA, H., GOTO, K. & NAGAYAMA, M. 1976b. The effect of ferric hydroxide on the oxygenation of ferrous ions in neutral solutions. *Corrosion Science,* 16**,** 197-207.

TÜFEKCI, N. & SARIKAYA, H. Z. 1996. Catalytic effects of high Fe(III) concentrations on Fe(II) oxidation. *Water Science and Technology,* 34**,** 389-396.

VAN DER WOUDE, J. H. A., VERHEES, P. & DE BRUYN, P. L. 1983. Formation of colloidal dispersions from supersaturated iron(III) nitrate solutions. II. Kinetics of growth at elevated temperatures. *Colloids and Surfaces,* 8**,** 79-92.

VLEK, P. L. G., BLOM, T. J. M., BEEK, J. & LINDSAY, W. L. 1974. Determination of the Solubility Product of Various Iron Hydroxides and Jarosite by the Chelation Method1. *Soil Science Society of America Journal,* 38**,** 429-432.

WANG, K. 2012. *Impurity rejection in the nickel laterite leach system.* Curtin University.

WANG, K., LI, J., MCDONALD, R. & BROWNER, R. 2011. The effect of iron precipitation upon nickel losses from synthetic atmospheric nickel laterite leach solutions: statistical analysis and modelling. *Hydrometallurgy,* 109**,** 140-152.

WANG, K., LI, J., MCDONALD, R. G. & BROWNER, R. E. 2013. Characterisation of iron-rich precipitates from synthetic atmospheric nickel laterite leach solutions. *Minerals Engineering,* 40**,** 1-11.

WHITE, D., MILLER, M. & NAPIER, A. 2006. Impurity disposition and control in the Ravensthorpe acid leaching process. *Iron Control Technologies—3rd International Symposium on Iron Control in Hydrometallurgy, Canadian Inst. Min. Metall. & Petroleum.*

YUE, T., HAN, H., SUN, W., HU, Y., CHEN, P. & LIU, R. 2016. Low-pH mediated goethite precipitation and nickel loss in nickel hydrometallurgy. *Hydrometallurgy*.

CHAPTER 5
OXIDATIVE PRECIPITATION OF MANGANOUS ION USING POTASSIUM PERMANGANATE

5.1 Introduction

As discussed in Chapter 2, following the removal of iron, aluminium and chromium by hydroxide precipitation from the sulfate leach solution in partial neutralisation steps, nickel and cobalt sulfate solutions still contain significant amounts of impurities. The impurities include the alkaline earth metals, Mg and Ca and the transition metals, Mn, Cu and Zn. Among the transition metals, Mn is the main impurity post partial neutralisation stage. This makes it a bigger problem than Cu and Zn. There is no single technique of nickel and cobalt purification from nickel laterite solutions that has emerged as a clear processing route of choice following partial neutralisation steps used for iron, aluminium and chromium removal. Among the processes adopted in the processing of nickel laterite sulfate solutions are MHP, MSP and SX. This chapter presents oxidative precipitation of manganese as a process that can lead to the development of an alternative purification route for processing post partial neutralisation nickel laterite solutions.

Several studies on oxidative precipitation of manganese from sulfate solutions involve the use of SO_2/air (O_2) mixture (Zhang et al., 2000, Zhang et al., 2002, Zhang et al., 2010). It has been well established that potassium permanganate is an effective oxidant for manganous ion during the treatment of drinking water and wastewater (Van Benschoten et al., 1992, Ming, 2003, Tian et al., 2006, Roccaro et al., 2007, Zhu et al., 2009). Manganous ion easily oxidises to tetravalent manganese and precipitates as manganese oxides at circumneutral pH conditions. Although there is not much research on its use in highly contaminated solutions such as nickel laterite sulfate solutions and acidic conditions, the oxidative precipitation of manganese could prove to be a better separation technique than the existing MHP and MSP as it might also allow the recovery of valuable Mn product. In this regard, experiments were carried out to study the oxidative precipitation of manganous ion using potassium permanganate. Synthetic sulfate solutions simulating laterite solutions post partial neutralisation stage. The effect of various factors: pH, temperature, concentration of

manganous ion and dose of permanganate on the manganese removal efficiency and the associated cobalt and nickel losses to the precipitate is investigated.

Chapter 5 is divided into three parts. The first part is the preliminary experiments to determine the effect of the ageing time on the removal efficiency of manganese and nickel and cobalt losses. The second part determines the importance of the factors pH, temperature and dose of $KMnO_4$ on the responses: % manganese removal and % nickel and cobalt losses, using full factorial design. The permanganate dose is the amount of $KMnO_4$ added per mg Mn(II) in solution. The third part involves one variable at a time approach to optimise the significant factors determined in the second part.

5.2 Materials and methods

5.2.1 Reagents

The following analytical grade chemicals supplied by Chem-Supply were used during the experimental work: nickel sulphate hexahydrate, $NiSO_4.6H_2O$, cobalt sulphate heptahydrate, $CoSO_4.7H_2O$, manganese sulphate monohydrate, $MnSO_4.H_2O$, magnesium sulphate heptahydrate, $MgSO_4.7H_2O$, calcium sulphate dehydrate, $CaSO_4.2H_2O$, copper sulphate pentahydrate, $CuSO_4.5H_2O$, zinc sulphate heptahydrate, $ZnSO_4.7H_2O$, potassium permanganate ($KMnO_4$), sulphuric acid, H_2SO_4 (EMSURE®) and sodium hydroxide, NaOH pellets from Rowe Scientific.

5.2.2 Preparation of test solutions

Test solutions simulating those produced post iron, aluminium and chromium precipitation in the previous hydrolytic precipitation step were prepared by dissolving the required masses of the respective analytical grade reagents in a beaker with a minimum amount of deionised water under stirring using a magnetic stirrer. The solution pH was adjusted to pH values representative of the nickel laterite sulfate solutions leaving the neutralisation stages, and the volume made up to the mark on the volumetric flask with acidified water at the required solution pH. The target metal ion composition of the test solution used in the experimental work is given in Table 5.1.

Table 5.1: Target metal ion composition of the synthetic sulfate solutions simulating post partial neutralisation laterite sulfate solutions

Element	Ni	Co	Mn	Mg	Ca	Cu	Zn
Concentration (g/L)	3.50	0.25	5.00 – 1.50	10.0	0.50	0.10	0.15

The potassium permanganate solution was prepared by dissolving potassium permanganate crystals in deionised water and stored in brown bottles inside dark cupboards, to minimise the decomposition of permanganate due to exposure to a light source. Sodium hydroxide solution was made by dissolving NaOH pellets in deionised water.

5.2.3 Experimental set-up and procedure

A semi-batch precipitation procedure was used for the oxidative precipitation experiments, and the experimental set up is shown in Figure 5.10. All the oxidative precipitation experiments were carried in a four-neck 200 mL flat bottom glass reactor seated in a water bath to allow for temperature control. A magnetic stirrer coupled with a magnetic bar was used for mixing during the experiment, and the oxidant and the neutralising agent were added directly above the rotating magnetic bar for better mixing. The pH and temperature of the solution were monitored using a Mettler Toledo® Inlab Versatile pH probe with a working temperature ranging from 0 to 100 °C in combination with a thermometer immersed in the solution throughout the experiments. The oxidative precipitation experiments were carried out by transferring the test solution (50 mL) into the reactor, the temperature adjusted to the desired value (25 to 55 °C) while under continuous stirring. When the desired solution temperature was attained, the desired dose of 4% (w/v) potassium permanganate solution was added to the solution. Solutions of 0.05 to 1 M sodium hydroxide and 1 M sulfuric acid solution were manually added using a pipette to achieve the target equilibrium pH value. The experiments were carried out in three different ways (mode of experiment) described in Table 5.2, which relates to oxidant addition and the control of pH. Samples were collected at pre-determined time and filtered using a 0.2 μm syringe filter membrane and concentrated sulphuric acid solution was added to filtrate as a quenching agent. The target pH was maintained for the desired time interval, the slurry vacuum filtered using a circular hardened ashless filter paper (Whatman No 542/110

mm) at the end of the experiment. The precipitate residue was thoroughly washed with acidified deionised water to recover co-precipitated nickel and cobalt. The test solution (synthetic sulfate solution), filtrate and wash liquor recovered were analysed for manganese, nickel, cobalt, copper, magnesium and zinc using ICP-OES. The precipitate was air dried. XRF and EDS analysis were carried out to determine the components of the precipitate. The mineralogy was determined by XRD using a Bruker D8 Advance diffractometer with a Cu-Kα radiation source operated at 40kV and 40 mA at step scan of 0.015° with a LynxEye detector. The morphology analysis was determined by SEM using ZEISS NEON 40EsB FIBSEM, particle size distribution by a Malvern Mastersizer 3000 Hydro EV and zeta potential measurements were carried out using a zetasizer (Malvern Nano Z, UK).

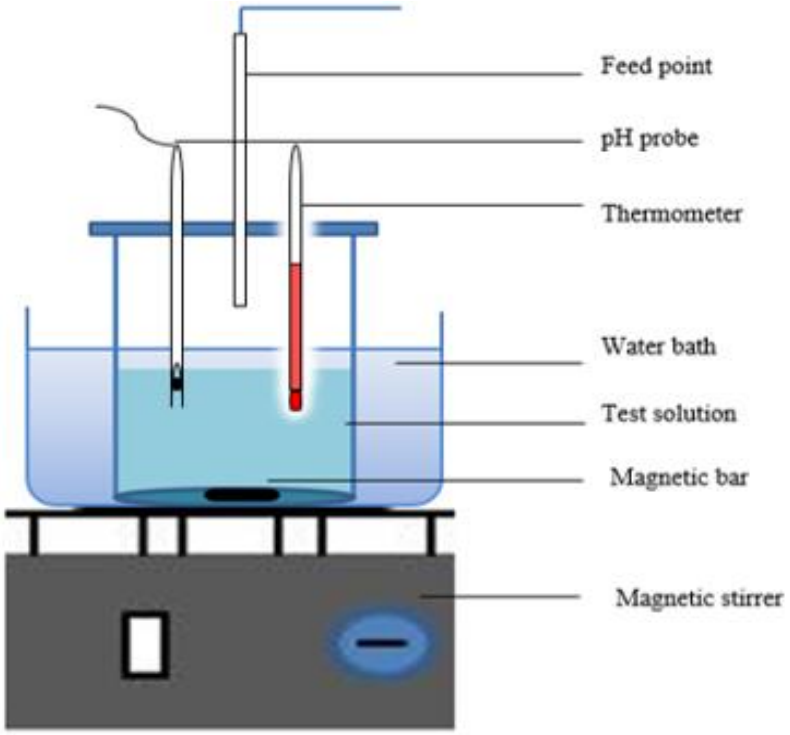

Figure 5.1: Schematic diagram of the experimental set-up for oxidative precipitation experiments.

Table 5.2: Experimental strategy (mode of operation) used on the oxidation precipitation of manganous ions

Mode	Description
A	Oxidation of divalent ions of manganese was carried out by quickly adding potassium permanganate solution to the test solution at the desired temperature without pH control while continuously stirring the solution mixture. Samples were collected at different time intervals and analysed for Co, Cu, Mg, Mn, Ni and Zn.
B	Potassium permanganate was quickly added to the test solution as in A and, after that, the equilibrium pH raised to the desired value. Sampling and sample analysis was carried out as in A.
C	The addition of potassium permanganate was done slowly while the solution pH was simultaneously controlled at a desired value. Sampling and analyses carried out as in A.

5.3 Preliminary experiments

Preliminary experiments were carried out to determine the effect of ageing time on the percentage removal of manganese and the amount of nickel and cobalt losses. The ageing time refers to the time the reaction is left to run after permanganate addition is complete. To study the effect of ageing time, Mode A was used in acidic manganese sulfate solution and a multi-element sulfate solution containing 2.5 g/L manganese mixed with 3.5 g/L nickel and 0.25 g/L cobalt at 25 ℃. The acidity of the test solution was approximately pH 3.5 at the start of the experiment.

5.4 Full factorial design experiments

In this chapter, a full factorial design (FFD) experimental procedure was used to evaluate the effect of equilibrium pH, temperature and oxidant dose (amount of $KMnO_4$ per mg Mn(II)) and their interaction effects on three responses. The responses were the % removal of manganese and % nickel and % cobalt losses to the precipitate. The factors investigated were evaluated at the low (-) and high (+) level, using Minitab

18 to generate the experimental matrix and statistical analysis of the experimental results. The factors investigated, and the design of experiment matrix is given in Table 5.3 and Table 5.4, respectively. The low and high levels for pH value were set at 1.75 and pH 4; The low pH was inherent from the oxidative precipitation of manganous ion by permanganate due to the release of hydrogen ions (Equation 2.31), and pH 4 was chosen because it is a typical pH for aluminium removal by hydroxide precipitation at reasonable nickel losses (Chapter 4). The minimum and maximum temperature were set at 25 and 40 ℃, which could be close to ambient temperatures for lower energy and operational costs. The experiments were carried out using Mode A and Mode B and multi-element synthetic sulfate solutions containing 2.5 g/L Mn(II) and the other cations as given in Table 5.1.

Table 5.3: Factors and the selected levels in a 2^3 full factorial design

Factor	Units	Low level (-)	High Level (+)
A= pH	-	1.75	4.0
B= $KMnO_4$ dose	mg/mg	0.09	0.102
C=Temperature	° C	25	40

5.5 Results and discussions

5.5.1 Preliminary experiments

In precipitation reactions, equilibrium is not always instantaneously reached upon the addition of the final drop of the reactant but can take several hours of additional contact time referred to as ageing time. The study by Freitas et al. (2013) on the oxidation of manganese from pure manganese sulfate solution at 25 ℃ has shown that oxidation with $KMnO_4$ is fast and the time required to reach equilibrium slightly depends on pH value. They found that 10 mins were required for equilibrium to be reached at pH value 5 and 7 and 20 mins at pH value 3. Also, the presence of other metal ions such as cobalt and zinc have been found to influence the equilibrium of the system. Cobalt and zinc are reported to substitute for both manganese and hydrogen in the hydrous manganese oxide matrices, with reaction equilibrium times found to vary from one hour (Morgan and Stumm, 1964) to several days (Loganathan and Burau, 1973).

In this regard, experiments were carried out using single element manganese solution and multi-element solution to determine the effect of ageing time and other metal ions on manganese precipitation and nickel losses to the precipitate. The results are given in Table 5.5.

Table 5.4: Design matrix for the three factors, 8 experiments replicated twice, A=pH, B =$KMnO_4$ dose and C=temperature.

	Factor		
Run	A	B	C
1	(-)	(+)	(-)
2	(+)	(+)	(+)
3	(+)	(-)	(+)
4	(+)	(+)	(+)
5	(-)	(-)	(-)
6	(-)	(-)	(+)
7	(-)	(-)	(+)
8	(+)	(-)	(-)
9	(+)	(+)	(-)
10	(+)	(-)	(-)
11	(-)	(+)	(+)
12	(-)	(+)	(+)
13	(-)	(-)	(-)
14	(-)	(+)	(-)
15	(+)	(-)	(+)
16	(+)	(+)	(-)

The effect of ageing time on manganese removal efficiency is shown in experiment P1 to P3 given in Table 5.5, carried out at slightly different $KMnO_4$ doses. The precipitation of manganese with permanganate occurs instantaneously with the maximum removal recorded immediately after the last addition of permanganate. There is a sudden drop in pH when adding permanganate into the test solution which is expected as the oxidation of manganese with permanganate is suggested to occur according to reaction given in Equation 5.1 (recalled from Section 2.6.4.1).

Table 5.5: The effect of the ageing time on the removal efficiency of manganese from synthetic sulfate solutions containing initial Mn(II) concentration about 2.5 g/L in the absence (P1) and presence of other metal ions (P2 and P3) at 25 °C and stirring speed of 200 rpm using Mode A.

Run	$KMnO_4$/ Mn(II) (mg/mg)	Ageing time (mins)	Metal ion concentration (mg/L)			% Metal removal		
			Mn	Ni	Co	Mn	Ni	Co
P1	1.34	<1	61.80	N/A	N/A	97.78	N/A	N/A
		10	65.40	N/A	N/A	97.65	N/A	N/A
		30	70.00	N/A	N/A	97.49	N/A	N/A
		60	84.00	N/A	N/A	96.99	N/A	N/A
P2	1.36	<1	95.40	3401.60	136.60	96.14	3.78	49.49
		10	103.80	3390.60	134.80	96.42	4.07	50.13
		30	112.80	3385.40	136.60	95.48	4.21	49.49
		60	126.40	3425.20	141.80	94.97	3.15	47.66
P3*	1.36	<1	89.40	3281.20	132.40	95.51	3.15	48.70
		60	109.20	3212.20	137.00	94.65	3.43	47.20
		1440	175.40	3151.80	139.00	91.79	5.47	45.55

Note: * Repeat Experiment, N/A stands for not added in solution

The effect of ageing time on manganese removal efficiency is shown in experiment P1 to P3 given in Table 5.5, carried out at slightly different $KMnO_4$ doses. The precipitation of manganese with permanganate occurs instantaneously with the maximum removal recorded immediately after the last addition of permanganate. There is a sudden drop in pH when adding permanganate into the test solution which is expected as the oxidation of manganese with permanganate is suggested to occur according to reaction given in Equation 5.1 (recalled from Section 2.6.4.1).

$$2MnO_4^-{}_{(aq)} + 3Mn^{2+}{}_{(aq)} + 2H_2O_{(l)} \leftrightarrow 5MnO_{2\,(s)} + 4H^+{}_{(aq)} \qquad 5.1$$

The pH dropped by at least approximately 1.75 units when using the multi-element sulfate solution containing Mn, Ni and Co and 2 pH units in pure manganese solution. The results show that the % removal of manganese is highest following the complete addition of permanganate (ageing time < 1 mins), which is followed by a slight decrease in overall manganese removal with an increase in ageing time. The continued decrease in manganese removal with an increase in ageing time indicates that the reaction has not reached equilibrium after 60 minutes. The lack of equilibrium during manganese oxidation in acidic conditions (pH 3) was also observed by Freitas et al. (2013), where manganese concentration in solution continued to change, increasing and decreasing in a cyclic pattern from 20 mins to 100 mins reaction time. In this study, a decrease in manganese removal when ageing the slurries occurs both in the absence (P1) and presence (P2 and P3) of other metal ions in solution suggesting re-dissoultion of ions from the manganese precipitate. This suggests that the release of manganese into solution is not only due to the presence of foreign metal cations substituting for manganese on the manganese oxides but probably because the manganese oxides are unstable in acidic solutions. The removal of Mn(II) is suggested to occur through a combination of oxidation to Mn(IV) that forms MnO_2 in solution and adsorption of Mn(II) onto hydrous MnO_2 followed by surface oxidation (Van Benschoten et al., 1992, Roccaro et al., 2007). It is, therefore, possible that the adsorbed Mn(II) is desorbed and released back into solution during ageing at the low pH values. Also, cobalt and nickel losses from the solution increased with increase in ageing time although cobalt loss is excessive, almost 50% compared to that of nickel at approximately 5%. The observed high losses of cobalt confirm findings by other

researchers that cobalt has a high sorption potential on hydrous manganese oxides compared to other divalent metal ions such as nickel, copper and zinc (Morgan and Stumm, 1964, Loganathan and Burau, 1973). There is no benefit in extended ageing times and thus shorter ageing time of 5 to 15 mins was used in subsequent factorial design experiments.

5.5.2 Full factorial design experiments

Full factorial experimental design was used to evaluate the significance of factors, pH, the dose of $KMnO_4$ and temperature on % manganese removal and the % cobalt and nickel losses to the precipitate. The advantage of using full factorial design is that the factors and all possible interactions of the factors are taken into consideration unlike in fractional factorial designs. Half-normal probability plots and ANOVA were used to estimate the statistical significance of both the main and interaction factors on the responses. The experimental results of the two replicates are given in Table 5.6.

Table 5.6: Elemental analysis for the full factorial design experiments

Run	Factor			% Metal Precipitated		
	A	B	C	Mn	Co	Ni
1	(+)	(-)	(-)	95.31	73.63	2.32
2	(+)	(-)	(+)	92.91	79.03	3.77
3	(+)	(+)	(-)	99.72	86.05	6.64
4	(-)	(+)	(-)	99.92	58.02	2.33
5	(-)	(-)	(-)	96.12	49.24	3.25
6	(+)	(+)	(+)	98.99	86.63	5.49
7	(-)	(+)	(-)	99.29	55.21	0.09
81	(-)	(+)	(+)	97.96	56.91	3.18
9	(+)	(-)	(+)	93.06	82.18	2.37
10	(+)	(+)	(+)	98.96	88.69	4.30
11	(-)	(-)	(+)	91.24	44.71	2.18
12	(-)	(-)	(-)	92.85	41.64	2.85
13	(+)	(+)	(-)	99.65	82.54	6.53
14	(+)	(-)	(-)	95.51	73.47	3.15
15	(-)	(+)	(+)	98.39	56.76	3.25
16	(-)	(-)	(+)	91.50	46.41	1.14

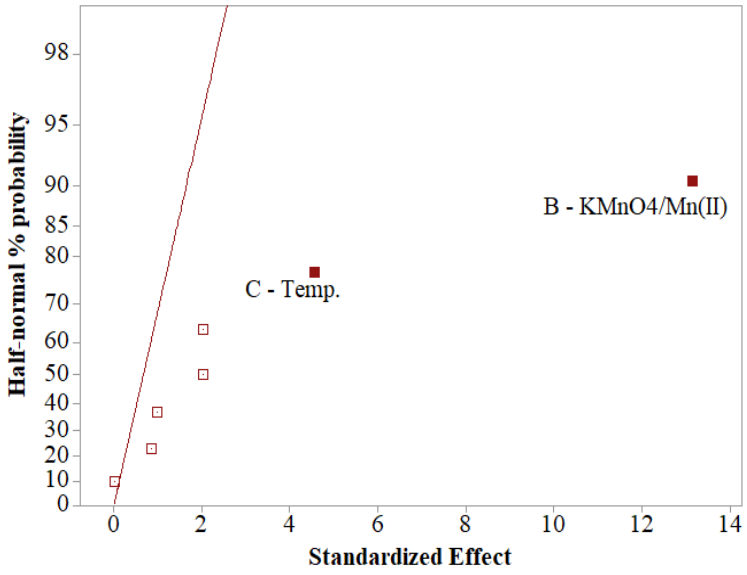

Figure 5.2: Half-normal probability plot of the standardised effects for manganese removal (%).

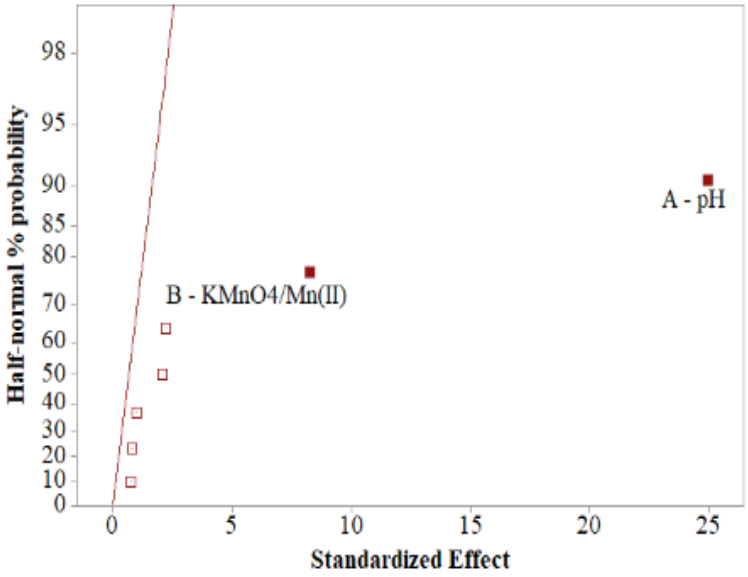

Figure 5.3: Half-normal probability plot of the standardised effects for cobalt losses (%).

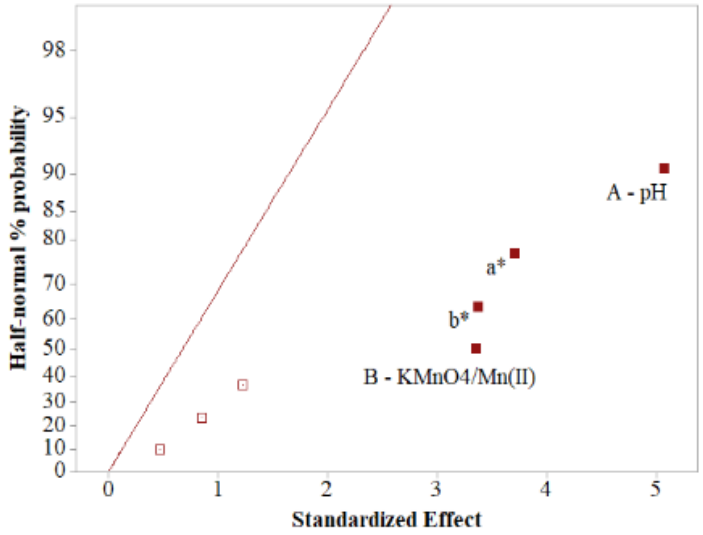

Figure 5.4: Half-normal probability plot of the standardised effects for nickel losses (%), a*= AB and b*=ABC.

Figure 5.2, Figure 5.3 and Figure 5.4 show half-normal probability plots for manganese removal (%), cobalt and nickel losses (%), respectively. A variable is considered significant when it has a non-zero mean value and falls further from the straight line and the p-value is less than 0.05 in ANOVA tests. Figure 5.2 shows that $KMnO_4$ dose and temperature have large effects on % Mn removal while Figure 5.3 and Figure 5.4 show that pH and $KMnO_4$ dose have large effects on the % cobalt and nickel losses. The $KMnO_4$ dose is the most important factor for manganese removal while pH is the most important factor for cobalt and nickel losses from the solution at 95% confidence interval shown by the very small p-values ($0.0001<<<0.05$) (Table 5.7). The interaction terms AB and ABC were found significant for nickel loss. The three factors, pH, $KMnO_4$ dose and temperature showed statistical significance in either manganese removal or nickel and cobalt losses and therefore were further studied in detail to optimise the process. One important observation from both preliminary and factorial experiments was that cobalt loss is extremely high even at the low equilibrium pH value which is an inherent condition when using Mode A as acid is produced via Equation 5.1. The minimum percentage loss of nickel was at least about 42% when using Mode A and increased to about 89% when using Mode B at pH value 4. Due to high affinity of manganese oxides for cobalt, the focus in the subsequent studies is the co-removal of manganese and cobalt without losing significant nickel to the precipitates.

Table 5.7: ANOVA analysis for the responses.

Source	% Manganese removal					% Cobalt loss					% Nickel loss				
	DF	Adj SS	Adj MS	F-Value	p-value	DF	Adj SS	Adj MS	F-Value	p-value	DF	Adj SS	Adj MS	F-Value	p-value
Model	7	144.845	20.692	29.01	<0.0001	7	4171.87	595.98	100.29	<0.0001	7	41.6695	5.9528	9.21	0.00277
Linear	3	140.769	46.923	65.81	<0.0001	3	4134.25	1378.08	231.91	<0.0001	3	24.0055	8.0018	12.38	0.00225
A-pH	1	2.924	2.924	4.13	0.0775	1	3700.29	3700.29	622.68	<0.0001	1	16.6056	16.6056	25.69	0.00097
B-$KMNO_4$/Mn(II)	1	123.099	123.099	172.61	<0.0001	1	405.02	405.02	68.16	<0.0001	1	7.2630	7.2630	11.24	0.01005
C-Temperature	1	14.746	14.746	20.68	0.0019	1	28.94	28.94	4.87	0.0584	1	0.1369	0.1369	0.21	0.65760
2-Way interactions	3	4.076	1.359	1.91	0.2073	3	34.03	11.34	1.91	0.2067	3	10.3198	3.4399	5.32	0.02614
AB	1	0.689	0.689	0.97	0.3545	1	5.41	5.41	0.91	0.3681	1	8.8804	8.8804	13.74	0.00598
AC	1	0.497	0.497	0.72	0.4280	1	25.40	25.43	4.27	0.0725	1	0.9702	0.9702	1.50	0.25534
BC	1	2.892	2.890	4.05	0.0789	1	3.22	3.22	0.54	0.4826	1	0.4692	0.4692	0.73	0.41896
3-Way interactions	1	0	0	0	0.9863	1	3.59	3.59	0.60	0.4593	1	7.3441	7.3441	11.36	0.00977
ABC	1	0	0	0	0.9863	1	3.59	3.59	0.60	0.4593	1	7.3441	7.3441	11.36	0.00977
Error	8	5.705	0.713			8	47.54	5.94			8	5.1706	0.6463		
Total	15	150.552				15	4219.41				15	46.8401			

DF, Adj SS and Adj MS denotes degrees of freedom, adjusted sum of squares and adjusted mean squares, respectively

5.5.3 Process optimisation

5.5.3.1 The effect of oxidant dose on the removal of divalent cations in solution

A set of oxidative precipitation experiments was carried out using Mode A under comparable conditions: initial manganous ion concentration of 2.5 g/L and temperature 25 ℃, except that $KMnO_4$ dose was varied. The results are summarised in Figure 5.5.

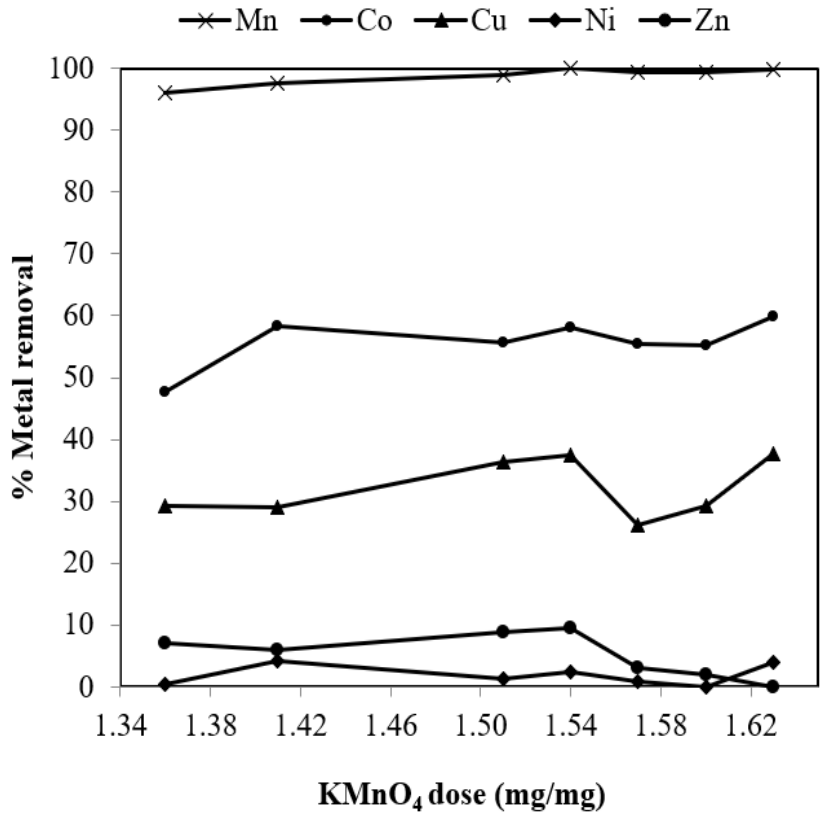

Figure 5.5: Variation in % metal removal as a function of the ratio of the amount of permanganate to that of manganous ion initially in solution using Mode A at 25 ℃.

Figure 5.5 shows that an increase in $KMnO_4$ dose results in an increase in manganese removal and a slight increase in the removal of cobalt and copper. Manganese removal was almost complete (greater than 99%) at a dose of 1.54 mg $KMnO_4$ per mg Mn(II) at reasonable nickel loss of less than 2%. Cobalt and copper removal were high at approximately 60% and 38 %, respectively. A similar trend in higher uptake of divalent ions of cobalt and copper compared to those of magnesium, nickel and zinc was observed by Murray (1975), when investigating the interaction of divalent ions and manganese

dioxide. Given the standard reduction potential ($E°$) for the reduction of Co(III) to Co(II) is +1.92 V (Equation 5.2) and is higher than +1.7 V for Mn(VII) to Mn(IV) (Equation 5.3), the most likely mechanism for Co(II) removal is by adsorption and surface oxidation and not solution phase oxidation by permanganate. It is suggested that the removal of cobalt is likely through a two-reaction mechanism as proposed by Burns (1976). Co(II) is rapidly adsorbed on the manganese oxide and then oxidised to Co(III) by nearby Mn(IV) in the lattice and is incorporated in the lattice (Burns, 1976), which could be the explanation for low recovery of cobalt from the washing of the solids.

$$Co^{3+}_{(aq)} + e^- \leftrightarrow Co^{2+}_{(aq)} \qquad E^{\theta} = 1.92\ V \qquad 5.2$$

$$MnO_4^-{}_{(aq)} + 8H^+_{(aq)} + 5e^- \leftrightarrow Mn^{2+}_{(aq)} + 4H_2O_{(l)} \qquad E^{\theta} = 1.7\ V \qquad 5.3$$

It is also suggested that because cobalt and copper easily undergo hydrolysis to form complex ions, which enhance metal ion adsorption on the manganese oxide surfaces (Stumm and O'Melia, 1968, Murray, 1975), this may be the reason for high removal during manganese oxidative precipitation. In this study, the results show that the $KMnO_4$ dose required for complete manganese removal was at least 1.54 mg $KMnO_4$ /mg Mn(II) without pH control, which is lower than the 1.63 mg $KMnO_4$ /mg Mn(II) by Freitas et al. (2013) and the stoichiometric amount of 1.92 mg $KMnO_4$ /mg Mn(II). This is probably owing to the large amounts of hydrous manganese oxides formed at the high Mn(II) concentrations used in this study, which enhances surface adsorption of Mn (II) (Adams, 1960, Morgan and Stumm, 1964).

5.5.3.2 Effect of seeding with manganese oxide precipitates on manganese removal

The effect of seeding with manganese oxide precipitates on the extent of oxidative precipitation of manganese was investigated without pH control (Mode A). The manganese precipitates from previous experiments at seed loading of 1 g MnO_x/L of sulfate solution was used at 1.55 mg $KMnO_4$ /mg Mn(II) and 25 °C. The initial metal ion concentrations were approximately those given in Table 1. The metal removal in the absence and addition of manganese oxide precipitate is given in Table 5.8.

Table 5.8: Effect of adding manganese oxide precipitate on metal precipitation at 25 °C

Run	pH	Ageing time (mins)	Seeding	Metal ion concentration in solution at given ageing time (mg/L)					Metal Precipitated %				
				Mn	Ni	Co	Cu	Zn	Mn	Ni	Co	Cu	Zn
1	N/C	5	X	13.6	3169.4	110.2	69.2	146.8	99.4	0.8	55.4	26.1	3.2
		15		19.2	3176.4	111.4	70.0	146.2	99.2	0.6	55.0	25.3	3.6
2	N/C	5	X	9.0	3384	116.6	74.4	141.0	99.6	0.4	54.9	29.1	8.7
		15		25.4	3354	114.4	66.6	140.6	98.9	1.2	55.7	36.3	8.9
3	3.5	5	X	9.8	2791.8	12.4	10.6	95.6	99.4	4.8	93.3	84.9	24.7
		15		22.4	2752.4	18.8	19.2	113.2	98.8	6.0	90.7	75.5	13.0
4	N/C	5	√	32.2	3105.4	110.4	67.2	142.0	98.6	0.8	54.4	26.5	4.4
		15		38.6	3081.8	109.8	66.8	141.2	98.3	1.5	54.6	27.2	4.9
5	N/C	5	√	29.2	3087.6	108.2	65.8	140.2	98.7	1.7	55.3	28.2	5.6
		15		36.0	3108.6	110.0	68.4	143.8	98.4	1.1	54.6	25.5	3.3
6	N/C	30	√	32.8	23.1	1.6	12.7	7.3	0.8	7.9	1.4	15.9	33.4
		60		32.2	29.4	1.7	13.3	7.7	0.8	10.1	1.5	16.5	35.5
		120		30.9	35.6	1.7	13.4	7.9	0.8	12.2	1.5	16.7	36.3

X and √ indicate the absence and presence of seed (manganese oxide precipitate) respectively and N/C indicates pH was not controlled.

The first three experimental results given in Table 5.8, Run 1 to Run 3 were carried out without the addition of manganese oxide seed precipitate while manganese oxide precipitate was added at the beginning of the experiment in Run 4 to Run 6. The experimental results show that the removal of manganese decreases with time and is lower when manganese oxide precipitate was added as seeding material initially (Run 4 and Run 5). Run 6 was a control experiment, with the manganese oxide precipitate agitated in acidified water at pH 1.75 and the results indicate that there was dissolution of the cations from the precipitate which is in good agreement with findings in Section 5.5.1. This suggested that the decrease in overall manganese removal with time is due to dissolution of the precipitates in acidic conditions. The results are in good agreement with the findings by Van Benschoten et al. (1992), in which manganese concentration at pH 3 fluctuated during retention time unlike at higher pH values (>5) were equilibrium was reached. In Run 3, the pH value was raised to 3.5 after complete addition of permanganate solution and as expected more cobalt and copper were removed but at the expense of increased nickel loss (from observation in FFD). Therefore, the effect of pH value on the removal and separation of the cations was further studied.

5.5.3.3 Effect of pH on oxidative precipitation

It was shown earlier (Section 5.5.2) that pH value has the largest effect on cobalt removal and the level of nickel loss, although an insignificant factor on manganese removal. Cobalt loss to the precipitate is excessive during oxidative precipitation. Therefore, it becomes feasible to design and develop an oxidative precipitation process to simultaneous remove manganese and cobalt and probably copper leaving nickel and the other divalent ions in solution. In this regard, experiments were carried out to determine the effect of (i) pH control during the reaction and ageing time and (ii) the equilibrium pH value on the removal of Mn, Co and Cu and the level of nickel loss to the precipitate at 25 ℃. This was achieved by using the three experimental procedures, Mode A, B and C described in Table 5.2 at various permanganate dose. The results for the comparison of the three different modes when equilibrium pH in Mode B and C is controlled at 3.5 is given in Figure 5.6.

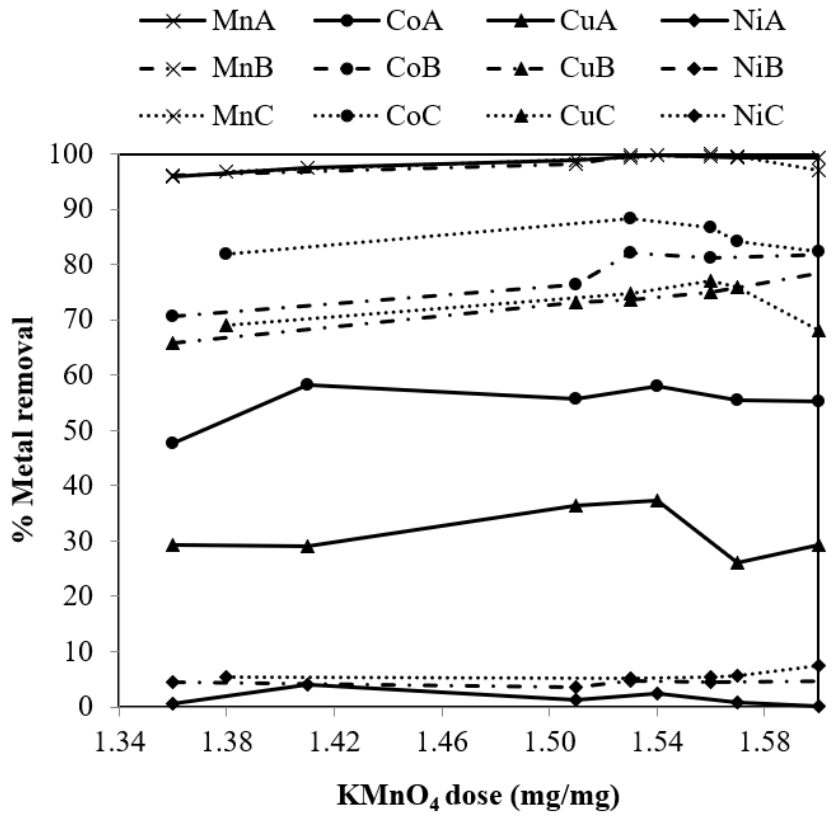

Figure 5.6: Effect of using the three experimental procedures (Mode A, B and C) on metal removal and the permanganate dose at pH value 3.5 for Mode B and Mode C and temperature 25 ℃.

The experimental results in Figure 5.6 show that the % Mn removal increases with an increase in the amount of permanganate added into the solution, which is expected from the proposed equation of reaction (Equation 5.1). Theoretically, 1.92 mg $KMnO_4$ per mg Mn(II) is required for complete removal of Mn(II) from solution. In this study, the amount of $KMnO_4$ required was only 81% of the stoichiometry amount. This supports the removal mechanism of Mn(II) in the process as a result of a combination of oxidative precipitation in solution and adsorption on MnO_2 surface and surface oxidation (Van Benschoten et al., 1992, Roccaro et al., 2007). Furthermore, the % Mn removal showed no dependence on pH value in that in the different modes of operation the pH value during reaction time or ageing time varied but still % Mn(II) removal is comparable at any given amount of permanganate added per mg of Mn(II) in solution.

For example, comparison of the results for the experiments with the same dose of 1.51 mg $KMnO_4$ per mg Mn(II), but different equilibrium pH values of 1.75 (Mode A) and 3.5

(Mode B) gave almost similar % Mn removal of 98.93% and 98.30%, respectively. Manganese removal was comparable at any given amount of permanganate added per mg of Mn(II) in solution for the three experimental procedures (Mode A, B and C). Noticeably, there is a substantial increase in overall cobalt and copper removal when using Mode B and Mode C, but at the cost of greater nickel loss to the precipitate. It is clear that the equilibrium pH value used during ageing and reaction time affects the amount of cobalt and copper removal. For instance, the removal of cobalt and copper using Mode A at 136 mg $KMnO_4$ /mg Mn(II) were quite low, about 47% and 29% compared to 70% and 65% when using Mode B where the respective equilibrium pH values are 1.75 and 3.5. In this regard, the removal of the cations as a function of equilibrium pH value using Mode B and Mode C and 1.57 mg $KMnO_4$ /mg Mn(II) at 25 ℃ was studied, and the experimental results are given in Figure 5.8a and Figure 5.8b, respectively.

It was observed that increasing the pH value during either ageing time (Mode B) or reaction and ageing time (Mode C) increases the % cobalt and copper removal. However, the amount of nickel lost to the precipitate is higher when using a high pH value (≥ 3) throughout the experiment, that is when using Mode C. As can be seen from Figure 5.7a and Figure 5.7b, more than 99.5% manganese, 90% cobalt and 80% copper were removed using Mode C. The increase in the overall amount of manganese, cobalt and copper removed by oxidative precipitation with an increase in pH is consistent with the dependence of the equilibrium concentration on pH. Coughlin and Matsui (1976) proposes that as pH increases, hydrated Mn(II) ions can easily hydrolyse to form complex species, monomers and dimers which undergo polymerisation, and if other cations are present in solution, they are likely incorporated into the polymeric species of manganese which are the precursors of the precipitates.

Precipitates of manganese dioxide have a variable point of zero charge (pzc) which depends on the crystallinity of the precipitate. The pzc was determined by zeta potential measurements carried out on a solution containing suspended fine particles of the manganese oxide precipitate at 25 ± 2 ℃ after coarse particles were allowed to settle. Figure 5.8 shows the experimental results of the zeta potential measurement of the manganese oxide precipitate.

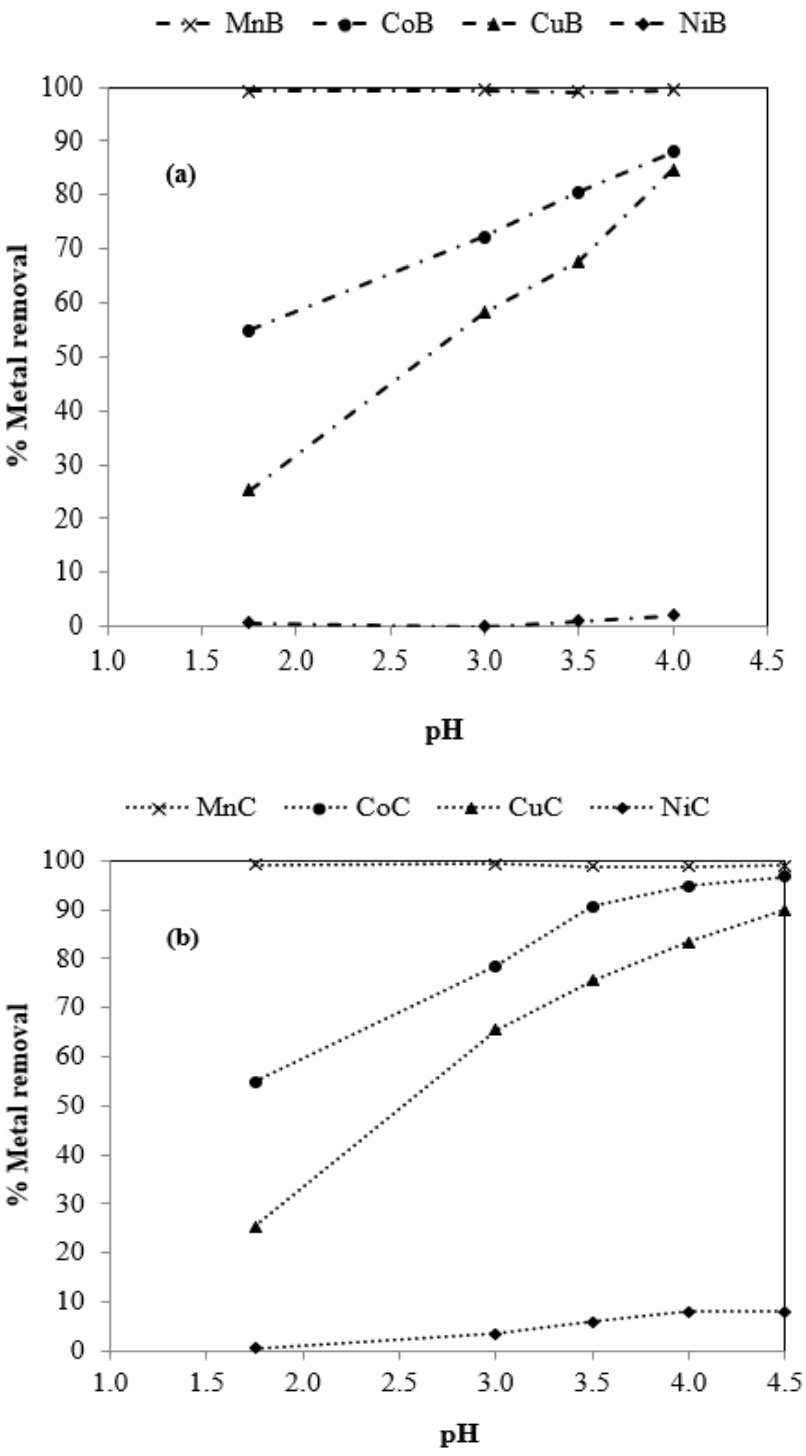

Figure 5.7: Effect of pH on metal removal and nickel loss using (a) Mode B and (b) Mode C, 1.57 mg $KMnO_4$/mg Mn(II) at 25 ℃.

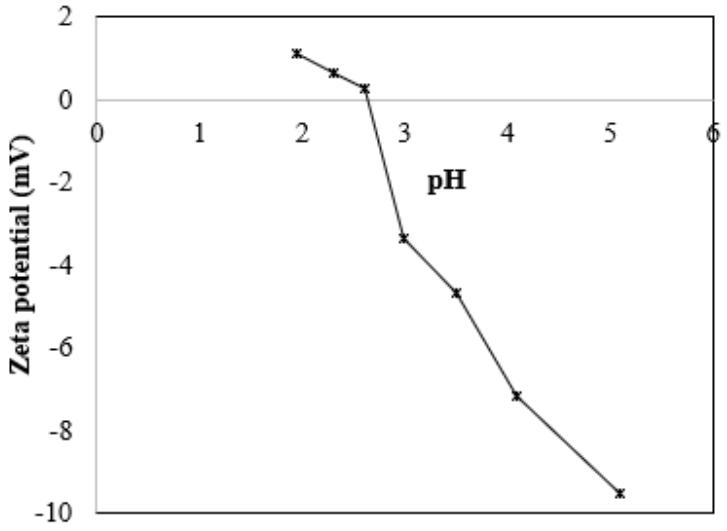

Figure 5.8: Zeta potential measurement of manganese oxide precipitate produced at the optimum conditions of pH 40 using Mode C.

The plot shows that the point of zero charge of manganese oxide is around pH value 2.7, which agrees with findings by Morgan and Stumm (1964), were the pzc of amorphous manganese dioxide was found to be around 2.8 ± 0.3. This means that manganese oxide is positively charged below pH 2.7 and negatively charged above pH 2.7 in deionised water. Cations and anions from solution are adsorbed as counterions to maintain electroneutrality on the charged oxide surfaces. In this study, higher cobalt and copper removals at pH 3 and above was possibly due to the enhanced adsorption of the cations on the negatively charged surface of manganese oxide precipitates.

5.5.3.4 Effect of temperature on metal removal during oxidative precipitation of manganese

It was observed in factorial design experiments (Section 5.5.2) that temperature has a large effect of the removal of manganese. The effect of temperature on the removal of the manganese, cobalt, copper and nickel at 1.56 mg $KMnO_4$/ mg Mn(II), pH 3.5 using Mode B is shown in Figure 5.9.

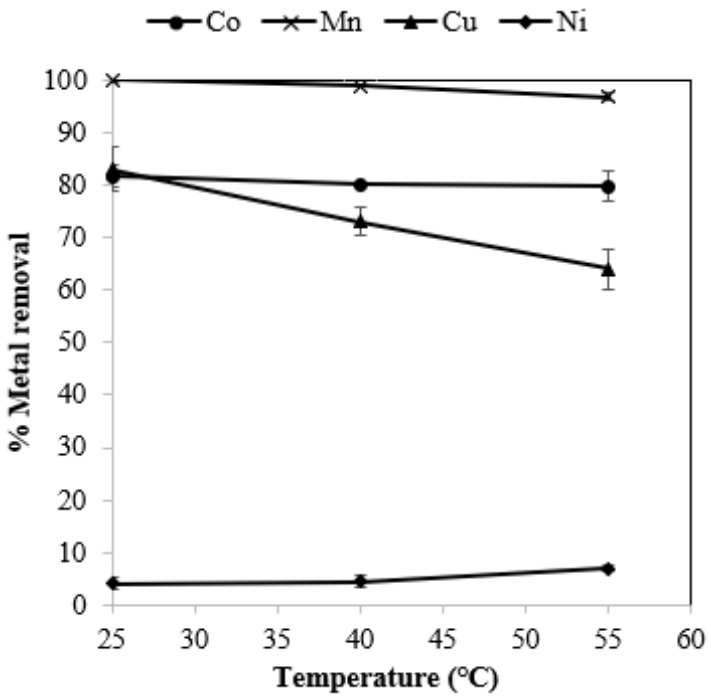

Figure 5.9: Variation on % manganese, cobalt, copper and nickel removal as a function of temperature at 1.56 mg $KMnO_4$/ mg Mn(II), pH 3.5 and using Mode B.

The results in Figure 5.9 indicate that at the studied temperature range of 25 ℃ to 55 ℃, the removal of manganese and cobalt decreased as temperature increased while the change in the amount of nickel loss and copper removal was minimal with an increase in temperature. The decrease in manganese and cobalt removal could be due to the dissolution of the precipitates and the similar trend in manganese and cobalt removal suggests the association of cobalt and manganese in the lattice structure of manganese oxide precipitates. The optimum temperature for oxidative precipitation of manganese and cobalt was 25 ℃, which has a practical advantage of lower costs.

5.5.3.5 Effect of initial Mn(II) concentration on permanganate dose and nickel loss

A series of experiments were also carried to determine the effect of the initial manganous ion concentration on the amount of permanganate required to achieve almost complete removal of manganese (99.5%) and the amount of nickel loss to the precipitate. The concentrations of the various metal ions in solution were kept constant and only varying manganous ion concentration as follows: 1.25, 2.5 and 5 g/L. The experiments were

carried out using Mode B, ageing pH 3.5 at 25℃. The % manganese removal and nickel loss as a function of mg $KMnO_4$ per mg Mn(II) at the different initial manganese concentration is given in Figure 5.10.

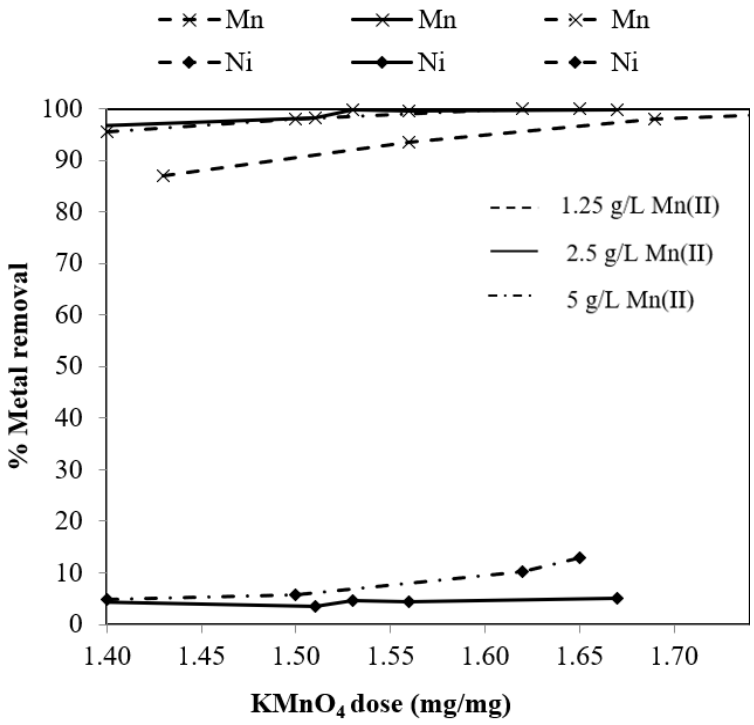

Figure 5.10: Effect of initial Mn(II) concentration on nickel loss and the permanganate dose

The experimental results indicate that the permanganate dose required for oxidative precipitation of manganese increases at low initial Mn(II) concentration, while lesser nickel loss to the precipitate are obtained at lower initial Mn(II) concentration. At initial manganese concentration of 1.25 g/L, more than 1.7 mg $KMnO_4$/mg Mn(II) was required for optimal Mn removal compared to 1.55 mg $KMnO_4$/mg Mn(II) at 2.5 g/L and 5 g/L. However, there was negligible nickel loss at 1.25 g/L compared with 5 to 10% at higher initial manganese concentrations of 2.5 g/L and 5 g/L. High metal removal from solution at high manganese concentration is due to large amounts of MnO_2 precipitate formed which probably provide more surface area for adsorption and enhanced co-precipitation of divalent ions of manganese (Freitas et al., 2013, Van Benschoten et al., 1992, Phatai et al., 2014, Phatai et al., 2010) and the other cations in solution including nickel. In addition, the high supersaturation level at high initial manganese concentration promotes rapid

precipitation which could enhance the incorporation and co-precipitation of other species contained in the solution. Higher doses of permanganate at low pH values of 3 were also obtained by Freitas et al. (2013) when processing less concentrated synthetic sulfate solutions and AMD solutions. The control of manganese concentration in highly concentrated manganese solution is therefore necessary for optimal manganese removal and reasonably nickel loss and permanganate demand. In this study, the optimal initial Mn(II) concentration was 2.5 g/L. Therefore, dilution of highly concentrated solutions to 2.5 g/L or less during oxidative precipitation in continuous mode could possibly minimise nickel loss and optimise the required permanganate dose.

5.5.4 Analysis of the precipitates

The precipitates from the oxidative precipitation of manganous ion with permanganate were brownish-black in colour, dense and were easily filtered regardless of the experimental procedure (Mode A, B and C) used. The particle number distribution of the particles formed when using Mode B and Mode C after 30 minutes of reaction at pH 4 and 25 ℃ is shown in Figure 5.11.

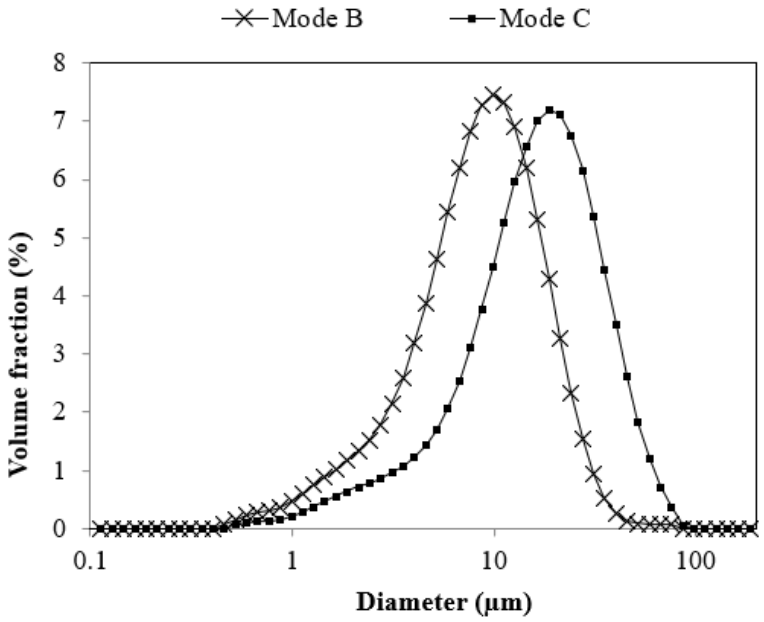

Figure 5.11: Particle size distribution after 30 minutes of reaction using Mode B and Mode C at pH 4 and 25℃.

The particle size distribution curves show the formation of smaller particles when permanganate is quickly added with Mode B. The smaller particles when using Mode B is probably due to increased oxidation rates, which resulted in a high nucleation rate and inhibited particle growth. Permanganate is a powerful oxidising agent, and its reaction with manganous ion is instantaneous which result in high supersaturation levels, and the formation of amorphous manganese oxides as shown in the XRD pattern for the manganese oxide produced using Mode C, in Figure 5.12. The amorphous nature of the precipitate is supported by the SEM micrograph (Figure 5.13), which shows that the crystal structure is not well-defined, and the precipitate is made up of aggregates of nanoparticles. Two peaks were identified at around 37.3° 2θ and 66.2 ° 2θ (Figure 5.12), which were identified as manganese dioxide. There were no nickel, cobalt and copper phases detected in the XRD patterns most probably owing to the low concentration of the species in the precipitate, although the species were detected in the EDS and XRF composition analysis given in Figure 5.13. Weak acid dissolution tests of the precipitates carried out at pH 1.5 and 25 ℃ for 2 hours showed that only 1% to 5% cobalt could be recovered. This suggests that cobalt in the precipitate is strongly adsorbed and probably incorporated in the lattice structure (McKenzie, 1970).

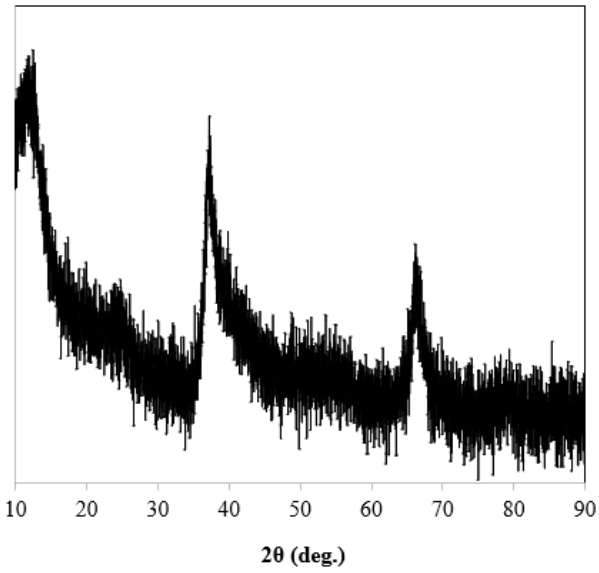

Figure 5.12: XRD diffraction pattern of dry manganese oxide precipitated with Mode C, at pH 4 and 25 ℃.

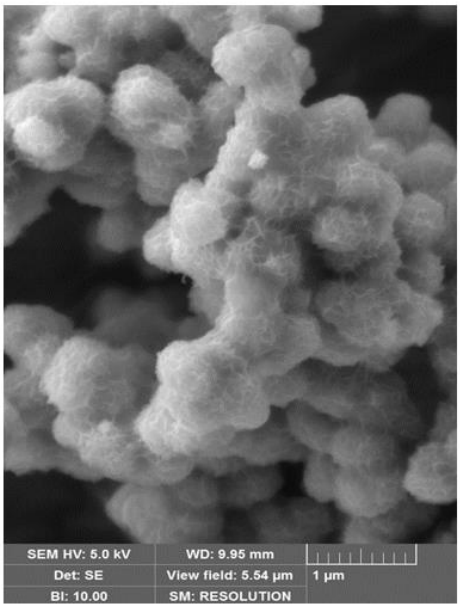

Element	Mn	Co	Cu	Zn	Ni	Mg
Weight %	65.52	3.72	1.29	0.35	4.96	0.46

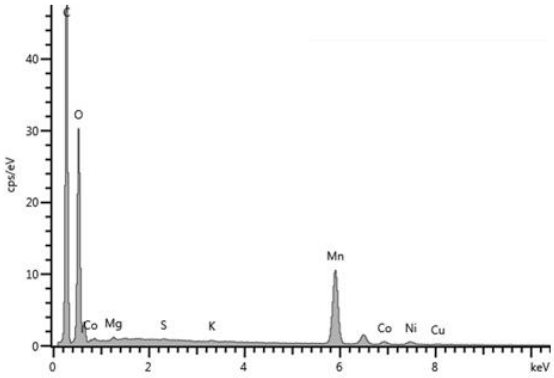

Figure 5.13: SEM micrograph, EDS and XRF elemental analysis of dry manganese oxide precipitated with Mode C, at pH 4 and 25 °C.

5.5.5 Proposed flowsheet for the processing of nickel laterite sulfate leach solutions

From the above exploratory experiments, it was found that manganese, cobalt and copper can be separated from nickel, magnesium, calcium and zinc by oxidative precipitation using potassium permanganate solution. A separation process based on the oxidative precipitation of manganese by $KMnO_4$ is proposed in Figure 5.14.

It is well known that in addition to the effectiveness of any process, the ability to produce by-products and recycle any products as reagent impacts on the viability of any potential process. This process flowsheet provides a potential to produce manganese as a by-product and the ability to produce a recyclable Mn product that can be useful in the processing of nickel laterite ores. The presence of manganese minerals in nickel laterite ores is found to influence the amount of ferrous ion reporting on the sulfate leach solution. The Ravensthorpe HPAL discharge liquor, for example, contained significant ferrous ion because manganese oxide content of the ore is low and not sufficient to oxidise ferrous ion from the iron (II) containing minerals (White et al., 2006). Manganese oxide precipitates can be recycled into the leaching step and serve as an oxidising agent for the

ferrous ion. The oxidative precipitation is advantageous as it is optimal at low temperatures which means that ambient conditions can be used. Although the oxidation precipitation process has shown success in removing manganese and cobalt at reasonable nickel losses, there is need to investigate the auxiliary process, associated with the downstream processing of the precipitates, its dissolution and the recovery of both cobalt and manganese and its optimisation using real nickel laterite sulfate solutions. The major concern in implementing this process is the cost of potassium permanganate. The process is comparable to MSP but has an advantage of using reagents that are not hazardous and comparable to DSX as used in Bulong nickel operation as it offers separation of nickel and cobalt following neutralisation stages.

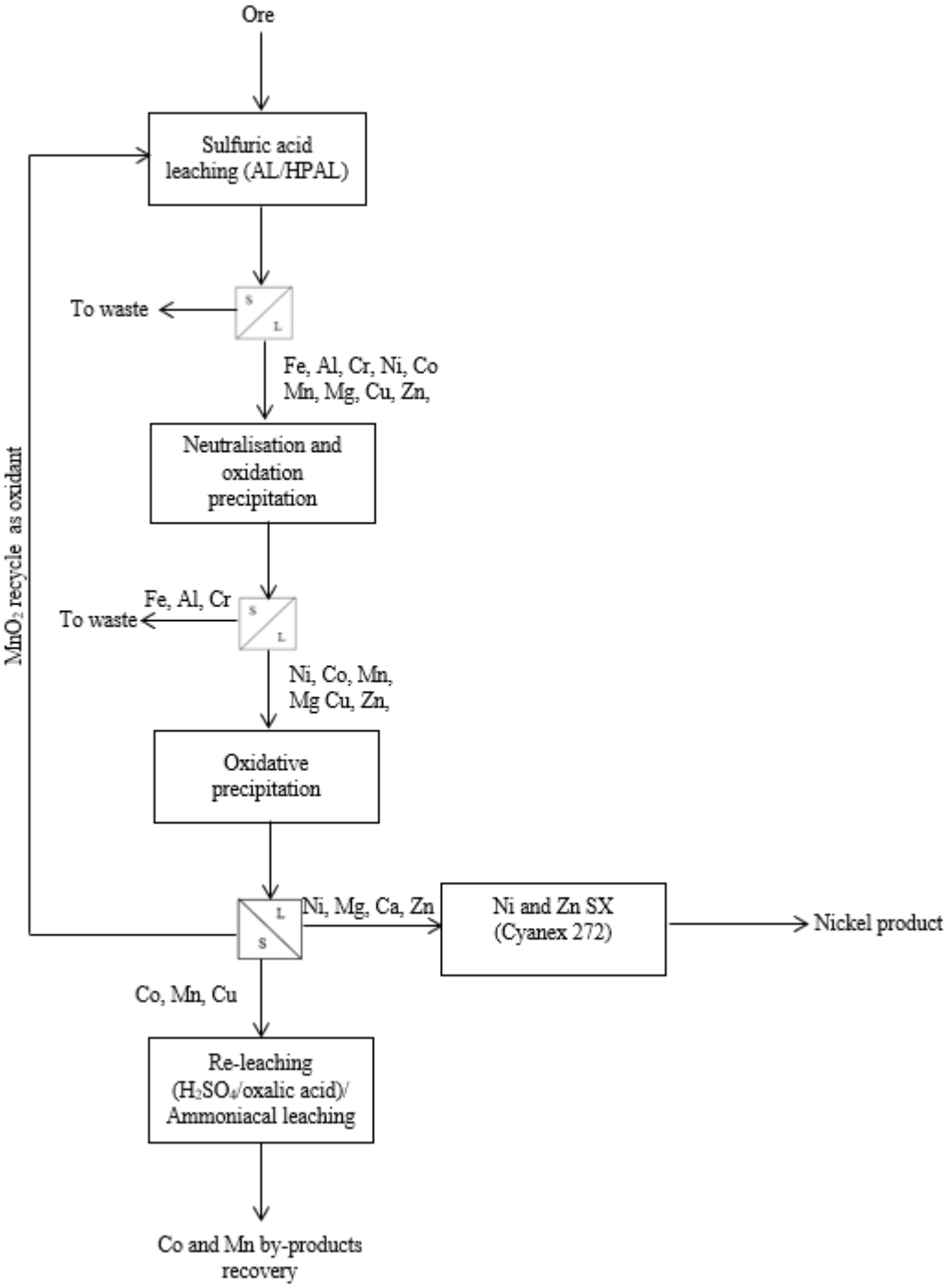

Figure 5.14: Proposed flowsheet for the processing of nickel laterite sulfate leach solutions. S and L refer to solid and liquid, respectively.

5.6 Conclusions

The removal of manganese with cobalt and the level of nickel loss from synthetic sulfate solutions simulating nickel laterite sulfate solutions post iron neutralisation was investigated.

The results showed that permanganate could effectively remove manganese, cobalt and to certain extent copper from sulfate solutions by oxidation precipitation. Comparison of the three experimental procedures used (Mode A, B and C) in the precipitation experiments, shows that the % manganese removal depends on the dose of permanganate and is not influenced by the operating pH value. On the contrary, greater removal of cobalt and copper and nickel loss to the precipitates occurs when a higher pH value is used during the reaction time and ageing time. When using Mode C at pH 4, 99.9% manganese, 95% cobalt and 83% copper could be easily removed from solution at 25 ℃ and significant amount of nickel are lost to the precipitate (>5%). Low equilibrium pH when using Mode A lowers the level of nickel loss and does not favour the co-removal of cobalt and copper. About 99.2% manganese, 55% cobalt and 25% copper were removed at equilibrium pH 1.75 (Mode A); and, the nickel loss to the precipitate was negligible at about 0.59%. Manganese and cobalt can be effectively removed by oxidative precipitation by carefully controlling pH. The removal of manganese is best at low temperature of 25℃ and decreases with increasing temperature. The optimum conditions devised as a result of the investigations were using Mode C, equilibrium pH 4, temperature 25 ℃, at least 1.54 mg $KMnO_4$ per mg Mn(II) and ageing time of 5 minutes. The permanganate dose required shows slight dependence on the concentration of manganese in solution, and thus the control of manganous ion concentration during precipitation is crucial.

Both cobalt and copper were not recovered by acid washing, and the congruency in the dissolution of manganese with an increase in temperature suggests that cobalt must be incorporated in the lattice and strongly adsorbed on the manganese oxide. Liquid-solid separation of the sludges is not an issue as the brownish-black manganese oxide precipitates are dense and easily settle and filter.

Although the experiments were carried out in a bench scale, the results show that oxidative precipitation by $KMnO_4$ process has potential application for the processing of nickel laterite sulfate solutions post iron, aluminium and chromium removal in partial neutralisation stages. It can be easily used in conjunction with re-leaching and solvent extraction as the other separation techniques, MHP and MSP.

References

ADAMS, R. B. 1960. Manganese removal by oxidation with potassium permanganate. *Journal (American Water Works Association),* 52**,** 219-228.

BURNS, R. G. 1976. The uptake of cobalt into ferromanganese nodules, soils, and synthetic manganese (IV) oxides. *Geochimica et Cosmochimica Acta,* 40**,** 95-102.

COUGHLIN, R. W. & MATSUI, I. 1976. Catalytic oxidation of aqueous Mn(II). *Journal of Catalysis,* 41**,** 108-123.

FREITAS, R. M., PERILLI, T. A. & LADEIRA, A. C. Q. 2013. Oxidative Precipitation of Manganese from Acid Mine Drainage by Potassium Permanganate. *Journal of Chemistry,* 2013.

LOGANATHAN, P. & BURAU, R. 1973. Sorption of heavy metal ions by hydrous manganese oxide. *Geochimica et Cosmochimica Acta,* 37**,** 1277-1293.

MCKENZIE, R. 1970. The reaction of cobalt with manganese dioxide minerals. *Soil Research,* 8**,** 97-106.

MING, T. 2003. Reduction of Mn content in municipal water supply by permanganate [J]. *Water & Wastewater Engineering,* 2**,** 009.

MORGAN, J. J. & STUMM, W. 1964. Colloid-chemical properties of manganese dioxide. *Journal of Colloid Science,* 19**,** 347-359.

MURRAY, J. W. 1975. The interaction of metal ions at the manganese dioxide-solution interface. *Geochimica et Cosmochimica Acta,* 39**,** 505-519.

PHATAI, P., WITTAYAKUN, J., CHEN, W.-H., FUTALAN, C. M., GRISDANURAK, N. & KAN, C.-C. 2014. Removal of manganese(II) and iron(II) from synthetic groundwater using potassium permanganate. *Desalination and Water Treatment,* 52**,** 5942-5951.

PHATAI, P., WITTAYAKUN, J., GRISDANURAK, N., CHEN, W. H., WAN, M. W. & KAN, C. C. 2010. Removal of manganese ions from synthetic groundwater by oxidation using KMnO4 and the characterization of produced MnO2 particles. *Water Science and Technology,* 62**,** 1719-1726.

ROCCARO, P., BARONE, C., MANCINI, G. & VAGLIASINDI, F. G. A. 2007. Removal of manganese from water supplies intended for human consumption: a case study. *Desalination,* 210**,** 205-214.

STUMM, W. & O'MELIA, C. R. 1968. Stoichiometry of coagulation. *Journal (American Water Works Association),* 60**,** 514-539.

TIAN, X.-Y., CHEN, L.-J., LIU, H.-C. & CHENG, Y.-L. 2006. Progress of potassium manganate preoxidation method for source of drinking water. *Jilin Jianzhu Gongcheng Xueyuan Xuebao(Journal of Jilin Architectural and Civil Engineering Institute),* 23**,** 15-18.

VAN BENSCHOTEN, J. E., LIN, W. & KNOCKE, W. R. 1992. Kinetic modelling of manganese (II) oxidation by chlorine dioxide and potassium permanganate. *Environmental science & technology,* 26**,** 1327-1333.

WHITE, D., MILLER, M. & NAPIER, A. 2006. Impurity disposition and control in the Ravensthorpe acid leaching process. *Iron Control Technologies—3rd International Symposium on Iron Control in Hydrometallurgy, Canadian Inst. Min. Metall. & Petroleum.*

ZHANG, W., CHENG, C. Y. & PRANOLO, Y. 2010. Investigation of methods for removal and recovery of manganese in hydrometallurgical processes. *Hydrometallurgy,* 101**,** 58-63.

ZHANG, W., SINGH, P. & MUIR, D. 2002. Oxidative precipitation of manganese with SO2/O2 and separation from cobalt and nickel. *Hydrometallurgy,* 63**,** 127-135.

ZHANG, W., SINGH, P. & MUIR, D. M. 2000. SO2/O2 as an oxidant in hydrometallurgy. *Minerals Engineering,* 13**,** 1319-1328.

ZHU, J.-W., ZHANG, Z., LI, X.-M., XU, X.-H. & WANG, D.-H. 2009. Manganese removal from the Qiantang River source water by pre-oxidation: A case study. *Journal of Zhejiang University-SCIENCE A,* 10**,** 450-457.

CHAPTER 6
SUMMARY AND FUTURE WORK

6.1 Summary

Specific conclusions were drawn at the end of chapter's two to five and this chapter provides a general summary of the conclusions and suggestions for future work. This thesis consists of three main parts: (i) use of Visual MINTEQ (version 3.1) in the simulation of a dilute sulfate solution containing trivalent ions of Fe, Al and Cr and also divalent ions of Ni and Co; (ii) detailed experimental investigations on the removal of major impurities including analysis of the associated nickel and cobalt losses; and (iii) characterisation of the iron-rich precipitates and manganese-rich precipitates obtained from the impurity removal processes.

Experimental investigations were carried out using synthetic sulfate solutions simulating nickel laterite leach solutions and nickel and cobalt simulation solutions following an iron precipitation process when processing nickel laterite ores.

6.1.1 Visual MINTEQ simulation

Visual MINTEQ software was used to calculate the speciation diagrams of the individual cations and the SI values of the individual metal phases at pH range 0 to 4.5 at 25 ℃ and 40 ℃. The behaviour of the cations in solution is influenced by both pH and temperature. It was found that in sulfate solutions, the metal ions exist as a mixture of metal sulfate species and metal hydroxo species. The trivalent cations of Fe, Al and Cr are precipitated as a mixture of metal oxyhydroxides and oxyhydroxysulfates. The simulation results predicted selective removal of the trivalent ions of Fe, Al and Cr from the divalent ions of Ni and Co in multi-element sulfate solutions. This can be achieved by adjusting the solution pH. The separation of cobalt would depend on the kinetics of the formation of $CoFe_2O_4$ which is predicted at pH values less than 4.5. Experimental results obtained using synthetic sulfate solutions were slightly different from simulation results. The experimental results confirmed that iron, aluminium and chromium could be recovered at pH range 0 to 4.5, but nickel and cobalt losses were incurred in the experimental results

using simulated solutions. This could have been a result of nickel and cobalt cations being adsorbed on the iron-rich precipitates since no phases of the species were identified. It was found that ferrihydrite and schwertmannite, iron oxyhydroxide and oxyhydroxysulfate, respectively were formed in the experimental results confirming predictions from the SI diagrams.

6.1.2 Impurity removal and nickel and cobalt losses

Detailed studies were carried out using synthetic sulfate solutions to establish the correlation between the process parameters and the impurity removal and the associated effect on nickel and cobalt losses to the precipitates. The one variable at a time approach and design of experiment were used in the following two studies: (i) co-removal of iron, aluminium and chromium by hydrolytic and oxidative hydrolytic precipitation, and (ii) manganese removal by oxidative precipitation.

In iron precipitation, simple and complex synthetic sulfate solutions with different metal ion combinations were used to determine the effect of various factors on the impurity removal efficiencies and nickel and cobalt losses. The same experimental procedure was used for all tests without dilution to control ferric ion concentration and supersaturation level during precipitation.

The first stage examined the impact of different neutralising agents, including $CaCO_3$, MgO and $MgCO_3$ slurries and NaOH solution on iron precipitation and the amount of nickel and cobalt losses. This was achieved using a ternary sulfate system [Fe(III)+Ni(II)+Co(II)] and multi-element sulfate solution (composition given in Table 3.1). The experimental results showed that $CaCO_3$ slurry is a better neutralising agent when compared to the other three, with the lowest nickel and cobalt losses of about 2 % and below from the sulfate solutions at pH 2.5. Nickel and cobalt losses were higher in multi-element sulfate solution than in ternary sulfate system. It was also found that the precipitates for all neutralising agents were instantaneously filtered when using the ternary sulfate system, but slow filtration rate was observed when using multi-element sulfate solution.

The second stage involved examination of the effect of aluminium, chromium and magnesium presence on the amount of nickel and cobalt losses and iron precipitation using $CaCO_3$ that gave the least amount of nickel and cobalt losses and produced iron-rich precipitates with the best filtration and washing characteristics was selected in the preceding study. This was conducted using synthetic sulfate solution with different metal combinations. It was observed that greater nickel and cobalt losses are incurred in the systems containing aluminium and chromium. The presence of magnesium affected the iron precipitation process in that it caused the formation of viscous iron precipitates with poor filtration properties which enhances the uptake of nickel and cobalt in the precipitates. Nickel and cobalt losses increase as the individual cations in solution increase resulting in the highest nickel and cobalt losses being observed when using multi-element sulfate solution, containing ten different cations (Table 3.1).

Full factorial design experiments were carried out using the multi-element sulfate solution, where several factors are changed simultaneously. The results showed that pH, temperature and the concentration of $CaCO_3$ slurry and their interactions were of statistical significance on the removal of the impurities and also on nickel and cobalt losses. Temperature and pH had the largest effect on nickel and cobalt loss and impurity removal efficiency. The effect of these parameters was studied further using one variable at a time approach. This was done to estimate the optimal conditions for removal of the iron, aluminium and chromium without excessive nickel and cobalt losses. The optimal conditions for removal of iron, aluminium and chromium was higher equilibrium pH and temperature of 3.5 and 85 °C, respectively, but at the cost of greater nickel and cobalt losses ($\leq$10%). Increasing the operating temperature increases the removal of aluminium and chromium but showed a minimal effect on the removal of ferric ion. At a pH range of 2.5 to 4, ferrous ion was not precipitated from multi-element sulfate solution containing both ferrous and ferric ion.

The removal of ferrous ion by oxidative precipitation from multi-element sulfate solution was studied as a secondary impurity removal process following the first impurity removal process. The results indicated that the process is largely influenced by the type of oxidant, pH and temperature. Hydrogen peroxide is a better oxidant than oxygen or air. Increasing pH and temperature favoured the oxidative precipitation of ferrous ion and the co-

precipitation of aluminium and chromium when using oxygen. However, this also increased nickel and cobalt losses. Reduction of nickel and cobalt losses in oxidative precipitation can be achieved by using multistage oxidative precipitation. Amorphous iron phases were still formed during oxidative precipitation experiments, regardless of the ferric ion concentration being below 2 g/L in the multi-element solutions during precipitation as is in E.Z. and V.M. methods. The precipitates obtained in oxidative precipitation were instantaneously filtered like the iron-rich precipitates produced at high ferric ion concentration using FNC, FANC, FCrNC and FACrNC sulfate system. Comparison of the filtration properties of the iron-rich precipitates from multi-element solutions in the first precipitation process (Chapter 3) and oxidative precipitation process suggests that ferric iron concentration control is crucial in magnesium-rich solutions. Low ferric ion concentration in multi-element sulfate solution resulted in lower supersaturation which promoted particle growth over nucleation. The iron phases formed during precipitation are largely dependent on the composition of sulfate solutions. The investigations of the removal of iron (ferrous and ferric ion), aluminium and chromium and the losses of nickel and cobalt indicate that a two-stage impurity removal process is best for processing nickel laterite leach sulfate solutions. The first stage was purely hydrolytic precipitation with the second stage oxidative hydrolytic precipitation of Fe, Al and Cr. The optimum conditions for the first stage are an equilibrium pH of 3.5 and temperature of 85 °C while for the second stage an oxidative precipitation pH value of 3.5, an ageing pH of 4.5, and temperature of 85 °C. Solids from the second stage could be recycled to the leaching stage to recover nickel and cobalt lost during precipitation. Aluminium build up can be minimised by using a high pH value of about 3.5 in the first step which means minor concentrations of Al and Cr in the oxidative precipitation feed solution.

Extensive experimental investigations were carried out using synthetic nickel and cobalt sulfate solutions with composition comparable to those obtained following Fe, Al and Cr precipitation. This was done to establish the relationship between manganese removal by oxidative precipitation using $KMnO_4$ and nickel and cobalt losses to the precipitates. The experiments were carried out using simple synthetic manganese sulfate solution containing manganese only, Mn(II)+Ni(II)+Co(II) ternary system and a more complicated

sulfate system [Mn(III)+Ni(II)+Co(II)+Cu(II)+Mg(II)+Zn(II)+Ca(II)]. To determine the important factors, full factorial design experiments were applied. One variable at a time approach was used to optimise the important factors determined in factorial design experiments. Three different experimental procedures referred to as Mode A, Mode B and Mode C were used (Table 5.2). Initially, the effect of ageing on the removal of manganese and nickel and cobalt losses was determined using pure synthetic manganese sulfate solution and [Mn(II)+Ni(II)+Co(II)] ternary system. It was found that there is a reduction in manganese removal with an increase in ageing time, most likely caused by the re-dissolution of the manganese-rich precipitates. Cobalt losses are extremely high regardless of the experimental procedure used and oxidative precipitation was used for co-removal of manganese and cobalt. Results of the full factorial design experiments showed that temperature and $KMnO_4$ dosage have a significant effect on manganese removal while pH and $KMnO_4$ dosage are significant factors on the removal of cobalt and nickel loss to the precipitate. The optimum $KMnO_4$ dosage for manganese removal was about 1.54 mg $KMnO_4$/mg Mn(II) and this was not dependant on the experimental procedure applied. Further studies on the important factors using one variable at a time approach showed that by controlling the equilibrium pH, the co-removal of cobalt could be maximised. The removal of manganese and cobalt was favoured at high pH values but at the cost of increased nickel losses. Increasing the operating temperature resulted in a decrease in manganese removal. The optimum conditions for oxidative precipitation of manganese were Mode C, at temperature 25 ℃, pH value 4.5 and oxidant dosage of 1.54 mg $KMnO_4$/mg Mn(II). Higher nickel losses were also observed with an increase in initial manganese concentration (>2.5 g/L) during precipitation.

6.1.3 Characterisation of iron-rich precipitates and manganese-rich precipitates

In this study, iron-rich precipitates were produced at high and low ferric ion concentrations. Several techniques such as XRD, SEM, EDS and AAO dissolution were applied to analyse the precipitates. Effect of the neutralising agent type, ferric ion concentration and other impurities, on the nature and crystallinity of the precipitate formed during iron precipitation was determined. XRD and SEM analysis results indicated that ferric ion was precipitated as a mixture of amorphous and metastable iron oxyhydroxides

and oxyhydroxysulfates. The XRD patterns and the SEM micrographs indicated the formation of amorphous iron phases and schwertmannite when slurries of $CaCO_3$, $MgCO_3$ and MgO are used. It also showed the formation of jarosite when sodium hydroxide solution is used at high ferric ion concentration. The formation of schwertmannite was confirmed during co-removal of aluminium and chromium in the quaternary systems FANC and FCrNC, however, it was difficult to identify the iron phases formed when magnesium is present in the high ferric ion synthetic sulfate solutions. The iron precipitates were a mixture of amorphous and metastable iron phases during oxidative precipitation with hydrogen peroxide as an oxidant and at low ferric ion concentration. The AAO dissolution experiments confirmed that no goethite was formed when using H_2O_2 as the precipitates were completely dissolved in acidified ammonium oxalate solution. The AAO dissolutions curves of the iron-rich precipitates were congruent showing that nickel, cobalt and other impurities are incorporated in the crystal lattice of iron minerals. It was found that at high ferric ion concentration and in the presence of magnesium clayey precipitates were formed.

To characterise the manganese-rich precipitates several techniques were used including XRD, SEM, EDS and zetasizer analysis. XRD and SEM analysis of the manganese precipitates showed that manganese was precipitated as amorphous manganese dioxide, a brownish-black precipitate. The manganese dioxide precipitates were found to have a pzc value at about pH of 2.7.

6.2 Future work

In consideration of the findings made in this study, the following suggestions for future work are recommended:

- Processing of ores high in magnesium silicates, the saprolite ores, is best conducted using AL and HP and thus the leach solutions contain significant amounts of magnesium. The nature of iron-rich precipitates in this study was affected by the concentration of magnesium ions relative to ferric ion concentration, and the mechanism responsible for this behaviour is not clear. The effect of Mg(II): Fe(III) ratio must be studied further to better understand the correlation with the iron precipitation and the associated nickel and cobalt loss.

This could help in establishing a benchmark for the blending of limonite and saprolite ores.

- Characterisation of the iron precipitates obtained showed that metastable phase schwertmannite was formed in simple sulfate solutions at high ferric ion concentration. The precipitates were less amorphous compared to those produced at low ferric ion concentrations of multi-element sulfate solutions during oxidative precipitation. The crystallinity of the iron phases affects nickel and cobalt uptake to the precipitates; for this reason, the formation of goethite is the driving force in most iron removal processes studied. The use of E.Z. and V.M. methods is mainly to enhance the formation of goethite through controlling supersaturation levels. It is worth conducting systematic investigations to establish whether the failure to obtain goethite formation is a result of supersaturation control or the presence of other species. This could eliminate unnecessary high dilutions and lead to savings in water usage.

- Magnesium-containing reagents are expensive, however, the iron residues produced are less bulky. There are also natural minerals such as magnesite and dolomite which are cheaper and are less reactive for good control of supersaturation. For example, the Murrin Murrin nickel operation has such deposits (Motteram et al. 1996). It is worth investigating the applicability of the cheaper and less reactive forms of neutralising agents to alleviate the gypsum problem caused by calcium-containing neutralising agents.

- The uptake of cobalt during oxidative precipitation of manganese is extremely high, although the mechanism responsible for this uptake is not clear. Further studies using variable concentrations of the cations in manganese-rich solution and the characterisation of the precipitates using different solid analysis techniques is necessary to establish the mechanisms.

- The viability of the manganese oxidative precipitation process rests on the ability to re-leach the manganese oxide precipitates to recover manganese and cobalt in downstream processing. It also relies on the usefulness of the manganese oxide as

an oxidant in upstream leaching. The weak sulfuric solution at pH 1 to 1.5 was not able to recover cobalt, copper, zinc and nickel co-removed with manganese. An investigation into the leaching behaviour of the manganese oxide precipitates using different reagents is necessary. The reagents that can be investigated include but are not limited to the following:

i. Strong inorganic acids such as sulfuric acid and hydrochloric acid.

ii. Aqueous mixture solutions of an organic reductant and inorganic acid such as using oxalic acid in sulfuric acid solution.

- The precipitation experiments were carried out in a batch-wise mode, however, supersaturation control is more stable and controlled better in a continuous mode operation. To improve the precipitation quality which is crucial in controlling the nickel and cobalt losses incurred, it is suggested that further investigation be carried out in a continuous mode operation.

Appendix 1: Particle size distribution

Particle size distribution was measured using a Malvern Mastersizer 3000 Hydro EV. The instrument gives the result as a volume distribution as illustrated below:

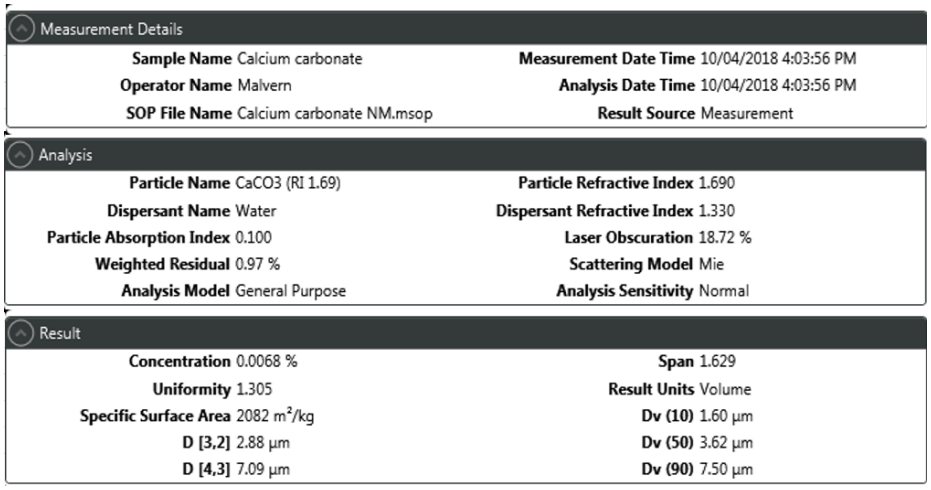

Measurement Details

Sample Name Calcium carbonate	**Measurement Date Time** 10/04/2018 4:03:56 PM
Operator Name Malvern	**Analysis Date Time** 10/04/2018 4:03:56 PM
SOP File Name Calcium carbonate NM.msop	**Result Source** Measurement

Analysis

Particle Name CaCO3 (RI 1.69)	**Particle Refractive Index** 1.690
Dispersant Name Water	**Dispersant Refractive Index** 1.330
Particle Absorption Index 0.100	**Laser Obscuration** 18.72 %
Weighted Residual 0.97 %	**Scattering Model** Mie
Analysis Model General Purpose	**Analysis Sensitivity** Normal

Result

Concentration 0.0068 %	**Span** 1.629
Uniformity 1.305	**Result Units** Volume
Specific Surface Area 2082 m^2/kg	**Dv (10)** 1.60 µm
D [3,2] 2.88 µm	**Dv (50)** 3.62 µm
D [4,3] 7.09 µm	**Dv (90)** 7.50 µm

Size (µm)	% Volume In	Size (µm)	% Volume In	Size (µm)	% Volume In	Size (µm)	% Volume In
0.01	0	0.243	0	5.92	5.11	144	0.1
0.0114	0	0.276	0	6.72	3.5	163	0
0.0129	0	0.314	0	7.64	2.09	186	0
0.0147	0	0.357	0	8.68	1.02	211	0
0.0167	0	0.405	0	9.86	0.36	240	0
0.0189	0	0.46	0.07	11.2	0	272	0
0.0215	0	0.523	0.3	12.7	0	310	0
0.0244	0	0.594	0.65	14.5	0	352	0
0.0278	0	0.675	0.97	16.4	0.1	400	0
0.0315	0	0.767	1.17	18.7	0.2	454	0
0.0358	0	0.872	1.22	21.2	0.3	516	0
0.0407	0	0.991	1.22	24.1	0.37	586	0
0.0463	0	1.13	1.28	27.4	0.42	666	0
0.0526	0	1.28	1.54	31.1	0.44	756	0
0.0597	0	1.45	2.12	35.3	0.44	859	0
0.0679	0	1.65	3.06	40.1	0.43	976	0
0.0771	0	1.88	4.31	45.6	0.42	1110	0
0.0876	0	2.13	5.75	51.8	0.41	1260	0
0.0995	0	2.42	7.19	58.9	0.41	1430	0
0.113	0	2.75	8.41	66.9	0.41	1630	0
0.128	0	3.12	9.22	76.0	0.41	1850	0
0.146	0	3.55	9.46	86.4	0.38	2100	0
0.166	0	4.03	9.08	98.1	0.34	2390	0
0.188	0	4.58	8.12	111	0.27	2710	0
0.214	0	5.21	6.73	127	0.18	3080	0

The results from the instrument were converted into a number distribution on an excel spreadsheet. The excel spreadsheet for the volume distribution to number distribution is given below:

Delta $L_{(0.0114)}$ = (0.0114-0.01)/1000000 = 1.40E-09

Lbar = 0.01 + (Delta L)/2

Number density = (Concentration*%Volume $in_{(0.0114)}$)*(π/6*$Lbar_{(0.0114)}^3$*100)=0.00E+00

Size µm	Delta L (m)	Lbar (m)	Number density
0.01			
0.0114	**1.40E-09**	**1.07E-08**	**0.00E+00**
0.0129	1.50E-09	1.22E-08	0.00E+00
0.0147	1.80E-09	1.38E-08	0.00E+00
0.0167	2.00E-09	1.57E-08	0.00E+00
0.0189	2.20E-09	1.78E-08	0.00E+00
0.0215	2.60E-09	2.02E-08	0.00E+00
0.0244	2.90E-09	2.30E-08	0.00E+00
0.0278	3.40E-09	2.61E-08	0.00E+00
0.0315	3.70E-09	2.97E-08	0.00E+00
0.0358	4.30E-09	3.37E-08	0.00E+00
0.0407	4.90E-09	3.83E-08	0.00E+00
0.0463	5.60E-09	4.35E-08	0.00E+00
0.0526	6.30E-09	4.95E-08	0.00E+00
0.0597	7.10E-09	5.62E-08	0.00E+00
0.0679	8.20E-09	6.38E-08	0.00E+00
0.0771	9.20E-09	7.25E-08	0.00E+00
0.0876	1.05E-08	8.24E-08	0.00E+00
0.0995	1.19E-08	9.36E-08	0.00E+00
0.113	1.35E-08	1.06E-07	0.00E+00
0.128	1.50E-08	1.21E-07	0.00E+00
0.146	1.80E-08	1.37E-07	0.00E+00
0.166	2.00E-08	1.56E-07	0.00E+00
0.188	2.20E-08	1.77E-07	0.00E+00
0.214	2.60E-08	2.01E-07	0.00E+00
0.243	2.90E-08	2.29E-07	0.00E+00
0.276	3.30E-08	2.60E-07	0.00E+00
0.314	3.80E-08	2.95E-07	0.00E+00
0.357	4.30E-08	3.36E-07	0.00E+00
0.405	4.80E-08	3.81E-07	0.00E+00
0.46	5.50E-08	4.33E-07	0.00E+00
0.523	6.30E-08	4.92E-07	0.00E+00
0.594	7.10E-08	5.59E-07	0.00E+00

0.675	8.10E-08	6.35E-07	0.00E+00
0.767	9.20E-08	7.21E-07	0.00E+00
0.872	1.05E-07	8.20E-07	0.00E+00
0.991	1.19E-07	9.32E-07	0.00E+00
1.13	1.39E-07	1.06E-06	0.00E+00
1.28	1.50E-07	1.21E-06	0.00E+00
1.45	1.70E-07	1.37E-06	0.00E+00
1.65	2.00E-07	1.55E-06	0.00E+00
1.88	2.30E-07	1.77E-06	0.00E+00
2.13	2.50E-07	2.01E-06	0.00E+00
2.42	2.90E-07	2.28E-06	0.00E+00
2.75	3.30E-07	2.59E-06	0.00E+00
3.12	3.70E-07	2.94E-06	7.86E+11
3.55	4.30E-07	3.34E-06	1.47E+12
4.03	4.80E-07	3.79E-06	2.03E+12
4.58	5.50E-07	4.31E-06	2.32E+12
5.21	6.30E-07	4.90E-06	2.35E+12
5.92	7.10E-07	5.57E-06	2.16E+12
6.72	8.00E-07	6.32E-06	1.84E+12
7.64	9.20E-07	7.18E-06	1.47E+12
8.68	1.04E-06	8.16E-06	1.10E+12
9.86	1.18E-06	9.27E-06	7.81E+11
11.2	1.34E-06	1.05E-05	5.26E+11
12.7	1.50E-06	1.20E-05	3.40E+11
14.5	1.80E-06	1.36E-05	2.09E+11
16.4	1.90E-06	1.55E-05	1.25E+11
18.7	2.30E-06	1.76E-05	7.21E+10
21.2	2.50E-06	2.00E-05	4.11E+10
24.1	2.90E-06	2.27E-05	2.34E+10
27.4	3.30E-06	2.58E-05	1.35E+10
31.1	3.70E-06	2.93E-05	7.94E+09
35.3	4.20E-06	3.32E-05	4.85E+09
40.1	4.80E-06	3.77E-05	3.10E+09
45.6	5.50E-06	4.29E-05	2.10E+09
51.8	6.20E-06	4.87E-05	1.52E+09
58.9	7.10E-06	5.54E-05	1.16E+09
66.9	8.00E-06	6.29E-05	9.33E+08
76	9.10E-06	7.15E-05	7.73E+08
86.4	1.04E-05	8.12E-05	6.33E+08
98.1	1.17E-05	9.23E-05	5.11E+08
111	1.29E-05	1.05E-04	4.01E+08
127	1.60E-05	1.19E-04	2.97E+08
144	1.70E-05	1.36E-04	2.08E+08
163	1.90E-05	1.54E-04	1.39E+08

186	2.30E-05	1.75E-04	8.60E+07
211	2.50E-05	1.99E-04	4.90E+07
240	2.90E-05	2.26E-04	2.54E+07
272	3.20E-05	2.56E-04	1.19E+07
310	3.80E-05	2.91E-04	4.38E+06
352	4.20E-05	3.31E-04	4.45E+05
400	4.80E-05	3.76E-04	0.00E+00
454	5.40E-05	4.27E-04	0.00E+00
516	6.20E-05	4.85E-04	0.00E+00
586	7.00E-05	5.51E-04	0.00E+00
666	8.00E-05	6.26E-04	0.00E+00
756	9.00E-05	7.11E-04	0.00E+00
859	1.03E-04	8.08E-04	0.00E+00
976	1.17E-04	9.18E-04	0.00E+00
1110	1.34E-04	1.04E-03	0.00E+00
1260	1.50E-04	1.19E-03	0.00E+00
1430	1.70E-04	1.35E-03	0.00E+00
1630	2.00E-04	1.53E-03	0.00E+00
1850	2.20E-04	1.74E-03	0.00E+00
2100	2.50E-04	1.98E-03	0.00E+00
2390	2.90E-04	2.25E-03	0.00E+00
2710	3.20E-04	2.55E-03	0.00E+00
3080	3.70E-04	2.90E-03	0.00E+00
3500	4.20E-04	3.29E-03	0.00E+00

Publications

The following peer-reviewed conference publications have been made from the work completed by the author of this thesis.

Mbedzi, N., Ibana, D., Dyer, L. and Browner, R., 2017, January. The effect of oxidant addition on ferrous iron removal from multi-element acidic sulphate solutions. In *AIP Conference Proceedings* (Vol. 1805, No. 1, p. 030002). AIP Publishing LLC. https://doi.org/10.1063/1.4974413